THE FUNCTIONS OF MOUSE SPINAL V3 INTERNEURONS IN LOCOMOTION

by

Han Zhang

Submitted in partial fulfilment of the requirements
for the degree of Doctor of Philosophy

at

Dalhousie University
Halifax, Nova Scotia

August of 2020

TABLE OF CONTENTS

LIST OF TABLES

LIST OF FIGURES

ABSTRACT

V3 interneurons (INs) are a major group of glutamatergic commissural neurons in the mouse spinal cord. They directly innervate motor neurons (MNs) as well as other ventral INs. Although it has been shown that V3 INs are crucial in generating stable and robust rhythmic locomotor activities, the mechanisms underlying their functions are still unclear. In my current study, I delete the expression of Vesicular Glutamate Transporter 2 (vGluT2) in V3 INs in *Sim1*$^{Cre/+}$;*vGluT2* $^{flox/flox}$ (V3OFF) mice, and systematically examine their locomotor behaviours, including their gaits at various treadmill speeds, as well as their kinematics and muscle activities in different locomotor tasks. Firstly, I identify a subset of V3 INs that might regulate the coordination of fore- and hind-limbs for trotting movements. Secondly, I find that V3 INs have task-dependent functional roles in regulating proximal or distal joints. They facilitate hip joint movements in all locomotor tasks, while only regulating distal joint activities in weight-bearing behaviours. In addition, using optogenetic tools, I also investigate the functions of V3 INs in fictive locomotion of the neonatal spinal cord. In combination with computational modelling studies, we provide convincing evidence that V3 INs contribute to the synchronization of the left-right locomotor outputs by providing mutual excitation between the extensor centres in the left and right central pattern generator (CPG) circuits. Thus, my study reveals that spinal V3 INs potentially have multiple functional subpopulations that play various specific and critical roles in regulating locomotor behaviours under different conditions.

LIST OF ABBREVIATIONS USED

Anterior biceps	AB
Bone Morphogenetic Proteins	BMPs
Central pattern generator circuits	CPGs
Channelrhodopsin2	ChR2
Cholera-toxin B	CTB
Commissural interneurons	CINs
Deep peroneal nerve	DPc
Developing brain homeobox 1	Dbx1
Diagonal trot	D-trot
Dorsal root ganglia	DRG
Dorsal V3	V3D
Electromyography	EMG
Electroneurogram	ENG
Engrailed 1	En1
Enhanced yellow fluorescent protein	EYFP
Even-skipped homologue protein 1	Evx1
Extensor digitorum longus	EDL
Flexor digitorum longus	FDL

Flexor halluces longus	FHL
Flexor reflex afferent	FRA
Gastrocnemii medialis and lateralis	GM and GL
Glutamic acid decarboxylase 2	GAD2
Golgi tendon organ	GTO
Ia inhibitory interneurons	IaINs
Iliopsoas	IP
Inhibitory interneurons for Extensor	InE
Inhibitory interneurons for flexor	InF
Interneuron	IN
Lateral walk	L-walk
Light-emitting diode	LED
Loosely coupled	LC
Mesencephalic locomotor region	MLR
Motor neuron	MN
N-methyl-D, L-aspartate	NMA
Numerical aperture	NA
Paired box protein 7	Pax7
Paired-like homeodomain transcription factor	Pitx
Parvalbumin	PV

Pattern formation	PF
Peroneus longus	Plong
Posterior biceps	PB
Postnatal day #	P#
Power stroke	PS
Primary afferent depolarization	PAD
Rectus femoris	RF
Renshaw cells	RCs
Retinoid-related orphan receptor alpha	RORα
Return stroke	RS
Rhythm generator	RG
Sartorius anterior and medial	Sart A and M
Semimembranosus anterior	SmA
Semitendinosus	ST
Sim1$^{Cre/+}$; *vGluT2* $^{flox/flox}$	V3OFF
Soleus	Sol
Sonic hedgehog	Shh
Stance	St
Standard deviations	StDv
Statistical parametric mapping	SPM

Swing	Sw
Tibialis anterior	TA
Tightly coupled	TC
Vastus	VA
Vastus lateralis	VL
Ventral V3	V3V
Vesicular glutamate transporter 2	vGluT2
Wild-type	WT

ACKNOWLEDGEMENTS

My deepest gratitude goes first to Dr. Ying Zhang, my supervisor, for all of her careful guidance and constant encouragement. She rescued me from the darkness when I first got to Halifax looking for an acceptance of graduate program to let me stay in Halifax and stay with my wife. She provides me a free and creative scientific environment and teaches me how to think as a scientist. Without her patient instruction, insightful criticism, and expert guidance, completing this thesis would not have been possible.

I also would like to express my heartfelt gratitude to my committee, Dr. Turgay Akay, Dr. Victor Rafuse and Dr. Stefan Krueger. We had several committee meetings together. After each meeting I could get very helpful feedbacks from them. I want to especially thank Dr. Turgay Akay for his instruction of experiment procedures and valuable suggestions in the academic studies. I also thank Dr. Ronald Morgan Harris-Warrick for agreeing to sit as my external examiner.

I must thank all of the members of Dr. Zhang's lab: Mary Li and Dallas Bennett for taking care of my experimental mice and tons of genotyping of those mice; Dylan Deska-Gauthier for the help in my experiment, studies, and language skill, support in the basketball game, and great discussion about science and life; Dr. Joanna Borowska-Fielding for the instruction of electrophysiology experiments. In addition, I need to thank Dr. William P. Mayer and Olivier Laflamme from Dr. Akay's lab. They helped me a lot in the past years.

I appreciate the sacrifice of all of my experimental mice. Wish the soul of them of a decedent eternal rest and peace.

Last my thanks would go to my beloved family for their loving considerations and great confidence in me all through these years. Especially, I want to thank my wife, Mingwei Liu, who support me all the time!

CHAPTER 1. INTRODUCTION

Locomotion is the primary motor function that allows humans and other mammals to interact with their environments. It encompasses many behaviours such as walking, climbing, and swimming. A proper understanding of animal locomotion presents the researcher with an extraordinarily broad range of challenges and complexities, and even comprehending limited ranges of locomotion requires detailed and sophisticated analysis.

Movement is generated by the activity of neuronal circuits mediating and integrating external and internal information, and ultimately leading to precisely timed skeletal muscle coordinations. Under normal circumstances, the planning and initiation of locomotor tasks take place in supraspinal areas, including the cerebral cortex (Drew & Marigold, 2015), the basal ganglia (Garcia-Rill, 1986; Takakusaki, 2013; Grillner & Robertson, 2015), the midbrain (Ryczko & Dubuc, 2013, 2017; Mena-Segovia & Bolam, 2017), the hindbrain (Ferreira-Pinto et al., 2018), and the cerebellum (D'Angelo & Casali, 2012; Grillner & El Manira, 2019). The precise timing and patterns of muscle contractions, however, are controlled by neural circuits located in the spinal cord (Graham Brown, 1911; Grillner, 1981, 2006; Kiehn, 2006, 2011; Rossignol et al., 2006). Spinal neuron assemblies receive signals from the supraspinal regions and peripheral input and then generate the rhythmic patterns of locomotion. The spinal neuronal circuits involved in locomotion are often referred to as central pattern generator circuits (CPGs). Uncovering the functional operations of spinal CPGs and linking cellular activity to specific motor circuits remains the most formidable challenge in the field of locomotion research.

There is a broad range of research on different aspects of locomotor control. For the purpose of this thesis, I will cover three basic principles of stereotyped locomotion in mammals: 1) The principles of mechanical kinematics and muscular kinetics in mammalian locomotion; 2) the organization of sensory regulation; and 3) spinal locomotor circuits.

1 Basic mechanical principles of locomotion in mammals

The mechanical aspects of movement exhibit both kinematic and kinetics properties. The kinematics of a movement produce its trajectory in space, while the kinetics of a movement constitute the cause for movement's excursion, for example, the amplitude and the pattern of corresponding muscle activity and the torques of angular motion. Understanding these basic mechanical principles is fundamental to comprehending locomotion and should serve as a starting point for us before we delve deeper into the investigations of locomotor circuits. As Grillner stated: "this is analogous to airplane design: it is pointless to try to develop the detailed control machinery without knowing the type of motor to be used or the shape of the plane and its fins." (Grillner, 1981)

I will begin by introducing the basic principles of walking. Then, I will extend those principles to different forms of locomotion, such as its different speeds.

1.1 Basic mechanical principle of stereotypic locomotion (walking)

1.1.1 Subphases of the step cycle

During stereotyped terrestrial movement, each limb sequentially performs a complete step cycle that is composed of a stance and a swing phase. During the stance phase, the paw is in contact with the ground supporting the animal's weight while it moves backward in order to support the next push forward. During the swing phase, the paw is lifted and brought forward.

In mammals, like cats, dogs and rodents, the distal joints (knee and ankle) display a more complex kinematic pattern than the hip joint during walking. After analysing Marey's photographs of dogs in locomotion, Phillipson further divided the swing phase into a flexion phase (F) and an extension phase (E1) and the stance phase into its own flexion phase (E2) and an extension phase (E3) (Philippson, 1905) (Figure 1). The F phase starts from the moment of lifting the foot off the ground. In this phase, the flexion movement is observed in all three hindlimb joints: the hip, knee, and ankle joints. This movement lifts the foot off the ground and moves it to a rostral position. When the foot reaches the highest

point in the air required for the motion, the ankle and knee start extending, entering the E1 phase, while the hip continues its flexion movement. The extension of knee and ankle joints lower the foot back to the ground while the flexion of the hip moves the leg forward. Then, the hip starts to extend, and the toe touches the ground, initiating the stance phase. After the toe contacts the ground, the knee and ankle are passively flexed during weight acceptance (E2 or the yielding phase). During the third extension phase, all joints extend to propel the body forward (Grillner, 1981; Halbertsma, 1983; Rossignol, 1996) (Supplementary Video 1.1).

This general subdivision has also been used in cats and rodents. (Grillner, 1981; Halbertsma, 1983; Rossignol, 1996). However, it should be noted that this four-phase description is based on the knee and ankle joint angular excursions, which does not totally correspond to the hip joint angular excursion. The hip flexion phase, which lasts throughout almost the entire swing phase, is longer than the flexion phase of distal joints. The hip flexion or extension cannot be subdivided since hip joint proceeds monotonically. The onset of the flexion phase in hip, knee and ankle does not always coincide but follow sequential orders (Goslow et al., 1973; Kuhtz-Buschbeck et al., 1994).

Humans are bipeds, but also walk with the swing and stance phases. Similar to other mammals, human's hip joint is rotated monotonously forward and backward, showing a stereotyped alternation between flexion and extension. The ankle and knee joints in humans also move similarly to those in cats and rodents, and their step cycle can also be divided into four phases (Grasso & Lacquaniti, 1998). Different from quadrupeds, however, human's heel strikes the ground before the front part of the foot, and so their foot E1 phase occurs during the stance phase instead of swing (Grillner, 1981; Nilsson et al., 1985).

1.1.2 Muscle activity

Electromyography (EMG) measures muscle electrical activity during locomotion, which is the most common method to study the function of a muscle during locomotion. Each joint is controlled by multiple flexors and extensors working together to ensure its smooth movement. The EMG signals can reliably reflect the activity patterns of these muscles during different locomotor tasks under different conditions. While interspecific differences

of locomotor EMG activity exist, many muscles in different species, especially cats, rodents, and, in many cases, humans, share more or less similar activity patterns. Characterization of the 'normal' EMG activities in behaving animals provide important information for us to interpret the motor defect observed from animals with injury, disease or genetic manipulations (Akay et al., 2006; Leblond et al., 2003; Quinlan et al., 2017; Tysseling et al., 2013; Zagoraiou et al., 2009).

In the 1960s, Engberg and Lundberg conducted an EMG analysis of the hindlimb muscular activity of cats during unrestrained locomotion (Engberg & Lundberg, 1962; 1969). These two papers were the first to provide the real time EMG recordings in correspondence with joint angular changes. In general, all extensors were active during the stance phase, with flexors in swing phases. They noticed, however, that the activity of extensors for all (hip, knee, and ankle) joints started before the foot contacted the ground. This extensor activity in the late E1 phase was separate from their subsequent main activities during E2, the yielding phase since there was a gap between these two bursting. This observation was the first evidence to indicate that cutaneous sensory inputs from toe contacting the ground was not responsible for the initiation of E2 phase, the weight acceptance, muscle activities. Similar results were also confirmed by others (Rasmussen et al., 1978, Gruner et al., 1980). Interestingly, Gorassini and colleagues showed that ankle and knee extensor muscles were initiated no matter if the toe touched the ground or stepped in a hole (Gorassini et al., 1994). Rasmussen et al. also measured detailed activities of muscle controlling hip, knee and ankle joints, respectively, in cats during different gaits, showing that their extensor muscles shared a common general activity pattern, that is, they were active prior to the toe contact and then activated during the stance phase (Rasmussen et al., 1978).

Further studies showed that extensor muscles for hip, knee and ankle were active with different patterns in each sub-phase during stance. The hip extensor muscles, such as anterior bicep femoris, semimembranosus and adductor femoris, conformed to the same pattern, in which their activities quickly reached peak in the yielding phase and then maintained till the onset of flexor muscles of next step (Engberg et al., 1969; English & Weeks, 1987). Although all ankle and knee extensor muscles were also active throughout the stance phase like hip extensors, they displayed distinct activation patterns. After toe

touch, vastus lateralis (VL), the primary muscle extending the knee, was active during the major parts of both E2 and E3 stance phases, but VL activity peaked in the E3 phase (Cat: Engberg & Lundberg, 1962; 1969; Rasmussen et al., 1978; Halbertsma, 1983; Gorassini et al., 1994; Markin et al., 2012; Rat: Gruner et al., 1980; Mouse: Leblond et al., 2003; Pearson et al., 2005; Akay et al., 2006; Tysseling et al., 2013). Such activity pattern suggests that VL muscle might play important roles in supporting body weight and propelling body forward. Differently, the activity of gastrocnemii medialis (GM) and lateralis (GL), both ankle extensors, generally peaked during the E2 phase (Engberg & Lundberg, 1962; 1969; Rasmussen et al., 1978; Walmsley et al., 1978; Gorassini et al., 1994; Gruner et al., 1980), but then gradually decrease in E3 phase, which indicates that GS muscles are crucial for supporting body weight after toe touching the ground.

The main flexor muscles of the hip (Iliopsoas, IP), knee (Semitendinosus, ST) and ankle (tibialis anterior, TA) joints all start their activities in a sequential manner in the later part of E3; however, they each stops in different phases (Akay et al., 2014; Rossignol, 1996). Hip flexor muscle, IP, stops during the late E1 phase as the hip joint is flexing and rotating during the swing phase (Akay et al., 2014; Halbertsma, 1983; Rasmussen et al., 1978). The activities of knee flexor muscles are more complex than other flexors because of their anatomical position. For example, ST, a knee flexor and a hip extensor, shows double bursts in one step (Perret & Cabelguen, 1976; Rasmussen et al., 1978; Perret& Cabelguen, 1980; Halbertsma, 1983; English & Weeks, 1987; Hutchison et al., 1989; Smith et al., 1993; Markin et al., 2012). As a knee flexor, ST starts firing in the late E3 phase and is active throughout the early part of the swing phase while the paw is lifted off the ground; but then in the E1 phase, it could fire again with its synergist muscle, Semimembranosus, before the toe contacts the ground. This second burst was suggested to be related to the need for a great torque in flexion to decelerate both the hip and knee joints at the end of the swing phase in preparation for directing the foot placement, because this second burst was more obviously appeared during high-speed locomotion (Wisleder et al., 1990; Smith et al., 1993). Ankle flexor, TA, always shows monophasic activation pattern, and it only discharges in F phase, during trotting and walking in both cats and rodents (Cat: Perret & Cabelguen, 1976; Rasmussen et al., 1978; Markin et al., 2012; Rat: Gruner et al., 1980;

Mouse: Leblond et al., 2003; Pearson et al., 2005; Akay et al., 2006, 2014; Tysseling et al., 2013). The muscle activities mentioned above are illustrated in Figure 2 (Markin et al., 2012).

1.2 Moving under different speeds

1.2.1 Kinematics

In 1983, Halbertsma's study gave a general assessment of locomotor patterns for both the over ground and treadmill activities at different speeds of the intact cat (Halbertsma, 1983). He showed that the length of stance phase duration had a positive linear correlation with the cycle period time, while the swing phase kept relatively constant across the tested speeds. This indicates that it is the stance time that decides the speed of the movement of the animals. Similar results were also observed in rodents (Clarke & Still, 1999, 2001; Leblond et al., 2003; Herbin et al., 2007; Batka et al., 2014; Mendes et al., 2015). Furthermore, the sub-phases of the step cycle related to speed were analysed in Halbertsma's study (1983): E3 phase duration was highly correlated to the speed, while F, E1 and E2 phases did not correspond to speed changes (Halbertsma, 1983). However, there was no study showing such subphase/speed correlation in the rodents.

1.2.2 Interlimb coordination: the gaits

The four legs of a quadruped coordinate with different patterns across different speeds. These patterns are identified as gaits (Philippson, 1905). Gaits can be generally classified as symmetrical (alternating) or asymmetrical (non-alternating) (Grillner, 1975; Hildebrand, 1976, 1989). To describe the phase relationship, the phase value is always corresponded to the time of foot touching the ground relative to the reference limb step cycle. Phase values normally range from 0 to 1, as 0 or 1 indicate perfect synchrony (in-phase coupling), while value of 0.5 indicates a perfect alternation (anti-phase coupling) between the two limbs. Symmetrical, or alternating, gait is defined as two limbs of the same girdle (homologous pair) alternating, that is, the footfall of each pair of feet (fore and hind) evenly spaced in time, but the phase relationship of the homolateral pair could be either in-phase (pace) or out-of-phase (walk and trot). Walking, trotting, and pacing are all symmetrical gaits (Miller

et al., 1975). Asymmetrical (Hildebrand, 1989) or non-alternating (Grillner, 1981) gait is a term for the gait that either homologous pair of limbs (pair of fore- or hindlimbs) is synchronized and contacts the ground simultaneously. The most typical asymmetrical gait is bound, as both fore and hind girdles move synchronously (Hildebrand, 1976, 1977), and half-bound (hop), when only hindlimbs move in-phase (Grillner, 1975). In gallop, the phase relationship between hind limbs is somewhat out-of-phase, in which one girdle can be 0.2 out of phase, and the other can be as much as 0.4, but it still is classified into asymmetrical gait (Grillner, 1975, Hildebrand, 1977, 1989). The gallop can also be subdivided into transverse gallop and rotatory gallop, depending on whether the order of forelimb's fall is the same as the hindlimb's or not (Grillner, 1975). For example, if the left forelimb touches the ground slightly before the right forelimb, and correspondingly the left hindlimb also contacts ground slightly before the left hindlimb, this gait will be a transverse gait; on the other hand, if that right hindlimb contacts the ground slightly before the left hindlimb, the gait will be classified into rotatory gallop.

1.2.3 Gaits under different speeds

Goslow et al. (1973) showed that cats used walking gaits below 0.7 m/s, trotting gaits between 0.7 and 2.7 m/s, and galloping gaits above 2.7m/s (Goslow et al., 1973; Rossignol, 1996). Similarly, Hildebrand stated in 1989: at low speeds, most symmetrical gaits were selected by mammals, since they provided higher stability than asymmetrical ones (Hildebrand, 1989), which, in another word, means that the animals would have to scarify the stability to reach high speeds. Recent studies on mice have shown the same trend in gaits (Serradj & Jamon, 2009; Bellardita & Kiehn, 2015; Lemieux et al.; 2016). Serradj & Jamon studied two strains of mice, 129/Sv and C57BL/6 and found both used stable gaits until their running speed reached 70 cm/s, when mice transitioned from symmetrical to asymmetrical gaits (Serradj & Jamon, 2009). Recently, Bellardita & Kiehn did more systematic analyses of the gait patterns under different speeds, and they identified 4 types of gaits, walk, trot, gallop and bound in mice, with quantifiable measurements. They then further demonstrated that walk, trot, and bound gaits were expressed in distinct stepping frequencies, while gallop, as an intermediate gait, was expressed in overlapping frequencies with trot and bound (Bellardita & Kiehn, 2015). The mice in this study were

stepping on a static corridor and performing a flight reaction to escape the experimenter. This enabled the animals to show natural locomotor behaviours as escaping potential predators, in which mice used all gaits. However, researchers noticed that bounding was barely seen when animals ran on a treadmill (Herbin et al., 2004, 2006, 2007; Serradj and Jamon, 2009). Only most recently, Lemieux et al. (2016) observed bounding in mice at very high speeds, > 90 cm/s, during treadmill locomotion. They identified and classified eight types of gaits in mice moving on the treadmill, including lateral walk, trot, rotary gallop, transverse gallop, half-bound, full-bound, hop, and out-of-phase walk (Lemieux et al.; 2016). Comparing to previous studies in other species, they found one more gait performed by mice moving on the treadmill,, the out-of-phase walk, which had similar limb coordination as gallop but its duty cycle of stance was more than 50% and was a low speed walking gait (Hildebrand, 1968, 1977; Heglund and Taylor, 1988; Abourachid et al., 2007; Maes and Abourachid, 2013; Lemieux et al.; 2016). More interestingly, they further defined two attractor gaits at different speed levels, the trot for low-medium speed, 15 cm/s to 60 cm/s, and bound for the highest running speeds, 120-150 cm/s. They also found out-of-phase walk and half-bound were two semi-attractor gaits for very low walking speed or low-running speed, respectively, since these two gaits were less stable and had a narrower range of suitable speeds than attractor gaits. The other gaits were defined as transition gaits. The attractor gaits, trot and full-bound, occurred more frequently, persisted longer, and were the most ‘attractive’ than other gaits, which means all other gaits tend to transfer to them at any given speed (Lemieux et al.; 2016).

2 Sensorimotor interaction during locomotion in mammals

In this section, I will mainly focus on the dynamic interaction of non-nociceptive cutaneous and proprioceptive afferent from muscle spindle and Golgi tendon organs (GTO) with locomotion in mammalian system. Experimentally inducing the sensory loss has been a useful approach to determine the contribution of peripheral sensation to locomotion. Therefore, this section starts with reviewing studies utilizing various methods to depress the transmission of sensory afferents during locomotion. Furthermore, under natural conditions, the movement is an interactive process between centrally generated motor activities and afferent input from sensory receptor on body that are activated by the

movement. Spinal sensorimotor networks integrate sensory afferent information into ongoing locomotor program thus adapt the locomotor pattern and ensure coordinated locomotion to the requirements of the environment. Both cutaneous and proprioceptive sensory afferents for dynamic modulation of response to unexpected perturbation are also likely involved in the sensorimotor system for regulation of normal step cycle (Gossard & Rossignol, 1990; Gossard et al, 1994; Panek et al, 2014; Koch, 2018; Rossignol et al, 2006). Interfering the ongoing locomotor activity by stimulating certain types of sensory afferent enables us to explore the contribution of this type of sensory afferent to different aspects of ongoing locomotion. Thus, in the later section, I will discuss the function of cutaneous and proprioceptive sensory afferent on locomotion by illustrating the studies utilizing different techniques to interfere the locomotion.

2.1 Removal of all sensory afferents

To test the importance of sensory feedback during locomotion, many studies have investigated the locomotor behaviours after the removal of all sensory afferents from the hindlimbs to the spinal cord. Firstly, these studies indicated that the removal of all dorsal roots to lower spinal cord does not impair the locomotor rhythmogenesis. For example, Brown demonstrated that rhythmically alternating activities of hind limb flexor and extensor muscle, evoked by cutting off the thoracic spinal cord, continued for multiple cycles after the dorsal rhizotomy (Brown, 1911, 1912). Later, Giuliani & Smith found that after deafferentation of one hindlimb in spinal cats, rhythmic locomotion of both hindlimbs were still appearing (Giuliani & Smith, 1987). Goldberger also confirmed that partial and complete deafferentation of both hindlimbs in cats did not impair their rhythmogenic capability in locomotion (Goldberger, 1988). Similarly, the mesencephalic cat retained their basic locomotor patterns after the dorsal root transection (Grillner & Zangger, 1984). Further investigations using *in vitro* preparations have provided more compelling evidence. It has been shown that electrical stimulation of mesencephalic locomotor region (MLR) or bath application of excitatory amino acids could evoke rhythmic locomotor activities in isolated brainstem-spinal cord preparations or spinal cords of rodents (Abstract: Smith and Feldman, 1985; Smith et al., 1986; Paper: Smith and Feldman, 1987; Kudo & Yamada, 1987). These early *in vivo* and *in vitro* studies indicate that the sensory inputs are not

essential for basic locomotor rhythms and patterns, which are generated by the neural circuits in the spinal cord.

Nonetheless, without sensory feedbacks, the animals lost the ability to perform complex locomotor activities requiring precise feedback regulations. In Smith & Giuliani (1987) showed that deafferented spinal animals could not produce a balanced activities between two hind limbs. Kinematic data suggested that the loss of sensory feedbacks impaired animal's postural reflexes, accurate limb placement and even overall step cycle phase divisions (Goldberger, 1988). Grillner & Zangger (1984) showed that although the general kinematics and EMG activity pattern during locomotion were retained after transection of all dorsal roots, the degrees of joint movements were decreased, and the patterns of muscle activities became more variable and sometimes even synchronized altogether (Grillner & Zangger, 1984).

2.2 Removal of cutaneous afferents

The cutaneous sensory organs in animal's foot provide information about the distribution of the pressure to the foot, the level and rate of loading of weight-bearing, and the step progression (Rossignol et al, 2006). Similar to the studies of complete denervation of sensory afferents, some early works also illustrated that cutaneous sensory afferents were not necessary to express fundamental motor activities. Sherrington in 1910 showed that removing cutaneous input did not prevent locomotion in the intact cats, or even in spinalization preparations (Sherrington, 1910). Stein and Duysen also mentioned that the deficits caused by cutting the posterior tibial and common peroneal nerve in cats could be compensated and did not affect the gait if sufficient recovery was allowed (Duysen&Stein, 1978).

However, the removal of cutaneous sensory afferents of the hindlimbs can interfere the animals performing precise and demanding tasks. Rossignol and Bouyer found that the cats were incapable of walking on a horizontal ladder or a narrow beam after cutting cutaneous nerves bilaterally at the ankle level, even though they could walk on a treadmill. After spinalization on T13, these deafferent cats were unable to place the plantar surface

of feet on the ground but the only thing they could do was to rapidly drag their rear feet back and forth across the treadmill. Also, they could not support their body weight or lift their paws. Rossignol and Bouyer also conducted a control experiment, in which one cat received a partially neurectomy, but its deep peroneal nerve (DPc) was left intact. This cat showed an "almost indistinguishable" locomotor pattern and weight support from the cat without neurectomy. However, after a local anesthesia was applied to the area innervated by DPc, the cat became similar to those completely denervated ones (Bouyer&Rossignol, 1998). Later, they re-examined the locomotor behaviours of intact cat after denervation in more details and they also evaluated the performance of these cats in more demanding locomotor tasks, such as walking on an incline and walkway embedded with force platforms (Bouyer & Rossignol, 2003a). In this study, they found that the cat's hindlimb kinematics during walking was also affected by cutaneous denervation. Denervated cats tended to extend their hindlimb further backwards and lifted their paws higher during the swing phase. When these cats walked on an inclined surface, which requires more control of the force amplitude and direction applied against the ground, these cates displayed worse deficiencies than walking on a flat surface after denervation. These results suggest that the cutaneous sensory afferents from the paw pads provide signals for the animal to assess the load on their limbs and regulate their movement on up-leaning slopes. (Bouyer & Rossignol, 2003a; Rossignol et al., 2006).

2.3 Removal of proprioceptive sensory input

Another crucial sensory feedback at spinal cord level is proprioceptive sensory feedback from muscle spindles and GTOs. These sensory afferents play more important roles in locomotion than cutaneous afferents (Duysens & Forner-Cordero, 2019; Grillner & El Manira, 2020; Pearson, 2004; Prochazka et al., 2017; Proske & Gandevia, 2012; Rossignol et al., 2006; Windhorst, 2007). The muscle afferent feedback system constantly regulates the timing and amplitude of muscle activities during various locomotor phases. Furthermore, muscle afferent feedbacks are to set the overall timing of the step cycle by adjusting the transitions and durations of the locomotor phases.

Due to the experimental limitations, it has been almost impossible to selectively eliminate proprioceptive afferent without interfering with other sensory afferents in cats. In contrast, genetic manipulation in mice and viral tools used in mice have provided possibilities to separate from muscle spindle or GTO afferents from other sensory inputs (Akay et al., 2014; Mayer et al., 2018; Mayer & Akay, 2018; Santuz et al., 2019; Takeoka & Arber, 2019; Tourtellotte & Milbrandt, 1998).

Proprioceptive sensory neurons in the dorsal root ganglia (DRG) express the calcium binding protein Parvalbumin (PV), based on which researchers generated useful genetic tools to target these neurons (Copray et al., 1994; Honda, 1995; Patel et al., 2003; Hippenmeyer et al., 2005). Using intercrossing PV^{cre} and $Advillin^{DTR}$ mouse line, Takeoka & Arber (2019) were able to selectively ablate proprioceptive sensory neurons in DRG along the whole spinal cord or in either cervical or lumbar segments during adulthood. They found that removal of proprioceptive inputs from the whole animal impaired the 'gait timing, limb movement trajectory, and intra- and interlimb coordination. Local ablation of proprioceptive inputs, however, only limited animal's ability to adapt to high locomotor speeds and 'disintegration' of interlimb coordination occurred only at their speed limit on treadmill. Those mice showed synchronized fore- and hindlimb stepping (Takeoka & Arber, 2019). Such impaired interlimb coordination did not exhibit in mice with removal of proprioceptive inputs from the whole body. (Takeoka & Arber, 2019). This discrepancy was likely due to the misbalancing proprioceptive sensory signaling between fore- and hindlimb sensorimotor circuit.

Akay et al. used another mouse line to selectively ablate the proprioceptive afferent during embryonic development stage via targeted expression of diphtheria toxin A chain in PV^{cre}; *Isl2 :: DTA* mutant mice (Akay et al., 2014). Wild-type (WT) mice always exhibited delayed or sequential activation of knee and ankle flexors with respect to hip flexors during walking and swimming, respectively. However, those mutant mice showed synchronized onset and offset phasing of flexor activities during treadmill walking and swimming (Akay et al., 2014). When only the afferents from muscle spindles were deleted while afferents from GTOs retained, as what happened in the Egr3 knock-out mice (Tourtellotte & Milbrandt, 1998), the animals only exhibited synchronous activities among flexors of

different joints during swimming. However, they showed largely normal locomotor activities during walking with slightly prolonged activity in ankle flexors which in turn affected the swing-stance phase transition during treadmill walking (Akay et al., 2014). Swimming is thought to have less GTO-derived signals than walking due to bodyweight supporting by buoyancy (Dagg & Windsor, 1971; Gruner & Altman, 1980). Therefore, these data suggested that proprioceptive afferents from muscle spindles mainly attribute to the swing-stance transition, and that afferent from GTOs plays important role than those from muscle spindles on the stance-swing phase transition.

2.4 Removal of genetically identified sensory-related IN populations

Recently, developmental studies combined with various genetic and molecular tools have led to the identification of several interneuron (IN) populations involved in sensorimotor integration (Lai et al., 2016). Currently, several spinal interneuronal populations have been demonstrated to directly receive inputs from cutaneous afferents and to regulate motor behaviors in a task-selective manner. These include INs expressing retinoid-related orphan receptor alpha (RORα) nuclear orphan receptor and RORβ orphan nuclear receptor, Satb2, and Isl1 (Abraira et al., 2017; Betley et al., 2009; Bui et al., 2013; Bui & Stifani et al., 2016; Fink et al., 2014; Haring et al., 2018; Hilde et al., 2016; Koch et al., 2017; Levine et al., 2014; Wildner et al., 2013).

A group of spinal inhibitory GABAergic INs in the dorsal spinal cord, expressing GAD2 (GAD65), one of two GABA-synthetic enzymes, form presynaptic contact onto primary afferent terminals that synapse with MNs and INs (Betley et al., 2009; Fink et al., 2014; Glasgow et al., 2005; Lai et al., 2016; Wildner et al., 2013; Windhorst, 2007). Selective genetic ablation of GAD2-expressing GABAergic INs in the cervical dorsal horn impaired smooth reaching movement and elicited forelimb scratching (Fink et al., 2014). The first phenotype indicates the crucial role of presynaptic inhibition in proprioceptive sensory filtering during the ongoing movement. The instantaneous scratching phenotype may be a secondary effect due to the loss of cutaneous sensory gating, since this phenotype was disappeared while reaching defects remained after blocking cutaneous sensory endings

inputs to forelimbs with lidocaine (Fink et al., 2014; Koch, 2019). Therefore, there might be different subpopulations of GAD2-expressing INs that contribute to this phenotype.

Del Barrio et al. (2013) identified several distinct subpopulations in the dorsal horn region related to mechanical sensory inputs. Among them, one group of INs expresses RORβ in and comprises of both excitatory and inhibitory neurons (Del Barrio et al., 2013). Koch et al. (2017) further identified an inhibitory subpopulation of RORβ expressing GABA transporter GAD2 in laminae V-VI (Koch et al., 2017). They also found that these RORβ/GAD2 INs received inputs from both low-threshold cutaneous and proprioceptive myelinated afferents from hindlimbs and form presynaptic inhibition, predominantly, onto hip flexor afferents (Koch et al., 2017). Inactivating RORβ in $Pax2^{+}$ inhibitory INs (*Pax2-RORβ* mutant mice) led to a loss of sensory afferent filtering function during swing phase and resulted in a 'duck gait', a hyperflexion phenotype, during walking (Koch et al., 2017). In the spinal cord of the *Pax2-RORβ* mutant mice, the threshold of sensory afferent-evoked reflexes and reduced primary afferent depolarization (PAD) amplitude were decreased (Koch et al., 2017). Therefore, the function of this population is to gate sensory afferent transmission and regulate the flexor reflex activity during locomotion thus ensure the smooth movement.

Another genetically identified sensory-related neuron population in the dorsal spinal cord was defined by their expression of RORα (Bourane et al., 2015; Del Barrio et al., 2013). This population, comprised of 86.1 % of excitatory and 1.2% of inhibitory neurons, was mainly restricted in laminae II/III and received afferent inputs from innocuous mechanosensory neurons (Bourane et al., 2015). Ablation of RORα INs impaired dynamic and static light touch without deficient in pain, thermosensation or itch. Bourane et al. also illustrated that RORα INs formed synapses onto MNs and some last-order INs, including V0c cholinergic neurons and V2a INs. Nonetheless, ablation of RORα INs did not cause any effect on locomotion but resulted in impaired corrective movements, increased hindlimb missteps and slips during raised beam test (Bourane et al., 2015). These data suggest that RORα INs mediate cutaneous feedback to the motor system for the precision of fine motor control.

Satb2 expressing INs are another population that has been shown to mediate cutaneous sensory inputs in locomotor circuits (Levine et al., 2014; Hilde et al., 2016). Sab2 INs directly receive inputs from motor cortex and sensory pathways and form monosynaptic connection with MNs (Levine et al., 2014). Satb2 INs were thought to integrate the sensory and supraspinal information to encode the circuit for motor synergies (Levine et al., 2014). A subset of Satb2 INs express GAD2 and are predominantly inhibitory (Hilde et al., 2016). Conditional deletion of Satb2 gene from spinal cord resulted in hyperflexion of the ankle joint during swing phase, and prolonged hyperflexion in response to noxious stimulation (Hilde et al., 2016). The former phenotype was thought to be mediated by the medial subpopulation of Satb2 INs which receive proprioceptive and cutaneous afferent inputs (Koch, 2019; Hilde et al., 2016).

Glutamatergic dI3 INs, defined by expression of transcription factor *Isl1*, directly project to MNs and are involved in low-threshold disynaptic reflex pathways (Bui et al., 2013). Deletion of spinal glutamatergic dI3 INs resulted in higher number of hindlimb missteps in horizontal ladder task and incapable of regulating grip strength (Bui et al., 2013). dI3 INs were also found to be integrated with walking related spinal cord circuits (Bui & Stifani et al., 2016). Elimination of dI3 INs did not impair fundamental rhythmic locomotion but contributed to some subtle changes of hindlimb movement, such as wider space between two hindlimbs, more frequent three or four feet on the ground and shorter swing phase (Bui & Stifani et al., 2016).

2.5 The functional roles of cutaneous and proprioceptive sensory afferents during locomotion

2.5.1 Cutaneous sensory afferents: stumbling corrective reaction

During locomotion, the cutaneous sensory inputs participate in correcting the leg movement in the case of uneven terrain or in response to obstacle, called stumbling corrective reaction (Forssberg, 1979; Quevedo et al., 2005; McVea & Pearson, 2007). When animals hit an obstacle during terrestrial locomotion, the cutaneous afferent signal from paw evokes a short-latency activation of the flexor muscles in knee and ankle which

in turn induce an additional flexion of the limb clearing the obstacle (Forssberg, 1979; Mayer & Akay, 2018). The stumbling correction reaction is a sophisticated and refined reflex mechanism and is phase (stance/swing)-, task (forward/backward walking)- and site (ventral/dorsal of the foot)- dependent.

When the mechanical stimulation was applied to a lifted limb during the swing phase, a situation similar to its hitting an obstacle, it could evoke a robust response of the affected limb, starting with a prominent knee flexion to rapidly withdraw the foot, followed by a flexion of the ankle and the hip to step over the obstacle and place the foot in front of it (Duysens and Pearson, 1976; Forssberg et al., 1975, 1977; Mayer & Akay, 2018). Such sequential reaction is important because if the ankle and hip responded at the same time with the knee, the foot would have just moved too close to the obstacle. Local anaesthesia on the dorsum of the foot abolished this reaction, which proved that it was the cutaneous sensory afferent evoked this response (Forssberg et al., 1975, 1977; Buford&Smith, 1993). When the mechanical stimulation was applied on the dorsum of the foot during stance phase, an increased extensor muscle activity was observed, but limb extension movement was not affected. The phenotype that extension movement in the limb did not change even though extensor muscle activities increased indicates that the actual limb movements appear less obvious during the weight-supporting phase than the effect caused by perturbations during swing.

Researchers also implanted cuff-electrodes on the various cutaneous nerve to mimic the situation of hitting obstacle (Duysens and Pearson, 1976; Mayer & Akay, 2018). This technique has been proved to evoke similar muscle activities as hitting the obstacle and to provide more precise stimulus timing that allows researchers to observe the activities in different periods of step cycle (Duysens and Pearson, 1976; Mayer & Akay, 2018). When the stimulation was applied during the swing phase, its effects varied depending on the precise swing phase period it was applied. The stimulus applied at the beginning of the swing phase caused the prolongation of the step cycle affecting the more extended ipsilateral flexor activity but not the extensor activity. When the stimulus was applied in the middle of the flexor phase, the step cycle became shorter. The stimulus train, starting at the end of the flexor phase and extending to the beginning of the extensor phase,

triggered a prolongation of flexor activity while at the same time reducing the extensor activity. This shorter extensor activity caused a shorter step cycle (Duysens and Pearson, 1976; Mayer & Akay, 2018). When the weak stimulus fell within the stance phase of the ipsilateral hindlimb, they observed that ipsilateral extensor activity increased both in amplitude and duration. Also, the subsequent ipsilateral flexor activity onset and contralateral extensor activities were delayed (Duysens and Pearson, 1976; Mayer & Akay, 2018).

Taken together, these studies showed that same muscle responds to the perturbations, cutaneous stimulations, in the opposite manner. The response could be either activated or not, during either swing or stance. Such phenomenon shows an example of a “reflex reversal”, which means that identical stimuli cause opposite effects based on the context of the stimulation. (Forssberg et al., 1975; Pearson & Collins, 1993; Mayer & Akay, 2018). This also reflects the complexity and preciseness of stumbling correction reflex pathways that are essential for an animal to avoid obstacles under different circumstances.

2.5.2 Proprioceptive sensory afferent initiate and halt the locomotion rhythm

Proprioceptive sensory feedback plays a significant role in detecting joint position. Afferents signalling muscle stretch at various joints are key components for the determination of limb position. The role of muscle afferent feedbacks across different joints have been studied in a various manner. Back in the 1900s, Sherrington had suggested that hip proprioceptors are prerequisite to the initiation of "reflex-stepping" (Sherrington, 1910). Similarly, Rossignol and Grillner found that in the chronic spinal cat, new rhythmic locomotion could be elicited when the hip joint, gradually extended by the researcher, surpassed a certain extension point (Rossignol & Grillner, 1978). Direct evidence that shows the hip position is critical for locomotion was from Rossignol and Pearson's study in 1991 (Pearson & Rossignol, 1991). When they gradually increased the hip angle of the chronic spinal cat during drug-evoked fictive locomotion, the rhythmic activity was started and became increasingly vigorous until the limit of the hip extension was reached (Pearson & Rossignol, 1991). This finding strongly indicates that afferents activated during hip extension produces an excitatory influence on the central system generating rhythmic

locomotion. Taken together, these findings suggest that the range of joint excursion, signalled by proprioceptive afferents mainly from muscle spindles, determines the on-off switch pattern of locomotion.

2.5.3 Proprioceptive sensory afferent entrain the locomotion

Muscle afferents can play crucial roles in setting locomotion frequency. The proprioceptive sensory system controls phase transitions by prolonging or ceasing the on-going phase, thus adjust the frequency of stepping. There have been many experiments specifically designed to evaluate how proprioceptive afferents can entrain locomotion. The results of these studies have made the convincing conclusion that proprioceptive input from muscles and joints are major contributors to the entrainment of locomotion.

In the 1980s, Andersson and Grillner found that curarizing the spinalized cat allowed the central pattern generator in the spinal cord still functioning, without ever producing any movement. This method permitted them to apply a passive movement of the hip joint while observing the influence from proprioceptive afferents of the hip joint on the drug evoked fictive locomotion (Andersson et al., 1978; Andersson &Grillner, 1981; Andersson & Grillner, 1983). Then they denervated the muscles controlling knee and lower limb and record from the nerves that innervate those muscles so that there was no proprioceptive afferent of those muscles sending back to spinal cord. Firstly, they found that the efferent burst activity could follow the superimposed movements of the hip joint over a vast range of frequencies (Andersson et al., 1978). Secondly, they found that the frequency of muscle bursting they recorded from TA and St changed with the frequency and flexion level of the manually moving hip joint (Andersson et al., 1978). Furthermore, the extension of the hip joint generally blocked the flexor activity (Andersson et al., 1978). In summary, hip extension and flexion levels, signals of muscle length, play a principal role in the entrainment of locomotor rhythm.

Group Ib afferents are also a significant component in the entrainment of rhythm. Sinusoidal stretches of the gastrocnemius-soleus at a frequency around spontaneous rhythm frequency could produce locomotor rhythm entrainment only when peak tensions approached three times the resting tension (Conway et al., 1987). At these tensions, group

Ib afferent are considered as the main contribution to the overall afferent discharge. Further evidence for group Ib afferents as major contributors to locomotor rhythm entrainment is from Pearson's team. They showed that when the tension was 15N, there was perfect entrainment, but not when the tension was 8N (Pearson et al., 1992). Also, they found that at 1.2 × threshold stimulation, at which a much higher percentage of Ia relative to Ib afferents are activated, there was a loss or weakening of the entrainment previous observed (Pearson et al., 1992).

2.5.4 Proprioceptive sensory afferent reset the locomotion

Resetting is different from entrainment. A reset is when the regular locomotor rhythm is interrupted and "restarted" in a coordinated fashion for all flexor and extensor muscles on the left and right sides. Typically, the rhythm will be reset by a prolongation or shortening of a stimulated cycle, after which the regular rhythm is resumed with step cycles of the original duration. Therefore, the resetting is likely to be thought as a situation when an animal encounters an unexpectedly short time-stretch or load followed by a resumed locomotion of the original frequency.

Hip joint movement not only can entrain the locomotor rhythm but can also reset it. After the studies mentioned above, Grillner and Andersson continued to systematically investigate the influence of proprioceptive afferents from hip during fictive locomotion by using a ramp stretch of the hip in various phases of the step cycle (Andersson & Grillner, 1981). They found that hip flexion imposed during the flexor burst prolonged and enhanced the ongoing activity, whereas flexion in the opposite period of extensor activity had a negative-feedback effect. This effect was also proved by another study done by Kriellaars et al. (Kriellaars et al., 1994). Electrical stimulus at a strength of 1.6 × threshold and higher, which thought to activate group Ia and Ib afferent, of hip flexor nerve could reset the rhythm in locomoting decerebrate cats (Lam & Pearson, 2002; McCrea et al., 2000; Perreault et al., 1995).

Other resetting evidence is from the stimulation of GTOs of extensors. Conway et al. first illustrated this idea in 1987 (Conway et al., 1987). They delivered a short train of electrical stimulus to the ankle or knee extensor muscle nerves recruiting group Ib afferents during

the flexion phase on the spinal cat during drug-evoked fictive locomotion. This stimulation immediately terminated the on-going flexor activity and evoked a new extensor burst (Conway et al., 1987). The recording from the MNs that innervates that flexor muscle showed a disfacilitation, but not a hyperpolarization since the same input at rest did not produce inhibition of the MNs (Conway et al., 1987). This stimulation also induced a reset of the locomotor rhythm when it was applied during the extension phase. When the stimulation was given during the extensor phase, the extensor burst was prolonged, and again reset the rhythm of locomotion (Conway et al., 1987).

3 Spinal cord CPG circuit for locomotion in mammals

In all vertebrates, neural circuits in the spinal cord generate the rhythmic timing and patterns to coordinate muscle activities during locomotion. This functionality can be preserved in the absence of any rhythmic inputs outside spinal cord, and this spinal neural circuitry is generally referred as central pattern generators (CPGs).

3.1 The history of discovery of locomotor CPG

The idea of CPG was proposed by Philippson in 1905. At the beginning of the 20th century, Philippson found that the suspended spinal animals often exhibited episodes of rhythmic hindlimb movement. Therefore, he suggested that there could be a spinal cord-controlled locomotion via both central and reflex mechanisms (reviewed by Clarac, 2008). By 1911, Thomas Graham Brown in his experiments compared the spontaneous rhythmic movements of hindlimbs of the spinal cats before and after deafferentation, and he found that after deafferentation, rhythmic activities of the hindlimb muscles lasted for at least another several episodes. These episodes were similar to those before the deafferent, and, importantly, there was no great difference of the movements of progression between deafferented muscles and those not deafferented. These results were the first experimental evidence of possible existence of a spinal centre that was responsible for rhythmic activity of hindlimb muscles without peripheral stimuli (Graham Brown, 1911). However, this idea was then forgotten for almost 60 years until late 60s of 20 century.

In a paper published in 1969, even though the original data were first reported in 1962 as an abstract, Engberg and Lundberg reported compelling evidence that extensor muscles became electrically active before the foot touches the ground at the onset of the E2 phase, and this activity was neither due to Ia stretch reflex nor cutaneous reflex from toe touch (Engberg & Lundberg, 1969). Engberg and Lundberg then claimed the existence of a central program, the CPG, for locomotion. More and more evidence of the spinal CPGs came after this report. For example, French researchers, Denise Viala and Pierre Buser also demonstrated the centrally controlled rhythmic locomotion in both decerebrate and spinal rabbits (Viala & Buser, 1971; reviewed by Clarac, 2008). Then, more detailed studies were done by Sten Grillner et al. They compared muscle activities in decerebrate walking cats before and after section of all dorsal nerves from one or both hindlimbs (Grillner & Zangger, 1975). They showed that the animals retained the intricate varied motor patterns of movement after the deafferentation, demonstrating the presence of a centrally generated motor output. Thus far, the spinal CPG concept had been well accepted.

Evidence of the presence of CPG centres in invertebrates also began to emerge in the 1930s after it was first shown that motor behaviour could be induced spontaneously in the isolated insect ventral cord of Dytiscus (Andrian, 1931). In 1960, Hughes and Wiersma demonstrated rhythmic swimmeret beating at a near-normal frequency (1 Hz) in the isolated crayfish abdominal cord with the complete absence of any peripheral afferent (Hughes & Wiersma, 1960). Shortly thereafter, Wilson and Wyman (1961) strengthened strong evidence of CPG activity in grasshoppers. The coordinated flight motor output pattern in this preparation could be evoked without head and wing proprioceptors (Wilson & Wyman, 1961). Following these truly seminal reports, an explosion of CPG researches undertook on a wide variety of invertebrate preparations.

3.2 Locomotor CPG network in mammals

3.2.1 Locomotor CPG circuitry and the network model

The existence and basic concept of spinal locomotor CPGs has been well accepted since late 1960s, but the organizational logic of the CPG system is still not completely well understood, despite big progresses have been made in the last 60 years.

The first conceptual model describing the CPG networks was originated from Brown in the early 20th century (Brown Graham, 1911, 1912, 1914). He proposed the 'half-centre' organization for spinal CPG network which contain two centres for coordinating flexor and extensor activity reciprocally inhibit each other (Brown Graham, 1914). He also suggest that the rhythmic alternating activities of flexor and extensor muscles were occurred when two centres were activated and then the inhibition from one centre waned and the other centre start activating the agonist muscles while inhibiting the antagonist 'half-centre' (Brown Graham, 1914). It has to been mentioned that in this model Brown assumed the recurrent motor axon collaterals were inhibitory and MNs were part of the 'half-centre' (Figure 3A).

In the 1960s, Lundberg's group conducted a series of experiments using spinalized cat intravenously injected with L-DOPA (Jankowska et al., 1967a, b). Under a resting condition, flexor reflex afferent (FRA) stimulation only evoked ipsilateral flexor MN activity. However, they found that when L-DOPA was applied to spinalized cat intravenously, FRA stimulation on both sides could suppress the ipsilateral flexor MN activity , but evoked a locomotor-like rhythmic, alternating activities in flexor and extensor α-motoneurons ipsilateral to the stimulated afferents. (Jankowska et al., 1967a). Moreover, they also suggested that these reciprocal organizations must occur at the interneuronal level. In their next paper, they further identified spinal INs that received inputs from ipsilateral or contralateral FRA and were located in the ventrolateral region of the lumbar spinal cord (Jankowska et al., 1967b). These experiments provided experimental evidence for a modified 'half-centre' architecture of the locomotor CPG in the lumbar spinal cord (Figure 3B).

Shortly after these experiments, Shik, Orlovsky, and Severin demonstrated that low strength repetitive electrical stimulation on a small region of midbrain, now known as the MLR, could evoke walking and high-speed running behaviours, such as trotting and

galloping, in response to increased stimulation strength in mesencephalic cat (Shik et al., 1966, 1969; reviewed in Shik & Orlovsky, 1976). Later on, the corresponding brainstem areas of lower vertebrates were also found to elicit locomotor behaviour (Rovainen, 1983; McClellan, 1984; Grillner et al., 1981; Grillner & Wallén, 1984). This preparation was further developed to combine with deafferentation and also INs recording. Orlovskii and Feldman recorded IN activities in lamina VII in deafferented mesencephalic cats during locomotion (Orlovskii & Feldman, 1972). They not only found that the activities of some INs were strictly phase-locked with stance or swing phase but also recorded other type of INs which were bursting during both stance and swing phase, and transition phase (Orlovskii & Fel'dman, 1972). Later, Grillner and Zangger demonstrated that intricate EMG patterns in flexor and extensor muscles, not just simple alternations, were preserved after deafferentation and spinalization (Grillner & Zangger, 1975). These results inspired people to rethink the 'half-centre' theory since it implied that all flexors and extensors respectively had an identical activation pattern, which was not consistent with the observation from EMG data in both intact cats and those decerebrated cats that activities of many flexor and extensor MNs are not strictly reciprocal. Questioning of the 'half-centre' hypothesis resulted in the development of the 'unit burst generator' hypothesis (suggested by Orlovskii & Feldman, 1972, then proposed by Grillner, 1975, 1981). They described multiple modules, called 'unit burst generators', for flexors and extensors that reciprocally inhibit each other around each joint. They further proposed that these individual 'units' were interconnected to each other but could also be individually regulated by supraspinal inputs to generate different types of locomotor behaviours (Grillner, 1981) (Figure 3C).

The brainstem-spinal cord preparation was then extended to rodents, since the size of a rodent spinal cord could be suitable to a small recording chamber. Smith et al., first demonstrated that isolated neonatal (postnatal 0-4 days) rat brainstem-spinal cord preparations were able to generate rhythmic patterns resembling locomotor activities by either chemical, electrical stimulation of the MLR or dorsal roots (Abstract: Smith and Feldman, 1985; Smith et al., 1986; Paper: Smith and Feldman, 1987). Then, Kudo and Yamada showed that bath application of excitatory amino acid, N-methyl-D, L-aspartate (NMDA), also could induce locomotor-like activity in isolated neonatal rat spinal cords

with hindlimbs attached. They found that this activity was dose-dependent; with higher NMDA doses the fictive locomotor frequency increased (Kudo & Yamada, 1987). After this revelation, a series of studies were conducted to show that the spinal fictive locomotion could be evoked by a variety of neurotransmitter agonists including dopamine (Kjaerulff and Kiehn, 1996; Smith et al., 1988), noradrenaline (Kiehn et al., 1999; Sqalli-Houssaini and Cazalets, 2000), acetylcholine (Cowley and Schmidt, 1994a,b; Kiehn et al., 1996) and specific peptides (Barthe and Clarac, 1997; Smith et al., 1988).

Further studies were focused on understanding the organization of the locomotor CPG. First, studies from three groups demonstrated that the CPG circuits controlling hindlimb movement were distributed along the caudal thoracic and lumbar spinal cord in neonatal rats, but with a rostral-caudal gradient of rhythmogenicity (Cazalets et al., 1995; Kjaerulff & Kiehn, 1996; Cowley & Schmidt, 1997). It was indicated that rostral lumbar segments were more capable of generating rhythms, particularly the fast and regular rhythmic activities than caudal segments (Cazalets et al., 1995, 1996; Kjaerulff & Kiehn, 1996; Cowley & Schmidt, 1997). Furthermore, these studies also showed that locomotor rhythmogenesis was primarily reliant on ipsilateral glutamatergic neurons (Bracci et al., 1996; Kjaerulff and Kiehn, 1997), whereas the alternating patterns of flexor-extensor and left-right activities were secured by GABAergic and glycinergic pathways (Cowley & Schmit, 1995; Bracci et al., 1996; Kjaerulff and Kiehn, 1996, 1997). Recent studies showed that optogenetic activation or inhibition of excitatory neurons could initiate or block fictive locomotion, respectively, in mouse-spinal cords, which further confirmed that spinal excitatory neurons are both sufficient and necessary for rhythm generation in the mammalian spinal cord (Hägglund et al., 2010, 2013). Hägglund et al also showed that, with regionally constrained optogenetic stimulation of excitatory INs, the rhythmic motor output could be limited to restricted flexor-related or extensor-related MNs, which further confirmed the ‘unit burst generator’ theory (Hägglund et al., 2013). By far, the architecture of ‘half centre’ could be extended to that rhythm generator (RG) activates commissural inhibitory INs, which mutually inhibit its ipsilateral antagonist RG and its contralateral counterpart, and there are many such units along the lumbar spinal cord that control different joints. Therefore, the term, ‘half-centre’ referred later in this thesis, was already

not as the same as proposed by Brown Graham. The ‘half-centre’ of Brown emphasized the hard-wire interconnection between flexor and extensor ‘half-centre’ and that the rhythm was produced by tonic activation of and mutual inhibition between the two centres. According to the studies provided above that the rhythmogenicity of individual flexor or extensor RG had been confirmed, the definition of ‘half-centre’ is used to describe the IN populations that are either control flexor or extensor activities and have reciprocal inhibitory connection between them (Brownstone & Wilson, 2007).

However, this architecture still hardly explains several experimental observations. Firstly, while a ‘half-centre’ organization can produce the alternating activity with one flexor and one extensor activity per step cycle, it is hard to generate multiple bursts within one-step cycle, which were shown in some bifunctional muscles, like ST (Perret & Cabelguen, 1980; Perret et al., 1988). Similarly, the flexor digitorum longus (FDL) muscle activity during locomotion also provided several pieces of evidence. Usual FDL was generally activated with a brief bursting during the transition from late stance to early swing (O’Donovan et al., 1982; Loeb, 1993); however, several groups showed some ‘odd’ activities of FDL. Sometimes. FDL could exhibit varied multiple activities during the stance phase under different conditions, for example, during either a ‘natural’ fictive locomotion state (O’Donovan et al., 1982; Burke et al., 2001) or the time when the steady excitation background was changed by varying MLR stimulation strengthes (Fleshman et al., 1984; Moschovakis et al., 1991; Degtyarenko et al., 1998). These ‘odd’ FDL activities could be generated by a circuit outside the RG but was activated by it. Thus, such a pattern formation circuit, which receives signals from RG circuits and directly regulates MN activities, would be required in the CPG model (Burke et al., 2001).

Secondly, the ‘half-centre’ and ‘unit burst generator’ theories failed to explain some observations of sensory influences over the locomotor CPGs. For example, if there were direct connections between RGs and MNs, the cycle timing of oscillation would not be able to be regulated independently of MNs amplitude and vice versa when it was required. The detailed information of sensorimotor interaction has been discussed in Chapter II. Here, I will only provide a few examples. One of the best understood examples is the stumbling corrective reaction. Several groups have observed that mechanical or electrical stimulation

to the dorsum of the foot, which mimics the real circumstance of the foot hitting an obstacle, evokes different muscle activities in a phase-dependent manner. That is, when the stimulation is applied during the swing phase, an additional flexion will be observed, while the same stimulation, during later stance phase, markedly enhanced extensor muscle activities, or, during the early stance phase, not change step cycle prominently, meanwhile shorten the extension duration (Forssberg et al., 1975, 1977; Forssberg, 1979). This phenomenon means that the circuit for step cycle timing and MN activity can be independently regulated during locomotion, and there is at least one more circuit that is likely involved.

Additional argument comes from investigations of the regulation of group I sensory afferents on locomotion. Stimulation of ankle extensor muscle nerves of a decerebrated cat during MLR-evoked locomotion could increase and prolong the ongoing extensor muscle activity differently in three joints without changing the step cycle period (Guertin et al., 1995). Thus, this work suggests that joint-specific CPGs can be regulated independently from one of the others.

Finally, the most problematic issue for the 'half-centre' theory is the 'non-resetting deletion'. The 'deletion' is the spontaneous disappearance of one MN pool activity during an on-going locomotion when other MN pools are still in rhythmic or tonic firing. 'Non-resetting' means the activity from that disappeared MN pool resumes at an integer number of locomotor cycles later without any change of the locomotion rhythm (Lafreniere-Roula & McCrea, 2005). The remaining types of deletions reset the phase of the next cycle, presumably through resetting the rhythm generating populations. Non-resetting deletions were first observed in a cat study by Duysens (Duysens, 1977), mentioned by Grillner and Zangger (Grillner & Zangger, 1979), and extensively described in turtles during the scratch reflex (Stein, 2004). The features of spontaneous deletions of MN burst have been systematically examined in cats during fictive locomotion and scratch in adult decerebrate cats (Lafreniere-Roula & McCrea, 2005). The evidence of non-resetting deletions strongly indicates that the CPG controlling each limb contains circuits that maintain the timing or amplitude of MN activity, respectively.

Accordingly, an advanced two-level half-centre CPG architecture has been described (Lafreniere-Roula & McCrea, 2005; Rybak et al., 2006; McCrea & Rybak, 2008). In this network, the half-centre RG is still preserved, which provides the rhythm timing, as a 'clock'. A pattern formation (PF) circuit is then embedded between the RG level and the MN level. The PF circuit is controlled by the RG, receives Ia sensory afferents, and activates multiple synergist flexor and extensor MN pools, respectively. Depending on the input from the RG and the interaction within the PF circuits, each PF population is active during a particular corresponding phase(s) of the step cycle and regulates the phase-specific synchronized activation of multiple synergist MN pools. The non-resetting deletions should come from neurons at the PF level and resetting deletions should come from those at RG level (Figure 4).

The original two-level half-centre CPG architecture was based on data from one limb. The knowledge of INs connecting left and right sides provided more information about the network structure of CPG circuits. Experiments from Kiehn's lab on isolated spinal cords of neonatal rats first systematically classified and characterized commissural interneurons (CINs) involved in left-right coordination (Butt et al., 2002; Butt & Kiehn, 2003). There was followed by series of studies using isolated spinal cords of neonatal mouse (Zhong et al., 2006a, b, 2012; Wilson et al., 2003; Quinlan & Kiehn, 2007). The mouse preparation has its advantages regarding the study of locomotor networks. The study from the Whelan's group showed that the isolated neonatal mouse spinal cord, in contrast to that of the rat, is adequately perfused at all tissue depths (Wilson et al., 2003). In these studies, they characterized L2 ascending, descending and bifurcating CINs (aCINs, dCINs and adCINs) and locally projecting CINs (sCINs) were characterized (Zhong et al., 2006a, b; Quinlan & Kiehn, 2007). Furthermore, Zhong et al., (2012) recorded molecularly identified INs while monitoring flexor and extensor related ventral root activity from both sides of the spinal cord. They found an asymmetrical pattern of antagonist motor activities during flexor and extensor non-resetting deletions where these non-resetting deletions were independent of contralateral motor activity.

Thereafter, Rybak and colleagues revised their previous two-level half-centre CPG model with new findings from those rodent studies and the Duysens-Pearson concept of an

asymmetric rhythm generator with a dominant flexor half-canter (Duysens & Pearson, 1976; Zhong et al., 2012). In the new model, the flexor RG neurons have strong intrinsic rhythmogenicity with abundant persistent sodium currents and mutual excitatory synaptic interactions among themselves, while extensor RG only show tonic firing. The activity of extensor RG still contributes to the extensor phase duration, but the transition timing to the next flexion phase is controlled by inhibitory INs, RG-E, driven by flexor RG neurons. The extensor PF population receives excitatory inputs from RE and fire rhythmically due to inhibition from flexor PF and rhythmic firing of RE caused by the network effect. Furthermore, in the new model, the CINs mediate left-right interactions only at RG level. The rhythmic activity of RG INs during fictive locomotion is not perturbed during non-resetting deletions (Zhong et al., 2012). They added three types of CINs, and type I and type II V2a INs (Cowley & Schmidt, 1995; Butt et al. 2002, 2003; Zhong et al. 2006a, b; Quinlan & Kiehn, 2007). This model simulated the experimental resetting and non-resetting deletion results and predicted the potential mechanism for them (Zhong et al., 2012; Harris-Warrick, 2014). (Figure 5)

3.2.2 Molecular identification of locomotor-related INs

Although the early studies using electrophysiological, pharmacological, and modelling approaches had provided a general structure of spinal CPG circuits, there were very limited knowledge about the identities of these neurons. Started in late 20th century, intensive studies were conducted to understand the development of spinal neurons during early embryonic stages. It was found that neuronal identity in the spinal cord was primarily determined by the dual activities of two morphogens that imparted dorsoventral positional information to dividing neural progenitors in the ventricular zone (Lee & Jessell, 1999; Jessell, 2000; Goulding & Lamar, 2000). The notochord and floor plate produce Sonic hedgehog (Shh), while the epidermis overlying the neural tube and roof plate secrete Bone Morphogenetic Proteins (BMPs). They distributed in gradients along the dorsal / ventral axis. The opposing activities of Shh and BMPs restrict the expression of patterning factors to spatially restricted subsets of ventricular zone progenitors, which in turn results in the ventricular zone being subdivided into discrete dorsoventral progenitor domains that generate different generic classes of embryonic neurons. Mainly, graded Shh signalling

activity determined the progenitor domains that generates MNs and four molecularly distinct classes of ventral INs from neural progenitor cells: V0, V1, V2 and V3 (Roelink et al., 1995; Ericson et al., 1997; Briscoe et al., 2000). In the mouse dorsal alar plate, six progenitor domains generate dI1-dI6 neurons (Lee & Jessell, 1999). These cell types express specific transcription factors (Figure 6, Alaynick et al., 2011). The four ventral populations and dI6 are considered as putative constituents of the spinal CPG circuits and play distinctive roles in locomotor control (Goulding, 2009; Arber, 2012; Kiehn, 2016; Gosgnach et al., 2017; Deska-Gauthier & Zhang, 2019).

The dI6 INs express the homeobox transcription factor Lbx1 in the progenitor stage and migrate ventrally to the ventromedial spinal cord (Gross et al., 2002; Müller et al., 2002). Since Lbx1 is also expressed in other dorsal IN populations, there is no unique molecular marker for the entire dI6 population (Gosgnach et al., 2017). Postmitotically, Lbx1-expressing cells divide into three genetically distinct subsets based on the expression of either DMRT3 or WT1 or both of them (Andersson et al., 2012). The DMRT3-expressing dI6 subpopulation has been shown to be exclusively inhibitory and project both ipsilaterally and contralaterally, forming synaptic connections to MNs (Andersson et al., 2012).

Dyck et al. applied whole-cell patch-clamp recording on dI6 INs and stated that about half of their recording cells were rhythmically active during drug-induced fictive locomotion in the isolated mouse spinal cord. They also demonstrated two subpopulations of dI6 INs based on their phase relationship with ventral root activities and their intrinsic membrane properties (Dyck et al., 2012). One subpopulation is referred to as loosely coupled (LC). The LC subpopulation showed significant firing preference to the root activity, inactivity and interburst period. Also, more than 15% of their action potentials were seen in their nonpreferred phase. These cells are suggested to be involved in rhythm generation. The other tightly coupled (TC) population has phase-locked activity to MN activity and is suggested to be part of pattern formation circuits (Dyck et al., 2012). Griener et al. then analysed the projection profiles of dI6 INs and their activity pattern during non-resetting deletions in isolated neonatal spinal cords (Griener et al., 2017). Their data further

confirmed that dI6 INs are involved in both rhythm generation and pattern formation locomotor circuits.

The Gosgnach group also studied the genetically identified subset of dI6, WT1-expressing dI6 INs. They showed that WT-1 expressing dI6 INs innervated other locomotor-related interneuronal populations and played important roles in securing left-right alternation during drug-evoked fictive locomotion in isolated spinal cords (Haque et al., 2018). The other genetically identified subset of dI6 INs is DMRT3+ INs. Andersson et al found the homozygosity for the DMRT3 nonsense mutation was required for the ability of horse to pace in Icelandic horse breed. DMRT3 mutated horses had difficulty to gallop at high speed, which is the natural high-speed gait of other breeds (Andersson et al., 2012). These horse data indicated that the DMRT3 neurons were important for both left-right and fore-hind limbs coordination.

V0 INs are characterized by their early expression of the transcription factor developing brain homeobox 1 (Dbx1) (Pierani et al., 2001). They are subdivided into multiple subpopulations, including V0d, V0v, and V0c neurons. Inhibitory V0d neurons derive from paired box protein 7 (Pax7) -positive progenitor cells. Excitatory V0v neurons derive from Pax7-negative progenitor cells and later express homeobox even-skipped homologue protein 1 (Evx1) (Pierani et al., 2001; Moran-Rivard et al., 2001; Lanuza et al., 2004). Lastly, cholinergic/glutamatergic V0C/G neurons express the paired-like homeodomain transcription factor 2 (Pitx2) (Zagoraiou et al., 2009).

V0 INs constitute a large proportion of CINs in ventral spinal cord and could form direct connections with contralateral MN pools (Lanuza et al., 2004). Genetic elimination of the whole population of V0 INs results in the loss of left-right alternation at all locomotor frequencies (Lanuza et al., 2004, Talpalar et al., 2013). The selective ablation of V0d neurons led to lethal genotypes owing to breathing impairments. Therefore, they only performed *in vitro* investigations on mutants. They found that the mutant cords lost left-right alternation only at low frequencies but remained normal alternation at high frequencies during drug-evoked fictive locomotion. On the other hand, to assess the role of excitatory V0v CINs, they selectively silenced the expression of vesicular glutamate

transporter 2 (Vglut2) in Evx1+ V0v INs. The mutant mice could survive to adulthood allowing them to *in vivo* locomotor analysis. They found that the mutant mice showed left-right alternating gait at low frequencies (2-4 Hz) and a hopping gait at high frequencies (4-10 Hz). The forelimbs stayed alternation at all frequencies (Talpalar et al., 2013). It has been introduced in section 1 that the increase in locomotor speed in rodents is accompanied by a transition from left-right alternating gaits, like walk and trot, to left-right synchronized gaits, like gallop and bound (Bellardita & Kiehn, 2015). After the ablation of V0 INs, only bound gait is reversed in mutant mice at all speeds (Bellardita & Kiehn, 2015). Ablation of V0v, however, results in the absence of trot gait at low frequencies, but walk is presented (Bellardita & Kiehn, 2015). This result indicates that the V0 population is vital for forming two distinct gaits, walk and trot, in non-overlapping frequencies of locomotion (Bellardita & Kiehn, 2015). Also, it indicates that the synchronization of left-right hindlimbs may be regulated by other IN populations (Kiehn, 2016). Although Pitx2 labels both V0C and V0G INs, only the function of V0C has been studied. V0C INs have been shown as the sole source of cholinergic inputs to spinal MNs and to regulate MN firing frequency and GS activity amplitude increase during swimming (Zagoraiou et al., 2009).

V1 INs are derived from the p1 progenitor domain, which expresses the transcription factors Pax6/Dbx2/Nkx6.2 and are defined by the postmitotic expression of engrailed 1 (En1) (Burrill et al., 1997; Saueressig et al., 1999). They are ipsilaterally projecting inhibitory neurons that can make direct connection to MNs (Sapir, 2004; Higashijima et al., 2004; Li et al., 2004). It has been shown that all Renshaw cells (RCs) and some of Ia inhibitory INs (IaINs) are subsets of V1 INs (Sapir, 2004; Alvarez et al., 2005; Benito-Gonzalez & Alvarez, 2012). Using 5'-bromodeoxyuridine birth dating, Benito-Gonzalez & Alvarez found that mouse V1 INs could be subdivided into early (E9.5-E10.5) and late (E11.5-E12.5) born groups. The RC was included in early born group and upregulated calbindin expression after postmitotic stage (Benito-Gonzalez & Alvarez, 2012). The differentiation of RCs is temporally controlled by the activation of several transcription factors, Onecut 1/2, Foxd3 and MafB (Stam et al., 2011). Later born V1-derived IaINs are calbindin-negative and express FoxP2 at the beginning of differentiation (Benito-Gonzalez & Alvarez, 2012).

Selective loss of V1 INs led to a significant reduction of the rhythm of fictive locomotion of isolated neonatal spinal cord and potentially locomotor speed of walking animals, which implies an essential role for V1 INs in generating fast locomotor output (Gosgnach et al., 2006). Furthermore, when the elimination of V1 INs was combined with silencing V2b INs, the isolated spinal cord showed a synchronized flexor-extensor activity during fictive locomotion, and neonatal mice were unable to move their limbs (Zhang et al., 2014). These data indicate the function of V1 and V2b in the coordination of flexor-extensor motor activity.

While it has been known that Renshaw cells and Ia INs are two subsets of V1 INs, they make up only a small section of the population. In 2016, utilizing a sparse Bayesian framework, fifty V1 subtypes were identified according to combinatorial expression of nineteen transcription factors (Bikoff et al., 2016; Gabitto et al., 2016). Some of these transcriptionally defined V1 subtypes exhibited distinct physiological signatures and situate in a highly restricted region within the neonatal spinal cord. Furthermore, the electrophysiological and anatomical analyses revealed variant microcircuit architectures, including V1 INs that control proximal and distal joint-related MN pool, respectively (Bikoff et al., 2016).

Mouse V2 INs are generated from the p2 progenitor domain expressing the combination of transcription factors, Nkx6.1/Irx3/Pax6 (Briscoe et al., 2000). Although both V2 INs and MNs express Lhx3 in the late progenitor stage, only MNs express Isl1, which distinguishes these two cell populations (Ericson et al., 1992, 1997; Thaler et al., 2002). There are two distinct subtypes of V2 INs: excitatory V2a INs expressing Chx10 and inhibitory (GABAergic/glycinergic) V2b INs expressing Gata2, Gata3 and Scl (Tal1) (Al-Mosawie et al., 2007; Ericson et al., 1997; Karunaratne et al., 2002; Lundfald et al., 2007; Muroyama et al., 2005; Peng et al., 2007; Smith et al., 2002; Zhou et al., 2000). Chx10+ V2a INs form ipsilateral excitatory connections with MNs and other ventral IN populations, including V0v (Lundfald et al., 2007; Crone et al., 2008). V2a INs were the first excitatory IN population that was shown to influence the left-right alternation in drug-evoked fictive locomotion and during high-speed treadmill running (Crone et al., 2008, 2009). The analysis of firing and membrane properties of V2a INs indicated that this subset was

electrophysiologically heterogeneous (Zhong et al., 2010; Dougherty & Kiehn, 2010). Furthermore, Zhong et al. (2010) observed that the number of rhythmically recruited V2a INs is increased when the fictive locomotion frequencies is higher as well as a significant amount of electrical coupling within the same class, either tonic or phasic V2a INs. Zhong et al., (2012) also found that V2a INs that are rhythmically active in phase with ipsilateral L2 ventral root during fictive locomotion could be subdivided into two types, type I and type II (Zhong et al., 2012). Type I V2a INs continued to receive rhythmic excitatory synaptic drive and oscillated regularly during deletions with no change of integrated synaptic drive. This type of V2a INs do not fire during spontaneous L2 activity during resting condition. Therefore, Zhong et al. (2012) suggested that type I V2a INs should be involved in the RG level. Type II V2a INs lost their synaptic drive and are silent during deletions, which is considered on the output paths from the PF circuit to MNs.

Sim1 expressing V3 INs derive from the most ventral Nkx2.2-expressing p3 progenitor domain (Briscoe et al., 1999; Goulding et al., 2002; Zhang et al., 2008). They are a major group of glutamatergic commissural INs in the mouse spinal cord (Zhang et al., 2008). The data from our lab has shown vast heterogeneity of V3 INs determined by their location, intrinsic membrane properties, axon projection profiles, and morphologies (Borowska et al., 2013, 2015; Blacklaws et al., 2015). The majority of ventral V3 (V3V) subpopulation form both commissural ascending and descending propriospinal axon projections, while a small part of them also exhibit ipsilateral or bifurcating projections (Chopek et al., 2018). V3 dorsal (V3D) INs displays exclusively commissural ascending projections (Blacklaws et al., 2015). V3V and V3D subpopulations were shown to be physiologically distinct at birth, but their electrophysiological properties undergo a significantly maturation process during the first three postnatal weeks (Borowska et al., 2015). Furthermore, Chopek et al. (2018) illustrate the local V3V circuit using whole-cell patch-clamp recordings in combination with holographic glutamate uncaging (Chopek et al., 2018). They found that smaller medial contralateral projecting V3V form synapses with larger lateral V3V, which in turn innervate adjacent MN networks. Ipsilateral MNs also excite both lateral and medial V3V, thus forming a positive V3-MN feedback microcircuit (Chopek et al., 2018). Genetic deletion of V3 INs did not affect left-right alternation, but caused unstable gaits in walking

mice, and generated imbalanced and less robust rhythmic fictive locomotion in isolated neonatal spinal cords (Zhang et al., 2008).

Although, these experimental data strongly suggest that V3 INs are involved in the control of locomotion, their exact function and commissural connectivity remain mainly unknown. In this thesis, I deleted the expression of Vesicular Glutamate Transporter 2 (vGluT2) in V3 INs in *Sim1*$^{Cre/+}$*;vGluT2* $^{flox/flox}$ (V3OFF) mice, and systematically examined their locomotor behaviours, including their gaits at various treadmill speeds, as well as their kinematics and muscle activities in different locomotor tasks. In chapter 2, I identified a lumbo-cervical projecting V3 propriospinal INs and found that these sub-population of V3 INs may have provided a direct excitatory drive to cervical locomotor CPGs and could be essential for the synchronization of diagonal limbs for proper trotting gaits. Chapter 3 demonstrates that spinal V3 INs may have multiple functional sub-populations that are involved in different modular circuits that regulate proximal or distal joints. In chapter 4, we combined our *in vitro* experimental and modelling results and shows that V3 CINs provide mutual excitation between the spinal neurons involved in the control of left and right extensor activity, which may promote left-right synchronization during locomotion.

4 Figures

Figure 1.1 the locomotor step cycle analysis from Philippson.

A

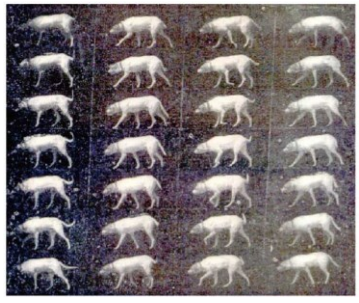

B

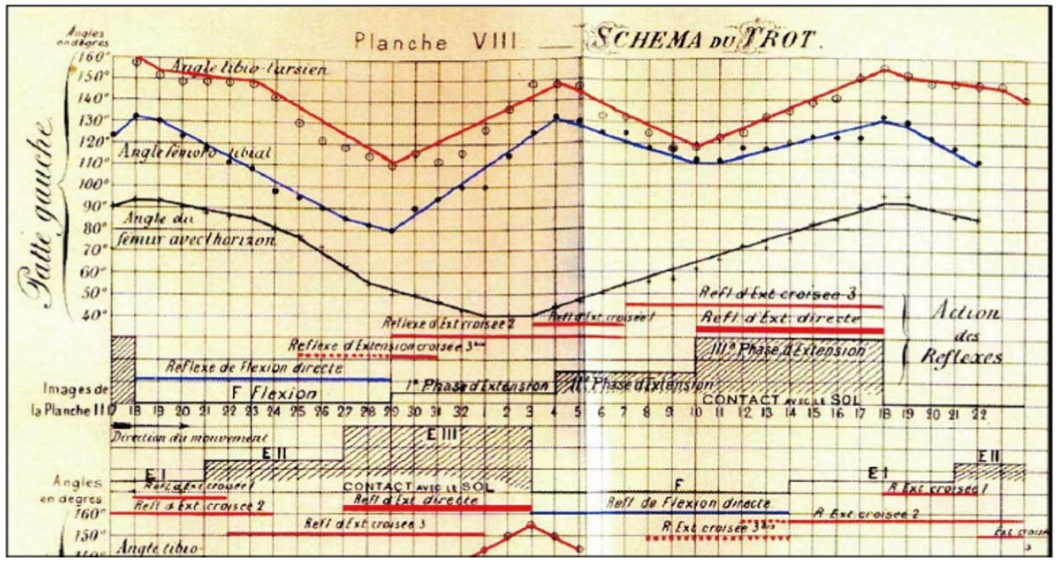

Figure 1.1 The locomotor step cycle analysis from Philippson.

(A) Photographs of dog locomotion which were given to Philippson by Marey (1905).

(B) Different phases of the step cycle, which Philippson defined as F (foot lift-off in the swing phase), E1 (foot descent in the swing phase), E2 (limb "give" in the stance phase) and E3 (limb thrust in the stance phase. Beneath these phases, Philippson drew the timings of reflexes which he believed to assist and/or bring about the successive step cycle movements (Clarac, 2009; Figure 1).

Figure 1.2 Schematic representation of rear limb muscles and pre-processed raw recordings of their activities from a cat walking on the treadmill.

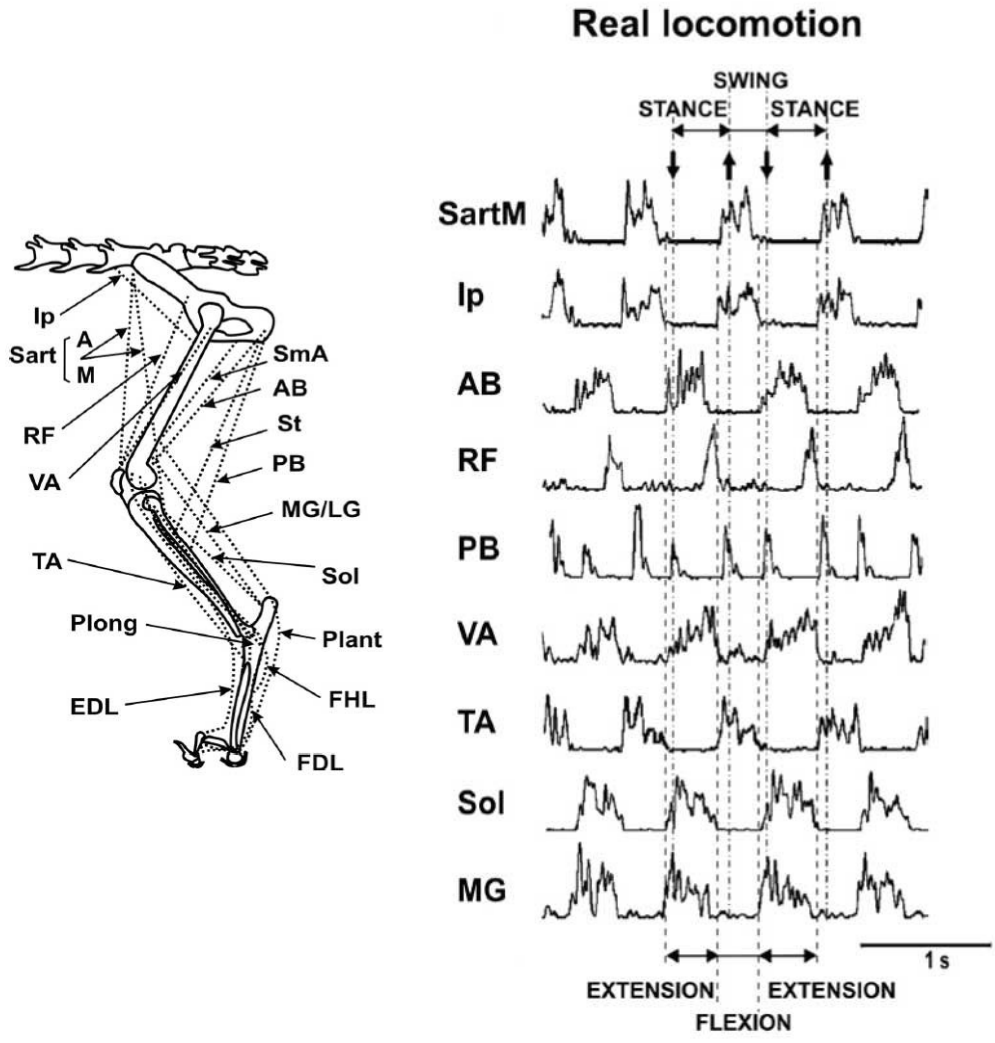

Figure 1.2 Schematic representation of rear limb muscles and pre-processed raw recordings of their activities from a cat walking on the treadmill.

Left: Muscles are represented by dashed lines. Flexors: Sart (A and M), sartorius (anterior and medial); Ip, iliopsoas; St, semitendinosus; TA, tibialis anterior; Plant, plantaris; FHL, flexor hallucis longus; Plong, peroneus longus; FDL, flexor digitorum longus. Extensors: SmA, semimembranosus anterior; AB, anterior biceps; VA, vastus; LG, lateral gastrocnemius; Sol, soleus; MG, medial gastrocnemius; EDL, extensor digitorum longus. Bifunctional muscles: PB, posterior biceps; RF, rectus femoris. (Markin et al., 2012; Figure 1)

Right: Preprocessed raw EMG recordings of muscle activities during treadmill walking. Note that flexor muscles, SartM, IP, and TA, start prior to the swing phase. Only the activities of hip flexor, IP and SartM, last through whole swing phase. Extensor muscles, AB, VA, Sol and GS are active in stance phase. RF and PB show two bursts either in stance or swing phase. (Markin et al., 2012; Figure 2B)

Figure 1.3 Scheme of different models for CPG circuitry.

A

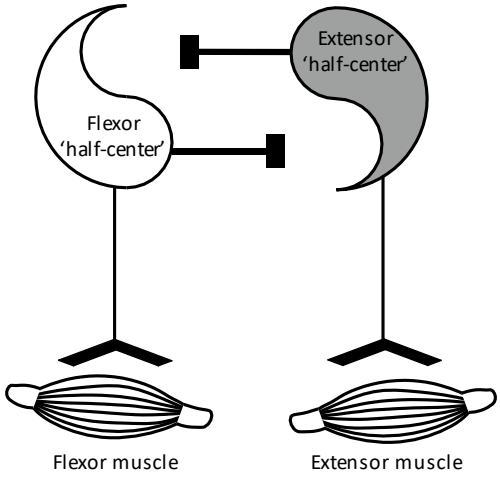

B

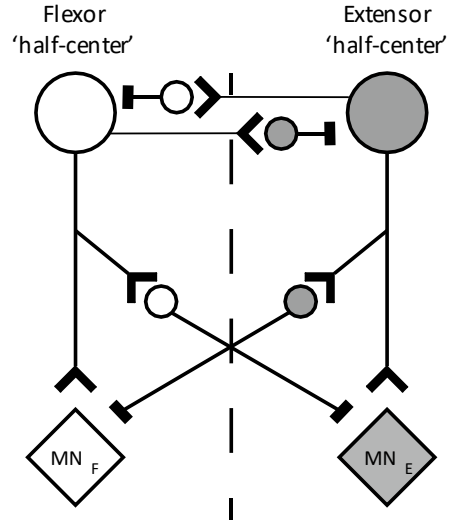

C

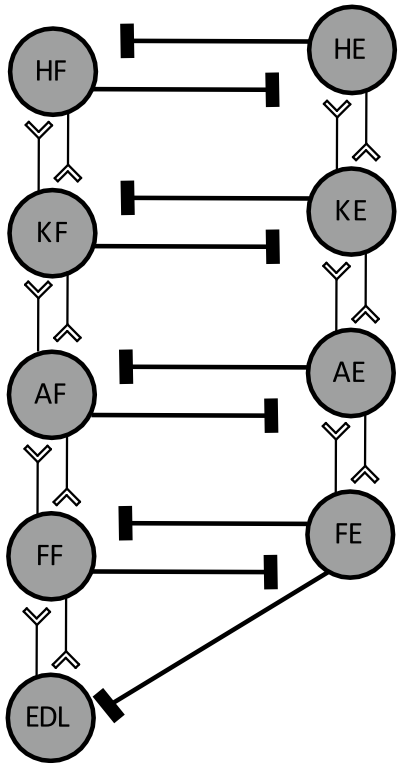

Figure 1.3 Scheme of models for CPG circuitry.

(A) Half-center theory proposed by Brown Graham. The two centers are reciprocally inhibiting each other, indicated by black solid bar. Flexor ‘half-center’ innervates flexor muscles while extensor ‘half-center’ innervate extensor muscles.

(B) Lundberg’s modified ‘half-center’ model. Small white circles represent excitatory INs and gray circles represent inhibitory INs.

(C) Unit burst generator theory proposed by Sten Grillner. H, hip; K, knee; A, ankle; F, foot; EDL, extensor digitorum longus. The black bars represent inhibitory synapse contacts and white ‘V’ shape icons represent excitatory synapse contacts.

Figure 1.4 Schematic of ‘two-level’ model.

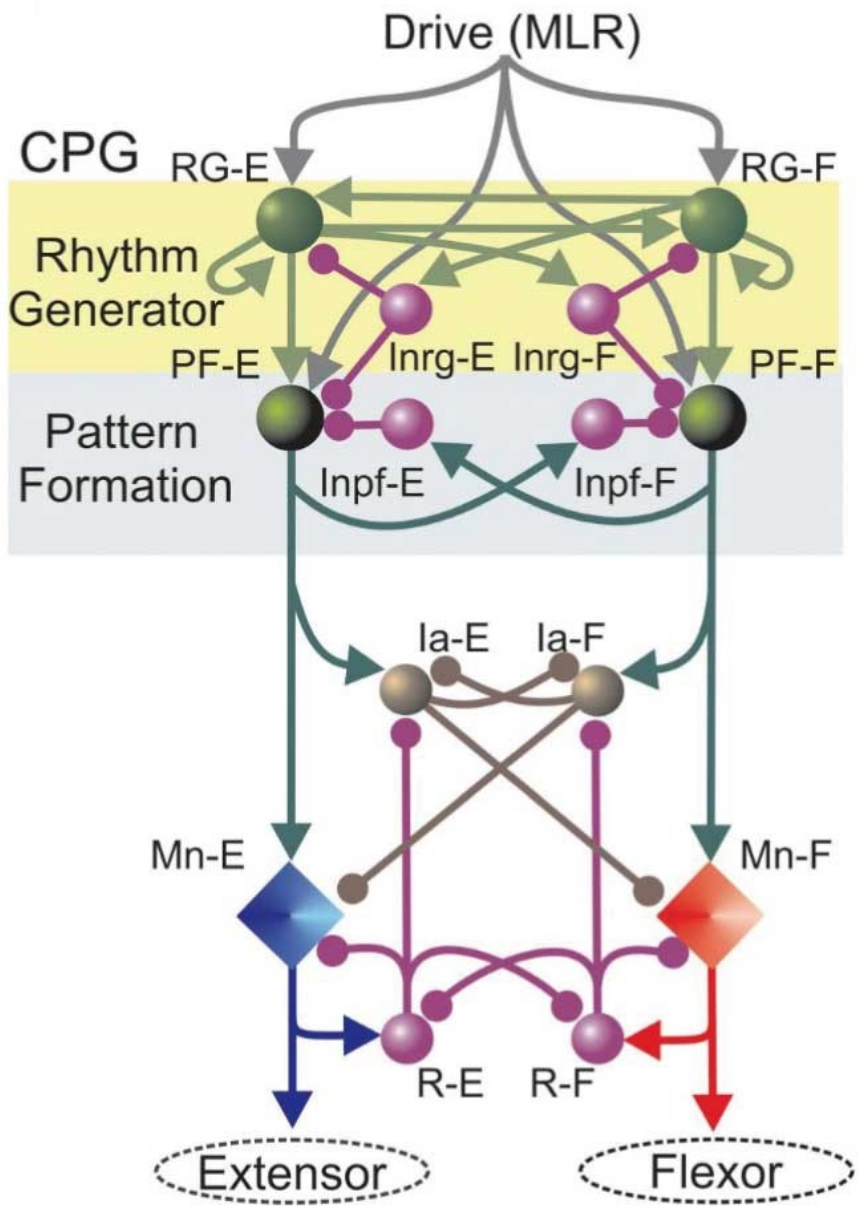

Figure 1.4 Schematic of ‘two-level’ model.

Populations of INs are represented by spheres. Excitatory and inhibitory synaptic connections are shown by arrows and small circles, respectively. Populations of motoneurons are represented by diamonds. RG, rhythm generator; PF, pattern formation; Inrg, inhibitory INs working in rhythm generation level; Inpf, inhibitory INs working in pattern formation level; Ia, Ia inhibitory INs; R, Renshaw cells; F, flexor; E, extensor; MLR represent descending drive to initiate rhythm in circuit. (Rybak et al, 2006; Figure 2A)

Figure 1.5 Schematic diagram of ‘two-level asymmetrical’ model.

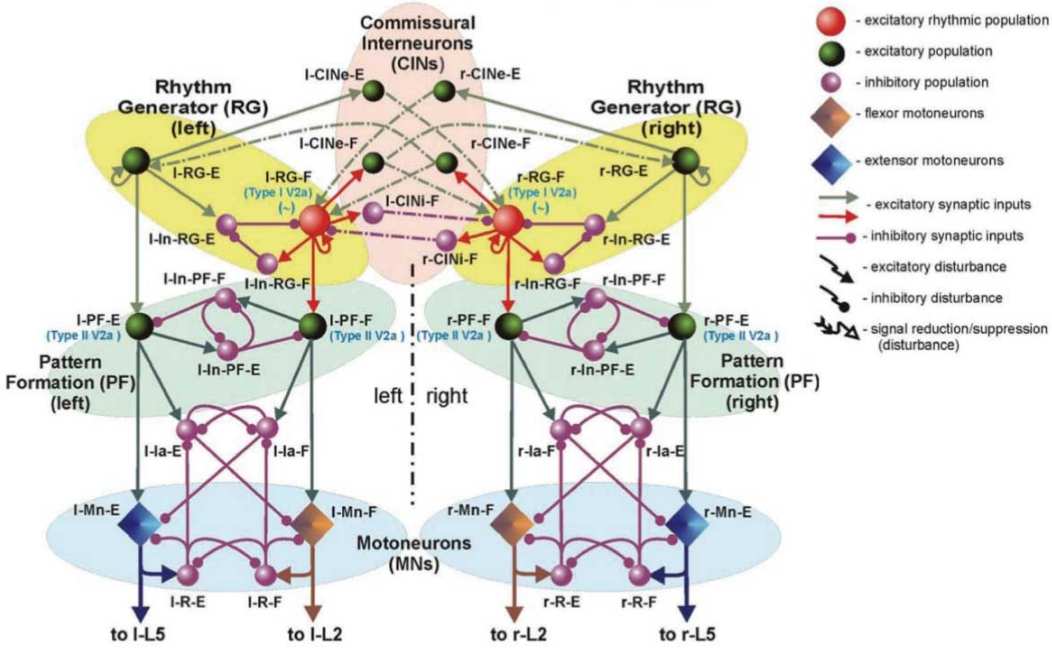

Figure 1.5 Schematic diagram of ‘two-level asymmetrical’ model.

Populations of INs are represented by spheres. Excitatory and inhibitory synaptic connections are shown by arrows and small circles, respectively. Populations of motoneurons are represented by diamonds. (Zhong et al., 2012; Figure 9)

Figure 1.6 Snapshot: spinal cord development.

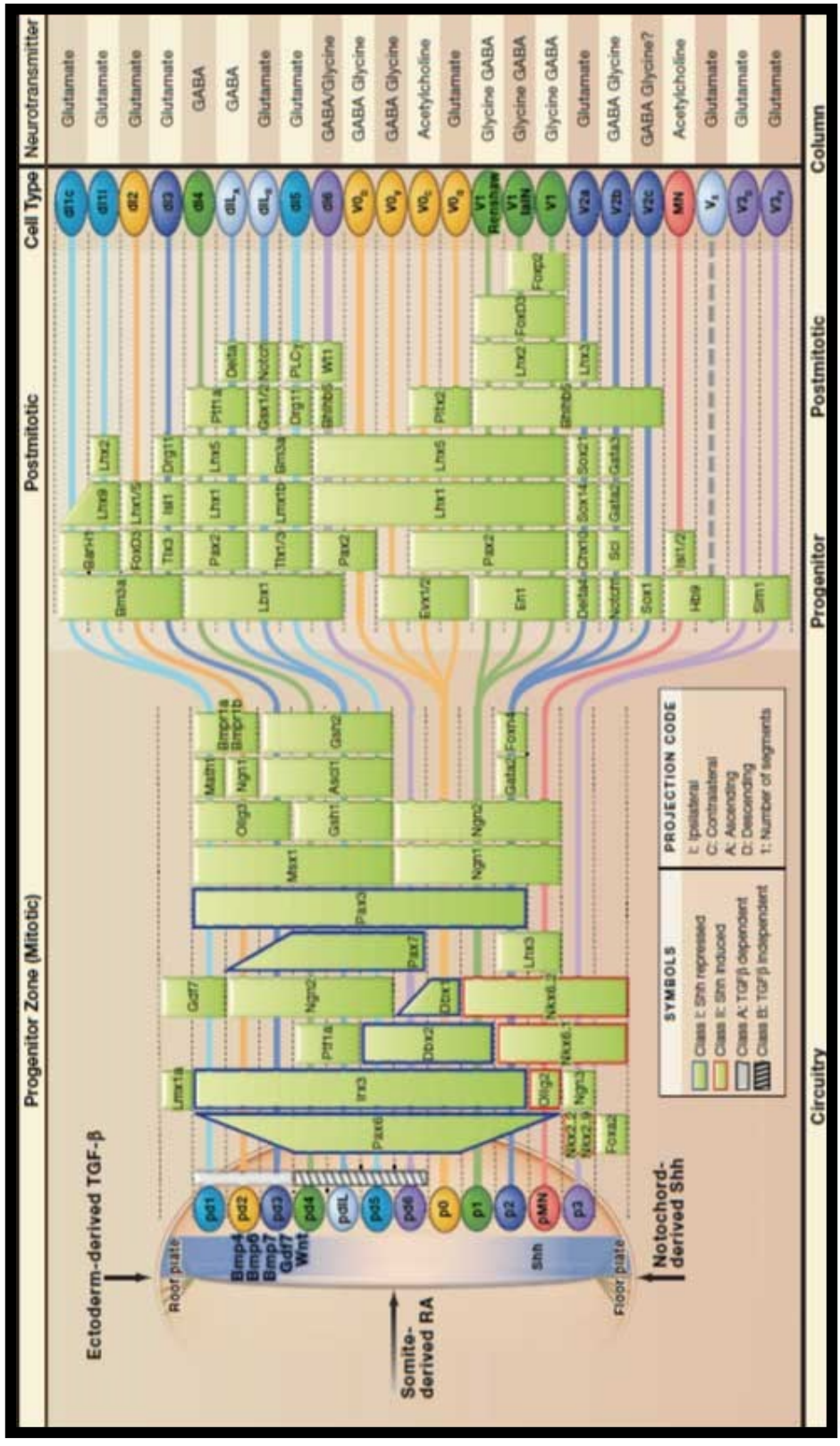

Figure 1.6 Snapshot: Spinal cord development.

This snapshot illustrates the sequential genetic steps that generate neuronal diversity within an idealized spinal segment of mouse.

CHAPTER 2. THE ROLE OF MOUSE SPINAL V3 INS IN QUADRUPEDAL INTERLIMB COORDINATION

Contribution statement

I would like to acknowledge Dylan Deska-Gauthier and Dr. Tiesong Li for the immunohistochemistry staining shown in this chapter; Dr. Christopher T. Jones for writing script of gait analysis; Mingwei Liu for developing MATLAB toolbox. I performed all behaviour experiments and statistical analysis described in this chapter. Immunohistochemistry staining of C-fos experiments was done by Dylan Deska-Gauthier and Dr. Tiesong Li. Cell counting of CTB/Sim1 cells in lumbar spinal cord was done by Dylan Deska-Gauthier. The MATLAB toolboxes for generating colour coded heating map and exporting the locomotion parameters were written by Mingwei Liu.

1 Summary

V3 INs are a major group of glutamatergic commissural neurons in the spinal cord. They directly innervate MNs as well as other ventral INs. Although it has been shown that V3 INs are crucial in forming stable and robust rhythmic locomotor activity, the mechanisms underlying their function is still unclear. In the current study, we specifically deleted the expression of Vesicular Glutamate Transporter 2 (vGluT2) in V3 INs in *Sim1*$^{Cre/+}$*; vGluT2* $^{flox/flox}$ (V3OFF) mice. We found that V3OFF mice were unable to run faster than 40 cm/s on a treadmill, a speed at which WT mice trotted constantly. At speed under 40 cm/s, V3OFF mice could not trot properly, mainly due to their inability to precisely synchronize their diagonal limbs. Using the track tracer, cholera toxin subunit B (CTB), we identified clusters of V3 INs within higher lumbar segments of the deep dorsal spinal laminae that had long ascending projections to the cervical region. Optical stimulation of V3 INs in the lumbar segments of the isolated spinal cord of the neonatal *Sim1*$^{Cre/+}$*; Ai32* mice could simultaneously evoke activities at the lumbar and cervical ventral roots. Blocking glutamatergic synapses exclusively in the lumbar region did not prevent this light-induced cervical activity, suggesting that lumbar V3 INs directly innervated cervical motor circuits. Next, we observed an increase in c-Fos expression in lumbo-cervical projecting spinal V3 INs from mice after they ran at 40cm/s on the treadmill, compared to corresponding expression from mice after walking at lower speeds. This result indicated that these long projecting V3 INs were highly active during medium-speed trotting. Taken together, we propose that lumbo-cervical projecting V3 INs provide a direct excitatory drive to cervical locomotor networks during medium locomotor speeds essential for performing robust and stable trotting gaits.

2 Introduction

Locomotion is a fundamental motor function in the animal kingdom. In quadrupeds, precise coordination of the four limbs is essential for generating smooth locomotor activities. Therefore, the relative phase relationship of the four limbs, interlimb coordination, must change to form different gaits under different conditions or speeds (Bellardita & Kiehn, 2015; Frigon, 2016; Grillner, 1981, 2006, 2019; Hildebrand, 1989; Lemieux et al.; 2016; Serradj & Jamon, 2009). It has been suggested that separate neural circuits in the spinal cord, named CPGs, generate basic rhythmic activities that control the movement of individual joint in each limb. These CPGs for each limb are connected with each other by propriospinal neurons (Ballion et al., 2001; Danner et al., 2017; Frigon, 2016; Grillner, 1975; Juvin et al. 2005, 2012; Yamaguchi, 2004; Zaporozhets et al., 2006). The propriospinal projections can be short, spinning a couple of spinal segments for CPGs within one leg, or longer reaching between cervical and lumbar segments for fore- and hindlimbs, respectively, or commissural for left-right limbs (Brockett et al., 2013; Dutton et al., 2006; Flynn et al., 2017; Ni et al., 2014; Reed et al., 2006; Ruder et al., 2016). The exact mechanisms underlying the functions and identities of these propriospinal neurons are still mostly unknown, particularly those mediating long projections between neural circuits in lumbar and cervical spinal segments to coordinate the movement of hind- and forelimbs (Miller, 1970; Miller & Van Der Meché, 1973; Juvin et al. 2005, 2012; Cowley et al., 2010; Ruder et al., 2016).

Track-tracing studies performed in rodents has shown that long descending propriospinal pathways, originating from neurons in cervical/upper thoracic segments, projected to the ipsilateral and contralateral lumbar spinal cord evenly. By comparison, more excitatory long-descending inputs were found in the contralateral than the ipsilateral lumbar segments, while long cervical inhibitory descending projections preferentially terminated ipsilaterally (Reed et al., 2006; Brockett et al., 2013; Ni et al., 2014; Flynn et al., 2017). On the other hand, long-ascending propriospinal projections originating from neurons in laminae VII and VIII lumbar segments were mainly excitatory and terminated more frequently in the contralateral than the ipsilateral cervical regions. (Dutton et al., 2006; Ruder et al., 2016).

Using isolated spinal cords from neonatal rats, Juvin et al. (2005) showed that the ascending contralateral excitatory drives from the lumbar region had more influence on CPG activity in the cervical region than descending pathways. By making midsagittal lesions on the spinal cord, several studies have shown that crossed propriospinal projections played an important role in the diagonal coordination of lumbar and cervical motor outputs (Cowley and Schmidt, 1997; Cowley et al., 2008, 2010; Juvin et al., 2012). More recently, Ruder et al. (2016) illustrated that the genetically identified Dbx-1 positive V0 INs were the major long descending projecting CINs, while V2s were the main ipsilaterally projecting INs from the cervical to lumbar region. They also showed that silencing of these cervico-lumbar long-projecting neurons resulted in a speed-dependent distortion of inter-limb coordination. However, the cellular identity of long-ascending propriospinal neurons and their functional role in speed-dependent gait expressions, *in vivo*, remain poorly understood. Based on our previous and current studies, we propose here that another population, V3 INs, as one of the long-ascending projections, may be a good candidate for coordinating fore-hind limb activities.

Sim1 expressing V3 INs derive from the most ventral Nkx2.2-expressing p3 progenitor domain (Briscoe et al., 1999; Goulding et al., 2002; Zhang et al., 2008). They are a major group of glutamatergic CINs in the mouse spinal cord (Zhang et al., 2008). Our previous studies have shown that V3 INs were heterogeneous with mixed projection profiles, including commissural ascending and descending and a small portion of ipsilateral projecting cells. Some of V3 INs showed potential to have long projections, although due to the limitation of our *in vitro* tract-tracing methods, we could not follow the axon up to the cervical region at that time. Previously, when we acutely suppressed the activity of V3 INs in the lumbar spinal cord, the mice showed unstable gaits during walking (Zhang et al., 2008). However, until now, we have not been able to characterize gait changes caused by the ablation of V3 INs and the function of V3 INs in coordinating the four limbs during locomotion.

In the current study, we employed *Sim1Cre/+; vGluT2*$^{flox/flox}$ (V3OFF) mice, in which the expression of glutamate transport vesicle (vGluT2) was specifically deleted from Sim1 expressing neurons. When we put these mice on a treadmill running at different speeds,

we found that V3OFF mice were unable to trot, observed as a lack of synchronized movements between diagonal limbs. Furthermore, we demonstrated that a subpopulation of lumbar V3 INs had long ascending projections to cervical locomotor network, and these long ascending propriospinal V3 INs were highly active when the mice ran at 40cm/s, at which speed mice mainly trot on the treadmill. Therefore, our results suggest that lumbo-cervical projecting V3 propriospinal INs may provide a direct excitatory drive to cervical locomotor CPGs, which should be essential for the synchronization of diagonal limbs for proper trotting gaits.

3 Results

3.1 Elimination of V3 INs resulted in deficits in fore-hind limb coordination of mice running on the treadmill.

To study the gait of V3OFF mice, we had them run on a treadmill at different speeds. We found that the highest speed the V3OFF mice could reach was only 40 cm/s (mean = 34.09 ± 7.00 cm/s, n=11), while WT mice normally could reach speeds up to 75 ± 7.56 cm/s (n=7) on the treadmill (Sup Figure 2.1). Next, we examined whether the deletion of V3 INs would affect the structure and pattern of animal's gaits. The mice were subjected to walk/run on the treadmill at 6 different speeds ranging from 15 cm/s - 40 cm/s with 5 cm/s increments. At each speed, the animal walked/ran at least 2x20s. Locomotor gaits were captured with a camera underneath the transparent belt of the treadmill.

We first calculated the phase relationship between different pairs of coupling legs: homologous couplings, between either two forelimbs or two hindlimbs; homolateral coupling, between left fore- and hindlimbs; and diagonal coupling, between left hindlimb and right forelimb (Sup Figure 2.2A). To evaluate the consistency of coordination at a given speed, we also compared standard deviation (StDv) of each mouse and phase value differences between two consecutive steps under different speeds.

Consistent with our previous studies, the left-right alternation, the homologous couplings, of both fore- and hindlimbs of V3OFF mice did not show any significant differences from those of WT mice (Figure 2.1Ai & Bi; Sup Figure 2.3A, B). The correlation analysis did not show changes in the phase values of both fore- and hindlimb at different speeds (Sup Figure 2.3A, B; Table 2.1), indicating that there was no correlation between homologous coupling and the speed. We then calculated the StDv within each mouse at different speeds and found that the variability of homologous coupling between hindlimbs within each V3OFF mice increased at higher speeds, while those of WT mice tended to decrease from low to medium speeds (Sup Figure 2.3A; Figure 1.1Aii; Table 2.1, R_{WT} = -0.32, P_{WT} = 0.01, R_{V3OFF} = 0.42, $P_{V3OFF} < 0.0001$). The homologous coupling between two forelimbs in V3OFF mice did not correlate with speed while those of WT mice was negatively

correlated with speed as shown in hindlimbs (Sup Figure 2.3B; Figure 2.1Bii; Table 2.1, R_{WT} = -0.44, P_{WT} = 0.0004, R_{V3OFF} = 0.05, P_{V3OFF} = 0.6136). The phase difference of homologous coupling between same girdles of WT mice also showed negative correlation with speed (Figure 2.1Aiii, Biii; Table 2.1, $R_{WT\_Hindlimb}$ = -0.48, $P_{WT\_Hindlimb}$ < 0.0001, $R_{WT\_Forelimb}$ = -0.48, $P_{WT\_Forelimb}$ < 0.0001). However, there was no such correlation observed in V3OFF mice (Figure 2.1Aiii, Biii; Table 2.1, $RV_{3OFF\_Hindlimb}$ = 0.18, $P_{V3OFF\_Hindlimb}$ = 0.0662, $R_{V3OFF\_Forelimb}$ = -0.04, $P_{V3OFF\_Forelimb}$ = 0.6833).These data indicates that WT mice tend to have a steadier left-right alternation than V3OFF mice when speed increases. Further, V3OFF mice perform a more variable left-right coordination between hindlimbs but not forelimbs as speed increases.

Although the alternation between forelimbs or hindlimbs was not changed, the affected homolateral and diagonal coupling, coordination between fore- and hindlimbs, was significantly changed in V3OFF mice (Figure 2.1Ci, Di). On treadmill, WT mice tend to have an alternating homolateral coordination (phase value ~ 0.5) and synchronized diagonal coupling (phase value ~ 1), especially at higher speed (Sup Figure 2.3C, D, WT; Figure 2.1Ci, Di, WT). However, V3OFF mice likely displayed an out-of-phase relationship between fore- and hindlimbs. For homolateral limbs, the phase value ranged from 0.125 to 0.375; and for diagonal coupling, it was 0.625 to 0.875. The means of these phase values increased with speeds in V3OFF mice while it stayed consistent in WT mice at all speeds (Sup Figure 2.3C, D, V3OFF; Figure 2.1Ci; Table 2.1, $R_{V3OFF\_Homolateral}$ = 0.43, $P_{V3OFF\_Homolateral}$ < 0.0001, $R_{V3OFF\_Diagonal}$ = 0.36, $P_{V3OFF\_Diagonal}$ = 0.0001). For WT mice, the StDvs of homolateral and diagonal coupling were negatively correlated with their speeds, indicating that the coordination of fore-hind limbs became more stable when their speed increased (Sup Figure 2.3C, D; Figure 2.1Cii, Dii; Table 2.1, $R_{WT\_Homolateral}$ = -0.38, $P_{WT\_Homolateral}$ = 0.0027, $R_{WT\_Diagonal}$ = -0.36; $P_{WT\_Diagonal}$ = 0.0036). In contrast, the StDvs of homolateral and diagonal coupling of V3OFF mice both increased with the speed (Sup Figure 2.3C, D; Figure 2.1Cii, Dii; Table 2.1, $R_{V3OFF\_Homolateral}$ = 0.27, $R_{V3OFF\_Homolateral}$ = 0.0041, $R_{V3OFF\_Diagonal}$ = 0.41; $R_{V3OFF\_Diagonal}$ <0.0001). The phase differences of homolateral coupling did not show correlation with speed in both WT and V3OFF mice (Figure 2.1 Ciii; Table 2.1, $R_{WT\_Homolateral}$ = -0.19, $P_{WT\_Homolateral}$ = 0.1358, $R_{V3OFF\_Homolateral}$

= 0.07, $P_{V3OFF\_Homolateral}$ = 0.4852). However, the phase differences of diagonal coupling did show opposite correlation between WT and V3OFF mice (Figure 2.1Diii; Table 2.1, $R_{WT\_Diagonal}$ = -0.44; $P_{WT\_Diagonal}$ = 0.0003, $R_{V3OFF\_Diagonal}$ = 0.30; $P_{V3OFF\_Diagonal}$ = 0.0014). Taken together, deletion of V3 INs resulted in more variable coupling between two hindlimbs and fore-hind limbs, and a change in fore-hind limb coordination, especially that of the diagonal coupling, at higher speeds.

3.2 Gait preferences at different speed were changed in V3OFF mice.

The overall relationships of the four limbs in mammals are expressed as gaits during locomotion. Bellardita & Kiehn (2015) and Lemieux et al. (2016) have systematically defined different gaits by the phase values of the interlimb couplings during over-ground and treadmill locomotion, respectively. Both studies have shown that at intermediate speeds, mice prefer trotting as the most steadied gait. Lemieux et al further demonstrated that lateral walk (L-walk) was used as a transitional gait under these speeds.

In this study, we mainly adopted methods described in Lemieux et al., (2016), using the phase of inter-limb coupling and duty cycle of stance durations to define most of gaits, except trot. Lemeiux et al. only considered two factors for trot identification, homologous and homolateral coupling. However, in V3OFF mice, the diagonal coupling showed the most problematic phenotype. To assess the diagonal coupling more accurately, we considered the diagonal coupling as the third factor for the classification of trot. Thus, we separated diagonal trot (D-trot) from regular trot. This gait had strict anti-phase homologous and homolateral coupling, and, more importantly, in-phase diagonal coupling. We then calculated the occurrence, persistency, and attractiveness of each gait to find the most preferred gaits at different speeds. The occurrence was the percentage of certain gait within the total steps. The persistence of certain gait was the percentage of two consecutive steps that both have the same gait out of all the consecutive steps that include every possible transition circumstance starting from this gait. The attractiveness represented how attractive the certain gait was. To detect the attractiveness of certain gait, we calculated the number of steps of certain gait and then this value was subdivided by the total number of

all possibilities that any type of gait transferred to this gait. Equation for these measurements are shown in Sup Figure 4.

Similar to other studies (Bellardita & Kiehn, 2015; Lemieux et al.; 2016), we observed that for WT animals, D-trot was the most preferred gaits at all speeds between 15-40 cm/s, and its dominancy increased with the speed (Sup Figure 2.2B, left), and its three parameters, the occurrence, persistency and attractiveness, all increased together along the speed as well (Figure 2.2A, B & C, WT). In contrast, the most occurred and attractive gait in V3OFF mice at low speeds < 30cm/s was L-walk, and then they lost any preferences of the gait choice when the speed increased (Sup Figure 2.2B, right; Figure 2.2A, B & C, V3OFF). More interestingly, at the speeds of 30-40cm/s, the medium speeds for adult mice (fast-walking speed, Lemieux et al., 2016), V3OFF animals started galloping, half-bounding and hopping, which were only seen in WT mice at high speeds (>80 cm/s) (Bellardita & Kiehn, 2015; Lemieux et al.; 2016). The appearance of such high-speed gaits and lack of a constant gait profile might indicate that 30 to 40 cm/s were already too fast for V3-OFF mice to catch easily. We would like to point it out that V3-OFF could trot at all speeds, but the trot gait was always used as a transit state instead of a steady state or attractive gait as that in WT animals (Figure 2.2A, B & C). Compared to most other gaits, the D-trot require robust alternation between left-right and ipsilateral fore-hind limbs, and more importantly, robust synchronization of diagonal fore-hind limbs. This enables the animals to distribute their body weight relatively equally on their diagonal limbs during stance phase keeping their body at the most stable state during locomotion. This result was consistent with our analyses above, which showed that V3-OFF animals had less diagonal synchronization and ipsilateral alternation.

All our results so far suggest that the deletion of V3 INs caused a lack of coordination between fore- and hindlimbs, particularly at higher speeds. This led us to predict that there might be subsets of V3 INs that serve as long projecting propriospinal neurons to connect the spinal circuits in lumbar and cervical regions for fore- and hindlimb coordination.

3.3 Long ascending V3 INs have direct excitatory inputs to the cervical locomotor circuit and are more active at intermediate than low speeds.

Previous studies indicated that there might be limited projections of V3 INs from cervical to lumbar region (Flynn et al., 2017; Ruder et al., 2016). Therefore, we decided to focus on the ascending projecting V3 INs from lumbar to cervical regions. To do so, we injected a retrograde tracer, cholera-toxin B (CTB), to the cervical C5-C8 region of *Sim1*$^{Cre/+;Rosafloxstop26TdTom\ mice}$, which express tdTomato fluorescent proteins specifically in Sim1-positive V3 INs (Figure 3A) (Borowska et al., 2013, 2015; Blacklaws et al., 2015; Zhang et al., 2008). After 7 days, we harvested the lumbar spinal cord, immune-stained and mapped the TdTomato and CTB double positive neurons, which should mainly be V3 INs with ascending axons to the cervical region (Figure 2.3A). We found that these long ascending V3 INs were predominately located contralateral to the injection sites, and at dorsal and intermediate region, mainly in lamina IV to VI, in higher lumbar segments, but moved to the intermediate and ventral lamina VII and VIII regions in lower lumbar segments (Figure 2.3B).

To test whether long ascending V3 INs in the lumbar segment could activate motor circuits in the cervical region, we generated *Sim1*$^{Cre/+}$*; Ai32* mice, which express channelrhodopsin2 (ChR2) specifically in Sim1 positive V3 INs. Isolated P0-3 spinal cord of *Sim1*$^{Cre/+}$*; Ai32* mice were placed in a perfusion chamber split into two parts. This split chamber was constructed over the T5 segment with petroleum jelly (Vaseline) walls. The suction electrodes for electroneurogram (ENG) recording were placed on the lumbar and cervical ventral roots of nerves innervating extensors and flexors (Figure 2.4A). Firstly, we found that photo-activation of V3 INs in the lumbar region evoked strong lumbar and cervical motor responses (Figure 2.4Bi). This indicated that lumbar V3 INs provided excitatory inputs to cervical MN pools. Then, to test if this excitatory drive was directly from V3 INs or from the other lumbar INs locally activated by V3 INs, we blocked the glutamatergic transmission selectively in the lumbar region with 4 mM of kynurenic acid (KYN), known to completely block NMDA and AMPA/Kainate receptors at this concentration (Hägglund et al., 2010). We found that although the optical stimulation of lumber V3 INs did not evoke any response in lumbar region, the motor responses in the cervical region were still present (Figure 2.4Bii). The lumbar response reappeared after the

drug was washed out (Figure 2.4Biii). These results clearly demonstrated that lumbar V3 INs directly provided an excitatory drive to cervical motor circuits.

Next, we tested if these long ascending neurons were truly active during locomotion, particularly at medium to high speeds. We first injected CTB in the cervical region of young adult (P35-40) *Sim1*$^{Cre/+;\ Rosafloxstop26TdTom}$ mice. After 7 days post injection, we let the animals run on the treadmill at either 15cm/s or 40cm/s. We then conducted post-hoc analysis of the expression of c-Fos protein, an indicator of neuronal activity, in V3 INs of whole lumbar spinal cord (Figure 2.5A). We found that c-Fos positive V3 INs at both speeds, but more V3 INs were recruited at 40cm/s than 15 cm/s and rest (P rest vs 40cm/s = 0.0185, P 15cm/s vs 40cm/s = 0.0183) (Figure 2.5B). Similarly, we found significantly increased c-Fos/CTB/V3 INs during 40 cm/s than 15 cm/s and rest (P rest vs 15cm/s = 0.0495, P 15cm/s vs 40cm/s = 0.0174, P rest vs 40cm/s = 0.0162) (Figure 2.5B).

Taken together, we propose that lumbo-cervical projecting V3 INs provide a direct excitatory drive to cervical locomotor networks during medium locomotor speeds essential for robust alternation between left-right and ipsilateral fore-hind limbs. This enables robust synchronization of diagonal fore-hind limbs to perform trotting gait.

4 Discussion

Proper coordination of the fore- and hindlimbs in terrestrial mammals is essential to maintain stability during the forward progression of quadrupedal locomotion. The propriospinal circuitry underlying inter-girdle coordination during quadrupedal locomotion remain poorly understood. In the present study, we demonstrated that selective ablation of V3 INs cause unstable gaits and a lack of fore- and hindlimb coordination. V3OFF mice were unable to trot due to a lack of synchronization between diagonal limbs. Using *in vivo* retrograde track tracing, we revealed a subpopulation of long ascending propriospinal V3 INs contralaterally projecting from the lumbar to cervical spinal cord. We then further demonstrated that these long ascending lumbar V3 INs could directly elicited cervical motor outputs and were highly active when mice were trotting on the treadmill.

4.1 V3OFF mice could not settle on trot.

A precise yet flexible control of interlimb coordination under any moving speed allows an animal to maintain dynamic stability in a continuously changing environment. Such inter limb coordination, expressed as gaits, at different speeds was well controlled by the locomotor circuits in the spinal cord (Batka et al., 2014; Bellardita & Kiehn., 2015; Lemieux et al., 2016).

For a mouse, lateral walk is preferentially performed at low frequency during over- ground locomotion (Bellardita & Kiehn., 2015). However, when mice were walking on the treadmill, lateral walk was only present up to 30 cm/s, and never occurred as a dominant gait at any other speeds (Lemieux et al., 2016). The most occurred, stable, and attractive gait was trot during medium speed treadmill locomotion (Lemieux et al., 2016). Our WT mice showed similar gait preference (Sup Figure 2.2B, left; Figure 2.2, WT). However, V3OFF mice preferred to use lateral walk when the treadmill speeds were below 35 cm/s (Sup Figure 2.2B, right; Figure 2.2, V3OFF). One main difference between L-walk and trot gait is the coordination of fore- and hindlimbs. Both trot and L-walk share alternating pattern within the same girdle but are different on coordination patterns of homolateral and

diagonal pairs. The homolateral and diagonal phase values of V3OFF mice were smaller than those of WT mice, which led that the gaits in the V3OFF mice were overwhelmingly classified as L-walk. Since we used the left hindlimb as the reference foot, the small phase value of homolateral coupling in V3OFF mice could be caused by that either the fore-limb contacted the ground earlier in the hindlimb stride cycle or the hindlimb contacted the ground later in fore-limb stride cycle. Later, data presented in the next chapter, we found that V3OFF mice had significantly longer swing phase duration in their hindlimb movement, while their forelimbs had normal phase durations. Therefore, one reason the lateral walk performed in V3OFF mice might be due to the delayed hindlimb stepping into the fore-limb stride cycle.

It has been suggested that ablation of long cervico-lumbar descending projection neurons, including V2-Shox2 and V0V INs, led to a predominant interlimb coordination defects of mice running on treadmill at speeds above 40 cm/s (Ruder et al., 2016). In addition, this study showed that after deletion of long cervico-lumbar descending projection neurons, at 40 cm/s, only hindlimb coordination was significantly affected yet forelimb left-right alternation remained normal. At the maximal treadmill speed that these mice were able to reach, coordinations at both hindlimbs and forelimbs were affected (Ruder et al., 2016). In our present study, deletion of V3 INs including the one with long ascending projections to cervical region, did not seem to affect forelimb alternation at all possible speeds for V3OFF mice (Figure 2.1B; Sup Figure 2.3B). At their maximal speed, 35 cm/s – 40 cm/s, V3OFF mice tended to show ‘high-speed’ like gaits, such as gallops. Under those circumstances, forelimbs of V3OFF mice kept alternating and had similar patterns as WTs, while their hindlimb coupling phases kept changing with increased variability at medium speeds. In another word, it appeared that the hindlimbs lost any influences on the forelimb locomotor circuits, particularly at medium speeds. Therefore, the disorganized gaits in V3OFF mice might be a combination of the defects of hindlimb movements and the decreased communication between hindlimb and forelimb locomotor circuits.

4.2 A subset of lumbar V3 INs that have long ascending projections to cervical segments may be involved in fore-hind limb coordination during medium speed locomotion.

In our previous studies, we have shown that lumbar V3 INs diverge into several subpopulations determined by their distribution, morphology, and electrophysiological properties (Blacklaws et al., 2015; Borowska et al., 2013, 2015). In the current study, we identified a subset of lumbar V3 INs, which have long ascending projections to the cervical segment. This subset of V3 INs might be involved in the coordination of fore- and hindlimb activities, particularly at medium speed movement like trotting.

Using retrograde tracing, we found that most of these long ascending V3 INs were in the deep dorsal horn and intermediate region of the higher lumbar spinal cord. The neurons in this region have been shown to receive intensive innervation from group Ib, group II and skin sensory afferents (Bannatyne et al., 2009; Edgley & Jankowska, 1987; Jankowska & Edgley, 2010). Previously, we also showed that V3 INs clustered in the dorsal region, named V3Ds, were more active during walking than in swimming (Borowska et al., 2013). We, then indeed, confirmed, in our present study, that long ascending lumbar V3 INs were more active during 40 cm/s than 15 cm/s treadmill locomotion. The trot gait was characterized by a robust alternation of fore-and hind-limbs and synchronized diagonal limbs, likely resulted from a well-orchestrated and coordinated actions between spinal locomotor circuits with sensory inputs. The diagonal synchronization contributes to an evenly distribution of body weight on the diagonal pairs of feet at stance, which produces the least body tilting (Fukuoka et al., 2009, 2015). To maintain such stable state, sensory feedback would be one of the most crucial factors (Fukuoka et al. 2015; Tsujita et al., 2001; Owaki et al., 2013). Therefore, we suggested that these long ascending lumbar V3 INs might play important roles mediating signals from both lumbar locomotor CPGs and direct sensory information from hindlimb muscles and joints to regulate the coordination of fore- and hindlimb movement during trotting.

In summary, our current study has demonstrated that V3 INs are crucial in generating coordinated and stable trotting gaits, and we have also identified a subset of V3 INs that

directly carry information from lumbar spinal cords to regulate the cervical locomotor circuits to ensure the coordinated movement between diagonal limbs.

5 Materials and Methods

Animals

The generation and genotyping of *Sim1*$^{Cre/+}$ mice were described previously by Zhang et al. (2008). Conditional knock-out of VGluT2 in Sim1-expressing V3 INs, *Sim1*$^{cre/+}$*;VGluT2* $^{flox/flox}$ (V3OFF mice), was described previously by Chopek et al. (2018). *Ai32* mice (RCL-ChR2(H134R)/EYFP, Jackson Laboratory, Stock No. 012569) was crossed with *Sim1*$^{Cre/+}$ to generate *Sim1*$^{Cre/+}$*; Ai32* mice. *TdTomato Ai14* mice (*Rosa26*^{TdTom,} Jackson Laboratory, Stock No. 007908) was crossed with *Sim1*$^{Cre/+}$ to generate ^{Rosafloxstop26TdTom} mice (Blacklaw et al., 2015). All procedures were performed in accordance with the Canadian Council on Animal Care and approved by the University Committee on Laboratory Animals at Dalhousie University.

Treadmill locomotion

Treadmill locomotion tests were performed using 11 (6 males, 5 females) V3OFF (*Sim1*$^{cre/+}$*;VGluT2* $^{flox/flox}$) mice and 7 (2 males, 5 females, *Sim1*$^{+/+}$*;VGluT2* $^{flox/flox}$ or *Sim1*$^{+/+}$*;VGluT2* $^{+/flox}$) control littermates (WT) at 40 to 48 postnatal days (P40-48). No training was performed before any locomotion tests.

Treadmill locomotion tests were performed using an Exer Gait XL treadmill (Columbus Instruments). Treadmill running started from 15 cm/s to 45 cm/s in 5 cm/s of increment. To avoid their fatigue, animals would not perform more than two trails for each speed during each experiment, and each trail was no more than 20s. The rest interval between two consecutive trials was > 1 minute. If the mouse hit the back wall of the chamber during running, the treadmill was stopped immediately. Gentle stimulations, such as a blow or touch the hind body of animals, were applied to encourage the animals to run. If the mouse failed to hold the speed more than three seconds after five tries, this speed was defined as the maximum speed for this mouse. A mirror was placed underneath the transparent treadmill belt with 45 degrees from vertical, which could reflect the paw movement to a high-speed camera with the capturing rate at 200 frames/s. Episodes with at least 10 consecutive steps were included for analysis.

Gait analysis

Four paws' movements were manually tracked using Vicon Motus software from the videos. The successive foot contacts were defined when the paw contacted the ground, the size of paw's image did not change for the next three frames, and then the first frame was chosen as the foot contacts. The foot lift was defined as the time of the frame when the front part of the paw was disappeared from the image. Data were exported and processed using a custom-written script in Spike2 (Version 7.09a, Cambridge Electronic Design). The stride duration was defined as the duration of two consecutive foot contacts. An stance (St) started from the foot contact and ended at foot lift. An swing (Sw) started from the offset of St and ended at the onset of next St. The phase value corresponded to proportion of the time of foot contact of the tested limb relative to the step cycle of the reference limb, which was the left rear-limb (RL) in this study. Phase values ranged from 0 to 1. The value of 0 or 1 indicated a perfect in-phase coupling (synchronization), and 0.5 indicated a perfect anti-phase coupling (alternation). The standards of the classification of different gaits that we utilized were the same as those in Lemieux et al. (2016a) did, except that we separated diagonal-trots (D-trot) from 'regular' trots based on their diagonal coupling. Therefore, we had a total of 11 gaits.

The occurrence was the percentage of certain gait within the total steps. The persistence of certain gait was the percentage of two consecutive steps that both have the same gait out of all the consecutive steps that include every possible transition circumstance starting from this gait. The attractiveness represented how attractive the certain gait was. To detect the attractiveness of certain gait, we calculated the number of steps of certain gait. Then this value was subdivided by the total number of all possibilities that any type of gait transferred to this gait. Example of how to calculate these parameters are illustrated in Sup Figure 2.5.

CTB injection and c-Fos expression

Retrograde tracer, cholera-toxin B (CTB), was injected into C5 to C8 segments of P30-35 Sim1TdTom mice to detect the cervical projection of V3 INs in different spinal cord regions. To accurately place the tracers at different spinal cord locations, we conducted

spinal laminectomy. Briefly, the mouse was placed in an induction chamber and anesthetized with isoflurane (4% in O2, 1.5L / minute), and then the mouse was transferred to a heating pad, and low dose isoflurane (?) was maintained through a mask throughout the surgery. A 1-cm sagittal incision was made centred over the sixth cervical spinous process. A laminectomy was performed, and the bone covering the upper half of the sixth cervical segment (C6) was removed. The glass micropipette filled with the tracer at the tip was lowered into the spinal cord. The manipulator adjusted the position of the micropipette. 500-700 nl of CTB was injected to one side of the spinal cord using a Nanoject II (Drummond). The pipette was the kept in place for an additional 5 minutes for diffusion. After injection, the muscles were sewn back together in layers with absorbable sutures, and the skin was sewn closed with polypropylene surgical sutures.

After 7 days for the tracer transportation, the animals were subjected to walk (15 cm/s) or run (40 cm/s) on a treadmill for 3 X 15 minutes with a 5-minute interval between trials. The animals in the control group were left in the home cage through the experiments. After all tasks, mice were put back to the home cage for 60 mins. Then, the animals were perfused with 4% PFA. Spinal cords were harvested and postfixed in 4% paraformaldehyde at 4°C for 3 hours and then cryoprotected in 20% sucrose before embedding in OCT and cryostat sectioning. The 30 μM thick sections were collected for immunolabeling. Sections were washed in 0.01 M PBS with 0.1% Triton X-100 (PBS-T), blocked for 1 hour in 5% normal goat serum in PBS-T, and incubated at room temperature over two nights in rabbit anti-CFos antibody (1:2000; Santa Cruz Biotechnology) in PBS-T with 2% goat serum. Sections were washed in 3 X PBS-T and incubated with goat anti-rabbit conjugated to Alexa Fluor 488 (1:500; The Jackson Laboratory) for 2 hours at room temperature. Sections were then washed in PBS three times and coverslipped with an anti-fade mounting medium (Dako).

The images were obtained using a Zeiss LSM 510 upright confocal microscope and a Zeiss Axiovert 200M fluorescent microscope. Total Tdtomato-positive V3 neurons and those co-expressing CTB and Fos protein were counted and mapped. For each animal, we sampled a total of 20 sections from the lumbar region and summarized the relative position of all double-labelled CTB/Tdtomato cells and triple-labelled CTB/Tdtomato/c-Fos cells

onto one schematic cross-section. In addition to using the central canal and Rexed's laminae as landmarks, we also set grids on the image of transverse sections of the spinal cord and the schematic section to map the double-labelled cells more accurately.

Electrophysiology

All experiments were performed using spinal cords from *Sim1*$^{Cre/+}$*; Ai32* mice at P2-P3. The mice were anesthetized, and the spinal cords caudal to C1 were dissected out in Ringer's solution (111 mm NaCl, 3.08 mm KCl, 11 mm glucose, 25 mm NaHCO3, 1.25 mm MgSO4, 2.52 mm CaCl2, and 1.18 mm KH2PO4, pH 7.4). The spinal cord was then transferred to the recording chamber to recover at room temperature for at least 1 hour before recording in Ringer's solution. The recording chamber was partitioned by a narrow petroleum jelly bridge into two parts with independent perfusion systems. The T6-T8 spinal segments were in the petroleum jelly and the whole lumbar (L) and cervical (C) region were exposed in the bath. The dye was added into one of the bathing systems to check the water tightness in the end of experiment. Electroneurogram (ENG) recordings of the L2/L5 and C5/C8 ventral roots were conducted using differential AC amplifier (A-M system, model 1700) with the band-pass filter between 300 Hz and 1 kHz. Analog signals were transferred and recorded through the Digidata 1400A board (Molecular Devices) under the control of pCLAMP10.3 (Molecular Devices).

To activate ChR2 in V3 INs, 488 nm fluorescent light was delivered by Colibri.2 illumination system (Zeiss) through 10x 1.0 numerical aperture (NA) objectives mounted on an up-right microscope (Examiner, Zeiss) onto the ventral surface of L2-L3 segments of the isolated spinal cord. Continuous light stimuli with duration of 200 ms were used. The stimulation was applied 10 times. Then 2 mM kynurenic acid was added into the bath system for lumbar spinal cord. The optical stimulation onto the same area was applied 10 times. After washing out the drug, another 10 times optical stimulation was applied onto the lumbar segment of spinal cord.

Statistical analysis

The statistical analysis was performed in Prism7 (GraphPad Software, Inc.) and MATLAB (Version R2018a, The MathWorks, Inc.). Pearson correlation coefficient were used to determine the relationship of phase value, StDv, and phase difference with speed. The correlation coefficient, r, ranged from -1 to +1. The P value represented the chance that random sampling would result in a correlation coefficient as far from zero as observed in the experiment if two values were not correlated overall. If the P values were small, the idea that the correlation was due to random sampling could be rejected. Kolmogorov-Smirnov test was used to compare the difference of maximum speed between WT and V3OFF mice. Welch's t-test were used to compare the difference of c-Fos expression in Sim1 cells and Sim1/CTB cells among different conditions.

6 Figures

Figure 2.1 Interlimb coordination in WT and V3OFF mice at different speeds.

Ai

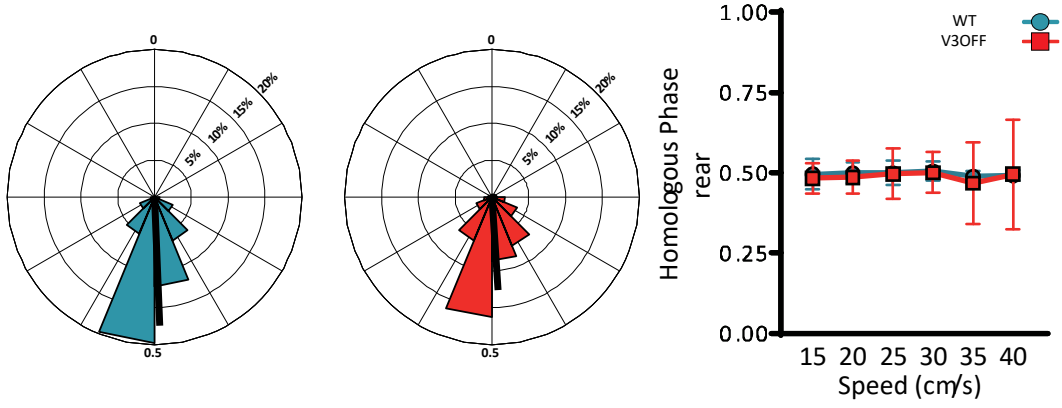

Aii

Aiii

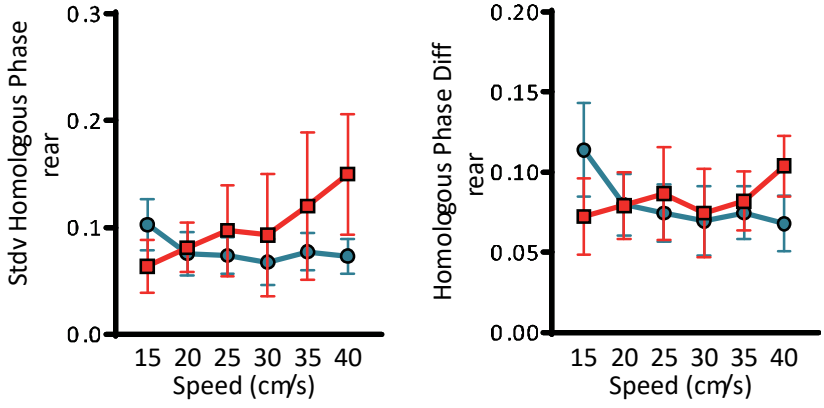

Bi

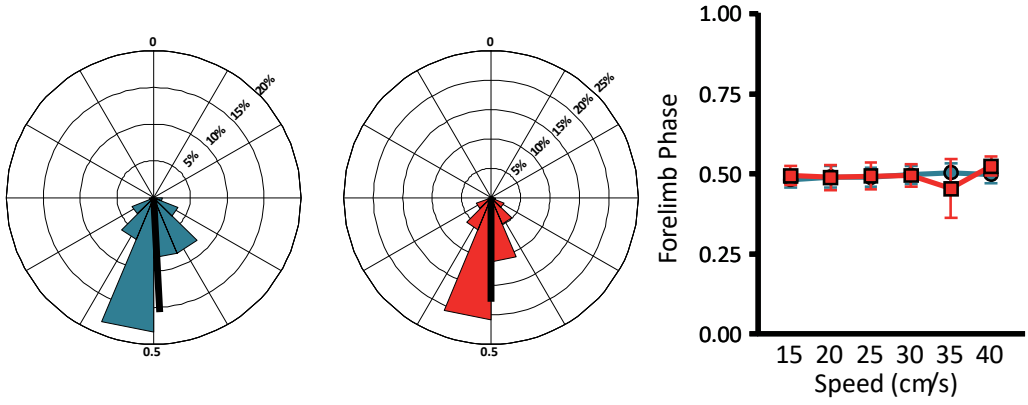
0
5%
10%
15%
20%
0.5
0
5%
10%
15%
20%
25%
0.5
Forelimb Phase
1.00
0.75
0.50
0.25
0.00
15 20 25 30 35 40
Speed (cm/s)

Bii

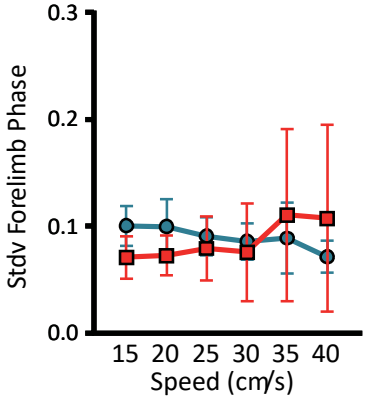
Stdv Forelimb Phase
0.3
0.2
0.1
0.0
15 20 25 30 35 40
Speed (cm/s)

Biii

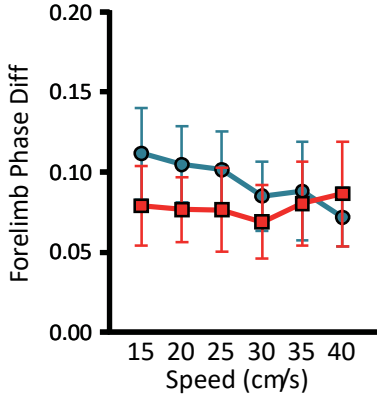
Forelimb Phase Diff
0.20
0.15
0.10
0.05
0.00
15 20 25 30 35 40
Speed (cm/s)

Ci

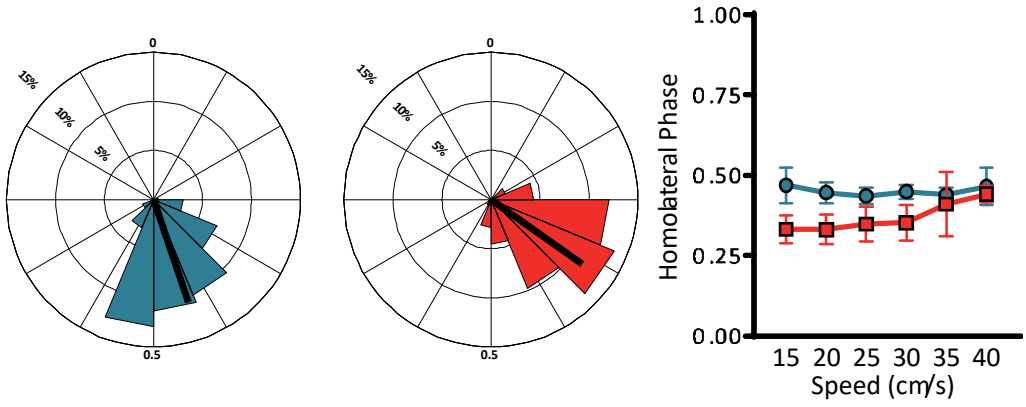
0
15%
10%
5%
0.5
0
15%
10%
5%
0.5
1.00
0.75
0.50
0.25
0.00
Homobateral Phase
15 20 25 30 35 40
Speed (cm/s)

Cii

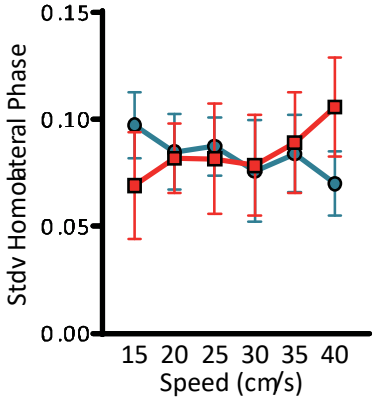
0.15
0.10
0.05
0.00
Stdv Homobateral Phase
15 20 25 30 35 40
Speed (cm/s)

Ciii

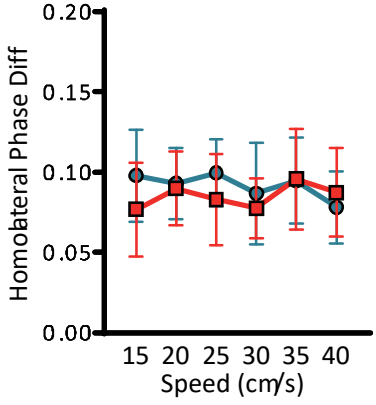
0.20
0.15
0.10
0.05
0.00
Homobateral Phase Diff
15 20 25 30 35 40
Speed (cm/s)

Di

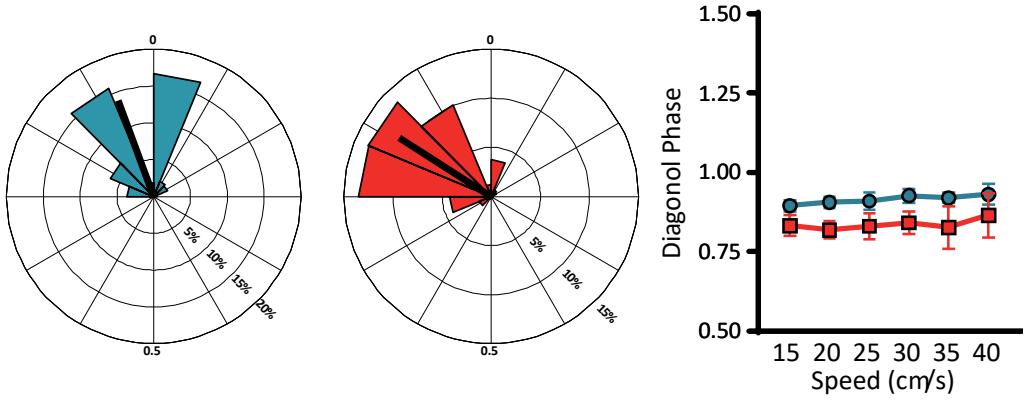
0
0.5
5%
10%
15%
20%
0
0.5
5%
10%
15%
1.50
1.25
1.00
0.75
0.50
Diagonol Phase
15 20 25 30 35 40
Speed (cm/s)

Dii

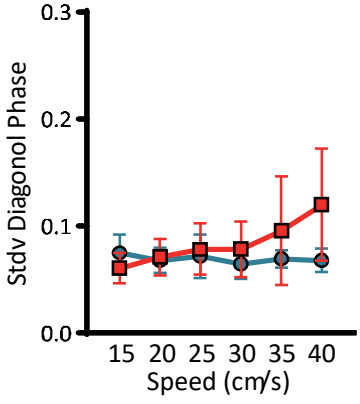
0.3
0.2
0.1
0.0
Stdv Diagonol Phase
15 20 25 30 35 40
Speed (cm/s)

Diii

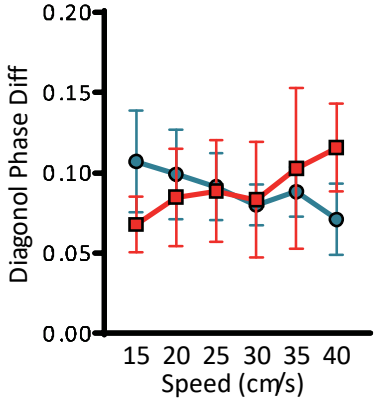
0.20
0.15
0.10
0.05
0.00
Diagonol Phase Diff
15 20 25 30 35 40
Speed (cm/s)

Figure 2.1 Interlimb coordination in WT and V3OFF mice at different speeds.

Circular plots of the means of phase value between (Ai) the left rear-limbs, the reference limb, and left fore-limb (homologous coupling), (Bi) the left-right fore-limbs (fore-limbs, left fore-limb as reference), (Ci) the left fore-limb and left rear-limb (homolateral coupling, left rear-limb as reference) and (Di) right fore-limb and left rear-limb (diagonal coupling, left rear-limb as reference) of WT (blue) and V3OFF (red) mice. Each vector (black bar in circular plot) indicates the mean phase (direction) and robustness (radial line) of the coupling. The circle is evenly separated into 12 fractions. The circular histograms represent the distribution of coupling phase of all steps. The percentage numbers indicate the proportion of steps fallen into this phase out of all steps. The means of coupling phase are also plotted against speed. The correlations between the StDvs of coupling phase and the phase differences with speeds are shown in ii and iii, respectively, for each foot coupling. The data shown in red are from V3OFF mice and blue are from WT mice.

Figure 2.2 Gait preference of WT and V3OFF mice at each speed.

A

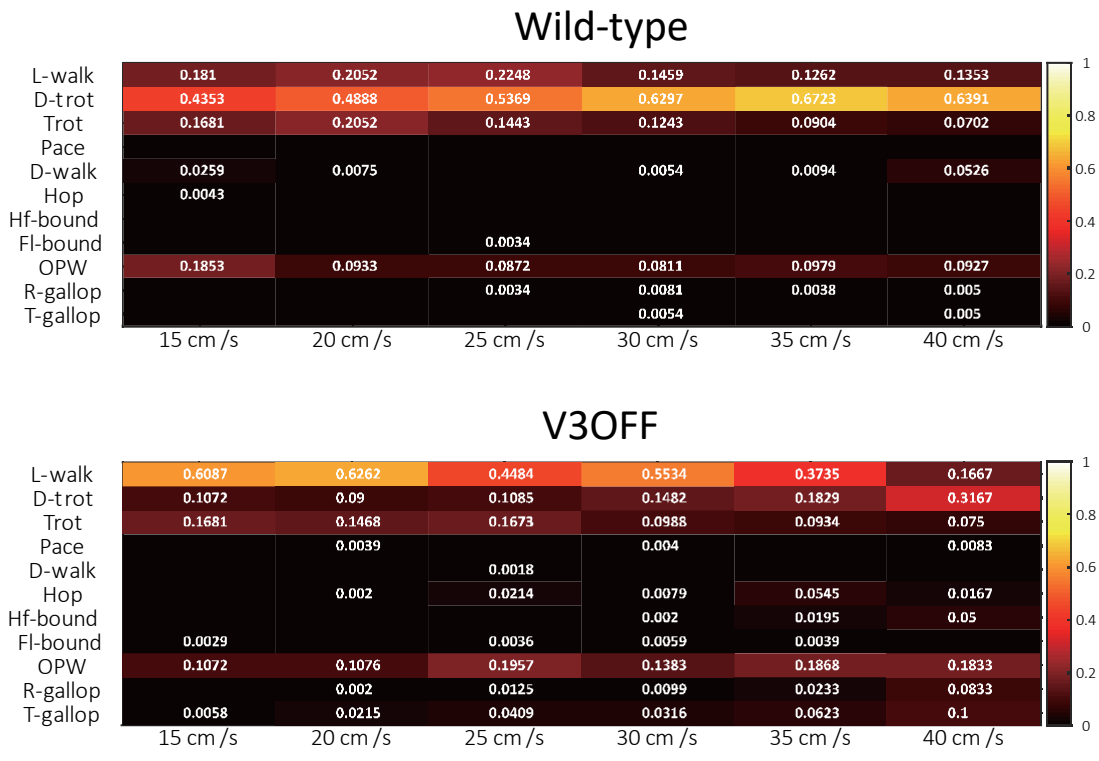

B

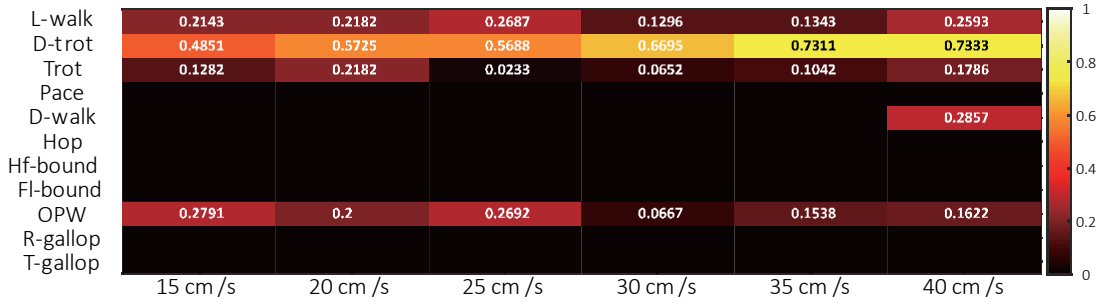

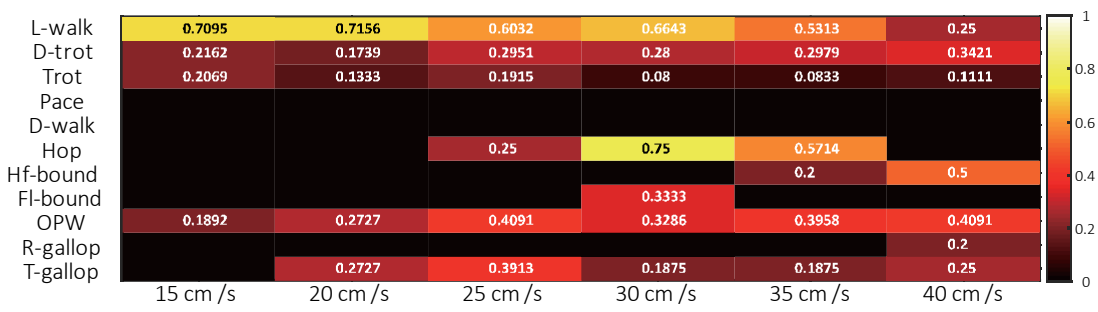
V3OFF
L-walk
D-trot
Trot
Pace
D-walk
Hop
Hf-bound
Fl-bound
OPW
R-gallop
T-gallop
0.7095 0.7156 0.6032 0.6643 0.5313 0.25
0.2162 0.1739 0.2951 0.28 0.2979 0.3421
0.2069 0.1333 0.1915 0.08 0.0833 0.1111
0.25 0.75 0.5714
0.2 0.5
0.3333
0.1892 0.2727 0.4091 0.3286 0.3958 0.4091
0.2
0.2727 0.3913 0.1875 0.1875 0.25
15 cm /s
20 cm /s
25 cm /s
30 cm /s
35 cm /s
40 cm /s
1
0.8
0.6
0.4
0.2
0

C

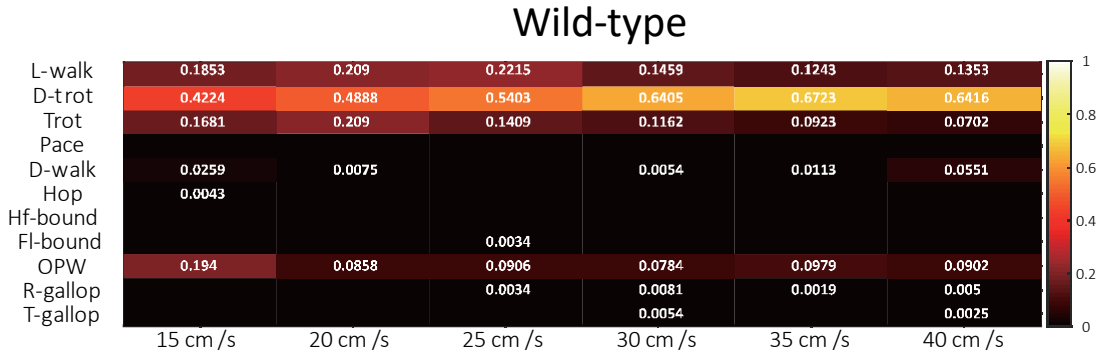
Wild-type
L-walk
D-trot
Trot
Pace
D-walk
Hop
Hf-bound
Fl-bound
OPW
R-gallop
T-gallop
0.1853 0.209 0.2215 0.1459 0.1243 0.1353
0.4224 0.4888 0.5403 0.6405 0.6723 0.6416
0.1681 0.209 0.1409 0.1162 0.0923 0.0702
0.0259 0.0075 0.0054 0.0113 0.0551
0.0043
0.0034
0.194 0.0858 0.0906 0.0784 0.0979 0.0902
0.0034 0.0081 0.0019 0.005
0.0054 0.0025
15 cm /s
20 cm /s
25 cm /s
30 cm /s
35 cm /s
40 cm /s
1
0.8
0.6
0.4
0.2
0

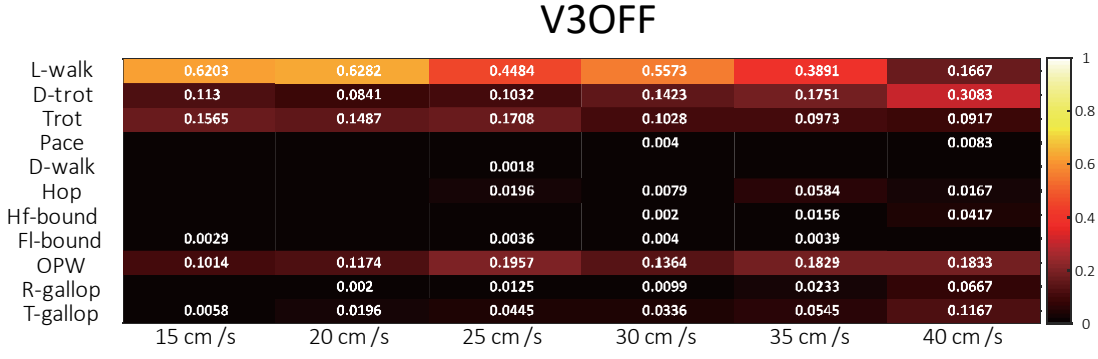
V3OFF
L-walk
D-trot
Trot
Pace
D-walk
Hop
Hf-bound
Fl-bound
OPW
R-gallop
T-gallop
0.6203 0.6282 0.4484 0.5573 0.3891 0.1667
0.113 0.0841 0.1032 0.1423 0.1751 0.3083
0.1565 0.1487 0.1708 0.1028 0.0973 0.0917
0.004 0.0083
0.0018
0.0196 0.0079 0.0584 0.0167
0.002 0.0156 0.0417
0.0029 0.0036 0.004 0.0039
0.1014 0.1174 0.1957 0.1364 0.1829 0.1833
0.002 0.0125 0.0099 0.0233 0.0667
0.0058 0.0196 0.0445 0.0336 0.0545 0.1167
15 cm /s
20 cm /s
25 cm /s
30 cm /s
35 cm /s
40 cm /s
1
0.8
0.6
0.4
0.2
0

Figure 2.2 Gait preference of WT and V3OFF mice at each speed.

Colour-coded-matrixes of the percentage of occurrence (A), persistence (B) and attractiveness (C) values of each type of gaits (raw) at each tested speed (column). The matrixes on the left are from WT and the right from V3OFF mice. A brighter colour indicates more higher percentage and the revers. The number in each cell shows the value of the parameter of corresponding gait and speed. L-walk: lateral-walking. D-trot: diagonal-trot. D-walk: diagonal-walk. Hf-bound: half-bound. Fl-bound: full-bound. OPW: out-of-phase walk. R-gallop: rotary-gallop. T-gallop: transverse-gallop.

Figure 2.3 Lumbar V3 INs projecting to the cervical spinal cord.

A

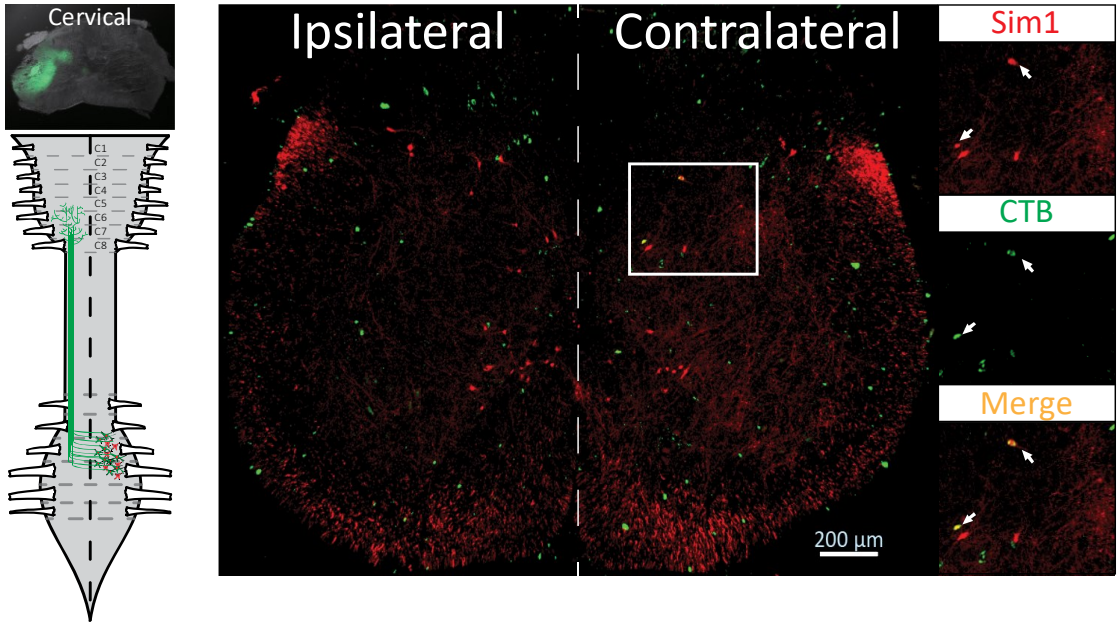

B

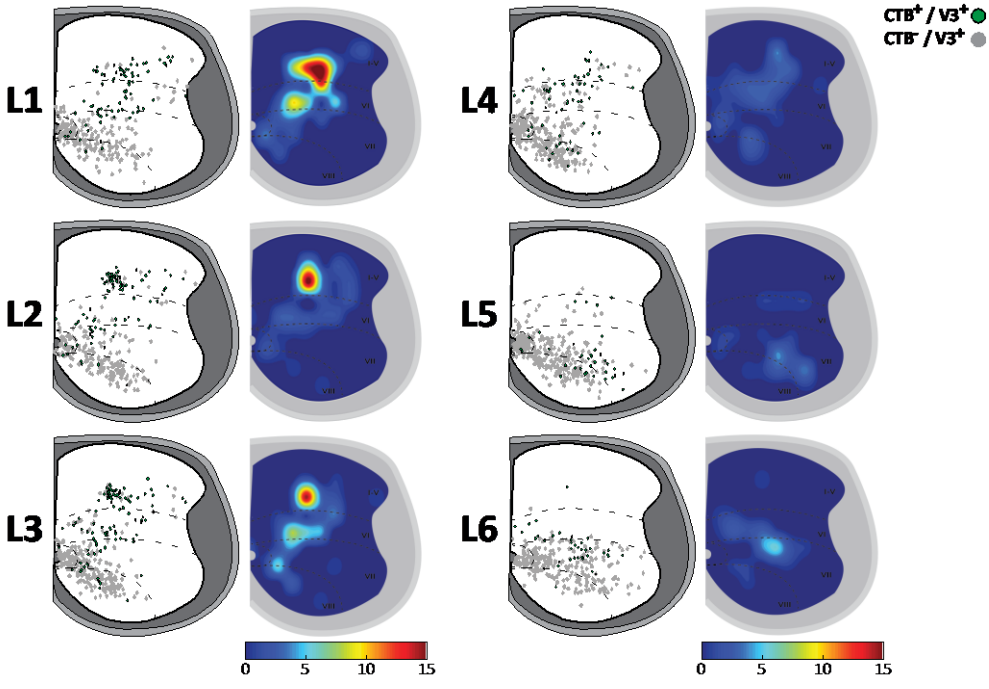

Figure 2.3 Lumbar V3 INs projecting to the cervical spinal cord.

A. Left top, representative image of cervical region of CTB injection site. Left bottom, illustration of the experimental strategy to visualize cell body distribution of long ascending V3 INs by CTB injection into the cervical region. Right, representative image of lumbar spinal cord section of *Sim1*$^{Cre/+;\ Rosafloxstop26TdTom}$ mouse immunostained for CTB and TdTom 7 days after the injection.

B. Distribution of long ascending V3 INs in the lumbar segments, L1-L6. Left columns: illustration of distribution of total (gray dots) and CTB positive (green dots) V3 INs of all analyzed sections (n=9) from injected corded on a half cross section at different lumbar segments. Each dot represents one neuron. Right columns: colour coded heating maps of the distribution pattern of long ascending V3 INs at each lumbar segment. Scale bars for heating map are shown under.

Figure 2.4 Optical activation of V3 INs at lumbar region directly activates the cervical motor outputs.

A

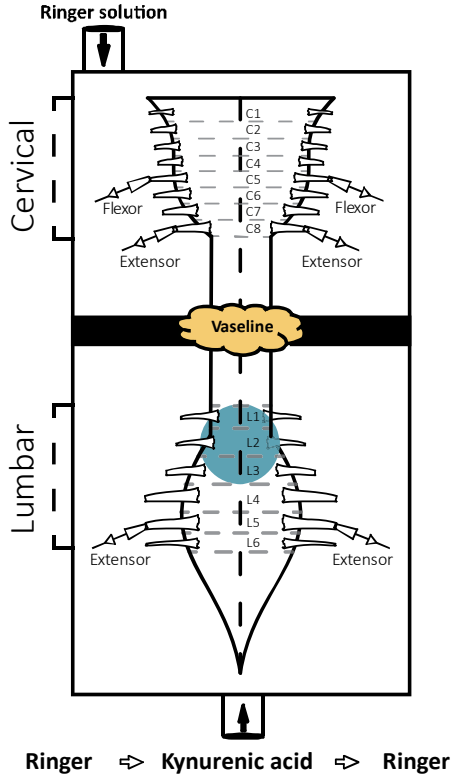

Bi Bii Biii

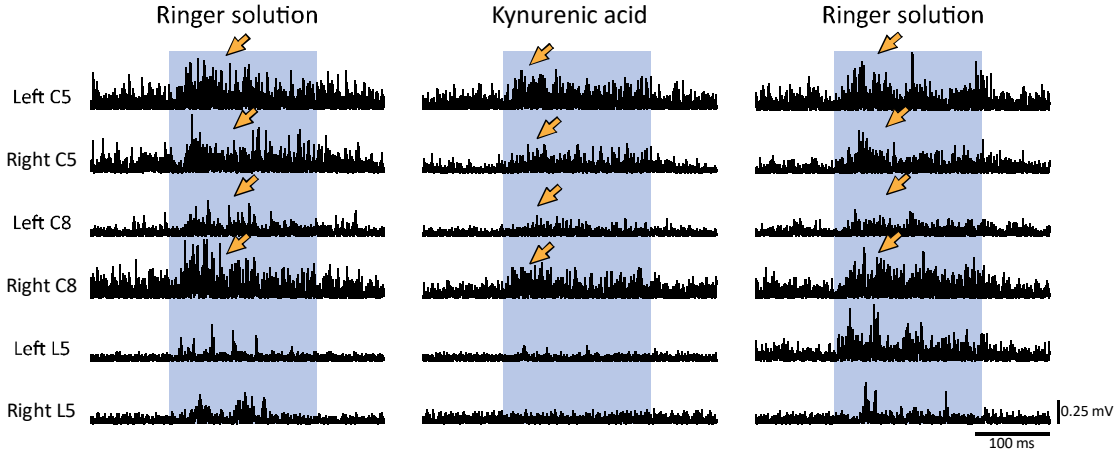

Figure 2.4 Optical activation of V3 INs at lumbar region directly activates the cervical motor outputs.

A. Schematics of the experimental strategy. Isolated spinal cord with ventral roots attached is placed in a split recording chamber. The chamber is partitioned into two sides with a Vaseline wall (represented by yellow cloud in the figure). The ENG activities of left and right, flexor- and extensor represented cervical roots, and the left and right flexor-represented lumbar roots were recorded. The blue fluorescent light indicated by the blue transparent circle is on the ventral side of higher lumbar segments.

B. Representative traces of rectified ENG recordings at ventral roots of both sides of cervical (C5, flexor related nerve, and C8, extensor related nerve) and lumbar (L5, extensor related nerve) spinal segments of P0 *Sim1*^{Cre}*;Ai32* mouse, before (Bi), during (Bii), and after wash-out kynurenic acid application (Biii). The optical stimulation period is indicated with the blue area. The persistent cervical ventral root activities responding to lumbar optical stimulation under all conditions are indicated with yellow arrows.

Figure 2.5 Lumbar long ascending V3 INs are more active during medium speed than low speed walking.

A

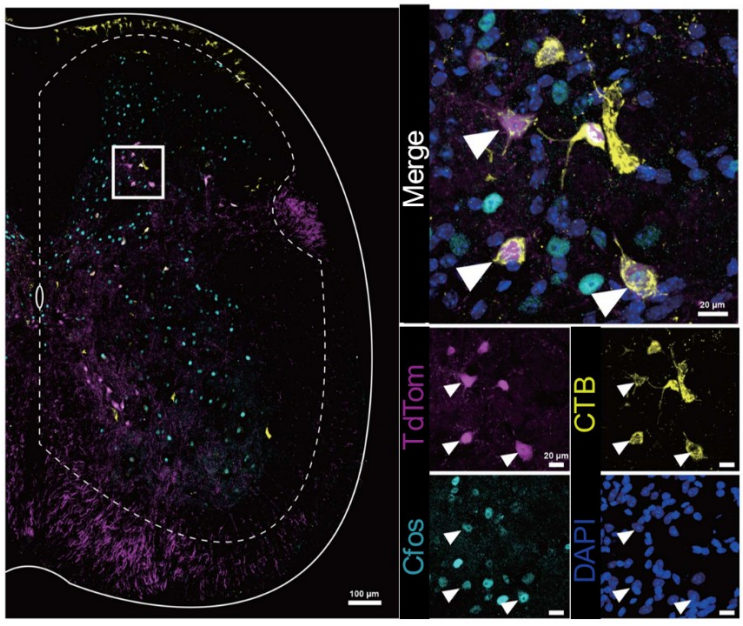

B

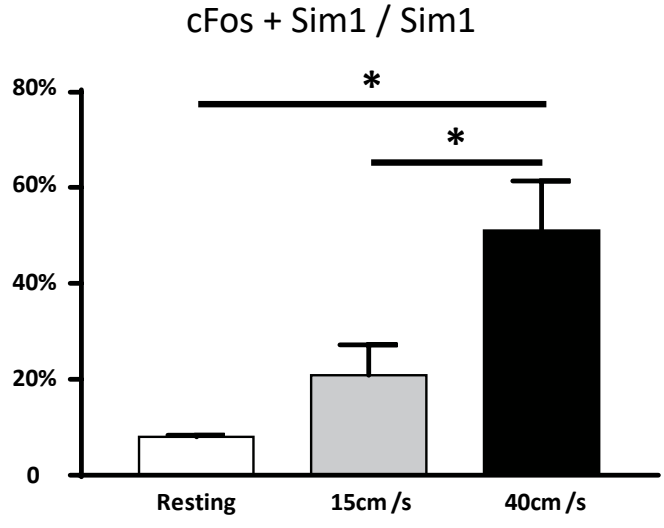

C

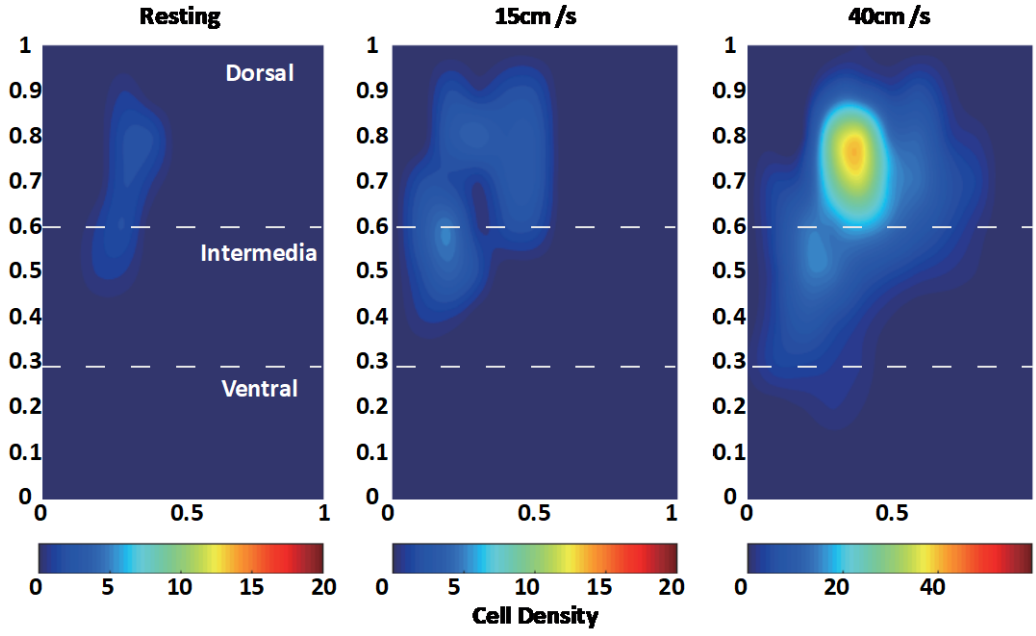
Resting
15cm /s
40cm /s
Dorsal
Intermedia
Ventral
1
0.9
0.8
0.7
0.6
0.5
0.4
0.3
0.2
0.1
0
0
0.5
1
0
5
10
15
20
0
20
40
Cell Density

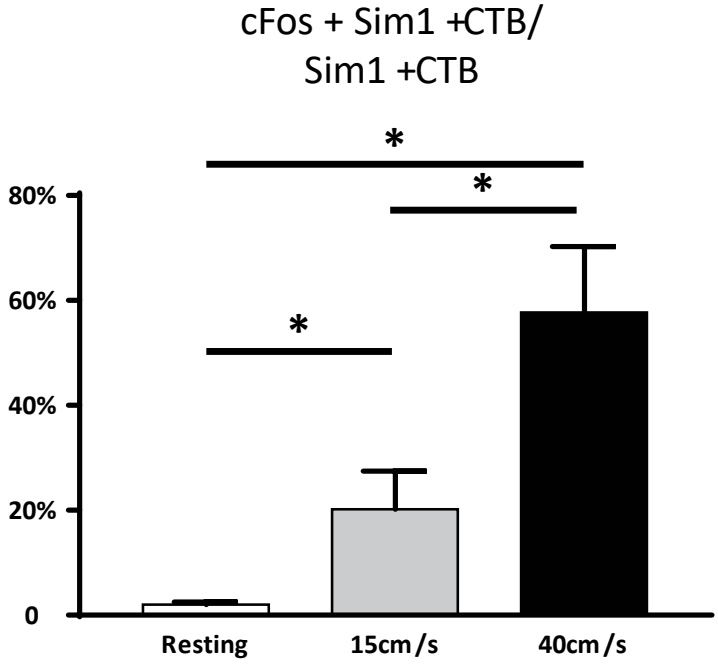
cFos + Sim1 +CTB/
Sim1 +CTB
*
*
*
80%
60%
40%
20%
0
Resting
15cm /s
40cm /s

Figure 2.5 Lumbar long ascending V3 INs are more active during medium speed than low speed walking.

A. Representative image of TdTom+ V3 INs (mediumvioletred), CTB (yellow) and c-Fos (turquoise) of a half cross-section of the spinal cord of *Sim1*$^{Cre/+;\ Rosafloxstop26TdTom}$ mouse. DAPI stained for cell nucleus. Enlarged images showing triple positive cells. (scale bars = 100μm and 10 μm).

B. Histograms of the percentage of c-Fos and TdTom double-positive V3 INs after different locomotor tasks (n=3). *, $0.01 < P < 0.05$.

C. Top, colour-coded heating map shows the distribution of c-Fos, CTB and TdTom triple-positive V3 INs on the cross section of lumbar spinal cord during resting, 15 cm/s and 40 cm/s treadmill locomotion. Bottom: histogram of the corresponding percentage of triple-positive cells indicating active in long ascending V3 INs during different locomotor tasks. *, $0.01 < P < 0.05$.

Supplementary Figure 2.1 Maximum speeds of WT and V3OFF mice on treadmill.

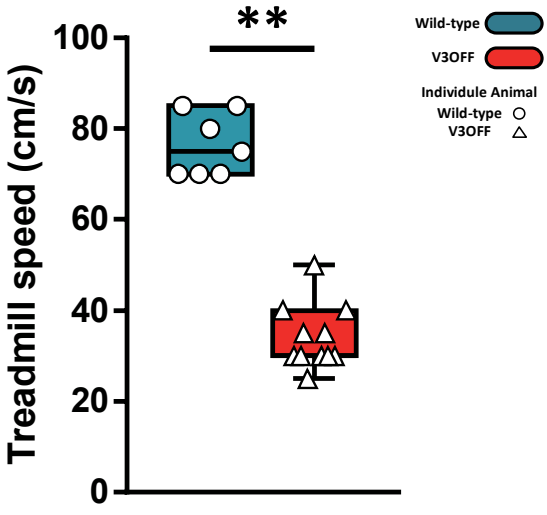

Supplementary Figure 2.1 Maximum speeds of WT and V3OFF mice on treadmill.

Histogram shows that the highest speed the V3OFF mice could reach was 40 cm/s (mean = 34.09 ± 7.006 cm/s, n=11), however, WT mice could in average reach 75 ± 7.559 cm/s (n=7) on the treadmill. **, $0.001 < P < 0.01$

Supplementary Figure 2.2 Diagram of foot coupling and examples of gait diagram of WT and V3OFF mice at low (15 cm/s and 25 cm/s) and medium (40 cm/s) speed.

Ai

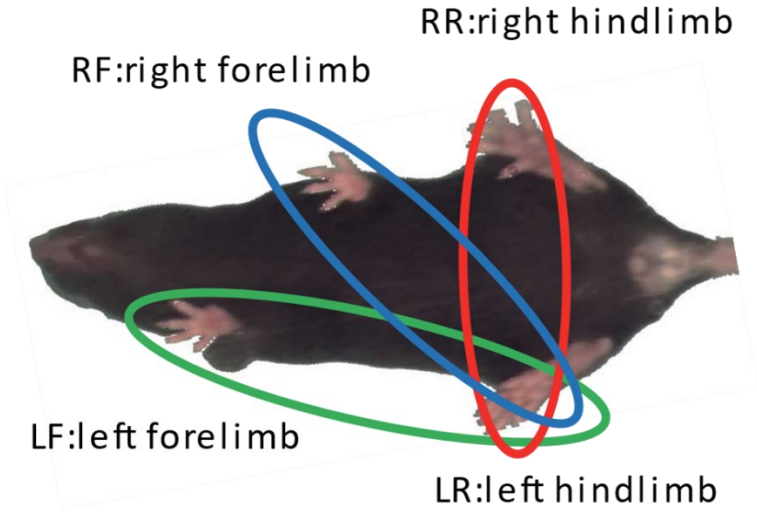

Aii

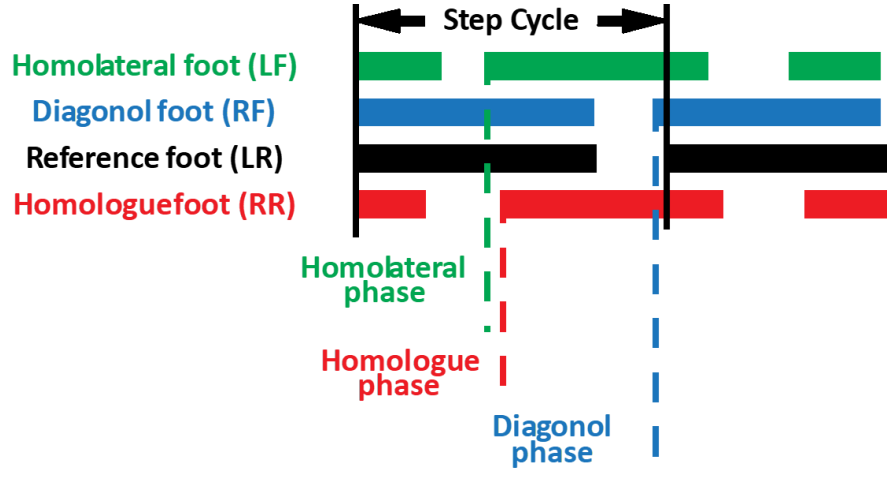

B

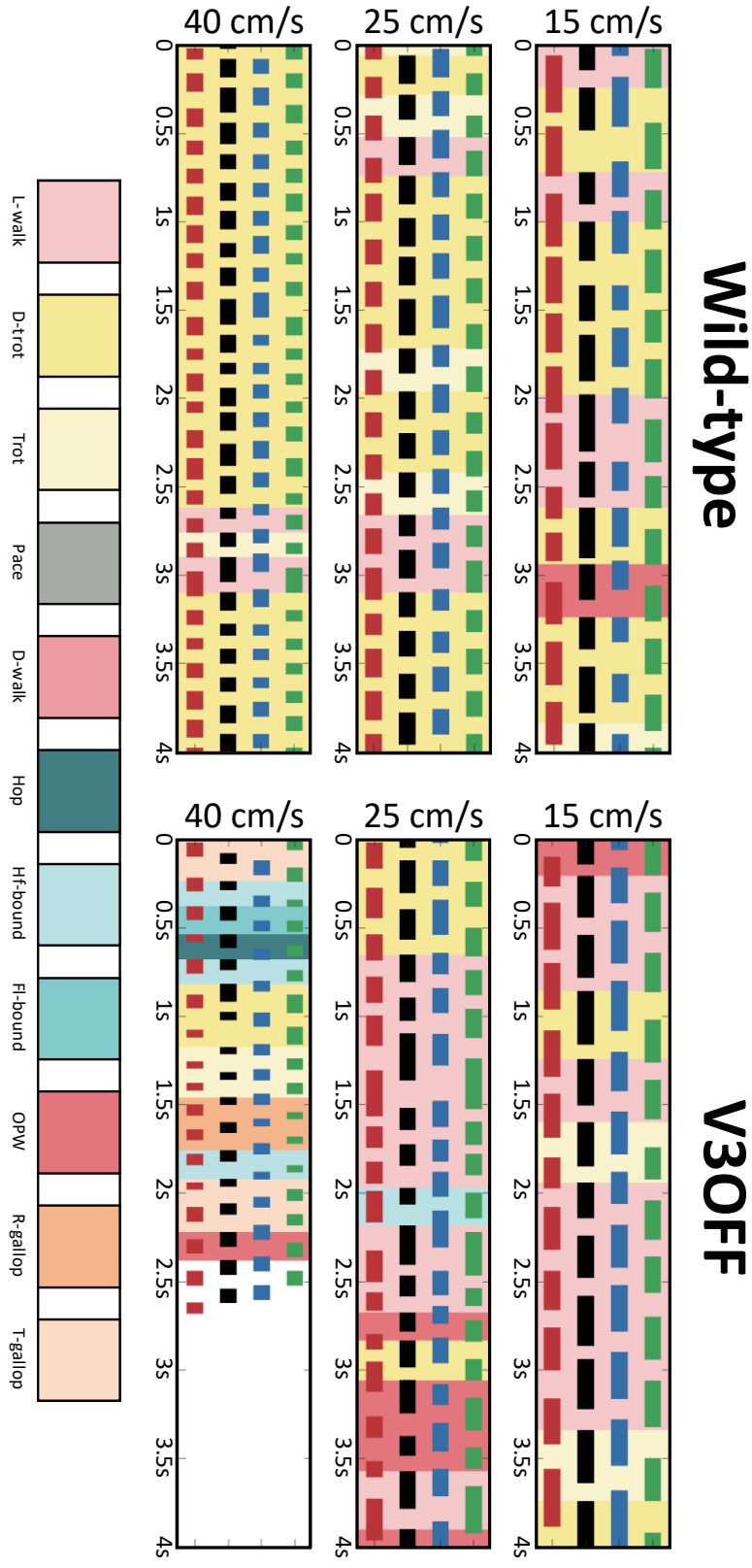
Wild-type
V3OFF
15 cm/s
25 cm/s
40 cm/s
0
0.5s
1s
1.5s
2s
2.5s
3s
3.5s
4s
L-walk
D-trot
Trot
Pace
D-walk
Hop
Hf-bound
Fl-bound
OPW
R-gallop
T-gallop

Supplementary Figure 2.2 Diagram of foot coupling and examples of gait diagram of WT and V3OFF mice at low (15 cm/s and 25 cm/s) and medium (40 cm/s) speed.

A. Homologous coupling was to describe the phase relationship between the same girdle. Homolateral coupling meant the phase relationship of the foot pair of same side. In our study, diagonal coupling was obtained from left rear-limb and right fore-limb as shown in i. The stance phase is shown with solid bar and swing phase is the interval between two bars. The step cycle was measured from the duration between the onset of contacts of two consecutive steps. Phase relationship was calculated by the duration of coupling foot contact to the first contact of reference foot divided by the current stride duration of reference foot.

B. The gait is colour-coded in the diagram. The black bars shows the stance phase of reference foot. The gait was identified by the combination of phase relationship, stance duty factor as previously described by Lemieux et al. (2016). The identification of D-trot was described in Method. L-walk: lateral-walking. D-trot: diagonal-trot. D-walk: diagonal-walk. Hf-bound: half-bound. Fl-bound: full-bound. OPW: out-of-phase walk. R-gallop: rotary-gallop. T-gallop: transverse-gallop.

Supplementary Figure 2.3 Foot couplings of WT and V3OFF mice at each speed.

A

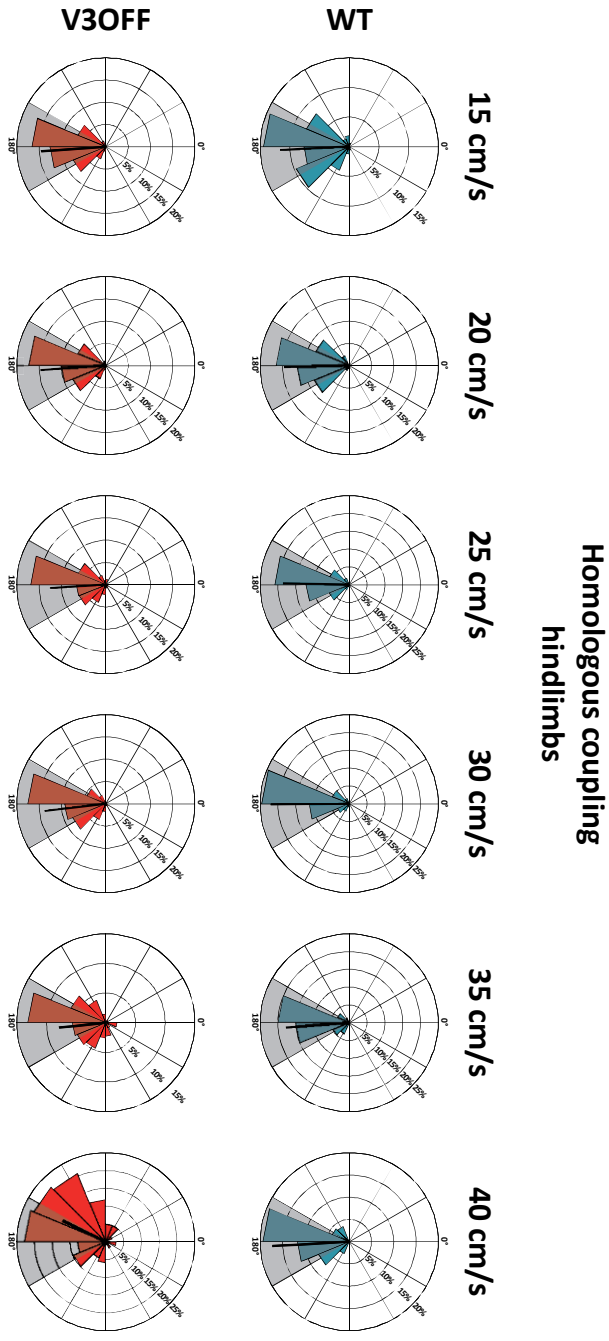

B

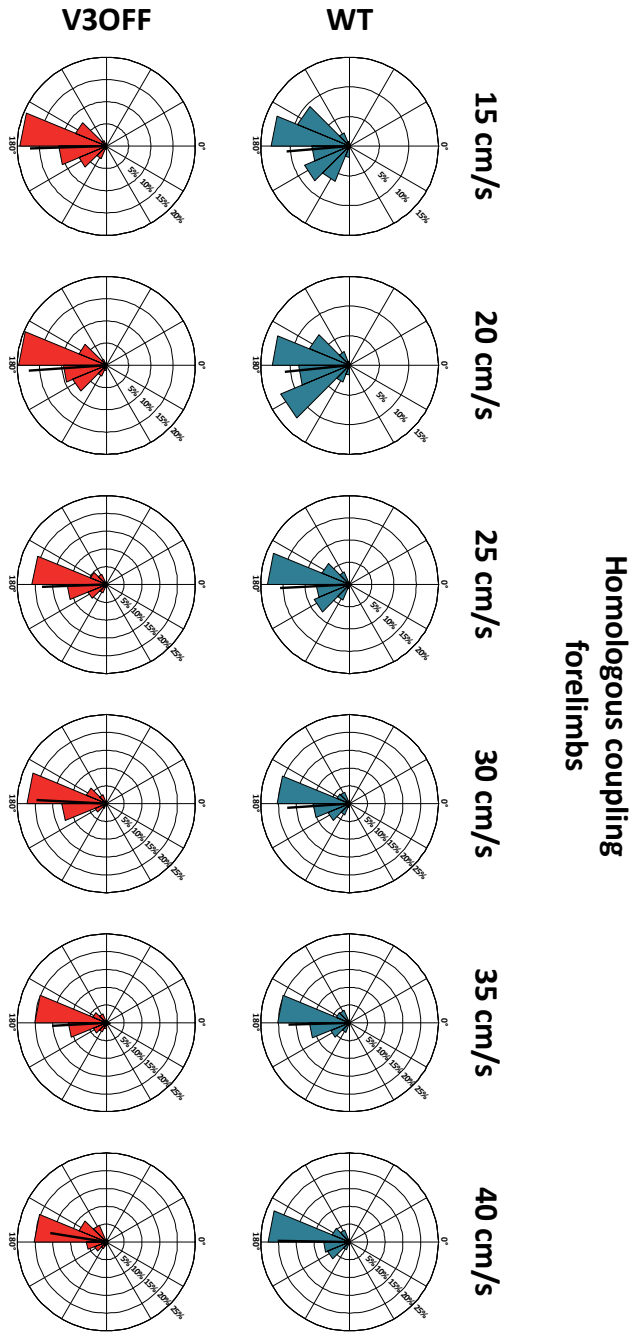
V3OFF
WT
15 cm/s
20 cm/s
25 cm/s
30 cm/s
35 cm/s
40 cm/s
Homologous coupling
forelimbs

C

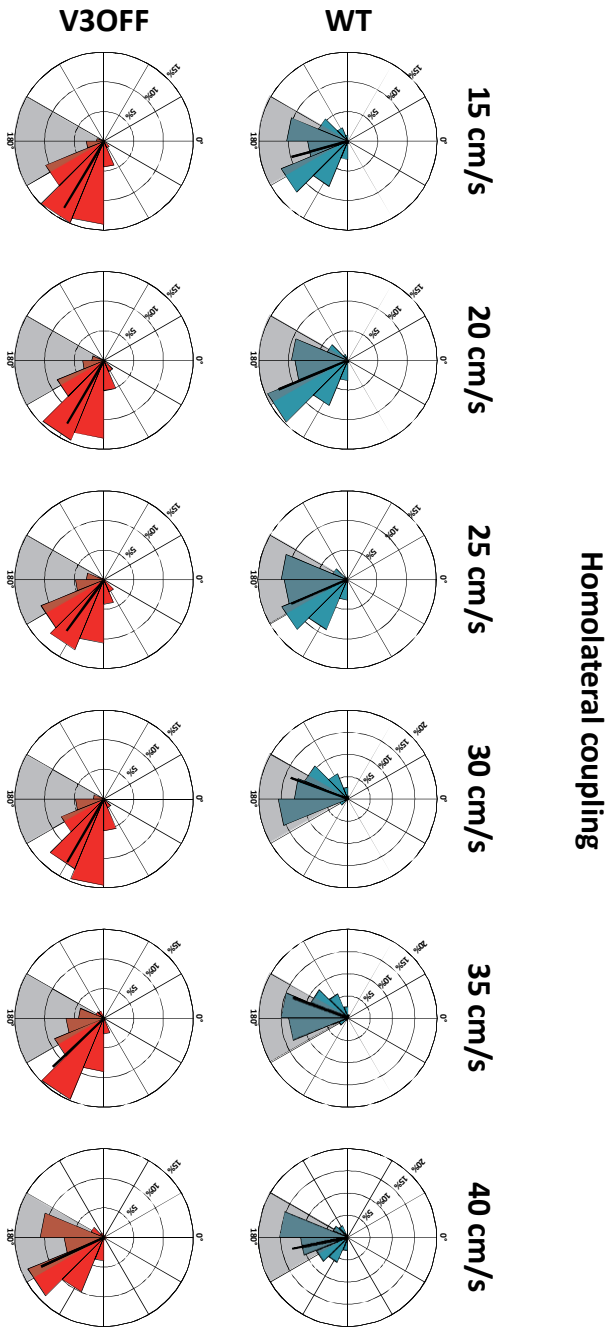
V3OFF
WT
15 cm/s
20 cm/s
25 cm/s
30 cm/s
35 cm/s
40 cm/s
Homolateral coupling

D

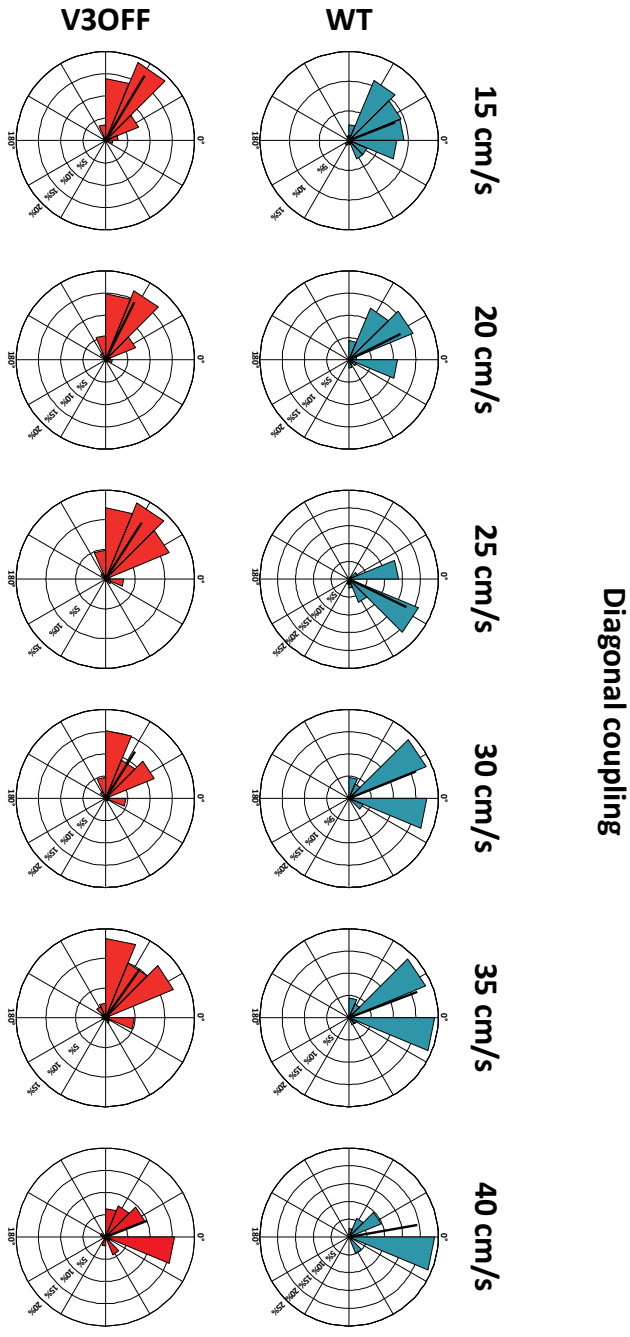
V3OFF
WT
15 cm/s
20 cm/s
25 cm/s
30 cm/s
35 cm/s
40 cm/s
Diagonal coupling

Supplementary Figure 2.3 Foot couplings of WT and V3OFF mice at each speed.

Circular plots show the mean phase coupling of all steps for (A) the left-right rear-limbs (homologous coupling, left rear-limb as reference), (B) the left-right fore-limbs (fore-limbs, left fore-limb as reference), (C) the left fore-limb and left rear-limb (homolateral coupling, left rear-limb as reference) and (D) right fore-limb and left rear-limb (diagonal coupling, left rear-limb as reference). Each vector (black bar in circular plot) indicates the mean phase (direction) and robustness (radio) of the coupling. The circle is evenly separated into 12 fractions. The circular histograms represent the distribution of coupling phase of all steps. The gray areas indicate the normal phase range observed from WT mice. The percentage numbers indicate the proportion of steps fallen into this phase out of all steps.

Supplementary Figure 2.4 Formula to calculate the occurrence, persistence and attractiveness.

Step sequence including gait A, B and C

A B A A B A C A A A

Formula for gait A:

$$\text{Occurence of A} = \frac{7A}{7A + 2B + 1C}$$

$$\text{Persistance of A} = \frac{3A\text{-}A}{3A\text{-}A + 1A\text{-}B + 1A\text{-}C}$$

$$\text{Attractiveness of A} = \frac{3A\text{-}A + 2B\text{-}A + 1C\text{-}A}{3A\text{-}A + 2B\text{-}A + 1C\text{-}A + 2A\text{-}B + 0B\text{-}B + 0C\text{-}B + 1A\text{-}C + 0B\text{-}C + 0C\text{-}C}$$

Supplementary Figure 2.4 Formula to calculate the occurrence, persistence, and attractiveness.

Example of a step sequence that include gait A, B and C. The occurrence was the percentage of certain gait out of total steps. The persistence of certain gait was the percentage of two consecutive steps that both have the same gait out of all the consecutive steps that include every possible transition circumstance starting from this gait. The attractiveness represent how attractive the certain gait is. To detect the attractiveness of certain gait, we first calculated the number of steps of this gait and then this value was subdivided by the total number of all possibilities that any type of gait transferred to this gait.

7 Table

Table 2.1 Correlation between phase relationship and speed.

	Homologous-hind		Homologous-fore		Homolateral		Diagonal	
	WT	V3OFF	WT	V3OFF	WT	V3OFF	WT	V3OFF
R (Phase)	0.09148	0.02567	0.229	0.07067	0.04319	0.4263	0.07241	0.3607
P value	0.4795	0.7891	0.0734	0.4611	0.7389	<0.0001	0.576	0.0001
R (StDv)	-0.3255	0.4152	-0.4395	0.04845	-0.375	0.2718	-0.364	0.4114
P value	0.0098	<0.0001	0.0004	0.6136	0.0027	0.0041	0.0036	<0.0001
R (Phase diff)	-0.4803	0.175	-0.4817	-0.03916	-0.1916	0.06693	-0.4413	0.3003
P value	<0.0001	0.0662	<0.0001	0.6833	0.1358	0.4852	0.0003	0.0014

CHAPTER 3. DIFFERENTIAL REGULATORY FUNCTION OF V3 INS IN DIFFERENT BEHAVIOURS

Contribution statement

I would like to acknowledge Dr. Christopher T. Jones for writing script for bootstrap method; Mingwei Liu for developing MATLAB toolbox. I performed all behaviour experiments, EMG implantation surgery, and statistical analysis described in this chapter. The MATLAB toolboxes for generating colour coded heating map and exporting the locomotion parameters were written by Mingwei Liu.

1 Summary

The high degree of coordination and individual flexibility of different joints in each limb ensure the smooth locomotion of all animals. Although it has long been understood that modular IN circuits in the spinal cords generate rhythmic activities that control these joint movements, the identity and organizational logic of the cells are still mostly unknown. Our series of studies have demonstrated that spinal V3 INs are crucial in generating coherent and stable gaits for animals. In the current study, through a systematic assessment of the kinematics and muscle activities of the hind-limbs of V3OFF mice during different locomotor activities, we discovered that V3 INs might play differential roles in spinal circuits that regulated the hip and ankle joints. We found that, without V3 INs, mice were unable to move their hip joints to full capacity while walking on a level or inclined treadmill or swimming. We then observed that, during walking on a level or inclined treadmill, V3OFF mice overextended their ankle joints when putting their feet on ground and exhibited less coherent hip and ankle movement. These outcomes could be due to disturbed activity patterns of hip flexor muscles, IP, and ankle extensor muscles, GS, in the transition from swing to stance. Furthermore, V3OFF mice also had insufficient propelling ankle muscle activities at the end of their stance phases. However, the phenotype of the ankle joint and the coordination of ankle and hip joints during swing-stance transitions only appeared during treadmill walking but not while swimming. In the end, after a spinal cord injury, V3OFF mice showed significantly fewer hip movements but regular knee and ankle movements during weight-supporting treadmill walking. These differences appeared to indicate that the involvement of V3 INs in distal joint regulation might be in a weight-bearing dependent manner. Therefore, we propose that spinal V3 INs may have multiple functional sub-populations that are involved in different modular circuits that regulate proximal or distal joints.

2 Introduction

To generate the huge variety of smooth movements displayed by animals, all the joints of their limbs have to tightly coordinate with each other and also maintain their own flexibility. Although a large body of research in the last several decades has shined some light on our understanding of neural circuits that control various motor behaviours, we still know little about the precise neural mechanisms underlying such tasks.

It has been suggested that in the spinal cord there are a series of IN circuits, known as central pattern generators (CPGs), which serve as modules to form a hierarchical organization (Grillner, 1981, 1985, 2006; Schouenborg, 2004; Bizzi et al., 2008; Stein, 2018). A variety of rhythmic movements comprising different motor patterns can be achieved by flexibly combining these different unit CPGs. For example, studies of the neuronal control of the turtle's hip and knee joint movements under different conditions strongly suggest the existence of separate hip- and knee-related spinal CPG modular circuits (Mortin et al., 1985; Robertson et al., 1985; Stein et al., 1995, 1998a, b; reviewed by Stein, 2018). Examinations of descending propriospinal IN firing pattern indicate that specific IN networks regulate hip- and knee-related spinal modules respectively (Stein and Daniels-McQueen, 2002, 2003, 2004). These modular circuits are broadly interconnected within the spinal cord (Grillner& El Manira, 2019; Kiehn, 2016; Pocratsky et al., 2017). At the same time, these circuits receive massive ascending sensory inputs as well as descending inputs from the brain to ensure that locomotion operates smoothly and is prepared to cope with any external or internal interruptions (Frigon & Rossigonal, 2006; Pearson, 2007; Grillner & El Manira, 2019).

One of the most important roles of sensory feedback during territorial locomotion is to control the timing of the phase transition between stance and swing. Stance-swing transition obviously plays a critical role in the maintenance and adjustment of speed, while swing-stance transition is a vital phase that ensures the correct placement of the feet during different locomotor tasks. It has been shown that the afferent feedbacks controlling hip position have the pivotal role in regulating both transitions (Andersson & Grillner, 1981, 1983; Grillner & Rossignol, 1978; Hieber et al., 1996; Kriellaars et al., 1994; Lam &

Pearson, 2001, 2002; McVea et al., 2005; Pearson & Duysens, 1976; Pearson & Rossignol, 1991). Additionally, the loading functions of ankle extensor muscles and cutaneous afferents emerging from mechanoreceptors in the foot have also been found to be an important factor in stance-swing transition (Dietz & Duysens, 2000; Frigon & Rossigonol, 2006; Donelan & Pearson, 2004; Duysens & Pearson, 1980; Whelan et al., 1995; Whelan & Pearson, 1997; Hiebert et al., 1995). Recently, small clusters of V1 IN subpopulations have been shown to receive specific sensory input from individual muscles, which implies that there could be particular IN groups serving as building blocks of individual joint CPG circuits (Bikoff et al., 2016).

V3 INs are a major group of glutamatergic commissural neurons located in the spinal cord. They are essential for producing coordinated, robust, and stable gaits. Our previous work has shown that V3 INs are highly heterogeneous and different subpopulations are activated differently for different locomotor tasks, such as walking or swimming. To further understand the function of V3 INs in locomotor activities, we systematically examined the kinematics and muscle activities of V3OFF mice. To our surprise, the V3OFF animals showed different defects in their hip and ankle joint movement under different locomotor tasks. Firstly, V3OFF mice had difficulties in moving their hip joints in all types of locomotion, including walking on a flat or inclined surface and during swimming, whereas defects in the timing and angular movement of ankle joints were only observed during weight-bearing behaviours, and not during swimming. Secondly, hip and ankle joint coordination during swing-stance transitions was also found weakened, which might be correlated with weakened contralateral ankle extension during the propelling phase, and only for weight-bearing behaviours. After complete thoracic spinal cord transection, V3OFF mice could hardly move their hips, but regained ankle movements similar to the WT animals during weight-supporting treadmill walking. Taking these results together, we suggest that spinal V3 INs are found in heterogeneous sub-populations that regulate proximal or distal joints differentially. At least, one subset of V3 INs adjusts hip joint excitability in all types of behaviours. The other subset of V3 INs regulates swing-stance transition only during weight-bearing movement.

3 Results

3.1 V3OFF mice have longer swing phase duration during treadmill walking.

In chapter 2, I indicated that V3OFF mice could not run fast. Particularly, after EMG electrodes implantation, we found that most V3OFF mice could only reach 20cm/s on a treadmill. Therefore, to evaluate the consistent leg movement of all tested mice, we set the treadmill at constant speed of 15cm/s for all the walking experiments.

Stance, swing, and stride duration were measured by manually tracing the toe on and off the ground in the videos recorded from the sideview of the animals (Figure 3.1Ai, ii). We found that the swing duration average of V3OFF mice (n = 14) was significantly longer than WT (n = 12) (Mean $_{WT}$ = 0.10 ± 0.017s, Mean $_{V3OFF}$ = 0.12 ± 0.02s, P = 0.0006), whereas the averaged stance duration remained similar (Mean $_{WT}$ = 0.23 ± 0.02s, Mean $_{V3OFF}$ = 0.22 ± 0.04s, P = 0.4786), as well as the stride duration (Mean $_{WT}$ = 0.33 ± 0.03s, Mean $_{V3OFF}$ = 0.35 ± 0.04s, P = 0.1862) (Figure 3.1Bi). Meanwhile, the stride duration of each V3OFF mouse was unstable (StDv $_{WT}$ = 0.05 ± 0.01s, StDv $_{V3OFF}$ = 0.07 ± 0.02s, P = 0.0200) (Figure 3.1Bii). This larger StDv was accompanied by a more variable swing duration (StDv $_{WT}$ = 0.02 ± 0.01s, StDv $_{V3OFF}$ = 0.02 ± 0.01s, P = 0.0200) but not stance duration (StDv $_{WT}$ = 0.043 ± 0.02s, StDv $_{V3OFF}$ = 0.05 ± 0.02s, P = 0.1040) (Figure 3.1Bii). This indicates that silencing V3 INs disturbs the timing of swing phases, which leads to an unstable stepping in V3OFF mice during treadmill walking.

3.2 Defects in hip and ankle joint movements of V3OFF mice during treadmill walking.

To further explore the causation of the walking defects in V3OFF mice, we tracked angular movements of hip and ankle joints using the reflective markers attached on one side of crest, hip, knee, ankle, paw, and toe (Figure 3.1A and 3.2A). Based on the peak and trough of joint angular values, the step cycle can be subdivided into different phases for each joint. For the hip joint, it flexes during swing, and extends during stance; for the ankle joint, each

step cycle includes the flexion phase and E1 phase, in swing, and another flexion phase (yield phase) and an extension phase (propel phase) during stance (Figure 3.2B) (Halbertsma, 1983; Grillner, 1981; Phillipson, 1905; Rossignol, 1996).

We found that the degrees of hip joint excursion in V3OFF mice (n = 14) were always smaller than WTs (n = 12) (hip flexion $_{WT}$ = 37.69 ± 4.32 º, hip flexion $_{V3OFF}$ = 26.75 ± 9.21 º, P = 0.0009; hip extension $_{WT}$ = 37.74 ± 4.51 º, hip extension $_{V3OFF}$ = 26.7 ± 9.29 º, P = 0.0006) (Figure3.2C top traces, Figure 3.3Ai). However, the phase duration of hip flexion and extension was not significantly different between V3OFF and WT mice (hip flexion $_{WT}$ = 0.1034 ± 0.02071s, hip flexion $_{V3OFF}$ = 0.10 ± 0.02s, P = 0.3067; hip extension $_{WT}$ = 0.23 ± 0.03s, hip extension $_{V3OFF}$ = 0.25 ± 0.04s, P = 0.0544) (Figure 3.2C top traces, Figure 3.3Bi). We did not find any differences in temporal or spatial angular parameters of knee joint movement between WT and V3OFF mice (data are not shown).

On the other hand, the changes of the ankle joint angular excursion were more complicated (Figure 3.2C bottom traces). As we mentioned above, the ankle joint goes through two consecutive two-phase-movement during both swing and stance phases in each step. During swing, the mean value of E1 duration and its StDv of V3OFF mice were significantly larger than WTs (Mean $_{WT}$ = 0.050 ± 0.011s, Mean $_{V3OFF}$ = 0.079 ± 0.015s, P <0.0001; StDv $_{WT}$ = 0.011 ± 0.0041s, StDv $_{V3OFF}$ = 0.019 ± 0.0061s, P = 0.0016) (Figure 3.3Bii). Ankle joint angular movement during E1 was also increased (Mean $_{WT}$ = 46.32 ± 15.02 º, Mean $_{V3OFF}$ = 70.63 ± 14.37 º, P = 0.0004) (Figure 3.3Aii) shown as over-reaching during swing phase (Mean $_{WT}$ = 1.8 ± 0.22cm, Mean $_{V3OFF}$ = 2.12 ± 0.46cm, P = 0.0324; StDv $_{WT}$ = 0.19 ± 0.047cm, StDv $_{V3OFF}$ = 0.26 ± 0.091cm, P = 0.020) (Sup Figure 3.1Ai, Bi, Ci). This increased E1 excursion and duration could account for the longer swing duration in V3OFF mice seen above, and it also led to an over-reaching position of the foot while landing on the ground. During stance phase, compared to WTs, V3OFF mice flexed more of their ankle joints during yield phase, but had smaller propelling movements (yield: Mean $_{WT}$ = 17.55 ± 7.47 º, Mean $_{V3OFF}$ = 31.11 ± 13.24 º, P = 0.0044; propel, Mean $_{WT}$ = 43.24 ± 14.75 º, Mean $_{V3OFF}$ = 23.86 ± 7.75 º, P = 0.0003) (Figure 3.2Aii & Bii). Therefore, at the end of the stance phase before toe lifting, the position of the toe relative to the hip horizontal position in V3OFF mice is shorter than WT animals. (Mean $_{WT}$ = 1.35 ± 0.27cm,

Mean $_{V3OFF}$ = 0.78 ± 0.34cm, P < 0.0001; StDv $_{WT}$ = 0.32 ± 0.11cm, StDv $_{V3OFF}$ = 0.32 ± 0.069cm, P = 0.83) (Sup Figure 3.1Aii, Bii, Cii). This lack of extension in their hindlimbs during propel phase would have caused less sufficient force for V3OFF animals to push their body moving forward.; propel, Mean WT = 43.24 ± 14.75 º, Mean V3OFF = 23.86 ± 7.75 º, P = 0.0003) (Figure 3.2Aii & Bii). Therefore, at the end of the stance phase before toe lifting, the position of the toe relative to the hip horizontal position in V3OFF mice was shorter than WT animals. (Mean WT = 1.35 ± 0.27cm, Mean V3OFF = 0.78 ± 0.34cm, P < 0.0001; StDv WT = 0.32 ± 0.11cm, StDv V3OFF = 0.32 ± 0.069cm, P = 0.8287) (Sup Figure 3.1Aii, Bii, Cii). This lack of extension in their hindlimbs during propel phase would have caused less sufficient force for V3OFF animals to push their body moving forward.

It has been shown that animals always display stereotypical and time-controlled sequential movements of hindlimb joints during treadmill walking at any constant speeds (Halbertsma, 1983). However, the combination of the unchanged hip flexion phase with a longer ankle E1 phase in V3OFF mice suggests that the timing of hip and ankle movement may be differentially changed by the V3 deletion. Accordingly, we measured the latency between the end of hip flexion phase and the termination of ankle extension in E1 phase or the moment when toe contacting the ground in WT and V3OFF mice (Figure 3.2C). Not surprisingly, WT mice showed a tightly synchronized movement between hip and distal joint with little time laps (delay ankle to hip = 0.0092 ± 0.0059s; delay toe to hip = 0.011 ± 0.0074s, n=12) (Figure 3.2C). However, V3OFF mice showed much delayed ending of ankle E1 phase or toe touching relative to the end of hip flexion (delay ankle to hip = 0.039 ± 0.016s; delay toe to hip = 0.043 ± 0.017s, n=14) (P <0.0001) (Figure 3.2C).

Taking together, we suggest that functional elimination of V3 INs resulted in a smaller hip joint movement and larger ankle extension, which led to a delayed hip-ankle coordination during swing-stance transition and incorrect foot placement during treadmill walking. Furthermore, V3OFF mice also had smaller ankle propulsion at the end of stance phase, which might have indicated an insufficient propelling power to move them forward.

3.3 Weight-bearing dependent function of V3 INs in coordinating the IP and GS activities during swing-stance transition phase.

These defects of hip and ankle joint movements, particularly at swing-stance transition and later stance phase, in V3-OFF mice prompted us to investigate if there were any dysregulations of particular muscle activities. We then measured the activities of hip muscles, IP and BF, and ankle extensor muscle, GS, in WT and V3OFF mice (Figure 3.4, Sup Figure 3.2). During swing-stance transition, IP muscle ended its activity to finish hip flexion, while BF started the hip extension and GS activity initiates during E1 ankle extension, respectively (Figure 3.4A, B, C). Using statistical parametric mapping (SPM), we could compare the EMG recordings during defined periods in V3OFF and WT mice. Interestingly, we noticed that the activity pattern of BF muscle was similar between V3OFF and WT animals during the entire activation period (Figure 3.4B), while IP and GS showed significant differences at different periods, particularly at swing-stance transition for both muscles, and in the propelling phase for GS (Figure 3.4A).

To further reveal the activity pattern of IP and GS during swing-stance transition period, we bootstrapped the traces of the EMG recordings from these two muscles to overcome the issue of low signal-noise ratio and high variability of EMG recordings in mice (Figure 3.5A). To accurately show the pattern changes, we processed EMG data in different episodes during the swing-stance transition period for each muscle. For IP, the episode started at 100ms prior to and ended at 50ms after the toe touching the ground, as IP reached the peak activity around 50ms before the toe touching the ground but its activity diminished after the toe touching the ground (Figure 3.4C, D). For GS, the episode was chosen to start at 50ms prior to and end at 100ms after the toe touching the ground, since GS was not activated till 50ms before the toe touching the ground and its activity would reach the peak around 50ms after the toe touching the ground (Figure 3.4C, D).

We found that in WT mice, IP activity reached the peak ~ 50ms prior to toe touching the ground (Figure 3.5Ai, Bii), but then started decreasing quickly and reached the resting state before toe touching the ground (Figure 3.5Ai, Bi). The decline took ~35ms. The GS was activated ~30ms prior to toe touching (Figure 3.5Aii) and quickly reached the peak within

5-10ms (Figure 3.5Bii). For V3OFF mice, however, the activity of their IP muscles reached the peak ~70ms prior to toe touching and was not completely inhibited even after toe touching (Figure 3.5Ai, Bii). Meanwhile, GS muscle of V3OFF mice was activated ~30ms before toe touching, which was similar to WT mice, but its activity did not reach the peak ~15ms after toe touching (Figure 3.5Aii, Bii). Accordingly, the distribution histograms of the slopes for IP termination phase and those for GS onset phase for WT and V3OFF mice were clearly separated (Figure 3.5Bi). The slope of IP in V3OFF was always larger than WT's, while the slope of GS in V3OFF was smaller (Figure 3.5Bi). Therefore, the absence of V3 INs might not affect the initiation of the swing-stance transition, but it might have cancelled feed forward regulatory signals to quickly terminate hip flexor or intensify the force of ankle extensor to move the corresponding joints precisely and smoothly at the swing-stance transition phase.

Such lack of the ability to build up intensified muscle activity was also shown in GS activity during ankle propelling phase in V3OFF mice, as we described earlier (Figure 3.4A). Interestingly, during slow walking, the ankle propelling phase usually superimpose with contralateral swing-stance transition phase (Sup Figure 3.2). We applied statistical parametric mapping (SPM) to identify regionally specific effects in GS (Sup Figure 3.2). When we superimposed the EMG traces of contralateral GS (oGS) with the trajectory ipsilateral leg movement, we found the weakened activity of oGS starting at ~30ms prior to ipsilateral foot touching ground to ~30ms after toe touching ground (Sup Figure 3.2). Thus, we speculated that the activity of oGS might have contributed to inhibit ipsilateral hip flexor but strengthened ipsilateral ankle extensor activity during swing-stance transition, and such left-right synchronization could have been mediated by V3 INs. Since one of the most important functions of GS muscle is to support body weight during walking, we further hypothesized that this V3 INs-mediated regulation of muscle activities could also be weight-bearing dependent.

3.4 V3 INs mediated regulations of joint movements with or without weight-bearing behaviours.

To test if V3 INs mediated regulations of hip and ankle movements were related to weight-bearing behaviours, we examined kinematics and EMG activities of V3OFF and WT mice during a weight-bearing increased activity, walking on inclined treadmill, and a task without weight-bearing behaviour, the swimming.

During inclined treadmill walking, V3OFF mice displayed very similar step cycles as they walking on flat surface. The means of their swing durations in V3OFF mice were larger than those in WT mice (Mean $_{WT}$ = 0.084 ± 0.021 s, Mean $_{V3OFF}$ = 0.12 ± 0.020 s, P = 0.0004) (Figure 3.6Ai). This longer swing duration led to longer stride duration in V3OFF mice (Mean $_{WT}$ = 0.32 ± 0.033 s, Mean $_{V3OFF}$ = 0.38 ± 0.034 s, P = 0.0009), but stance duration still did not show any difference between the two groups (Mean $_{WT}$ = 0.24 ± 0.026 s, Mean $_{V3OFF}$ = 0.26 ± 0.034 s, P = 0.1489) (Figure 3.6Ai). The steps in V3OFF mice became quite unstable with extremely higher StDv values in swing, stance and stride durations compared to those in WT mice (Swing: StDv $_{WT}$ = 0.015 ± 0.0073 s, StDv $_{V3OFF}$ = 0.023 ± 0.010 s, P = 0.046; Stance: StDv $_{WT}$ = 0.036 ± 0.023s, StDv $_{V3OFF}$ = 0.070 ± 0.026 s, P = 0.0007; Stride: StDv $_{WT}$ = 0.041 ± 0.024 s, StDv $_{V3OFF}$ = 0.081 ± 0.027 s, P = 0,0008) (Figure 3.6Aii).

During swimming, instead of swing and stance phases, mice flex (protraction) or extend (retraction) their limbs for each stroke. Interesting, we found no significant differences between WT and V3OFF mice in either of these phases during swimming (Protraction: Mean $_{WT}$ = 0.15 ± 0.021 s, Mean $_{V3OFF}$ = 0.16 ± 0.043 s, P = 0.6409; Retraction: Mean $_{WT}$ = 0.066 ± 0.011 s, Mean $_{V3OFF}$ = 0.070 ± 0.024 s, P = 0.9627; Step cycle: Mean $_{WT}$ = 0.22 ± 0.020 s, Mean $_{V3OFF}$ = 0.23 ± 0.063 s, P = 0.6004) (Protraction: StDv $_{WT}$ = 0.018 ± 0.0071 s, StDv $_{V3OFF}$ = 0.037 ± 0.024 s, P = 0.1047; Retraction: StDv $_{WT}$ = 0.0094 ± 0.0046 s, StDv $_{V3OFF}$ = 0.012 ± 0.0083 s, P = 0.4283; Step cycle: StDv $_{WT}$ = 0.020 ± 0.0063 s, StDv $_{V3OFF}$ = 0.039 ± 0.025 s, P = 0.1189) (Figure 3.6B).

3.4.1 V3OFF mice moved their hip less during all locomotor tasks.

Across different locomotor tasks in our experiments, walking, inclined-walking, and swimming, WT mice displayed similar ranges of hip motions (Figure 3.2C, 3.3Ai & 7A,

Bi & 8A, B). However, V3OFF mice always had smaller hip movement compared to WT mice in the same tasks.

Similarly to walking on flat treadmill, in the inclined-walking task, V3OFF mice (n= 11) showed less hip flexion and extension excursions than those of WT mice (n = 12) (Flexion: Mean $_{WT}$ = 42.27 ± 5.042 º, Mean $_{V3OFF}$ = 34.18 ± 8.37 º, P = 0.0098; Extension: Mean $_{WT}$ = 42.29 ± 5.17 º, Mean $_{V3OFF}$ = 33.73 ± 8.65 º, P = 0.0083) (Figure 3.7A hip traces & Bi). The hip flexion duration did not show any significant difference in WT and V3OFF mice (Mean $_{WT}$ = 0.10 ± 0.029 s, Mean $_{V3OFF}$ = 0.095 ± 0.022 s, P = 0.4102) (Sup Figure 3.3A). However, the mean of hip extension phase duration in V3OFF mice was significantly shorter than WTs (Mean $_{WT}$ = 0.27 ± 0.036 s, Mean $_{V3OFF}$ = 0.22 ± 0.029 s, P = 0.0028) (Sup Figure 3.3A).

During swimming, V3OFF mice exhibited smaller hip joint movement in either flexion (protraction) or extension (retraction) (Figure 3.8A). The excursion of hip flexion (protraction) and extension (retraction) were significantly smaller in V3OFF (n = 6) than WTs (n = 7) (Flexion: Mean $_{WT}$ = 45.78 ± 15.46 º, Mean $_{V3OFF}$ = 22.46 ± 5.27 º, P = 0.0062; Extension: Mean $_{WT}$ = 45.55 ± 15.41 º, Mean $_{V3OFF}$ = 22.67 ± 5.02 º, P = 0.0068) (Figure 3.8A, B). However, the phase duration of V3OFF mice during swimming were not shown significant different with those in WT (Flexion: Mean $_{WT}$ = 0.14 ± 0.020 s, Mean $_{V3OFF}$ = 0.14 ± 0.033 s, P = 0.8350; Extension: Mean $_{WT}$ = 0.074 ± 0.014 s, Mean $_{V3OFF}$ = 0.092 ± 0.037 s, P = 0.30) (Sup Figure 3.3B). Therefore, V3 INs may facilitate the hip movement in all locomotor behaviours and this function is not weight-bearing dependent.

3.4.2 Weight-bearing dependent function of V3 INs on distal joint movements and their coordination with hip joint.

During inclined-walking, similar to walking on flat surface, the step cycle can also be subdivided into one flexion phase and three extension phases, E1, yield and propel phases following ankle joint positions. During swimming, due to less restriction on their hip movement, mice sometimes move their leg in the transverse plane. Our single camera from one side of the body would not be able to catch the three-dimensional movements. Therefore, we were unable to study the full movement of ankle joint during swimming.

Instead, however, we traced the reflective marker on the toe of the mouse during swimming and used the toe trajectory to represent the distal joint movement and examine its relationship with the hip joint.

The relative changes of ankle movements of V3OFF mice compared to WT animals during inclined treadmill walking were similar to what we saw in treadmill walking on flat surface. For example, the duration and excursion of E1 phase in V3OFF mice were significantly increased (Phase duration: Mean $_{WT}$ = 0.040 ± 0.011 s, Mean $_{V3OFF}$ = 0.065 ± 0.015 s, P = 0.0003; Excursion: Mean $_{WT}$ = 37.08 ± 9.87 º, Mean $_{V3OFF}$ = 64.6 ± 9.13 º, P < 0.0001) (Figure 3.7A, Bii, iii) with increased ankle joint angular displacements during yielding but decreased propelling movement compared to WT mice (yield: Mean $_{WT}$ = 15.36 ± 6.81 º, Mean $_{V3OFF}$ = 27.79 ± 8.43 º, P = 0.0008; propel, Mean $_{WT}$ = 54.07 ± 9.30 º, Mean $_{V3OFF}$ = 39.5 ± 12.17 º, P = 0.0039) (Figure 3.7Biii), although V3OFF mice had longer yielding phase duration than WTs during inclined treadmill walking, which wasn't seen on flat surface (Mean $_{WT}$ = 0.0702 ± 0.01824 s, Mean $_{V3OFF}$ = 0.095 ± 0.025 s, P = 0.017) (Figure 3.7Bii). Nonetheless, the longer delay of ankle E1 extension termination/toe touch relative to the hip flexion termination still remained in V3OFF mice (delay ankle to hip: WT = 0.010 ± 0.004 s, n=12; V3OFF = 0.031 ± 0.011 s, n=11; P < 0.0001. delay toe to hip: WT = 0.012 ± 0.005 s, n=12; V3OFF = 0.034 ± 0.011 s, n=11; P < 0.0001) (Figure 3.7C).

During normal mouse swimming, there was a latency of the time between toe reach anterior extreme and the termination of hip flexion. This latency was similar in V3OFF mice (delay toe to hip: WT = -0.0078 ± 0.0130 s, n=7; V3OFF = -0.0028 ± 0.0142 s, n=6; P= 0.3328) (Figure 3.8C). Therefore, the dysregulation of ankle movement and the coordination of hip and distal joints during swing-stance transition phase during walking could be weight-bearing context dependent.

3.4.3 Weight-bearing dependent regulation of the hip flexor/ankle extensor activities mediated by V3 INs during swing-stance transition phase.

To further understand the task-dependency of V3 functions, we analysed the muscle activities of V3OFF and WT mice during these two behaviours.

We observed that during inclined-walking, V3OFF mice displayed similar changes in IP and GS activities as what we discovered in their walking on the flat surface (Figure 3.9A, B; Figure 3.10A). All the parameters that we measured for termination of IP activity and the activation of GS for V3OFF mice showed similar trends as walking on flat surface and were all significantly different from WT mice under the same conditions (Figure 3.9A, B). Interestingly, during inclined walking, the peaks of GS activities of WT mice were shifted to ~6ms after the toe touching the ground, while, correspondingly, the peaks of GS activity in V3OFF mice were shifted to even further, ~25ms after toe touching ground (Figure 3.10Aii).

Conversely, during swimming, the descending slope of IP activity of V3OFF mice were almost overlapped with those of WT mice (Figure 3.9C & 3.10Bi, ii). Most of arising rate (the slope) for the GS activity of V3OFF mice was even more positive than that of WT (Figure 3.10Bi, ii). This means the deceleration of IP activity was similar between V3OFF and WT mice; but the acceleration of GS activity of V3OFF mice was faster than WT mice (also see Figure 3.10Bi, ii). The peak positions of IP and GS activities were closer to each other in V3OFF mice than WT mice (Figure 3.10Bi, ii). The discrepancy of IP/GS transition in inclined treadmill walking and swimming verifies our hypothesis that one function of V3 INs is to coordinate the hip flexor and ankle extensor activity transition and it is weight-bearing behavioural context dependent.

Furthermore, the discrepancy of ankle extensor muscle regulation during different locomotor tasks in V3OFF mice was also shown in the changes of the rectified and smoothened EMG activities (Figure 3.11). We found, for WT mice, all extensor muscle activities during inclined treadmill walking were increased ~85% compared to level treadmill walking (BF = 1.09 ± 0.48, n = 9; VL = 0.85 ± 0.73, n = 12; GS = 0.75 ± 0.43, n = 8) (Figure 3.11Bi). In comparison, however, V3OFF mice had much smaller increase in all extensor muscle activities (BF = 0.38 ± 0.34, n = 7; VL = -0.10 ± 0.18, n = 9; GS = 0.20 ± 0.29, n = 7) ($P_{BF} = 0.0051$, $P_{VL} < 0.0001$, $P_{GS} = 0.0127$) (Figure 3.11Bi). Moreover, the increase of IP integrated EMG (iEMG) activity in V3OFF mice during inclined treadmill walking was also smaller than those of WT ($IP_{WT} = 0.32 \pm 0.22$, n = 6; $IP_{V3OFF} = 0.01 \pm 0.20$, n = 8; $P_{IP} = 0.0385$) (Figure 3.11Bi). By contrast, during swimming, the increases of

iEMG of GS in V3OFF mice (GS_{V3OFF} = 1.9 ± 1.8, n = 7) did not shown statistically significant difference with those in WT mice (GS_{WT} = 3.5 ± 2.3, n = 8) (P = 0.1181) (Figure 3.11Bii). On the other hand, the hip muscles of V3OFF mice were not increased as much as that observed in WT (IP_{WT} = 0.52 ± 0.56, n = 6; IP_{V3OFF} = -0.07 ± 0.38, n = 7; BF_{WT} = 4.8 ± 1.3, n = 9; BF_{V3OFF} = 0.48 ± 0.54, n = 7) (P_{IP} = 0.048; P_{BF} <0.0001) (Figure 3.11Bii).

Therefore, we conclude that subsets of V3 INs may provide excitatory drives to the core motor circuits that control hip movement for all locomotor tasks; different subsets may regulate hip/distal joint coordination during swing-stance transition phase only in weight-bearing behaviours, like walking and inclined-walking. These two groups V3 INs could be recruited simultaneously for some tasks.

3.5 V3OFF mice did not recover the hip excursion after spinal cord injury.

Finally, to verify the phenotypes displayed by V3OFF were due to the deletion of spinal V3 INs, we analyzed the kinematics of hip and ankle joint in spinal WT and V3OFF mice. After spinal cord transection of T10-11 spinal cord segment, the mice were subjected to treadmill walking with the body weight supported. This task mimics the circumstance of none weight-bearing treadmill walking. The V3OFF mice did not recover any locomotor behaviour in the first post-surgery week. Therefore, the analysis of kinematics starts from the second post-surgery week and end at the sixth post-surgery week (Figure 3.12A). WT mice started recovery of hip joint and horizontal toe movement since the third post-surgery week. At post-surgery week six, with weight support, WT mice almost showed regular limb movement on the treadmill at low speed (Hip: Wk2 = 25.3 ± 7.6 º, Wk3 = 35.52 ± 3.64 º, Wk4 = 27.35 ± 3.42 º, Wk5 = 27.67 ± 5.96 º, Wk6 = 31.41 ± 4.42 º, n = 3. Horizontal toe: Wk2 = 1.40 ± 0.61cm, Wk3 = 2.04 ± 0.12cm, Wk4 = 1.9 ± 0.13cm, Wk5 = 1.9 ± 0.31cm, Wk6 = 2 ± 0.24cm, n = 3) (Figure 3.12A, Bi and Ci). However, V3OFF mice still could not move their hip joint until the sixth post-surgery week which was also shown as less toe horizontal movement (Hip: Wk2 = 11.07 ± 4.5 º, Wk3 = 7.6 ± 2.9 º, Wk4 = 15.68 ± 1.84 º, Wk5 = 14.4 ± 4.39 º, Wk6 = 15.27 ± 5.56 º, n = 3. Horizontal toe: Wk2 = 0.62 ± 0.27cm, Wk3 = 0.85 ± 0.21cm, Wk4 = 1.05 ± 0.17 cm, Wk5 = 0.99 ± 0.50 cm, Wk6 = 0.96

± 0.40 cm, n = 3) (Hip: $P_{Wk2} = 0.0493$, $P_{Wk3} = 0.0005$, $P_{Wk4} = 0.0065$, $P_{Wk5} = 0.0362$, $P_{Wk6} = 0.0170$. Horizontal toe: $P_{Wk2} = 0.1144$, $P_{Wk3} = 0.0011$, $P_{Wk4} = 0.0026$, $P_{Wk5} = 0.0499$, $P_{Wk6} = 0.0179$) (Figure 3.12A, Bi and Ci). Conversely, their ankle joint movements were recovered since the second post-surgery week which did not show difference with WT (WT: Wk2 = 60.59 ± 18.39 º, Wk3 = 55.23 ± 6.35 º, Wk4 = 57.21 ± 7.08 º, Wk5 = 52.72 ± 1.93 º, Wk6 = 58.3 ± 16.64 º, n = 3; V3OFF: Wk2 = 39.57 ± 10.06 º, Wk3 = 46.93 ± 11.31 º, Wk4 = 52.1 ± 8.48 º, Wk5 = 40.85 ± 8.51 º, Wk6 = 36.78 ± 19.94 º, n = 3). In addition, we could also observe the normal toe vertical movement since the second post-surgery week (WT: Wk2 = 0.18 ± 0.08 cm, Wk3 = 0.20 ± 0.08 cm, Wk4 = 0.29 ± 0.07cm, Wk5 = 0.31 ± 0.06 cm, Wk6 = 0.23 ± 0.09cm, n = 3. V3OFF: Wk2 = 0.20 ± 0.13cm, Wk3 = 0.18 ± 0.07cm, Wk4 = 0.33 ± 0.22cm, Wk5 = 0.33 ± 0.11cm, Wk6 = 0.32 ± 0.28cm, n = 3). In conclusion, spinal V3 INs are crucial for the hip joint movement and would be a key component in hip CPG modular circuits.

4 Discussion

In the current study, we have systematically examined the kinematics and EMG activities of V3OFF mice. We have observed that V3 INs had two main regulatory roles in locomotor control. The first one was weight-bearing dependent regulation of multiple muscle activity patterns during the swing-stance transition phase. The other one was facilitating hip joint angular excursion across all tested locomotor tasks. This study illustrates the behavioural context dependency of the functions of V3 INs, which further indicates the flexibility of the modular hierarchical organization of this IN locomotor circuitry.

4.1 V3 INs are involved in the regulation of swing-stance transition only during weight-bearing behaviours

The first main phenotype we observed in V3OFF mice was the uncoordinated movements of hip-distal joint during the swing-stance transition. V3OFF mice exhibited a longer transition during the swing phase accompanied by more variable StDv of swing phase duration, which resulted in an unstable gait. The hindlimb landing of V3OFF was also more anterior than WT. We suggest that these defects were caused by a longer ankle E1

phase as the duration of the hip flexion and extension did not show any difference between WT and V3OFF mice. These data indicate that in V3OFF mice, hip-distal joint coordination was interrupted during the swing-stance transition phase. Further analysis of the muscle activity patterns of the hip flexor muscle, IP, and the ankle extensor muscle, GS, in V3OFF mice indicates that the flexor-extensor transition was not as decisive as that of the WT mice during swing-stance transition.

Incline-walk is a type of walking that involves some important changes in the joint angles of the hind limbs and several notable changes in muscle recruitments (Donelan & Pearson, 2004; Frigon & Rossignol, 2006). Swimming is another stereotypical locomotion that is assumed to recruit a similar neural organization as walking, but it may be simpler because of less GTO-derived signals due to the fact that the body weight is supported by buoyancy (Dagg & Windsor, 1971; Gruner & Altman, 1980; Takeoka et al., 2014; Akay et al., 2015; Satoh et al., 2016). We found similar defects in V3OFF mice during increased weight-loading inclined-walking. On the contrary, during non- weight-bearing behaviour, such as swimming, the hip-distal joint coordination was tightly coordinated, with unchanged latency between hip to distal joint movement and with a shorter latency between the peak of IP and GS during protraction-retraction transition phase in V3OFF mice compared to those in WT mice. Therefore, we suggest that the function of V3 INs mediating the coordination of hip-distal joint during swing-stance (flexor-extensor) transition is context dependent in weight-bearing behaviour.

The second phenotype we observed in V3OFF mice during weight-bearing behaviours was the lack of propelling ankle extension and sustained ankle extensor muscle activity during the end of the ipsilateral stance phase and contralateral swing-stance phase. In addition, we found that, in V3OFF mice, the integrated EMG amplitude of GS increased as much as that of WT mice during swimming but not during inclined-walking compared to level walking. It has been shown in other studies as well as the current study that the amplitude of ankle extensor muscle, GS shows greater increases during both inclined-walking and swimming compared to level walking. The underlying mechanism of the amplitude increase during these two behaviours may be different. Increases during inclined-walking are due to the increased muscle torques and tendon forces during the stance phase, but

during swimming, it is due to a greater limb retraction rate (Fowler et al., 1993; Herzog et al. 1993; Smith et al. 1977; Walmsley et al. 1978; Gruner & Altman, 1980). Therefore, we suggest that V3 INs mediate ankle extensor muscle activity only during weight-bearing behaviours.

Furthermore, we found that during slow speed walking, the ankle propelling phase is always superimposed with the contralateral swing-stance transition phase. SPM analysis of contralateral ankle extensor activity during ipsilateral swing-stance transition revealed that the decline of contralateral ankle extensor activity happened ~30ms before ipsilateral toe contact in V3OFF mice, whereas GS started declining right before toe contact in WT mice. Therefore, we speculate that the swing-stance transition defect and lack of contralateral ankle propelling activity might be correlated with each other. That is, V3 INs, receiving proprioceptive sensory input, mediate ankle extensor activity during the propelling phase in turn activate the contralateral swing-stance transition by facilitating the excitation of ankle extension and inhibition onto the hip flexor, synchronizing left-right extensor activity to secure stereotypical stepping. Although, V3s have been identified as a class of the excitatory CIN population, Chopek et al. (2018) have been demonstrated the existence of the bilaterally projecting V3 INs. This study provides evidence that these bilateral projections of V3 INs may coordinate left-right synchronization to balance locomotor output across the spinal cord.

4.2 V3 INs provide excitation to hip network to ensure enough force for proper hip movement

We found that a main phenotype of V3OFF mice presented in all behaviours, including treadmill walking after spinal cord injury, was the reduction in amplitude of hip movements. The rectified and smoothened EMG activities of hip muscles in V3OFF mice did not increase as much as those in WT mice when they were required during inclined-walking and swimming compared to level-walking. These data indicate that V3 INs should be a main source of the excitation of the hip locomotor network. Furthermore, we found that, while there was a longer duration and larger StDv of the swing phase in V3OFF mice during weight-bearing behaviours, the temporal aspects of hip movement of the V3OFF

mice did not display any difference from WT mice. This indicates that the smaller hip movements and the smaller increase of hip muscle activity were not the cause of a longer swing phase and unstable gait during weight-bearing behaviours. Previous data from Zhang et al. have shown that V3 INs directly projected to MN pools (Zhang et al., 2008). Tracing data from our lab has also shown that V3 INs had direct inputs to hip muscles, including IP, GL, and BF muscles. Therefore, we suggest that V3 INs should be a major source of excitation to hip MN pools.

It has been shown that hip position is key for the swing-stance and stance-swing transitions during weight-bearing behaviours (Hultborn & Nielsen, 2007; Pearson, 2007; Rossignol et al., 2007). Therefore, it is possible that the significant smaller hip movement during weight-bearing behaviours contributes to disturbed hip-distal joint coordination in V3OFF mice. However, we did not find statistically significant differences between WT and V3OFF mice when we checked several hip position parameters related to the onset of GS in WT and V3OFF mice. The hip angle, hip excursion, and the proportion of hip movement in the whole hip flexion at the initiation of GS activation remained consistent. Since most V3 INs are CINs, we also checked these three parameters of the hip joint when contralateral GS were activated. Still, we did not find statistically significant differences between WT and V3OFF mice. Furthermore, in V3OFF mice, smaller hip movement was maintained during non-weight-bearing behaviours, such as swimming, and full weight supported treadmill-walking after spinal cord injury, whereas the hip-distal joint coordination was normal. Taken all together, we suggest that the less hip movement observed in V3OFF mice is not weight-bearing dependent and is controlled by the sub-set of V3 INs other than those introduce in the last section.

Therefore, our current study demonstrates that spinal V3 INs may have multiple functional sub-populations that are involved in different modular circuits that regulate proximal or distal joints. Our results have also provided experimental evident for separate modular circuits for different joints.

5 Materials and Methods

Animals

The generation and genotyping of *Sim1*$^{Cre/+}$ mice were described previously by Zhang et al. (2008). Conditional knock-out of VGluT2 in Sim1-expressing V3 INs, *Sim1*$^{cre/+}$*;VGluT2* $^{flox/flox}$ (V3OFF mice) was described previously by Chopek et al. (2018). Behavioural tests were performed on 14 (7 males, 7 females) V3OFF mice and 11 (6 males, 5 females) *Sim1*$^{+/+}$*;VGluT2* $^{flox/flox}$ or *Sim1*$^{+/+}$*;VGluT2* $^{+/flox}$, control littermates (WT) from 43 to 70 postnatal days (P43-P70).

Behavioural tests

EMG recording

All mice were implanted with bipolar EMG-recording electrodes (Akay et al., 2006; Tysseling et al., 2013). The IP, ST, TA, and GS muscles were implanted with twisted strains EMG electrodes as described by Akay et al. (2006). BF and VL muscles were implanted with EMG electrodes of separated strains, as described by Tysseling et al. (2013). The conductance of implanted electrodes was tested after the surgery and before recordings.

The EMG signals were recorded using Power1401 (model MA 102, custom built in the workshop of the Zoological Institute, University of Cologne, DEU) and Spike 2 (Version 7.09a, Cambridge Electronic Design) software.

To measure the kinematics of leg movement, small aluminate reflective markers were put on crest, hip, ankle, metatarsophalangeal joints, and toe of the animal's hind limb, as shown in Figure 3.1A and Figure 3.2A. The reflective markers were adhered to the skin with super glue.

Kinematics

A high-speed camera was used to record the joint movement from the side of the body. Mouse treadmill (Zoological Institute's workshop, University of Cologne) speed was set at 15cm/s. The inclined treadmill was set at 17.5°. Each trial was run no more than 20s. The rest interval between 2 consecutive trials was at least 1 minute. At least 2 trials of each

locomotor task were recorded. The recordings those were included in the analysis were the episodes when animals continuously walked in the front half of the chamber for 5 -7 s. The abnormal walking steps, such as crouching, jumping and bipedal walking, were excluded from the analysis.

A transparent Plexiglass tank (100 x 10 x 40cm) was filled with warm water (23-26C) to a depth of 25-30cm. A platform was placed at one end so that it was visible to the mouse from the opposite end of the tank. 10 dimensional reflective markers were placed on both legs of the mice. Mice were lowered carefully into the water and allowed to swim to the platform. Each mouse underwent 3-5 trials per session, and each trial was limited to 1 minute. Between trials, the mice were given a 2-minute rest period during which they were placed in a clean and dry cage with a paper towel on top of a heating mat set to 37ºC. Initially, some mice might require a short training period during which the distance required for the mouse to reach the platform was increased until the mouse was able to swim the full distance. Mice were carefully monitored during the test. Mice displaying underwater tumbling, or any distressing behaviours were scooped up and rescued immediately. For drying the mice following the testing session, the animals were placed in an empty cage with some paper towels on top of a heating mat set to 37ºC.

Data analysis

EMG recordings

The EMG recordings were initially rectified and smoothed (τ = 0.05 s) in Spike 2. All processed data were then transformed to MATLAB (Version R2018a, The MathWorks, Inc.). The toe touching point of each step in the video recording was used to synchronize the EMG activities with the leg movements. For the data of treadmill walking, the episode ranging from 150 ms before the toe touch to 250 ms after the toe touch was defined as the current step cycle's EMG activity. For the data of swimming, the anterior toe extreme was used as the reference point. The step range was between 150 ms before and 100 ms after the reference point. To detect the pattern of EMG activity, the EMG signals were normalized by the peak amplitude within the current step cycle.

To compare the pattern of IP termination and GS activation, we applied the Bootstrap method for a specific area of the EMG activities of IP and GS. Since the peaks and termination slopes of IP were always located within 150 ms before toe touch for both WT and V3OFF mice for weight-loading behaviours as shown in Figure 4B & 10A, B, we selectively chose the normalized EMG activities of IP in this area; For GS, as shown in Figure 4B & 10A, the data was selected in the 50 ms before and after toe touch. Based on the same principle, the EMG activities of IP and GS in swimming were selected in the 40 ms before and after anterior toe extreme (Figure 10B).

Kinematic analysis

The video data were analysed using the Peak Motus 8.2 motion analysis system (Peak Performance Technologies) and processed by customized scripts in Spike2 (Version 7.09a, Cambridge Electronic Design) and MATLAB (Version R2018a, The MathWorks, Inc.). For treadmill walking, the time points of toe touching and off the ground were manually marked for each step, as shown in Figure 3.11A. The knee joint was calculated triangulation from the position of hip and ankle joint markers using the femur and tibia's measured lengths. The step cycle was sub-divided into stance and swing based on the toe touch and toe lift. Each step's hip joint angular movement was sub-divided into flexion and extension based on the peak and trough. The ankle joint angular movement in each step was sub-divided into flexion, E1, yield, and propel sub-phases (Figure 2B). The flexion phase started from the peak of the last extension and terminated at the trough in the swing phase. Then the E1 phase started and terminated at the peak around toe touch followed by yield phase. The yield phase terminated at the first trough in the stance phase. In the end, the propel phase started and ended at the second peak in the stance phase. The excursion of the joint was measured as the difference between the peak and trough of each sub-phase.

Treadmill locomotion after complete spinal cord transection

Complete spinal cord transection

The animal was anesthetized using 4% isoflurane for approximately 5 minutes then reduced to 2% isoflurane through the surgery. The mouse was placed on a heated pad. A

laminectomy was performed, and the bone covering the upper half of the eighth thoracic vertebral (T8) was removed. A complete T10-11 spinal cord transection was performed. Fine scissors were used to cut across the edges of the spinal cord to ensure a complete transaction. Standard precautions were taken to minimize tissue damage and bleeding through the surgery. After the cut, muscles were sewn back together in layers, and the skin was sewn closed as well.

Post-operative care included buprenorphine analgesic, Baytril antibiotic and 1.0 ml subcutaneous saline twice/day for three days. The mice received care for the duration of the experiment, including manually compressing the bladder to release urine twice a day until automatic micturition returned.

One week after the surgery, treadmill tests were performed weekly. A homemade harness was used to support the hindquarters of the mice. The experimenter held and kept the harness in the right position. The speed of the treadmill was set at 20 cm/s. The tail of the animal was held by the experimenter to apply the pinching stimulus. The mice received a 5-10-minute session twice a week for six weeks. Reflective markers were attached to the hindlimb joints. A high-speed camera was used to record the leg movement from the side view. The videos and data were analysed as described above.

Statistics

The statistical analysis was performed in Prism7 (GraphPad Software, Inc.) and MATLAB (Version R2018a, The MathWorks, Inc.). Student t-test and Welch's t-test were used to compare the differences between WT and V3OFF mice's kinematics in three behaviours. The bootstrap method was used to compare the patterns of IP termination and GS activation. The statistical parametric mapping (SPM) was used to analyze the pattern of the ipsilateral BF and both side GS muscles.

6 Figures

Figure 3.1. V3OFF mice have longer swing phase duration during treadmill walking.

Ai

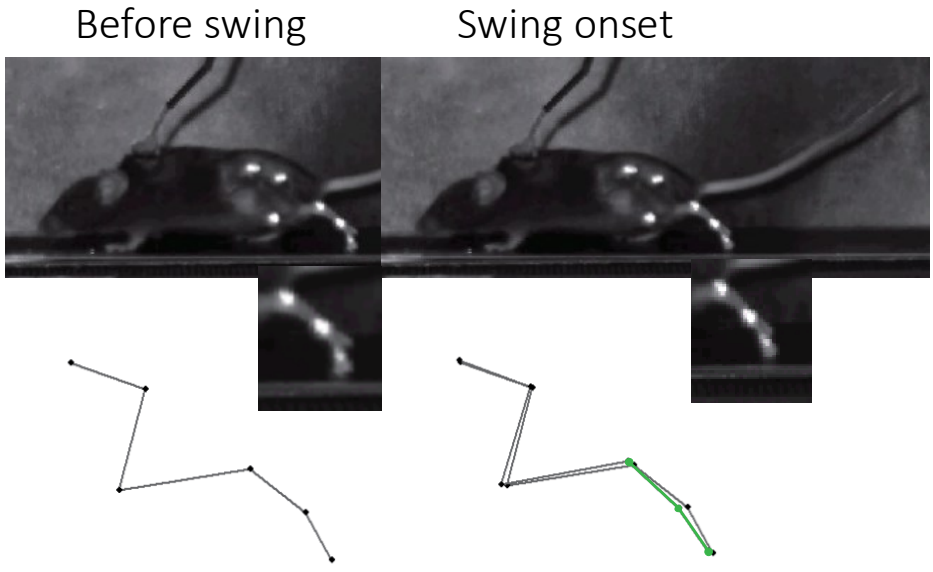

Aii

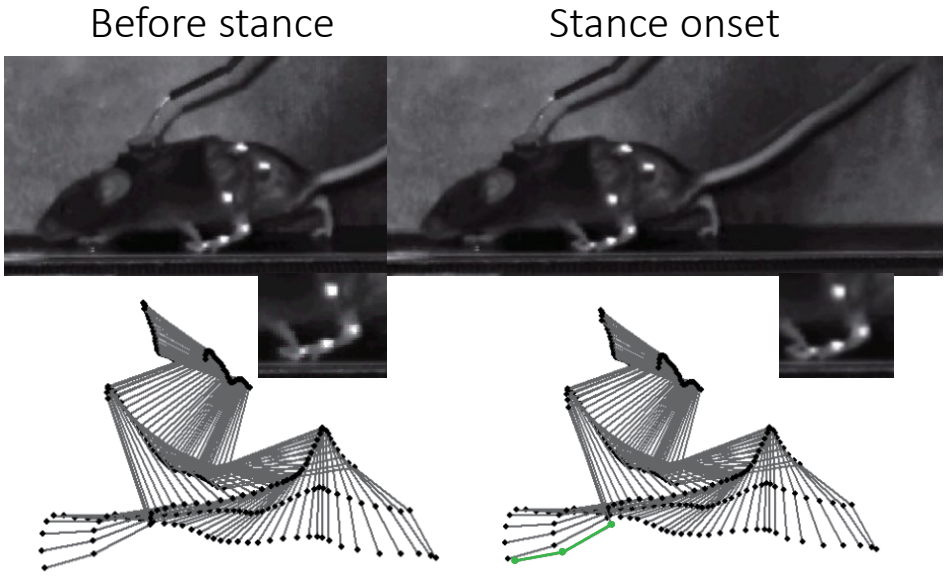

Bi

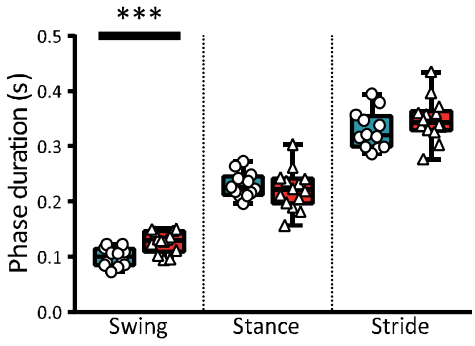
***
Phase duration (s)
0.5
0.4
0.3
0.2
0.1
0.0
Swing
Stance
Stride

Bii

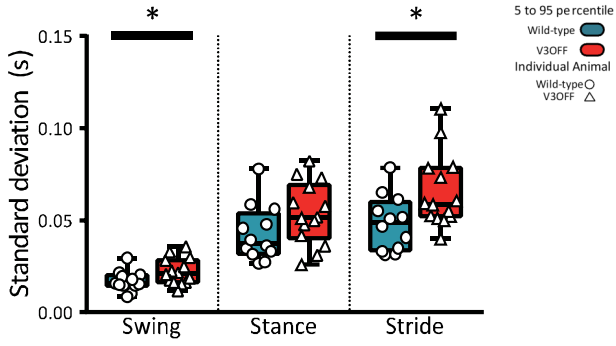
*
*
Standard deviation (s)
0.15
0.10
0.05
0.00
Swing
Stance
Stride
5 to 95 percentile
Wild-type
V3OFF
Individual Animal
Wild-type
V3OFF

Figure 3.1. V3OFF mice have longer swing phase duration during treadmill walking.

A. Top rows, representative photo image from videos recorded from the sideview of a WT mouse using high-speed camera (250 Hz). The reflective markers were adhered on the crest, hip, knee, ankle, metatarsophalangeal (MTP) joints, and the toe. The bottom rows: the stick plots frame-by-frame reconstructed hindlimb one step movement. The knee joint was calculated triangulation from the position of hip and ankle joint markers, using the measured lengths of the femur and tibia. i shows the frame before and after toe lifted as the whole paw was pulled forward, respectively. ii shows the frames before and after the toe touching the ground, respectively. The toe touching was identified as whole front paw touched ground. The reconstructed limb is indicated by green lines and joints are represented by green dots.

B. Box graphs of means (i) and StDvs (ii) of stride, stance, and swing durations of WT (blue, n=12) and V3OFF (red, n=14) mice during treadmill walking. The blue and red boxes indicate the 5 to 95 percentile of data distribution. The means of each mouse are shown as white circle for WT and as white triangle for V3OFF. *, $0.01 \leq P < 0.05$; ***, $0.0001 \leq P < 0.001$.

Figure 3.2. Schematics of experimental strategies and kinematics of V3OFF and WT mice during treadmill walking.

A

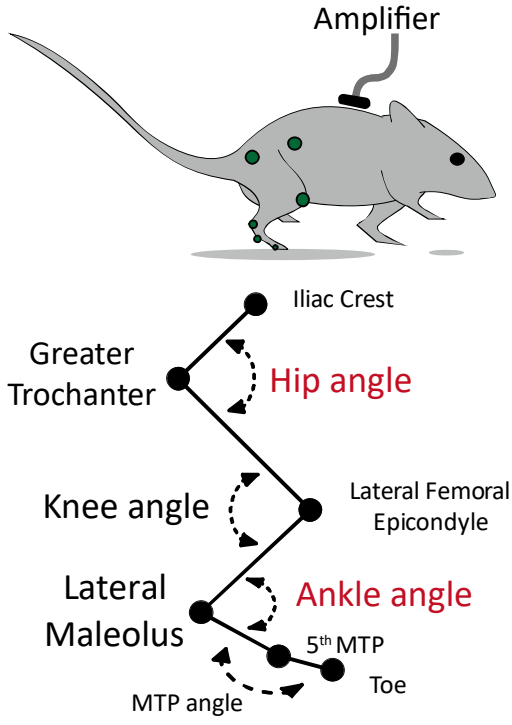

B

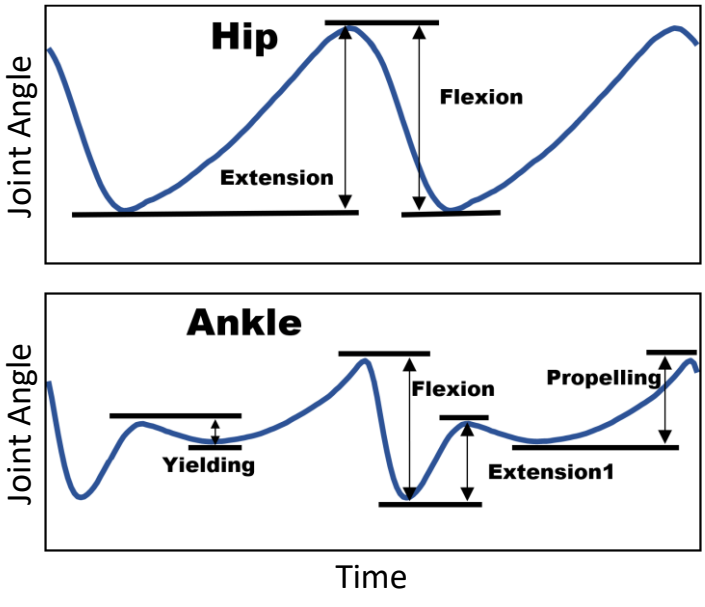

C

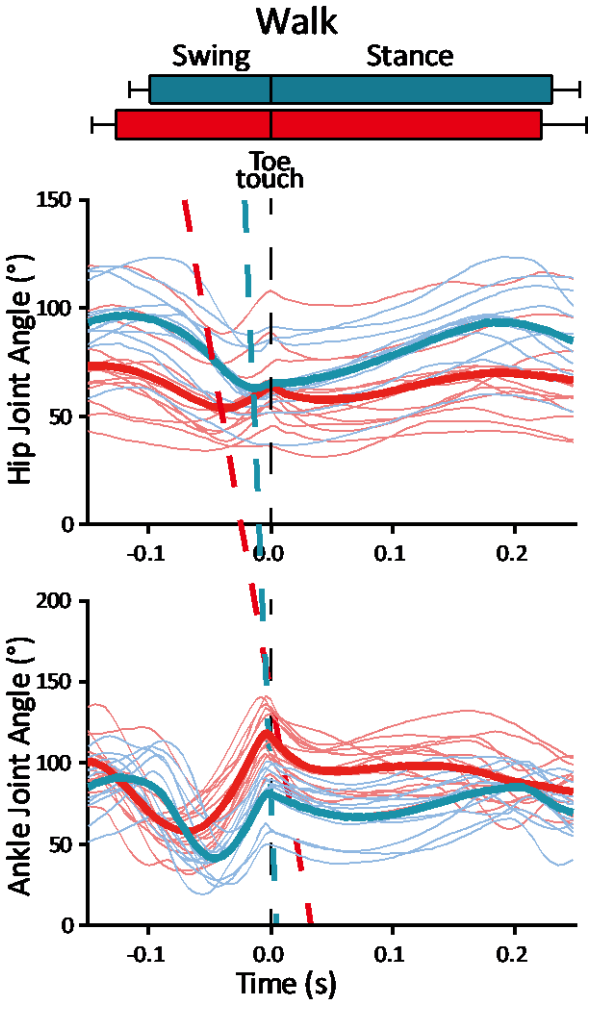
Walk
Swing
Stance
Toe
touch
150
100
50
0
Hip Joint Angle (°)
-0.1
0.0
0.1
0.2
200
150
100
50
0
Ankle Joint Angle (°)
-0.1
0.0
0.1
0.2
Time (s)

Figure 3.2. Schematics of experimental strategies and kinematics of V3OFF and WT mice during treadmill walking.

A. Illustration of the positions of reflective markers on the joints of a mouse right hind limb (top) and corresponding hindlimb geometry and joint angles used in this study (bottom). The black box on the back of the mouse indicates the connector for linking EMG electrodes to the amplifier.

B. Illustration of hip angular excursion and corresponding flexion and extension phases within a step cycle; and ankle joint angular movement and four subphases, in a step cycle.

C. Angular movement of hip (upper) and ankle (lower) joints during a step cycle of WT (blue) and V3OFF (red) mice. The thin lines are the average trace of 15-25 consecutive steps of individual animals, while the thick lines are the average of the corresponding group. The mean of swing and stance phase duration of all WT and V3OFF mice are shown on the top. The manually marked toe touch is used as reference point, indicated as black dashed line. Traces of joint angle (blue: WT; red: V3OFF) are triggered around toe touch. The blue and red dashed line connecting hip flexion termination and ankle E1 termination is for WT and V3OFF mice, respectively.

Figure 3.3. Comparison of joint angular excursion, phase duration of sub-phases and delay between hip and distal joint during swing phase.

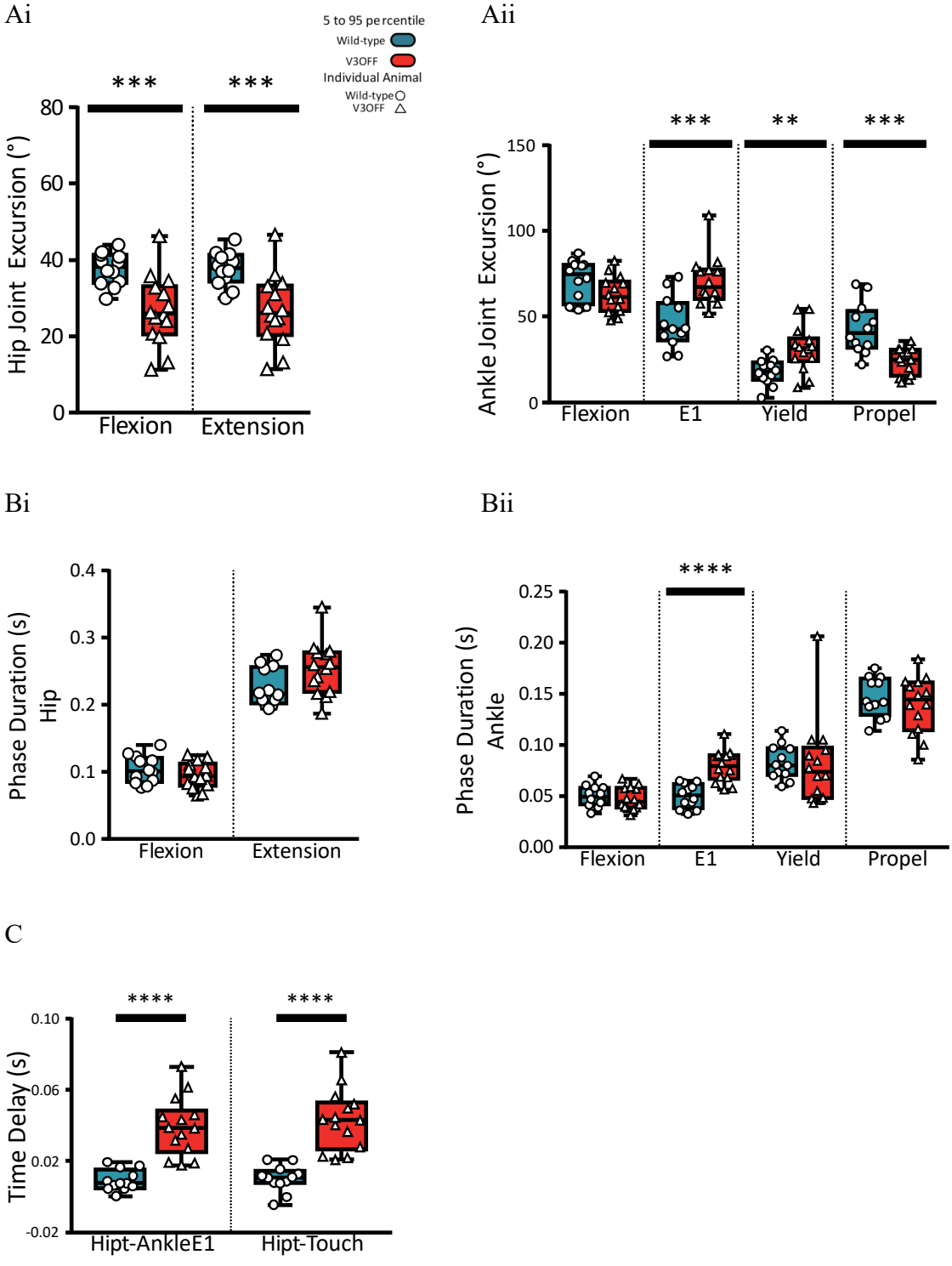

Figure 3.3. Comparison of joint angular excursion, phase duration of sub-phases and delay between hip and distal joint during swing phase.

A. Box graphs of means of extension and flexion excursion of hip joint (i) and flexion, E1, yield and propel excursion of ankle joint (ii) between WT (blue) (n=12) and V3OFF (red) (n=14) mice. The box indicates the 5 to 95 percentile of data distribution. The means of each mouse are shown as white circle for WT and as white triangle for V3OFF. **, $0.001 \leq P < 0.01$; ***, $0.0001 \leq P < 0.001$.

B. Box graphs of means of phase duration of hip joint (i) and ankle joint (ii) between WT (blue) (n=12) and V3OFF (red) (n=14) mice. The box indicates the 5 to 95 percentile of data distribution. The means of each mouse are shown as white circle for WT and as white triangle for V3OFF. ****, $P < 0.0001$.

C. Box graphs of delay latency of hip flexion phase termination to ankle E1 phase termination and toe touch between WT (blue) (n=12) and V3OFF (red) (n=14) mice. The box indicates the 5 to 95 percentile of data distribution. The means of each mouse are shown as white circle for WT and as white triangle for V3OFF. ****, $P < 0.0001$.

Figure 3.4. EMG pattern between WT and V3OFF mice during treadmill walking.

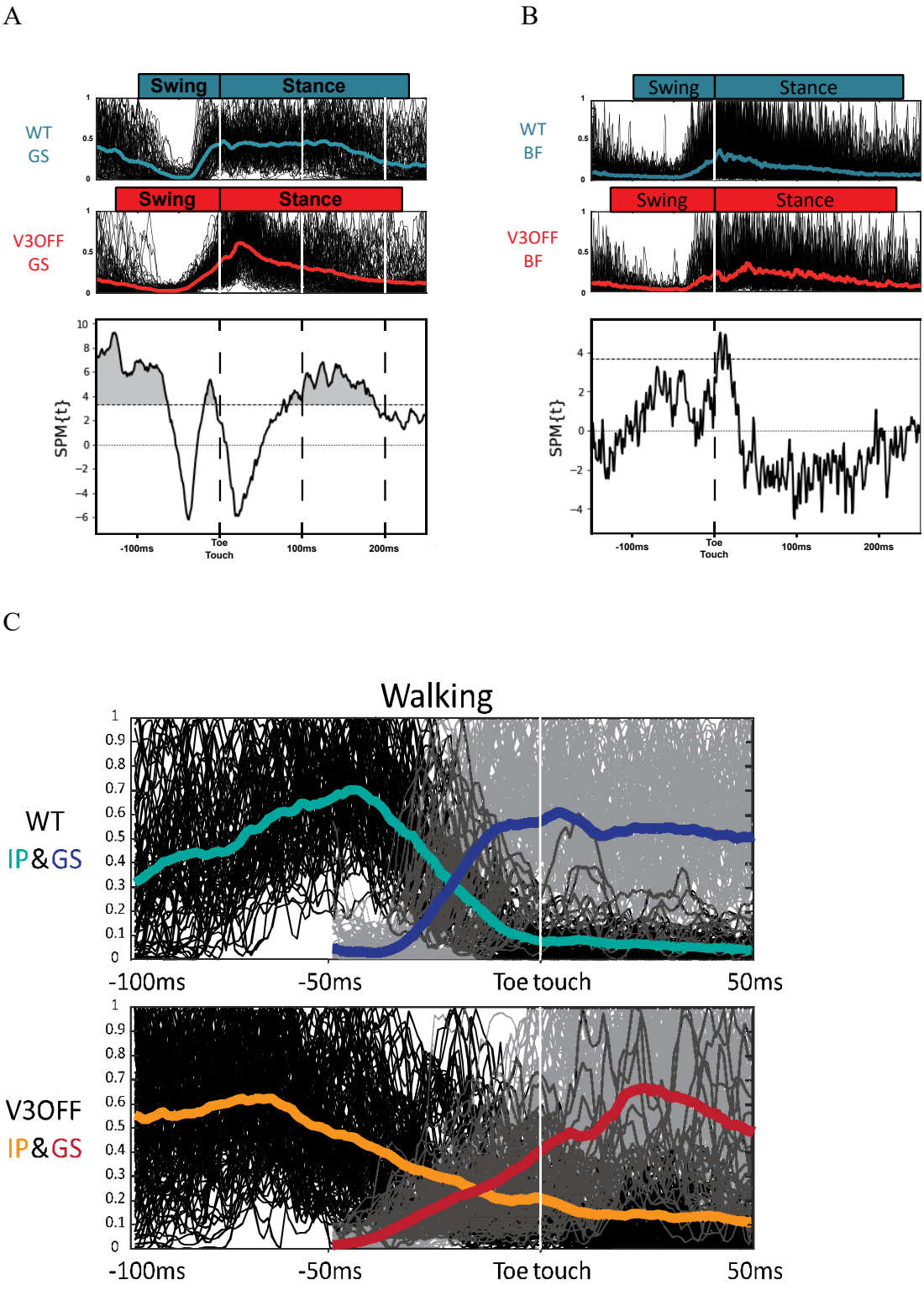

D

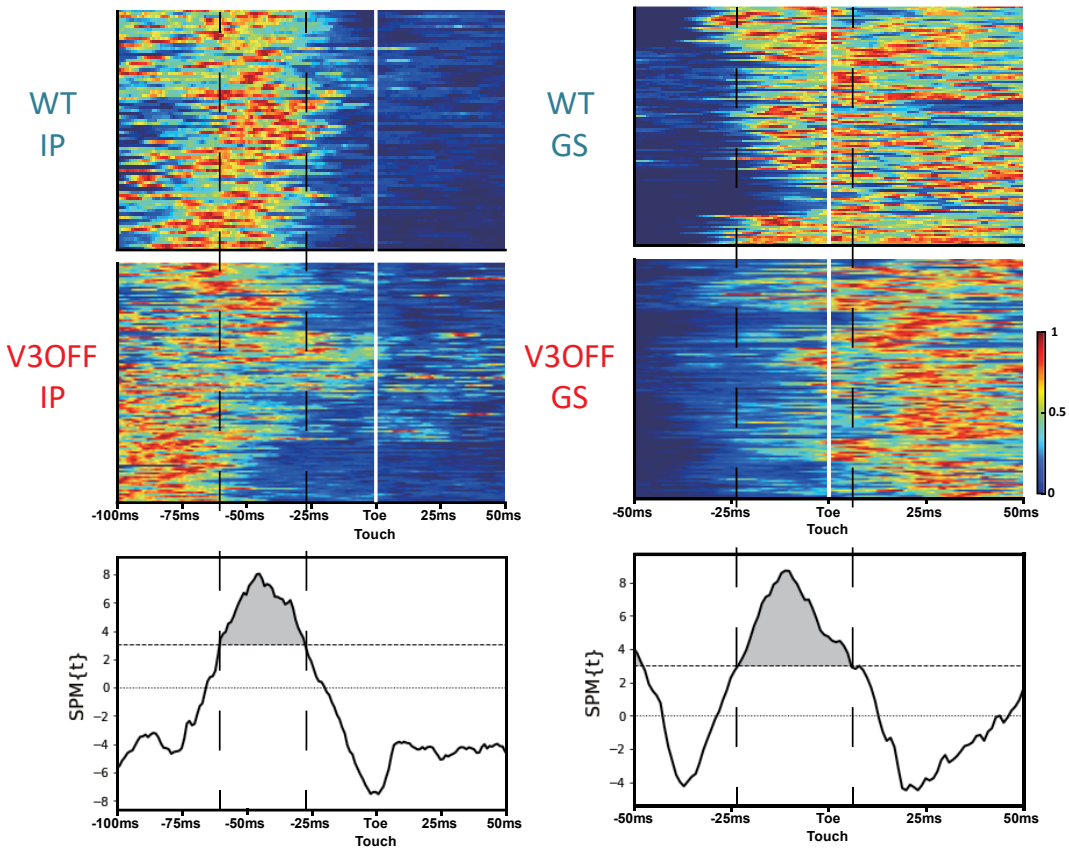
WT
IP
WT
GS
V3OFF
IP
V3OFF
GS
-100ms
-75ms
-50ms
-25ms
Toe
Touch
25ms
50ms
-50ms
-25ms
Toe
Touch
25ms
50ms
1
0.5
0
SPM{t}
8
6
4
2
0
−2
−4
−6
−8
SPM{t}
8
6
4
2
0
−2
−4
-100ms
-75ms
-50ms
-25ms
Toe
Touch
25ms
50ms
-50ms
-25ms
Toe
Touch
25ms
50ms

Figure 3.4. EMG pattern between WT and V3OFF mice during treadmill walking.

A, B. EMG activities of GS (A) and BF (B) are triggered around toe touch. Horizontal bar on the top indicates the mean of swing and stance phases in WT (blue) (n=12) and V3OFF (red) (n=14) mice. The processed EMG activities of each step are normalized by its peak amplitude in the episode of current step. Only the activities within the episode ranging from 150ms before ipsilateral toe touch to 250ms after ipsilateral toe touch are normalized. The thick trace is averaged EMG activity from all steps in WT (blue) and V3OFF (red) mice. The gray area in the SPM t-map shows where the EMG pattern differed between WT and V3OFF mice. The horizontal dotted line in the SPM t-map indicates the critical threshold of Random Field Theory (RFT) for significant difference between WT and V3OFF mice.

C. EMG activities of IP and GS. The processed EMG activities of each step are normalized by its peak amplitude in the episode of current step. For IP, the episode is from 100ms before toe touch to 50ms after toe touch. For GS, the episode is from 50ms before toe touch to 50ms after toe touch. Thin traces indicate the normalized IP (black) or GS (gray) activities of each step. Thick traces indicate the averaged activities of IP and GS from WT (IP, turquoise; GS, blue) and V3OFF (IP, orange; GS, red) mice.

D. Statistical parametric mapping (SPM) analysis for the pattern of IP (left) and GS (right). Top, colour coded heating maps show the pattern of IP (left) and GS (right) as shown in Figure 3.4C. The gray area in the SPM t-map shows where the EMG pattern differe between WT and V3OFF mice. The horizontal dotted line indicates the critical RFT threshold for significant difference between WT and V3OFF mice.

Figure 3.5. Bootstrap method to qualitatively analyze IP and GS patterns during swing-stance transition in treadmill waking.

Ai

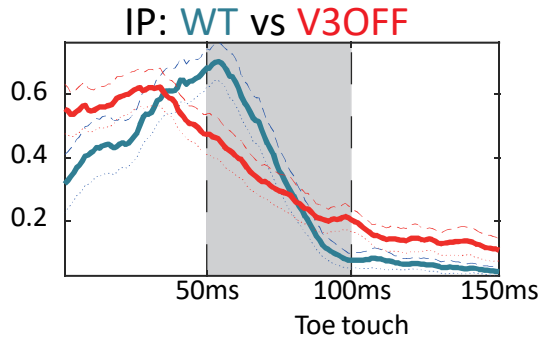

Aii

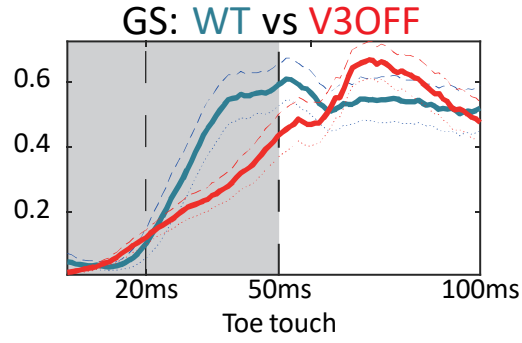

Bi

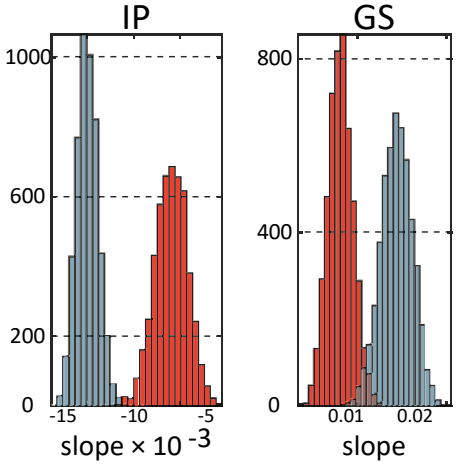

Bii

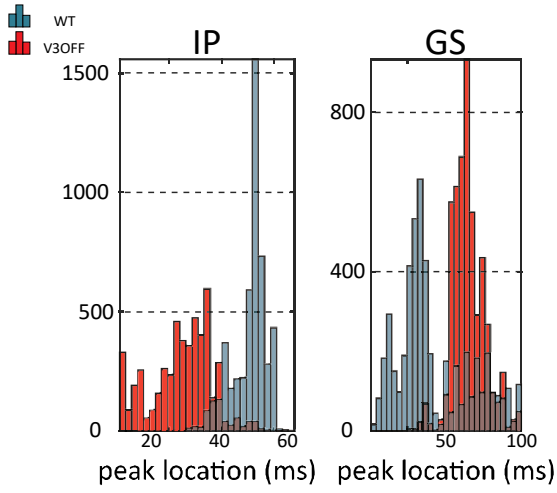

Figure 3.5. Bootstrap method to qualitatively analyze IP and GS patterns during swing-stance transition in treadmill waking.

A. Graph of mean traces ± 3*StDv of IP (i) and GS (ii) of WT (blue) and V3OFF (red) mice. Thick solid lines indicate the mean of bootstrapped data. Dashed lines indicate + 3*StDv. Dotted lines indicate - 3*StDv. Gray areas show the region of analyzed slopes.

B. Distribution of slope values (i) and peak locations (ii). Note the IP activities are decreasing with the time thus the slope values of IP are negative. The smaller slope value means the steeper slope. For the GS, the larger slope value means the steeper slope.

Figure 3.6. Temporal parameters of hind-limbs during inclined-walking and swimming.

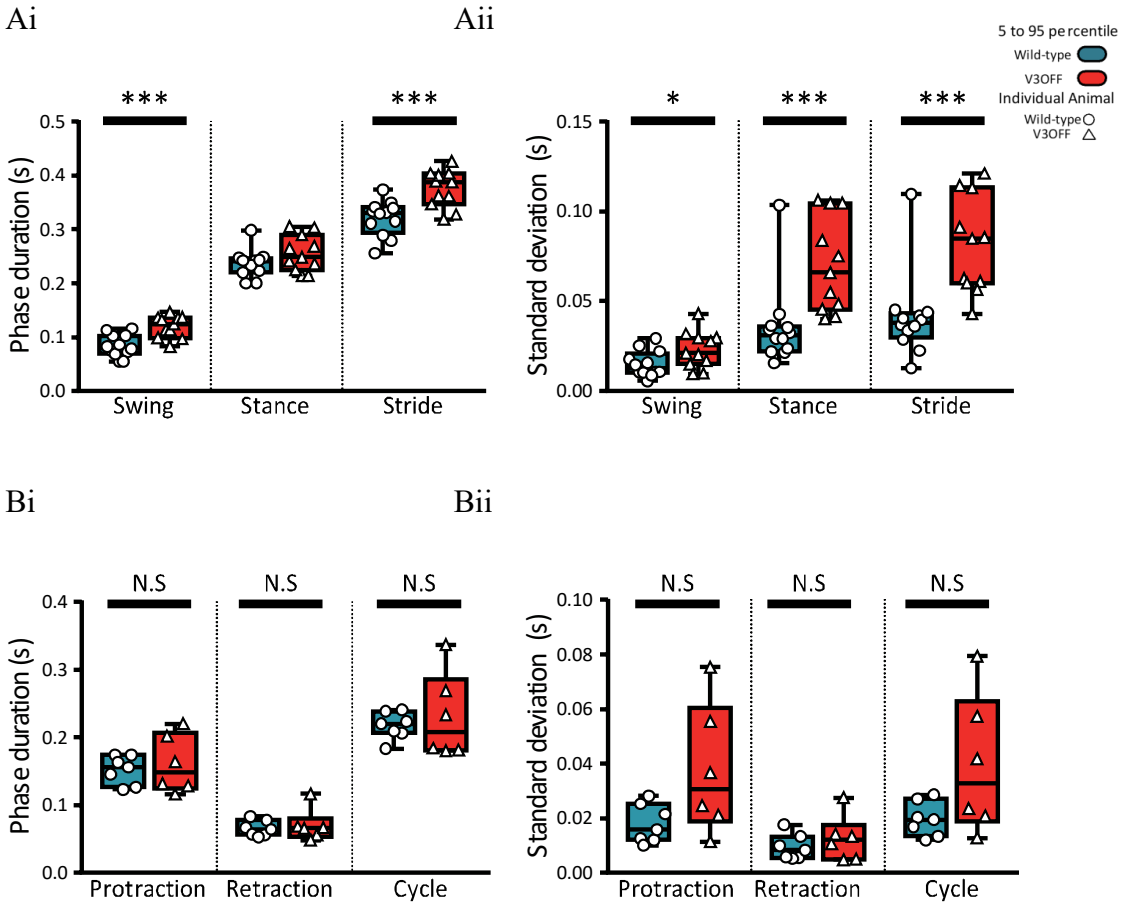

Figure 3.6. Temporal parameters of hind-limbs during inclined-walking and swimming.

Box graphs of means (i) and StDvs (ii) of stride, stance, and swing duration of WT (blue, n=12) and V3OFF (red, n=11) mice during inclined-walking (A) and swimming (B). The blue and red boxes indicate the 5 to 95 percentile of data distribution. The means of each mouse are shown as white circle for WT and as white triangle for V3OFF. *, $0.01 \leq P < 0.05$; ***, $0.0001 \leq P < 0.001$.

Figure 3.7. Kinematics of V3OFF and WT mice during inclined treadmill walking.

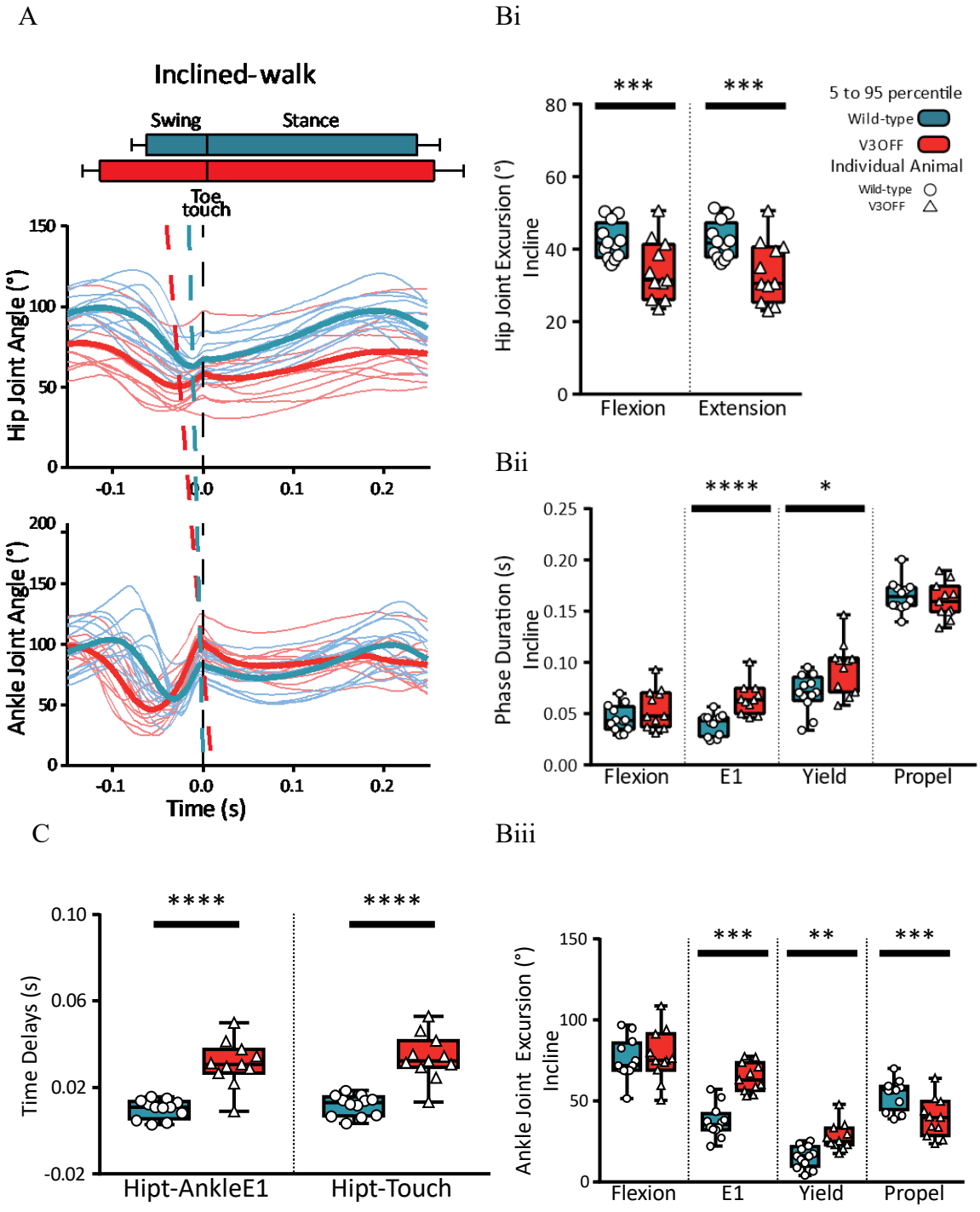

Figure 3.7. Kinematics of V3OFF and WT mice during inclined treadmill walking.

A. Angular movement of hip (upper) and ankle (lower) joints during a step cycle of WT (blue) and V3OFF (red) mice. The thin lines are the average trace of 15-25 consecutive steps of individual animals, while the thick lines are the average of the corresponding group. The mean of swing and stance phase duration of all WT and V3OFF mice are shown on the top. The manually marked toe touch is used as reference point, indicated as black dashed line. Traces of joint angle (blue: WT; red: V3OFF) are triggered around toe touch. The blue and red dashed line connecting hip flexion termination and ankle E1 termination is for WT and V3OFF mice, respectively.

B. Box graphs of means of extension and flexion excursion (i), and phase duration (ii) and excursion (iii) of ankle joint between WT (blue) (n=12) and V3OFF (red) (n=11) mice. The blue and red boxes indicate the 5 to 95 percentile of data distribution. The means of each mouse are shown as white circle for WT and as white triangle for V3OFF. *, $0.01 \leq P < 0.05$; **, $0.001 \leq P < 0.01$; ***, $0.0001 \leq P < 0.001$; ****, $P < 0.0001$.

C. Box graphs of delay latency of hip flexion phase termination to ankle E1 phase termination and toe touch between WT (blue) (n=12) and V3OFF (red) (n=14) mice. The box indicates the 5 to 95 percentile of data distribution. The means of each mouse are shown as white circle for WT and as white triangle for V3OFF. ****, $P < 0.0001$.

Figure 3.8. Kinematics of V3OFF and WT mice during swimming.

A

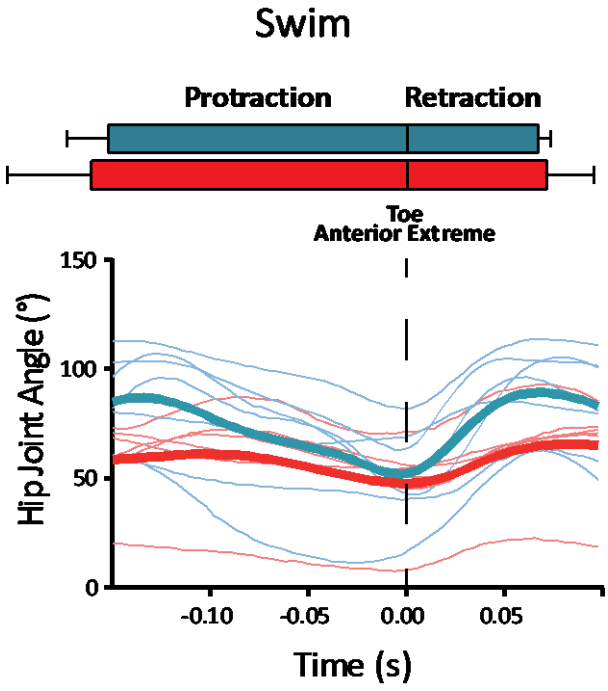

B

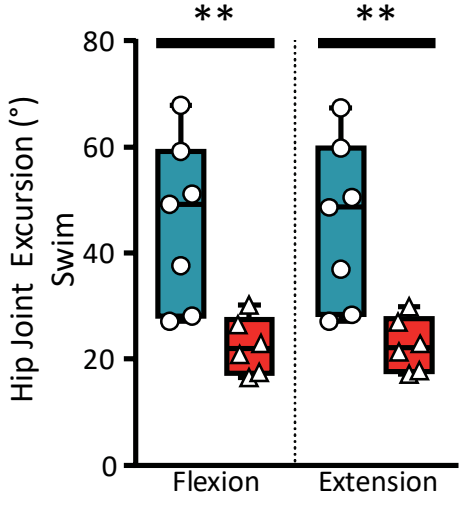

C

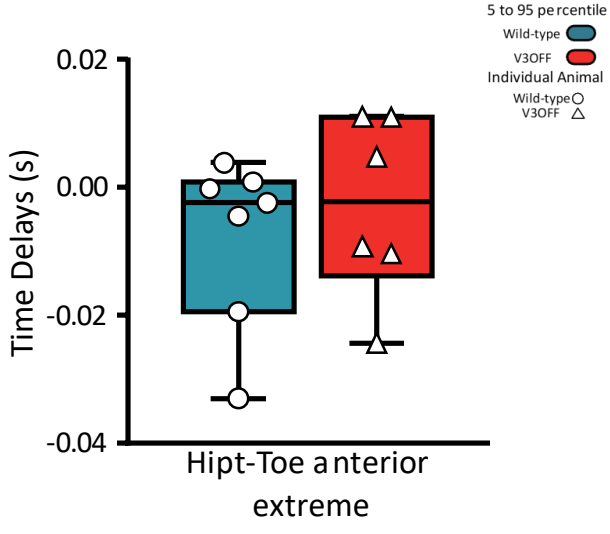

Figure 3.8. Kinematics of V3OFF and WT mice during swimming.

A. Angular movement of hip (upper) and ankle (lower) joints during a step cycle of WT (blue) and V3OFF (red) mice. The thin lines are the average trace of 15-25 consecutive steps of individual animals, while the thick lines are the average of the corresponding group. The mean of swing and stance phase duration of all WT and V3OFF mice are shown on the top. The manually marked toe touch is used as reference point, indicated as black dashed line. Traces of joint angle (blue: WT; red: V3OFF) are triggered around toe touch. The blue and red dashed line connecting hip flexion termination and ankle E1 termination is for WT and V3OFF mice, respectively.

B. Box graphs of means of extension and flexion excursion of hip joint between WT (blue) (n=7) and V3OFF (red) (n=6) mice. The blue and red boxes indicate the 5 to 95 percentile of data distribution. The means of each mouse are shown as white circle for WT and as white triangle for V3OFF. **, $0.001 \leq P < 0.01$.

C. Box graphs of delay latency of hip flexion phase termination to ankle E1 phase termination and toe touch between WT (blue) (n=7) and V3OFF (red) (n=6) mice. The box indicates the 5 to 95 percentile of data distribution. The means of each mouse are shown as white circle for WT and as white triangle for V3OFF. ****, $P < 0.0001$.

Figure 3.9. EMG pattern between WT and V3OFF mice during inclined treadmill walking and swimming.

A

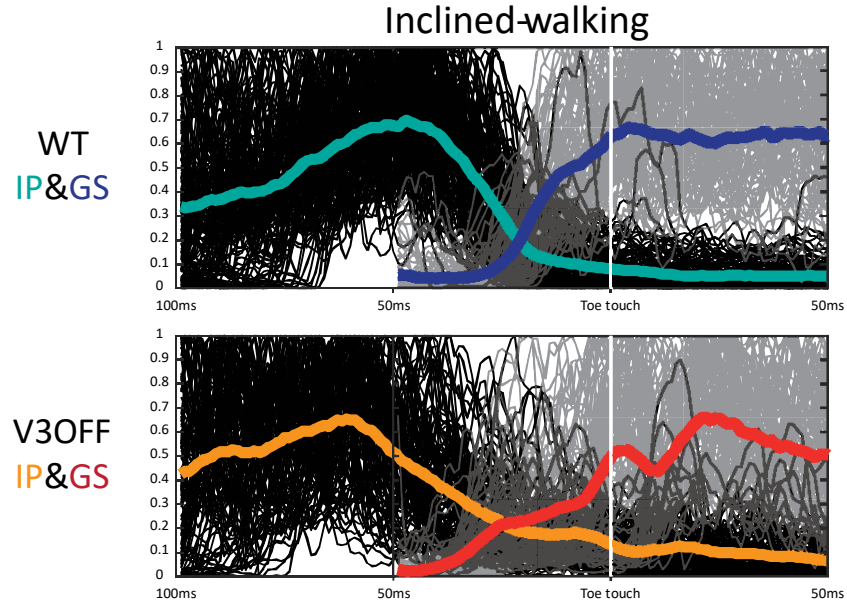

B

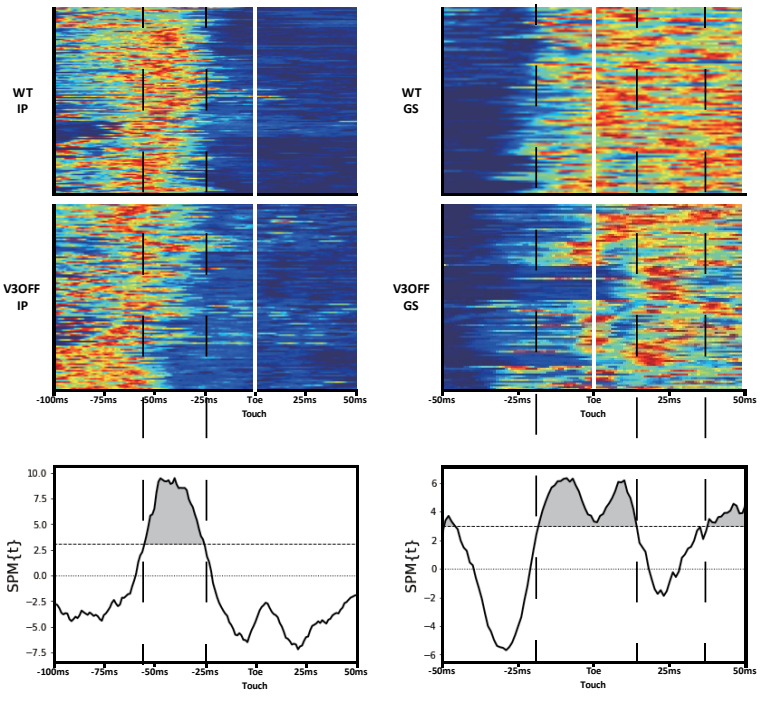

C

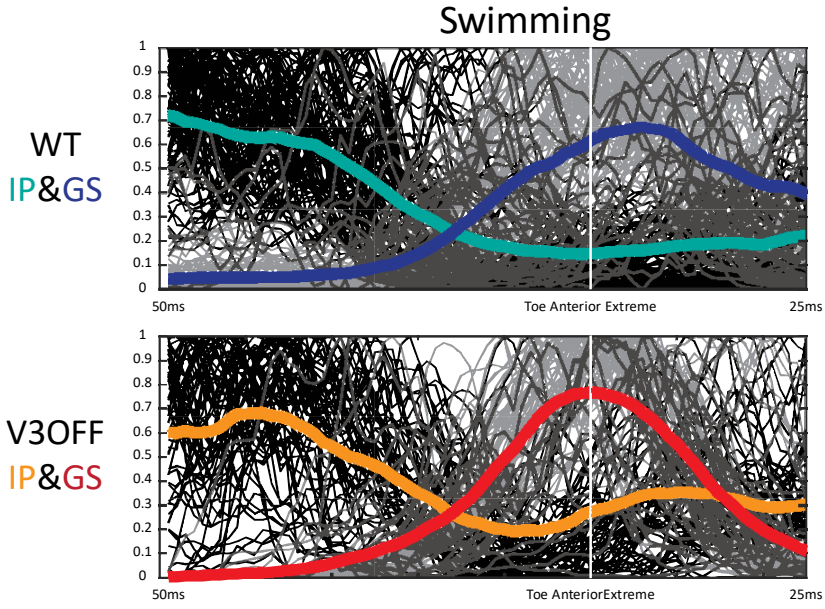
Swimming
WT
IP&GS
V3OFF
IP&GS
1
0.9
0.8
0.7
0.6
0.5
0.4
0.3
0.2
0.1
0
50ms
Toe Anterior Extreme
25ms
Toe AnteriorExtreme

D

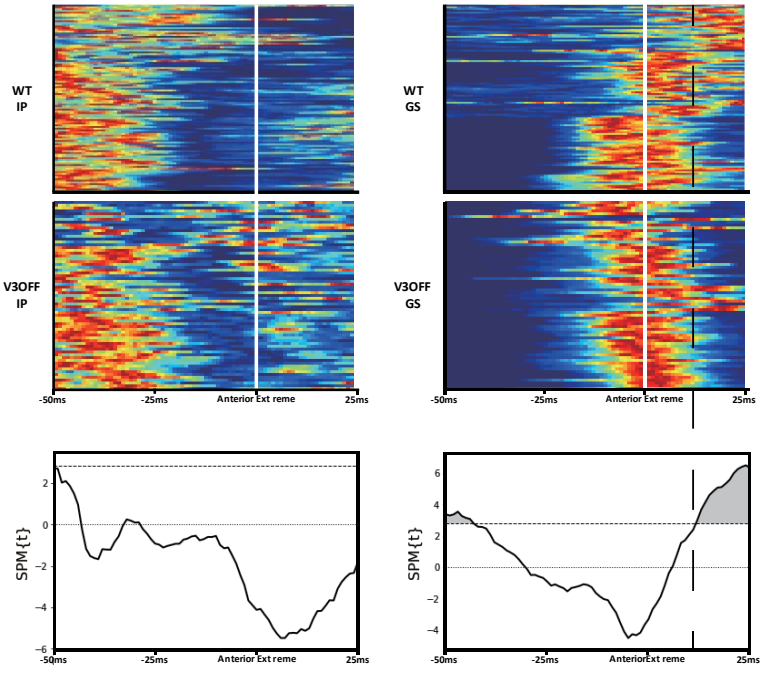
WT
IP
WT
GS
V3OFF
IP
V3OFF
GS
-50ms
-25ms
Anterior Ext reme
25ms
SPM{t}
2
0
−2
−4
−6
6
4
2
0
−2
−4

Figure 3.9. EMG pattern between WT and V3OFF mice during inclined treadmill walking and swimming.

A, C. EMG activities of GS (A) and BF (B) are triggered around toe touch. Horizontal bar on the top indicates the mean of swing and stance phases in WT (blue) (n=12) and V3OFF (red) (n=14) mice. The processed EMG activities of each step are normalized by its peak amplitude in the episode of current step. For IP in inclined-walking, only the activities within the episode ranging from 100ms before toe touch to 50ms after toe touch are normalized. The thick trace is averaged EMG activity from all steps in WT (blue) and V3OFF (red) mice. For GS in inclined-walking, only the activities within the episode ranging from 50ms before toe touch to 50ms after toe touch are normalized. For IP and GS in swimming, only the activities within the episode ranging from 50ms before toe reaching anterior extreme to 25ms after are normalized. Thin traces indicate the normalized IP (black) or GS (gray) activities of each step. Thick traces indicate the averaged activities of IP and GS from WT (IP, turquoise; GS, blue) and V3OFF (IP, orange; GS, red) mice.

B, D. Statistical parametric mapping (SPM) analysis for the pattern of IP (left) and GS (right). Top, colour coded heating maps show the pattern of IP (left) and GS (right) as shown in Figure 3.9C. The gray area in the SPM t-map shows where the EMG pattern differed between WT and V3OFF mice. The horizontal dotted line indicates the critical RFT threshold for significance.

Figure 3.10. Bootstrap method to qualitatively analyze IP and GS patterns during swing-stance transition in inclined treadmill waking and during protraction-retraction transition phase in swimming.

Ai

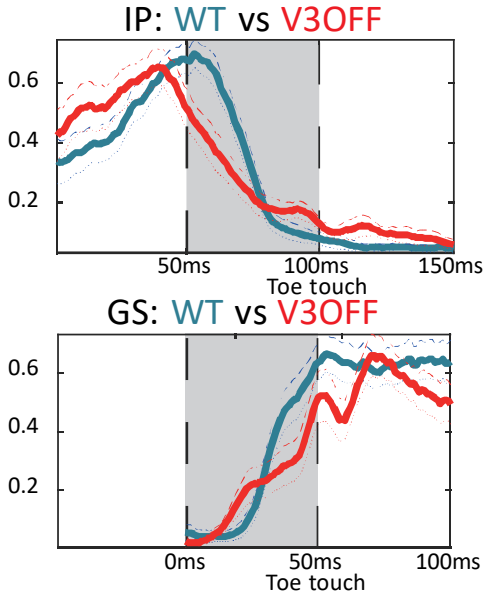

Aii

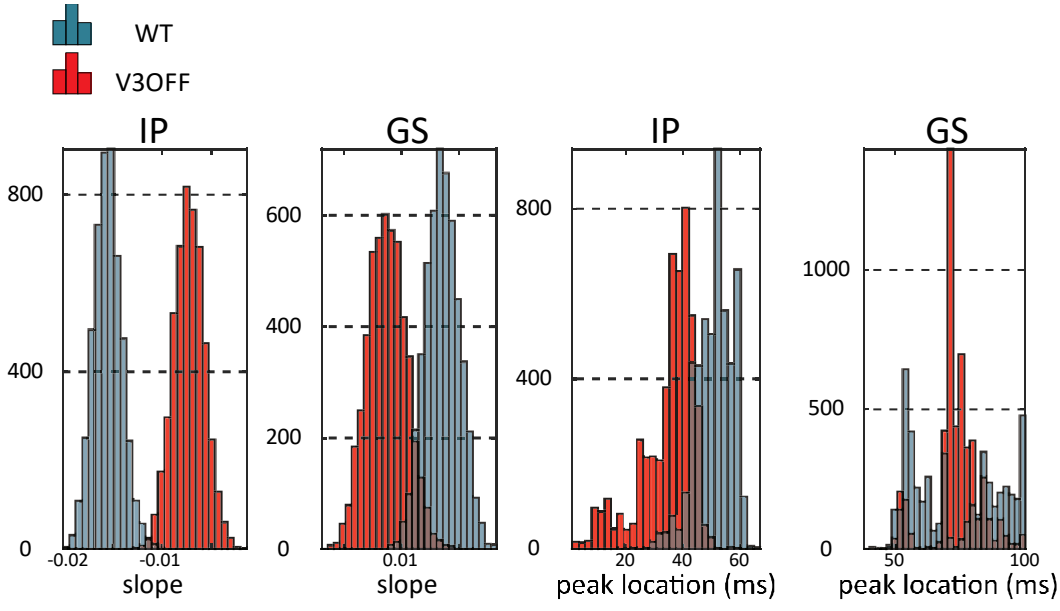

Bi

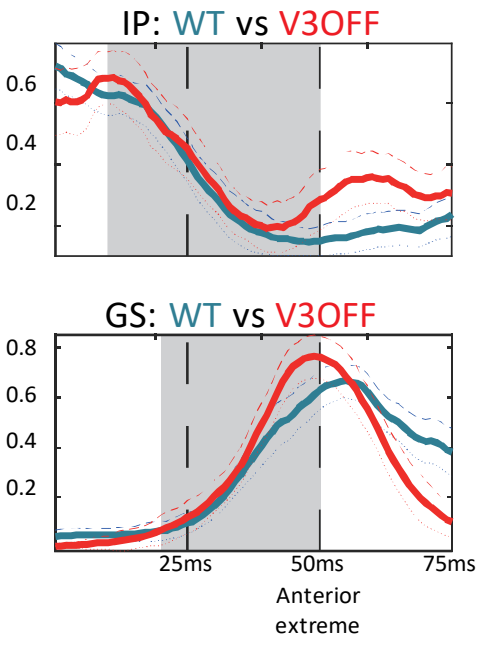
IP: WT vs V3OFF
0.6
0.4
0.2
GS: WT vs V3OFF
0.8
0.6
0.4
0.2
25ms
50ms
75ms
Anterior
extreme

Bii

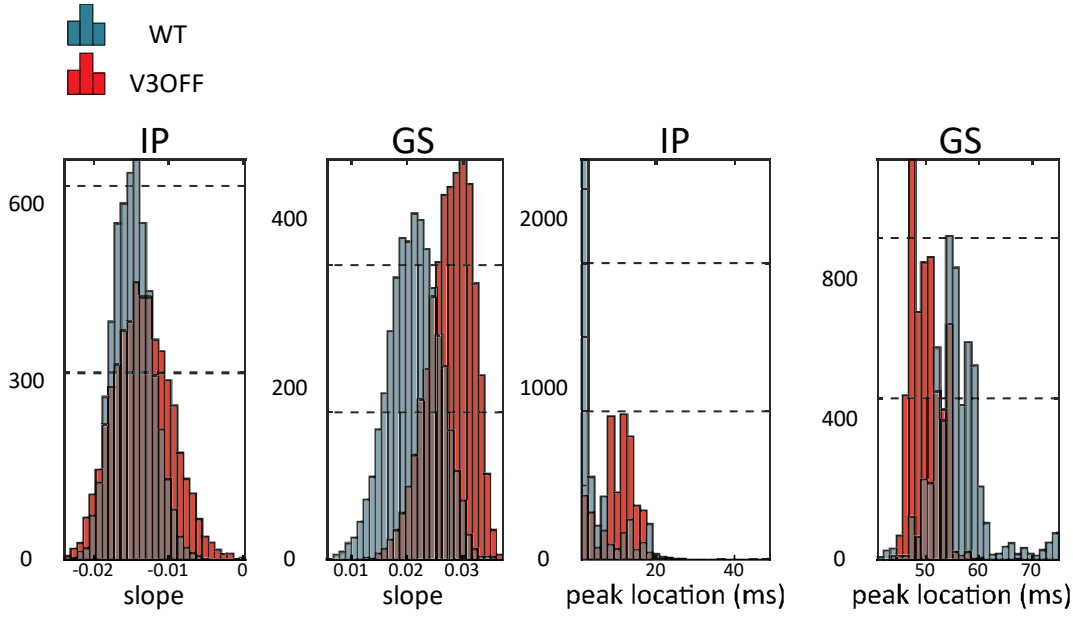
WT
V3OFF
IP
GS
IP
GS
600
300
0
400
200
0
2000
1000
0
800
400
0
-0.02
-0.01
0
slope
0.01
0.02
0.03
slope
20
40
peak location (ms)
50
60
70
peak location (ms)

Figure 3.10. Bootstrap method to qualitatively analyse IP and GS patterns during swing-stance transition in inclined treadmill waking and during protraction-retraction transition phase in swimming.

Ai, Bi. Graph of mean traces ± 3*StDv of IP (upper) and GS (lower) of WT (blue) and V3OFF (red) mice. Thick solid lines indicate the mean of bootstrapped data. Dashed lines indicate + 3*StDv. Dotted lines indicate - 3*StDv. Gray areas show the region of analyzed slopes.

Aii, Bii. Distribution of slope values (left) and peak locations (right). Note the IP activities are decreasing with the time thus the slope values of IP are negative. The smaller slope value means the steeper slope. For the GS, the larger slope value means the steeper slope.

Figure 3.11. Comparison of mean iEMG of hip, knee, and ankle muscles of WT and V3OFF mice during treadmill walking, inclined treadmill walking and swimming.

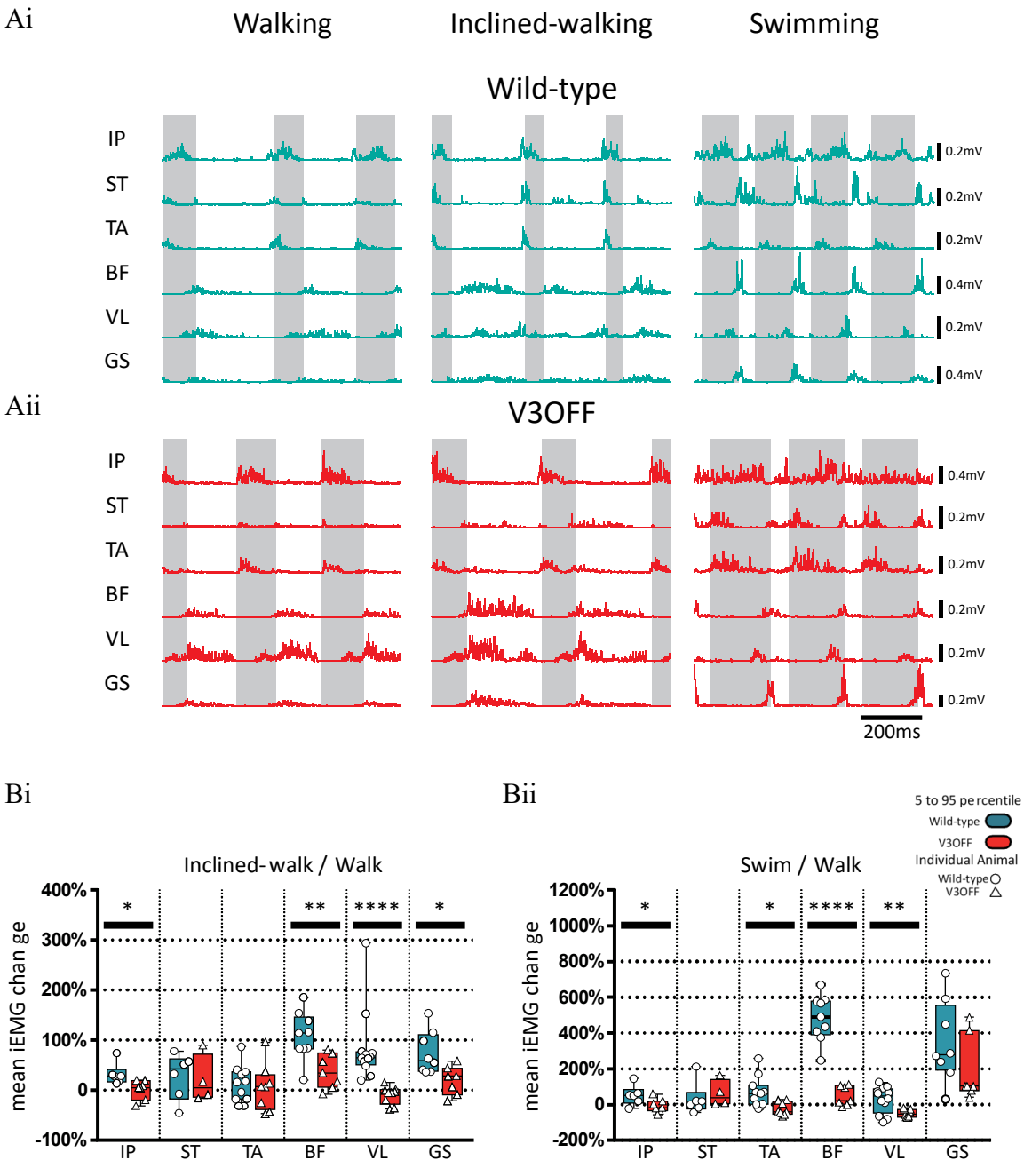

Figure 3.11. Comparison of mean iEMG of hip, knee, and ankle muscles of WT and V3OFF mice during treadmill walking, inclined treadmill walking and swimming.

A. Representative traces of WT (i) and V3OFF (ii) mice during level-walking, inclined-walking, and swimming.

B. Box graphs of means of the iEMG increase of each muscle in WT and V3OFF mice between level-walking (walk) and inclined-walking (inclined-walk) (i), and between level-walking (walk) and swimming (swim) (ii). The blue and red boxes indicate the 5 to 95 percentile of data distribution. The means of each mouse are shown as white circle for WT and as white triangle for V3OFF. *, $0.01 \leq P < 0.05$; **, $0.001 \leq P < 0.01$; ****, $P < 0.0001$.

Figure 3.12. V3OFF mice did not recover the hip excursion after spinal cord injury.

A

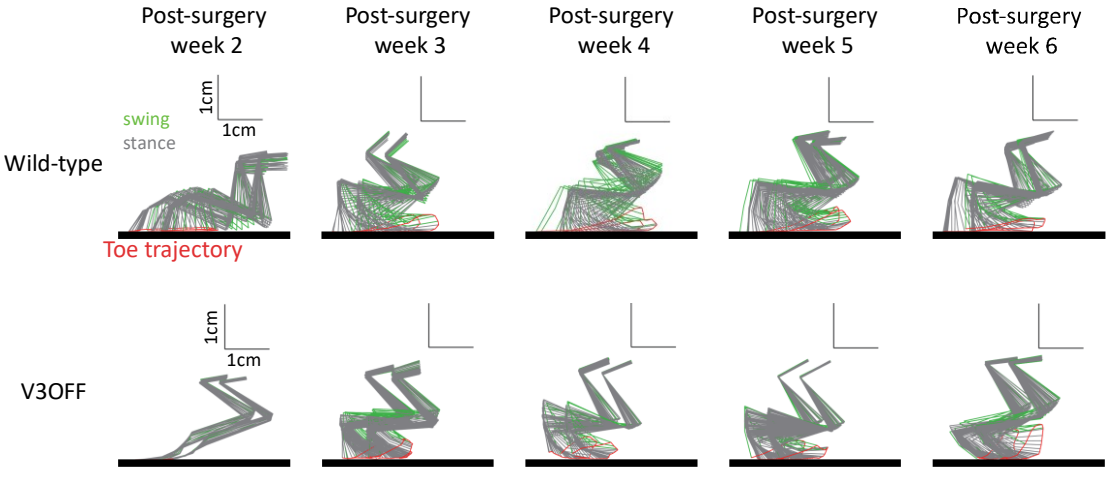

Bi Bii Biii

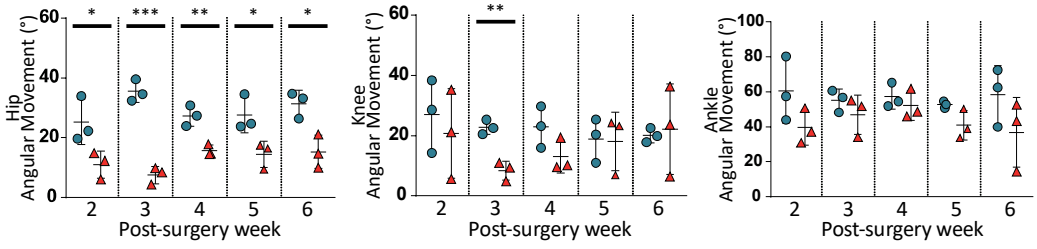

Ci Cii

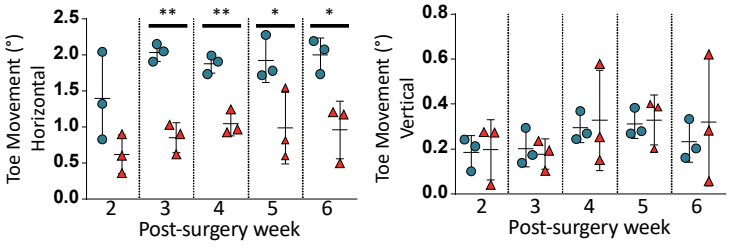

Figure 3.12. V3OFF mice did not recover the hip excursion after spinal cord injury.

A. Stick reconstructions and toe trajectories (red) of these two steps after spinal cord transection. The swing phase is represented by green sticks and stance is represented by gray sticks. *, $0.01 \leq P < 0.05$; **, $0.001 \leq P < 0.01$; ***, $0.0001 \leq P < 0.001$.

B. Comparison of joint angular movement for hip (i), knee (ii) and ankle (iii) of WT and V3OFF mice after spinal cord transection. Each circle or triangle represent data from individual mouse.

C. Horizontal (i) and vertical (ii) moving distance of toe of WT and V3OFF mice after spinal cord transection. Each circle or triangle represent data from individual mouse.

7 Supplementary figure

Supplementary Figure 3.1. Anterior and posterior extreme of WT and V3OFF mice during walking.

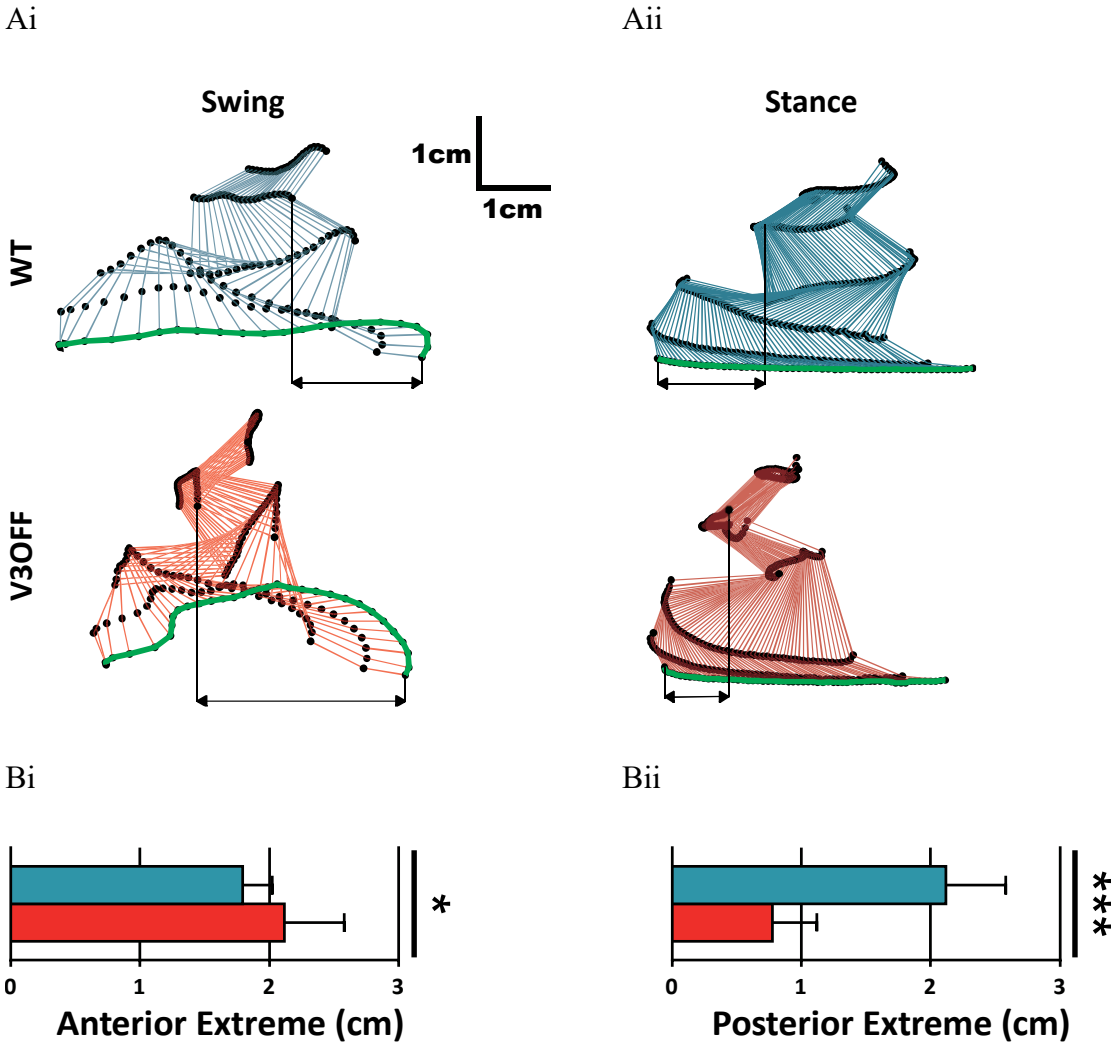

Ci

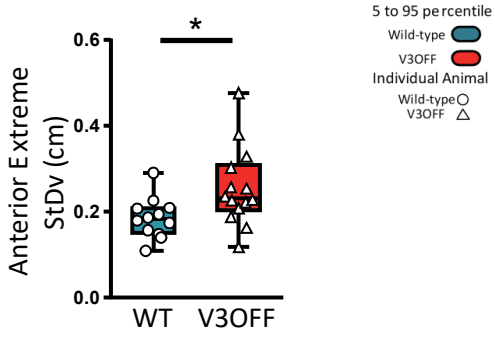
*
Anterior Extreme StDv (cm)
0.6
0.4
0.2
0.0
WT
V3OFF
5 to 95 percentile
Wild-type
V3OFF
Individual Animal
Wild-type
V3OFF

Cii

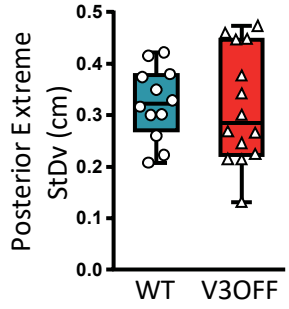
Posterior Extreme StDv (cm)
0.5
0.4
0.3
0.2
0.1
0.0
WT
V3OFF

Sup Figure 3.1. Anterior and posterior extreme of WT and V3OFF mice during walking.

A. The frame-by-frame reconstructed hindlimb movement of WT (blue) and V3OFF (red) mice during walking. The swing (i), and stance (ii) phase were separated by toe lifting and touching the ground. The horizontal distance between toe and hip joint was measured.

B. The means of distances between hip joint and toe at toe anterior (i) and posterior (ii) extreme position of WT (blue) and V3OFF (red) mice during walking were compared statistically. *, $0.01 \leq P < 0.05$; ***, $0.0001 \leq P < 0.001$

C. Box graphs of means of StDv of distances between hip joint and toe at toe anterior (i) and posterior (ii) extreme position of WT (blue) and V3OFF (red) mice during walking. The blue and red boxes indicate the 5 to 95 percentile of data distribution. The means of each mouse are shown as white circle for WT and as white triangle for V3OFF. *, $0.01 \leq P < 0.05$.

Supplementary Figure 3.2. Statistical parametric mapping identified lack of contralateral GS activity during ipsilateral swing-stance transition phase in V3OFF mice.

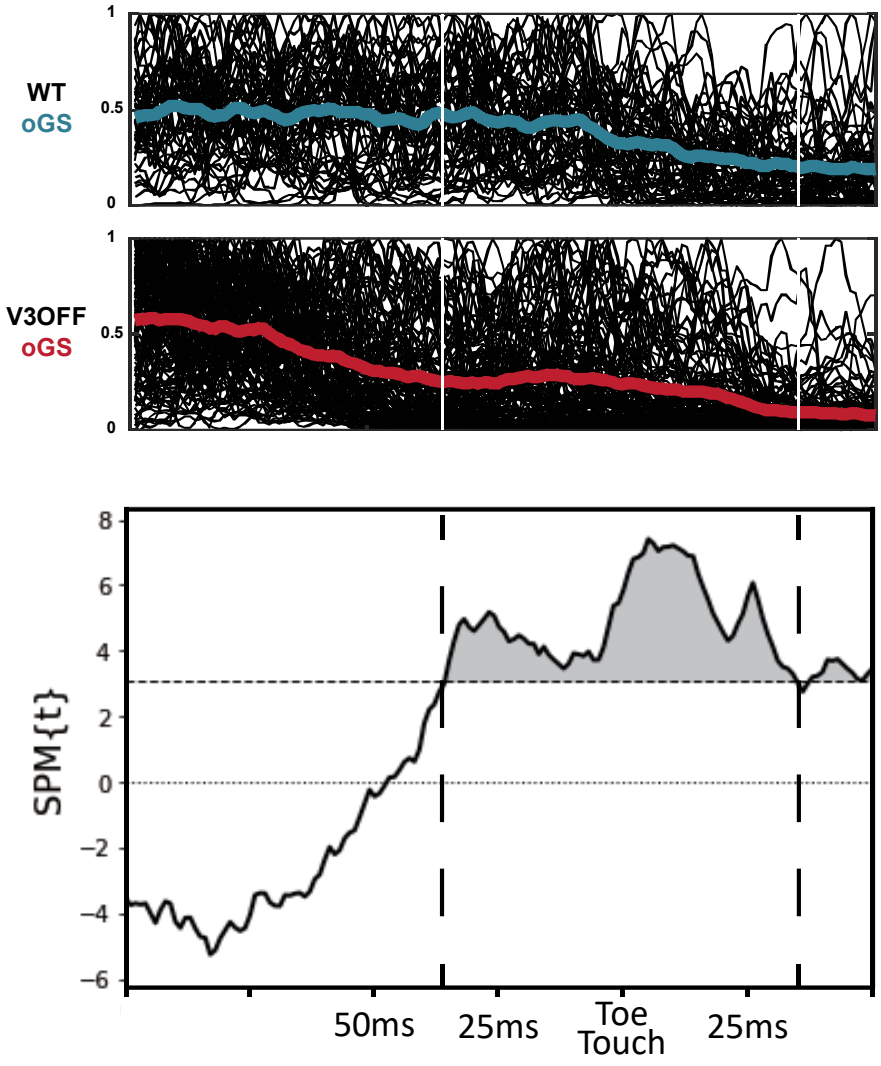

Sup Figure 3.2. Statistical parametric mapping identified lack of contralateral GS activity during ipsilateral swing-stance transition phase in V3OFF mice.

EMG activities of contralateral GS (oGS) of individual step are triggered around ipsilateral toe touch. Horizontal bar on the top indicates the mean of swing and stance phases in WT (blue) (n=12) and V3OFF (red) (n=14) mice. The processed EMG activities of each step are normalized by its peak amplitude in the current step. Only the activities within the episode ranging from 100ms before ipsilateral toe touch to 50ms after ipsilateral toe touch are normalized. The thick trace is averaged EMG activity from all steps in WT (blue) and V3OFF (red) mice. The gray area in the SPM t-map shows where the EMG pattern differed between WT and V3OFF mice. The horizontal dotted line in the SPM t-map indicates the critical threshold of Random Field Theory (RFT) for significant difference between WT and V3OFF mice.

Sup Figure 3.3. Comparison of hip phase duration between WT and V3OFF mice in inclined treadmill walking and swimming.

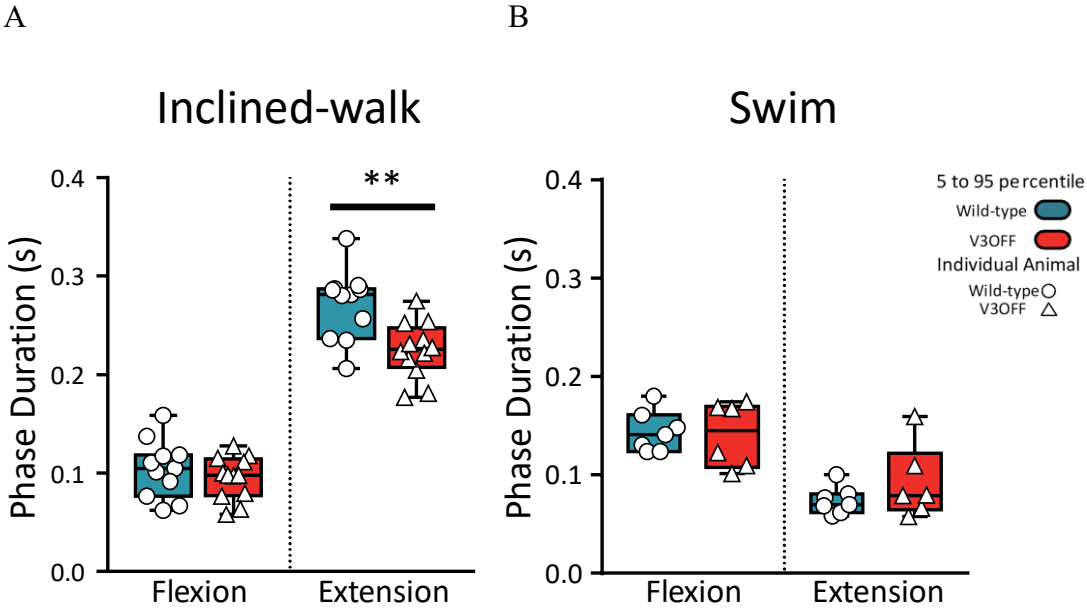

Sup Figure 3.3. Comparison of hip phase duration between WT and V3OFF mice in inclined treadmill walking and swimming.

Box graphs of means durations of hip joint angular movement during inclined-walking (A) and swimming (B). The blue and red boxes indicate the 5 to 95 percentile of data distribution. The means of each mouse are shown as white circle for WT and as white triangle for V3OFF. **, $0.001 \leq P < 0.01$

CHAPTER 4. SPINAL V3 INS AND LEFT-RIGHT COORDINATION IN MAMMALIAN LOCOMOTION

Contribution statement

I would like to acknowledge the laboratory of Dr. Ilya A. Rybak for the verification of the role of V3 INs in CPG circuits with modelling study; Dr. Joanna Borowska-Fielding for whole-cell patch-clamp recordings; Dylan Deska-Gauthier for the immunohistochemistry staining. This chapter contains portions of text co-written by Dr. Zhang, Dr. Ilya A. Rybak, Dr. Simon M. Danner, Dr. Natalia A. Shevtsova and me. I designed and performed all whole-cord recording experiments and statistical analysis for experimental data. Dr. Joanna Borowska-Fielding performed whole-cell patch-clamp recordings. Dylan Deska-Gauthier performed the immunohistochemistry staining. Dr. Simon M. Danner and Dr. Natalia A. Shevtsova performed model establishment and statistical analysis on modelling data. Dr. Simon M. Danner, Dr. Natalia A. Shevtsova and I performed data curation and visualization. This chapter have been published elsewhere (Danner, S.M., Zhang, H., Shevtsova, N.A., Borowska-Fielding, J., Deska-Gauthier, D., Rybak, I.A., & Zhang, Y. (2019). Spinal V3 INs and Left–Right Coordination in Mammalian Locomotion. Frontiers in Cellular Neuroscience, 13) and are reprinted here with permission.

1 Summary

CINs mediate interactions between rhythm-generating locomotor circuits located on each side of the spinal cord and are necessary for left-right limb coordination during locomotion. While glutamatergic V3 CINs have been implicated in left-right coordination, their functional connectivity remains elusive. Here, we addressed this issue by combining experimental and modelling approaches. We employed Sim1Cre/+; Ai32 mice, in which light-activated Channelrhodopsin-2 was selectively expressed in V3 INs. Fictive locomotor activity was evoked by NMDA and 5-HT in the isolated neonatal lumbar spinal cord. Flexor and extensor activities were recorded from left and right L2 and L5 ventral roots, respectively. Bilateral photoactivation of V3 INs increased the duration of extensor bursts resulting in a slowed down on-going rhythm. At high light intensities, extensor activity could become sustained. When light stimulation was shifted toward one side of the cord, the duration of extensor bursts still increased on both sides, but these changes were more pronounced on the contralateral side than on the ipsilateral side. Additional bursts appeared on the ipsilateral side not seen on the contralateral side. Further increase of the stimulation could suppress the contralateral oscillations by switching to a sustained extensor activity, while the ipsilateral rhythmic activity remained. To delineate the function of V3 INs and their connectivity, we developed a computational model of the spinal circuits consisting of two (left and right) rhythm generators (RGs) interacting via V0V, V0D, and V3 CINs. Both types of V0 CINs provided mutual inhibition between the left and right flexor RG centers and promoted left-right alternation. V3 CINs mediated mutual excitation between the left and right extensor RG centers. These interactions allowed the model to reproduce our current experimental data, while being consistent with previous data concerning the role of V0V and V0D CINs in securing left–right alternation and the changes in left–right coordination following their selective removal. We suggest that V3 CINs provide mutual excitation between the spinal neurons involved in the control of left and right extensor activity, which may promote left-right synchronization during locomotion.

2 Introduction

The rhythmic activities controlling locomotor movements in mammals are generated by neural circuits within the spinal cord, representing so-called central pattern generators (CPGs; Graham Brown, 1911; Grillner, 1981, 2006; Kiehn, 2006, 2011; Rossignol et al., 2006). It is commonly accepted that each limb is controlled by a separate spinal CPG and that CPGs controlling fore and hind limbs are located in the left and right sides of cervical and lumbar enlargements, respectively. These CPGs are connected by spinal CINs that coordinate their activities, hence defining locomotor gaits. CINs project axons across the spinal cord midline and affect INs and motoneurons located on the contralateral side of the cord (Kjaerulff and Kiehn, 1997; Butt and Kiehn, 2003; Quinlan and Kiehn, 2007; Jankowska, 2008).

Several classes of spinal CINs, including two subtypes of V0 CINs (excitatory V0V and inhibitory V0D) and the excitatory V3 CIN, have been identified based on their transcription factor profiles (Lanuza et al., 2004; Goulding, 2009; Gosgnach, 2011). Both subtypes of V0 CINs promote left–right alternation, and their functional ablation results in aberrant left–right synchronization. In vitro, selective ablation of V0D CINs disrupted left-right alternation at low locomotor frequencies while ablation of V0V CINs disrupted left-right alternation at higher locomotor frequencies (Talpalar et al., 2013). Thus, V0 CINs are necessary for securing left-right alternation.

In vivo, an increase of locomotor speed in rodents is accompanied by a transition from left–right alternating gaits (walk and trot) to left-right synchronized gaits (like gallop and bound). Yet, the CIN networks promoting left–right synchronization at higher locomotor speeds, or during V0 ablation, are poorly understood. Our previous modeling studies suggested that left-right synchronization could be performed by V3 CINs providing mutual excitation between the left and right rhythm-generating circuits (Rybak et al., 2013, 2015; Shevtsova et al., 2015; Danner et al., 2016, 2017; Shevtsova and Rybak, 2016). Although this suggestion allowed our previous models to reproduce the results of the above experimental studies, including the effects of V0 CIN ablation in vitro and in vivo, the role

and connectivity of V3 neurons suggested by these models have not been tested experimentally and remained hypothetical.

V3 INs, defined by their post-mitotic expression of the transcription factor single-minded homolog 1 (Sim1), are excitatory, and the majority of them project to the contralateral side of the spinal cord (Zhang et al., 2008). Genetic deletion of V3 INs did not affect left-right alternation, but caused unstable gaits in walking mice, and generated imbalanced and less robust rhythmic fictive locomotion in isolated neonatal spinal cords (Zhang et al., 2008). While these experimental data strongly suggest that V3 INs are involved in the control of locomotion, their exact function and commissural connectivity remain mainly unknown.

To address V3's functional connectivity between left-right spinal circuits, we used in vitro preparations of isolated spinal cords from neonatal mice, in which fictive locomotion was induced by neuroactive drugs. This preparation allows studying functional connectivity between genetically identified spinal INs, involved in CPG operation and left-right coordination. We took advantage of an optogenetic approach, which enabled us to specifically regulate the activity of V3 INs on each side of the isolated spinal cord during fictive locomotion. We then designed an updated computational model of spinal circuits that incorporated the connectivity of V3 CINs suggested from our experimental studies. Together our experimental and modelling results provide convincing evidence that V3 INs contribute to synchronization of the left-right locomotor activity (under appropriate conditions) by providing mutual excitation between the extensor centers of the left and right CPGs.

3 Results

3.1 Optical activation of lumbar V3 INs increases the intensity of extensor motor activity and slows oscillation frequency of drug-evoked fictive locomotion.

To assess the function of V3 INs in the spinal locomotor network, we used an optogenetic approach that allowed us to selectively activate V3 INs in different regions of the isolated

spinal cords from *Sim1*$^{Cre/+}$*; Rosa26* $^{ChR2\text{-}EYFP}$ (Sim1cre- Ai32) mice, which express ChR2 and EYFP in Sim1 positive cells.

To verify the expression of ChR2-EYFP in Sim1 positive V3 INs, we crossed Sim1cre-Ai32 with Rosa26tdTom (Ai14) to generate *Sim1*$^{Cre/+;\ tdTom}$*; Ai32* mice. Sim1$^{Cre/+;tdTom}$ has been well characterized and widely used in our previous studies (Borowska et al., 2013, 2015; Blacklaws et al., 2015). In *Sim1*$^{Cre/+;\ tdTom}$*; Ai3* spinal cords, ChR2-EYFP fusion protein could be specifically detected around all tdTom positive cells (Figure 4.1A), which demonstrated the co-expression of ChR2-EYFP and tdTom in Sim1+V3 INs. Using whole-cell patch-clamp recordings, we confirmed that the blue fluorescent light (488 nm) could produce membrane depolarization and evoke persistent spiking only in EYFP expressing cells (22/22) from the slices of Sim1cre-Ai32 or *Sim1*$^{Cre/+;\ tdTom}$*; Ai32* mice at postnatal day (P) 2–3 (Figures 4.1B1–B3). None of EYFP negative cells (10/10) showed any direct response to the light (Figure 4.1B1). The evoked spiking activity continued within a 20-s period with or without glutamatergic receptor blockers (CNQX and AP-5; Figures 4.1B2, B3). These results confirmed that V3 INs in the isolated spinal cords of Sim1cre-Ai32 mouse could be selectively activated by the blue fluorescent light.

To investigate the role of V3 INs and their interactions with CPG circuits, we shined fluorescent light onto the ventral spinal cord of neonatal Sim1cre-Ai32 mice during fictive locomotion evoked by a 5-HT/NMDA mixture (5-HT 8 μM, NMDA 7–8 μM) and analyzed the effects of light stimulation on the ongoing rhythmic activity (Figure 4.2). Flexor and extensor activities on each side of the cord were evaluated based on the recordings from L2 and L5 ventral roots, respectively. Optogenetic stimulation with blue fluorescent light applied on the whole L2 ventral spinal cord (Figure 4.2A) slowed down the ongoing rhythmic activity, as evident by an increased locomotor cycle period (Figures 4.2B, D; n = 12, left L5 P = 0.0005, right L5 P = 0.0010). The increased cycle duration was mainly attributed to an increase in the L5-burst durations, while L2-burst durations did not significantly change in response to the applied stimulation (Figures 4.2B, C). Furthermore, the optogenetic stimulation caused an increase in the amplitude of integral ENG bursts in L5, but not in L2 ventral roots (Figures 4.2B, E). These results suggest that

lumbar V3 neurons interact with locomotor CPGs and provide activation of extensor circuits, either directly or transynaptically.

3.2 Biased optical activation of V3 INs in spinal segment L2 leads to asymmetrical left–right motor activity.

Since most V3 neurons are CINs, activation of V3s on one side of the spinal cord should more strongly impact the contralateral circuits. To test this hypothesis, we used a 20x, 1.0 numerical aperture (NA) objective to deliver the light onto a small area on one side of the spinal cord (Figure 4.3A). We then selected the illuminated region by manually adjusting the field diaphragm to have the activation zone between approximately one-third to a half of the spinal cord (Figure 4.3B) and the intensity of the light-emitting diode (LED) light to regulate the number of V3 neurons being activated.

Under these experimental conditions, we found that optical activation of V3 INs on one side of the cord significantly prolonged L5 burst durations and step cycles on both sides (Figures 4.3C,D2,E; $P < 0.0001$), while L2 burst durations were not significantly affected (Figure 4.3D1). However, the contralateral L5 burst durations were influenced more strongly than those of ipsilateral L5 (Figure 4.3F). Consequently, the step-cycle period also changed more strongly on the contralateral side than the ipsilateral side (Figure 4.3E), which led to a left-right asymmetric activity with more bursts on the ipsilateral than on the contralateral side. Emergence of additional bursts in an integer relationship is a fundamental property of (weakly-) coupled oscillators, with asymmetric drive (Pikovsky et al., 2001; Pikovsky and Rosenblum, 2003; Rubin et al., 2011), suggesting that tonically activated V3 neurons mainly affect (and slow down) the contralateral CPG.

We also noticed a dose-response relationship between stimulation intensity and the prolongation of the contralateral cycle period and L5 burst duration (Figures 4.4A–C). At the highest applied light intensity, the rhythm of the contralateral cord can be suppressed, resulting in almost sustained extensor activity (Figure 4.4C). To further evaluate the relation between the asymmetric changes of the fictive locomotor activity in two sides of the spinal cord and the imbalanced activation intensity of V3 neurons, we systematically

manipulated the focal size and light intensity to study the response to three levels of stimulation (low, medium and high intensity; see methods). Interestingly, the L5 burst duration on the contralateral side to the light stimulation showed a positive linear correlation to the optical stimulation intensity (Figures 4.4D1,D2; $R^2 = 0.5081$, $P < 0.0001$), but not the ipsilateral L5 ($R^2 = 0.007813$) or both L2s ($R2 = 0.003418$, $R^2 = 0.1186$ for ipsilateral and contralateral sides, respectively). In turn, the changes of step cycle of contralateral locomotor activities also showed a positive linear correlation with the optical stimulation intensity (Figure 4.4E; $R^2 = 0.4842$, $P < 0.0001$). This result indicates that the asymmetric response is dependent on the activation of V3 neurons on one side of the spinal cord.

Together, our experiments showed that the activation of V3 neurons increased extensor activity, and prolonged burst and step cycle duration predominantly on the contralateral side with a smaller effect on the ipsilateral side. These resulted in left-right asymmetric rhythmic activity with lower-frequency bursting on the contralateral than on the ipsilateral side, suggesting that V3 neurons mainly affect the extensor activity of the contralateral CPG.

3.3 Modelling left–right interactions between rhythm generators.

To further delineate the function and connectivity of the spinal V3 INs involved in left–right coordination, we developed a computational model of the lumbar locomotor circuitry. We built upon our previous model (Shevtsova et al., 2015) with the assumption that V3 neurons slow down the contralateral rhythm by exciting the extensor centers of the contralateral rhythm generators and transsynaptically inhibiting the flexor centers. Our goal was to update the model so that it could reproduce the effect of bilateral and unilateral stimulation of V3 neurons revealed in the above experiments without disrupting its ability to reproduce previous experimental findings concerning the effects of ablation of V0V, V0D and all V0 CINs on the left-right coordination (Talpalar et al., 2013).

3.3.1 Model schematic

The updated model consisted of two rhythm generating networks (RGs), one for each side of the spinal cord (Figure 4.5). Each RG included two excitatory populations, representing flexor (F) and extensor (E) RG centers that mutually inhibited each other through populations of inhibitory INs (InF and InE). Similar to our previous model (Shevtsova et al., 2015), all neurons in both RG centers included a persistent (slowly inactivating) sodium current, allowing them to intrinsically generate rhythmic bursting. Because of the mutual excitation between the neurons within each center, which synchronized their activity, each center could intrinsically generate a population rhythmic bursting activity. However, according to the setup of initial neuronal excitability, under normal conditions, the extensor centers, if uncoupled, expressed sustained activation and the rhythmic activity of each RG were defined by the activity of flexor centers, which then provided rhythmic inhibition of the corresponding extensor centers via the InF populations (see Figure 4.5 and Zhong et al., 2012; Rybak et al., 2015; Shevtsova et al., 2015; Shevtsova and Rybak, 2016). Interactions between F and E centers of the left and right RGs were mediated by populations of V3, V0V and V0D CINs (Figure 4.5). Drug-induced fictive locomotion was modeled by an unspecific increase of the excitability of all neurons in the network through a depolarization of the leakage reversal potentials in each neuron. The drug concentration was defined by the parameter α (see section Materials and Methods).

In the present model, the organization of interactions between left and right RGs mediated by V0V and V0D populations of CINs followed that of our previous models (Shevtsova et al., 2015; Danner et al., 2016, 2017; Shevtsova and Rybak, 2016; Ausborn et al., 2019). Specifically (see Figure 4.5), the populations of inhibitory V0D CINs provided direct mutual inhibition between the left and right flexor centers of the RGs, while the populations of excitatory V0V CINs mediated mutual inhibition between the same flexor centers through oligosynaptic pathways (each V0V population received excitation from the ipsilateral flexor center through a local population of V2a neurons and inhibited the flexor center of the contralateral RG through a population of local inhibitory neurons, Ini). Both V0V and V0D pathways ensured left-right alternation.

The organization of V3 CIN pathways in the present model differed from the previous models and was constructed to fit our experimental results. Based on these results we

suggested that V3 populations mediate mutual excitation between the extensor centers of the left and right RGs (Figure 4.5) and promoted inhibition of the contralateral flexor centers.

Each population of neurons in our model (Figure 4.5) consisted of 50–200 neurons (Table 4.1). All neurons were modeled in the Hodgkin-Huxley style (for details see Materials and Methods, section Computational Modeling and Table 4.1). Heterogeneity within the populations was ensured by randomizing the baseline value for leakage reversal potential and initial conditions for the values of membrane potential and channel kinetics variables. Connections between the populations were modeled as sparse random synaptic connections. Model equations and simulation procedures are listed in Section "Materials and Methods." Population specific parameters are listed in Table 4.1 and connection weights and probabilities are specified in Table 4.2.

3.3.2 The model exhibits characteristic features of drug-induced fictive locomotion and frequency-dependent changes of left–right coordination following removal of V0 CINs.

First, we characterized the model performance under normal conditions by simulating drug-induced fictive locomotion (Figure 4.6). The model exhibited alternation between the rhythmic activities of the flexor and extensor RG centers on each side as well as alternation between the activities of the left and right RGs. By increasing α (simulating an increase in the drug concentration) the burst frequency increased (Figures 4.6A–C). The frequency increase was accompanied by an asymmetric decrease of the burst durations: extensor burst durations decreased more than flexor burst durations. At all frequencies, left–right alternation was maintained. Thus, the model reproduced the main characteristics of drug-induced fictive locomotion in mice.

To test whether the model is still consistent with the frequency-dependent changes in left–right coordination following the removal of V0 CINs (Talpalar et al., 2013), we simulated the selective removal of V0V, V0D or both V0 CIN populations by setting all connection weights from the selected types of neurons to 0. Removal of V0V CIN populations did not change left-right alternation at low locomotor frequencies (Figure 4.7A1) but demonstrated

left-right synchronized activity at high oscillation frequencies (Figure 4.7A2). Removal of V0D CINs had the opposite effect: left-right synchronization occurred at low frequencies (Figure 4.7B1), while left-right alternation was maintained at high frequencies (Figure 4.7B2). Finally, removal of both types of V0 CIN populations led to left-right synchronization at all frequencies (Figures 4.7C1, C2). Thus, similar to the previous model (Shevtsova et al., 2015) the present model was able to reproduce the experimental results on the speed-dependent role of V0V and V0D in support of left-right alternation (Talpalar et al., 2013).

3.3.3 The model reproduces deceleration of the rhythm by tonic stimulation of V3 neurons.

To simulate bilateral optogenetic stimulation of V3 CINs (see Section Optical Activation of Lumbar V3 INs Increases the Intensity of Extensor Motor Activity and Slows Oscillation Frequency of Drug-Evoked Fictive Locomotion), we incorporated a channelrhodopsin ionic current, IChR, in V3 neurons (see Materials and Methods, Section Simulations of Changes in the Locomotor Frequency by Neuroactive Drugs and Application of Photostimulation), which was activated in all V3 neurons for 15 s during ongoing locomotor activity. The results of these simulations with progressively increased stimulation intensity are shown in Figures 4.8, 4.9. At any value, the applied stimulation increased the firing rate of active V3 neurons and recruited new neurons that were silent before stimulation (Figures 4.8A2–C2, A3–C3). Immediately with its onset, V3-stimulation increased the cycle period and reduced the burst frequency of both RGs (Figures 4.8A1, B1). The frequency reduction was mainly caused by a prolongation of the extensor burst duration. Flexor-extensor and left–right alternations were preserved during this stimulation. With increasing value of stimulation, the frequency was progressively decreased (Figures 4.8A1, B1). At high stimulation values, the rhythm could be stopped, resulting in sustained activation of both extensor centers and suppression of both flexor centers (Figure 4.8C1). Once the stimulation was stopped, the model exhibited a short transitional period (one or two cycles) and then returned to the same burst frequency and pattern that were expressed before stimulation.

To study the effect of bilateral stimulation intensity on model behavior in more detail, we performed a simulation when the value of gChR (conductance of the channelrhodopsin ionic current, IChR, that characterizes the intensity of photostimulation in the model) was slowly changed from 0 to 0.4 (see section Materials and Methods). The results of this simulation (Figure 4.9A) show that both flexor and extensor phases increase with increasing intensity of stimulation and the slope of this increase is higher for larger values of gChR. To simulate experimental variability, in a series of simulations parameters α (defining the average level of neuron excitation in the model) and gChR were randomly chosen from a uniform distribution in intervals [0.01; 0.06] and [0.18; 0.4], respectively. For each pair (α, gChR) a simulation was run in which average flexor and extensor burst durations and period of oscillations were calculated and compared to the control condition (gChR = 0; see Figures 4.9B, C). These results qualitatively reproduce the experimental results shown in Figures 4.2D, E.

Altogether our results show that the model closely reproduces our experimental findings of bilateral optogenetic stimulation of V3 neurons during drug-induced fictive locomotion when stimulation was applied at the midline and equally affected left and right V3 neurons (see section Optical Activation of Lumbar V3 INs Increases the Intensity of Extensor Motor Activity and Slows Oscillation Frequency of Drug-Evoked Fictive Locomotion).

The reduction of the oscillation frequency when V3 neurons were stimulated occurred because both (left and right) extensor centers were activated by V3 neurons and they both provided an additional inhibition to the corresponding flexor centers through the corresponding inhibitory populations (InE), which reduced the average excitation of the flexor centers (Figure 4.5). In addition, activated V3 neurons provided direct excitation of the contralateral InE populations inhibiting the corresponding flexor centers. Note that the frequency of persistent sodium current-dependent oscillations positively correlates with the average excitation of a population of neurons with this current and mutually excitatory interconnection (Butera et al., 1999; Rybak et al., 2004, 2015). Since the rhythm in our model was generated by flexor centers, the reduction of their excitation during V3 neuron activation led to the reduction of oscillation frequency generated in both RGs. Furthermore, the reciprocal excitation of the extensor centers through V3 CINs created a positive

feedback loop that amplified the firing rates of its constituent neurons and consequently the net inhibition exerted on the flexor centers.

3.3.4 The model reproduces asymmetric changes of the locomotor rhythm by unilateral stimulation of V3 neurons.

To simulate the effects of unilateral activation of V3 neurons during locomotor activity (see section Biased Optical Activation of V3 INs in Spinal Segment L2 Leads to Asymmetrical Left–Right Motor Activity), we activated IChR in all V3 neurons located on one side of the cord. At a low value of unilateral activation of ipsilateral V3 population (Figure 4.10A), the extensor burst durations and the cycle periods increased on both sides, while the flexor-extensor and left-right alternation remained unchanged, which was similar to the effect of bilateral stimulation. With increasing value of stimulation (Figures 4.10B, C), the rhythm of the contralateral circuits was progressively slowed down, and additional bursts appeared ipsilateral to the stimulation. Figure 4.10B shows a stable 2-to-1 relationship between the number of burst ipsilateral and contralateral to the stimulation. In Figure 4.10C one can see both 2-to-1 and 3-to-1 relationships. In all cases, reciprocity between the flexor centers maintained. Our simulations shown in Figures 4.10B,C qualitatively reproduced the experimental results concerning the response of the fictive locomotor pattern to the weak and medium unilateral optical stimulation of V3 neurons (Figures 4.4A,B) where one can also see an unequal number of flexor bursts on ipsi- and contralateral sides (marked by asterisks in Figures 4.10B,C).

This effect is even more obvious on the bifurcation diagrams in Figures 4.11A1, A2 that show flexor and extensor phase durations plotted against parameter gChR, which has been gradually increased from 0 to 0.4. At lower values of gChR, both flexor and extensor phases progressively increase with an increase of parameter gChR. At a critical value of gChR, the curves characterizing dependence of flexor and extensor phase durations on gChR bifurcate into two and then three branches. The bifurcation diagram in Figure 4.11B1 demonstrates that the stable regime at lower gChR values is characterized by a 1:1 ratio between the numbers of bursts in the contra- and ipsilateral flexor centers and then with increasing gChR the model starts to exhibit also 1:2 and 1:3 burst ratios with multiple

bursts of the ipsilateral flexor center during one period of contralateral oscillations. In the diagrams in Figures 4.11A1, B1 the bifurcations (transitions between regimes) can be seen as discontinuities. Transitions between stable regimes of 1:1, 1:2, and 1:3 ratios happen through intermediate quasiperiodic regimes where 1:1 and 1:2 or 1:2 and 1:3 ratios between the numbers of contra- and ipsilateral bursts occur and alternate with different integer intervals. To assess transition between regimes in more detail, in a series of simulations we fixed parameter gChR at some values (marked by red circles and vertical dashed lines in Figure 4.11B1) and estimated the timing of burst onsets in ipsi- and contralateral flexor centers for 40 s of simulated time. The results of these simulations are shown as the diagrams of ipsi- and contralateral flexor burst onsets in Figure 4.11B2. These diagrams demonstrate how the 1:1 regime at lower values of gChR transitions to the 1:2 regime through an intermediate quasiperiodic {1:1; 1:2} regime as gChR increases, and then to the 1:3 regime though another quasiperiodic {1:2; 1:3} regime.

The 1:2, 1:3 and intermediate quasiperiodic regimes are characterized by increased variability of burst durations during a single recording (see Figures 4.11A1, A2). Such behavior obviously affects the estimated average phase duration and period in particular experiments. Indeed, in experimental results shown in Figures 4.3D1, 4.4D1, in individual recordings the flexor burst duration decreases during photostimulation as compared to the control condition, while on average there is either an increase (Figure 4.3D1) or no change (Figure 4.4D1). This is reproduced in our simulations (Figures 4.12A1,B), in which the results are shown for a series of computer experiments when parameters α and gChR were randomly chosen in intervals [0.01; 0.06] and [0.18; 0.4], respectively, and for each pair (α, gChR) a single simulation was performed to estimate average values for burst duration and oscillation period and compare with the control condition. These simulation results closely reproduce the experimental results shown in Figures 4.3D1,E. Interestingly, when the results of these simulations were conditionally separated according to the value of parameter gChR and the differences in flexor and extensor burst durations and period of oscillation in stimulated vs. control conditions were plotted against stimulation strength (similar to what was done in experiment in the spinal cord in vitro, see Figures 4.4D1,E), these results strikingly resembled the experimental results in Figures 4.4D1,E and

demonstrated asymmetric response in the ipsi- and contralateral RG centers. Altogether, our modeling results strongly support the hypothesis that activation of V3 INs on one side of the spinal cord more strongly impacts the contralateral circuits.

To simulate the effects of high intensity and larger focal area unilateral stimulation, an additional weak stimulation of the contralateral V3 neuron population was applied (Figure 4.10D). In this case, the rhythmic activity on the ipsilateral side slowed down during the stimulation and the contralateral extensor centers became constantly active, while irregular low-amplitude activity of the contralateral flexor centers occurred. This behavior of the model was similar to the results of experimental studies at a high intensity unilateral stimulation when the rhythm of the contralateral cord was suppressed, resulting in almost sustained extensor activity (Figure 4.4C). Based on our simulation results, we suggest that at high stimulation intensities the stimulation partly affected V3 neurons on the side contralateral to stimulation.

4 Discussion

In the current study, we combined experimental studies with computational modeling to investigate the potential roles that V3 INs play in the spinal locomotor network. In our experiments, we used the in vitro preparations of isolated spinal cords from neonatal (P2-P3) mice in which fictive locomotion was induced by a mixture of neuroactive drugs (NMDA and 5-HT). Although the isolated neonatal spinal cords are characterized by a lack of supra-spinal and sensory inputs and are from young animals whose weight bearing ability is not fully developed, this preparation allows studying basic CPG circuits and functional interactions between genetically identified spinal INs (Kjaerulff and Kiehn, 1997; Lanuza et al., 2004; Gosgnach et al., 2006; Zhang et al., 2008). Using optogenetic approaches, we were able to selectively activate V3 INs at different regions of the spinal cord during drug-evoked fictive locomotion. Our computational model of locomotor circuits was able to qualitatively reproduce the experimental results. Our study revealed that lumbar V3 INs strongly enhance the contralateral extensor activity and regulate the frequency of the locomotor oscillations. We suggest that spinal V3 CINs mediate mutual excitation between the extensor centers of the left and right rhythm generators in the

lumbar spinal cord, which might support the synchronization of left-right activity under certain conditions during locomotion. In addition, we show that unilateral activation of V3 CINs can produce left-right asymmetrical rhythmic outputs, which provides a potential mechanism for the separate regulation of left–right limb movements as required for changing direction or during split-belt locomotion (Kiehn, 2016).

4.1 Optogenetic activation of V3 INs

Mapping the functional connectivity among neurons in the central nervous system is vital to understand circuit mechanisms underlying behavior. This is especially true within the spinal cord, which generates the rhythmic and patterned motor outputs necessary for coordinated movement (Grillner, 2006; Kiehn, 2006, 2011; Danner et al., 2015). However, uncovering the functional circuitry within the spinal cord has proven difficult due to a lack of clear anatomical organization compared to other brain regions. In the current study, novel optogenetic tools (Dougherty et al., 2013; Hägglund et al., 2013; Levine et al., 2014) have enabled us to specifically, reversibly, and acutely regulate the activity of a molecularly identified group of spinal neurons. By using Sim1cre-Ai32 mice (Chopek et al., 2018), we were able to target V3 INs on both or just one side of the isolated spinal cord, allowing us to start dissecting the function of V3 CINs in spinal locomotor circuits.

Using whole-cell patch-clamp recordings, we could verify that all ChR2-EYFP-expressing cells in the lumbar spinal slices could be exclusively depolarized by blue fluorescent light and elicit spikes during periods of the light pulses (10–20 s). During our functional study, however, we had to keep the whole lumbar cord intact and deliver the LED light on the ventral surface of the isolated spinal cord. Thus, we expect to have activated V3 neurons that had cell bodies and terminals located or neurites passing the illuminated region that is relatively close to the ventral surface. Although we were not able to specify the particular group of V3s, which we might be activating, we kept the light intensity, size and position consistent to limit variability across experiments.

4.2 The V3 CINs provide excitation to the contralateral CPG extensor center.

The identification of genetically defined IN populations has enabled us to characterize their specific functions in locomotor behaviors (Goulding, 2009; Gosgnach et al., 2017; Deska-Gauthier and Zhang, 2019). Until now, however, most experimental data were obtained by genetically eliminating certain classes of spinal INs without clear understanding of connectivity among the spinal INs (Lanuza et al., 2004; Gosgnach et al., 2006; Crone et al., 2008; Zhang et al., 2008; Talpalar et al., 2013; Bellardita and Kiehn, 2015; Haque and Gosgnach, 2019). In the case of V3 INs, genetic deletion of entire V3 population reduced the general robustness of the rhythmicity of the in vivo and in vitro locomotor activity and led to unstable gaits (Zhang et al., 2008). Our previous anatomical studies were only able to show that V3 cells had broad projections to contralateral MNs and other ventral spinal INs along the lumbar spinal cord, but we still do not know their precise anatomical position and their role in the CPG network (Zhang et al., 2008; Blacklaws et al., 2015). The current spatially controlled activation of V3 neurons was the first step to overcome this limitation to decipher their functional role in the spinal cord.

We found that the bilateral photoactivation of V3 neurons in the isolated spinal cord during fictive locomotion increased the intensity and duration of L5 bursts and prolonged the step cycles in all recorded lumbar roots whereas the duration of bursts in L2 roots was not significantly affected. These results suggested that, under our experimental condition, the photoactivated V3 INs predominantly excited the circuits responsible for extensor activities, which in turn reduced the frequency of fictive locomotion oscillations. This conclusion became more evident when we activated V3 INs only on one-side of the cord with varied light intensities. With such stimulations, we found that only the increase of burst duration of contralateral L5 were positively correlated to the intensity of the illuminating light, and at high intensity of unilateral photostimulation the contralateral L5 activity could express a sustained activity. More interestingly, such uneven regulation of contralateral extensor excitability by V3 CINs significantly decreased the bursting frequency of the contralateral ventral root output, which led to asymmetrical oscillation of the motor outputs on the two sides of the spinal cord. Thus, our experimental results support the conclusion that the lumbar V3 INs, or at least a sub-group of them, strongly regulate the extensor activity and step cycle duration on the contralateral side of the cord.

Similar to other genetically defined types of spinal IN populations (Bikoff et al., 2016; Gosgnach et al., 2017; Deska-Gauthier and Zhang, 2019), the V3 population is heterogeneous and consists of sub-populations with different anatomical, physiological, and molecular profiles (Borowska et al., 2013, 2015). In the present study, however, we did not consider different subtype of V3 neurons. When we delivered the LED fluorescent light on the ventral surface of the spinal cord, we most likely activated a mixed group of different V3 neuron types in the illuminated region. Nonetheless, this discovery has provided direct evidence that some subtypes of V3 neurons can regulate the rhythm and pattern of the locomotor output through manipulating the contralateral extensor circuits.

4.3 Model prediction: V3 INs project to local contralateral inhibitory V1 neurons.

To reproduce the experimental results, it was necessary to model connections from the V3 CINs to the local contralateral inhibitory populations that inhibit the contralateral flexor centers (InE; Figure 4.5). The main function of these connections in the present model was to allow for the reduction in frequency with V3 stimulation. In our previous models (Danner et al., 2016, 2017), we had introduced hypothetical inhibitory CIN populations mediating inhibition from the extensor centers to the contralateral flexor centers. These connections allowed for perfect alternation (0.5 normalized phase difference) between the left and right RGs. In the present model, the V3 connection to the local contralateral inhibitory neurons achieved the same function while no additional populations were needed.

The classes of V1 and V2b inhibitory neurons have been implicated in mediating flexor-extensor alternation (Zhang et al., 2014). Specifically, V1 neurons were suggested to provide inhibition from the extensor to the flexor RGs (Zhang et al., 2014; Shevtsova and Rybak, 2016): the same connection pattern as the InE populations in our model (Figure 4.5). Thus, our model predicts that V3 CINs project to contralateral V1 neurons that inhibit the flexor center. This prediction awaits experimental verification.

4.4 Coordination of left–right activities by V3 INs during locomotion.

Until now, several types of CINs, including V0, V3, and dI6, have been identified in the ventral spinal cord (Lanuza et al., 2004; Zhang et al., 2008; Andersson et al., 2012; Talpalar et al., 2013; Bellardita and Kiehn, 2015; Haque et al., 2018). When each of these CIN types, except V3, was genetically deleted, the left–right hind-limb alternation was affected. Particularly, V0V and V0D CINs were shown to secure the speed-dependent left-right alternation at walking and trotting gaits without effects on hind-limb synchronization observed during gallop and bound (Talpalar et al., 2013; Bellardita and Kiehn, 2015). On the other hand, deletion of V3 CINs did not affect the left-right alternation of the limb movement during walk and trot (Zhang et al., 2008). We had suggested that V3 represent the CIN populations that mediate left–right synchronization in certain conditions (e.g., when some or all V0 CINs are genetically removed) and during gallop and bound. In our previous computational models (Rybak et al., 2013; Shevtsova et al., 2015; Danner et al., 2016, 2017; Shevtsova and Rybak, 2016), to perform this function the V3 CINs were assigned to explicitly mediate mutual excitation between the flexor centers of the left and right rhythm generators. However, our current experimental outcome contradicts this assumption, suggesting functional connections of V3 CINs to the contralateral extensor centers instead of the flexor centers. To match our experimental findings, we changed the connection of simulated V3 populations from the activation of contralateral flexor centers to the activation of contralateral extensor centers. With this change in the V3 connectivity we were able to qualitatively reproduce all our current and previous experimental results, including speed-dependent left–right alternation mediated by V0V and V0D.

This unification of the experimental and computational data confirmed that the proposed organization of our current computational model of spinal circuits is plausible, and that V3 INs can mediate the synchronization of left-right hind-limb activities through mutual excitation of extensor centers of the left and right spinal rhythm generators.

Excitatory commissural neurons (such as the V3 CINs) have been reported to mediate reticulospinal and vestibulospinal input as well as input from ipsilateral somatosensory afferents to contralateral motoneurons (Bruggencate et al., 1969; Bruggencate and Lundberg, 1974; Matsuyama et al., 2004; Cabaj et al., 2006). Kasumacic et al. (2015) further described a population of CINs that directly receives vestibulospinal input and

contributes to contralateral extensor activity. These pathways are thought to be involved in stabilizing posture during locomotion. Based on our results, the V3 class is a likely candidate for mediating and integrating these inputs. Thus, studying interaction and convergence of supraspinal and somatosensory afferent inputs on V3 might lead to a better understanding of the role and function of these pathways during locomotion.

Activation of V3s of one side of the spinal cord resulted in asymmetric modulation of extensor and flexor phase durations between the two sides of the cord. This allows a suggestion that V3 INs may play important functional roles in left–right coordination when changing the direction of movement, walking on a curved path (Courtine and Schieppati, 2003a, b), on unequal surfaces or a split-belt treadmill (Forssberg et al., 1980; Yang et al., 2005; Frigon, 2017). Such locomotor behaviors may be controlled by an additional supraspinal or afferent activation/suppression to V3 neuron populations on one side of the cord. In these situations, different speeds for left-right limbs are necessary for maintaining stable locomotion. The precise mechanisms underlying such movements are still unknown, but it has been indicated that the independent but closely coordinated CPG circuits in both sides of the spinal cord are involved (Frigon, 2017). In our current experimental and modeling studies, we could induce asymmetric rhythmic activities with an unequal number of bursts between the two sides of the spinal cord by unilaterally activating V3 neurons. These results closely resemble the findings in split-belt locomotion with a large speed difference for the left and right belts, in which additional steps were observed on the fast side (Forssberg et al., 1980; Yang et al., 2005; Frigon, 2017). Such activity patterns are reminiscent of those of (weakly-) coupled oscillators, with asymmetric drive (Pikovsky et al., 2001; Pikovsky and Rosenblum, 2003; Rubin et al., 2011) and since our data were obtained in an isolated spinal cord preparation, they provide even more convincing evidence of the existence of a CPG on either side of the cord.

In conclusion, our study provides strong evidence that spinal V3 CINs are involved in left-right limb coordination during locomotion presumably by providing mutual excitation between the extensor centers of the left and right rhythm generators and mediating inhibition from the extensor centers to their contralateral flexor centers through an additional inhibitor IN population. In addition, we have shown that unilateral activation of

V3 CINs can produce left-right asymmetric rhythmic outputs. Which led us to suggest that V3 neurons are involved in changing the direction of movements and/or in control of locomotion through complex environments.

5 Materials And Methods

5.1 Experiment materials and methods

Animals

The generation and genotyping of Sim1Cre/+ mice were described previously by Zhang et al. (2008). Ai32 mice were from the Jackson Laboratory (Stock No. 012569). It contains Rosa26-cytomegalovirus early enhancer element/chicken beta-actin promoter (CAG)-loxP–Stop codons–3x SV40 polyA–loxP (LSL)-channelrhodopsin2 (ChR2)-enhanced yellow fluorescent protein (EYFP)-woodchick hepatitis virus posttranscriptional enhancer (WPRE; RC-ChR2). Sim1cre-Ai32 mice were generated by breeding these two strains expressed ChR2/EYFP fusion-protein in Sim1 expressing cells. TdTomato Ai14 (Jackson Laboratory Stock No. 007908) conditional reporter (referred as tdTom) mice were generated and genotyped as previously described (Blacklaws et al., 2015). Sim1Cre/+; tdTom; Ai32 mice were generated by crossing Sim1Cre/+; tdTom mice with Ai32 mice. All procedures were performed in accordance with the Canadian Council on Animal Care and approved by the University Committee on Laboratory Animals at Dalhousie University.

Electrophysiology and immunohistochemistry

Preparation

All experiments were performed using spinal cords from Sim1cre-Ai32 mice (isolated spinal cord recording and whole-cell patch-clamp recording) and Sim1Cre/+; tdTom; Ai32 mice (whole-cell patch-clamp recording) at postnatal day (P) P2-P3. The mice were anesthetized, and the spinal cords caudal to thoracic (T) 8 segments were dissected in an ice-cold oxygenated Ringer's solution (111 mm NaCl, 3.08 mm KCl, 11 mm glucose, 25

mm NaHCO3, 1.25 mm MgSO4, 2.52 mm CaCl2, and 1.18 mm KH2PO4, pH 7.4). The spinal cord was then transferred to the recording chamber to recover at room temperature for 1 h before recording in Ringer's solution.

Isolated whole-cord recordings

Electroneurogram (ENG) recordings of the (lumbar) L2 and L5 ventral roots were conducted using differential AC amplifier (A-M system, model 1700) with the band-pass filter between 300 Hz and 1 kHz. Analog signals were transferred and recorded through the Digidata 1400A board (Molecular Devices) under the control of pCLAMP10.3 (Molecular Devices). Fictive locomotor activity was induced by applying 5-hydroxytryptamine (5-HT, 8 μM) and NMDA (7–8 μM) in the Ringer's solution.

Optical stimulation of v3 INs

To activate ChR2 in V3 INs, 488 nm fluorescent light was delivered by Colibri.2 illumination system (Zeiss) through 10x or 20 × 1.0 numerical aperture (NA) objectives mounted on an up-right microscope (Examiner, Zeiss) onto the ventral surface of the isolated spinal cord, a protocol adopted from other studies (Hägglund et al., 2013; Levine et al., 2014). This allowed us to have relative fixed focal areas. In addition, using the Colibri system, we were able to control the LED light intensity accurately. Only when we needed to compare the intensity-dependent changes, we would manually adjust the focal size of the field diaphragm and LED light intensity.

To perform unilateral stimulation, we manually adjusted the field diaphragm and LED light intensity to cover the whole half side of the spinal cord to be the largest illuminated area, and then to reduce the illuminated region between approximately one-third to a half of the spinal cord (Figure 4.4B) to regulate the number of V3 neurons being activated. For each cord, we set the stimuli with largest focal area and 100% light intensity as the high intensity group, then reduced focal area to medium group, and the smallest focal area less than medium group (one of third) and/or reduced light intensity to less than 50% as the low intensity group.

Continuous light stimuli with duration of 10 and 20 s were used. To use such long-lasting stimuli, we needed to make sure that they do not cause any damage of tissue and neuronal behavior. Our special studies did not find any damage produced by such stimulations in our experiments including possible effects on patch-clamp or whole cord recordings. The results of such experiments are shown in Supplementary Figure 4.1. Specifically, under whole cell-patch-clamp configuration, we used three consecutive 20-s light pulses to EYFP or tdTomato positive cell and showed that the firing patterns of cells were the same during each stimulation (Supplementary Figure 4.1A1) and their response to injected current the same before and after optical stimulation (Supplementary Figure 4.1A2; n = 22). In contrast, under the same conditions, the EYFP and tdTomato-negative neurons did not respond to the light stimulation (Supplementary Figure 4.1B1) but could generate normal spiking activity in response to injected current (Supplementary Figure 4.1B2; n = 10). To further verify that the optical stimulation did not affect neuronal activity, we applied maximum optical stimulation (100% light intensity, 10x objective) on the spinal cord of Cre negative Ai32 mice. The activity of all recorded nerves remained unchanged under and after the 20-s light pulses (Supplementary Figure 4.1C).

Whole-cell patch-clamp recordings

The experimental procedures were detailed in Borowska et al. (2013). Briefly, 300 μM slices from the spinal cord lumbar region (T13–L3) from P2-3 Sim1cre-Ai32 or Sim1Cre/+; tdTom; Ai32 mice were prepared in an ice-cold oxygenated sucrose solution (3.5 mm KCL, 25 mm NaHCO3, 1.2 mm KH2PO4, 1.3 mm MgSO4, 1.2 mm CaCl2, 10 mm glucose, 212.5 mm sucrose, and 2 mm MgCl2, pH 7.4) on a vibratome (Vibratome 300, Vibratome). Slices were incubated in an oxygenated Ringer's solution (111 mm NaCl, 3.08 mm KCl, 11 mm glucose, 25 mm NaHCO3, 1.25 mm MgSO4, 2.52 mm CaCl2, and 1.18 mm KH2PO4, pH 7.4) at room temperature for >30 min for recovery before recording. EYFP fluorescence-positive, tdTom fluorescence-positive and fluorescence-negative cells were visually identified using a 40× water-immersion objective (numerical aperture, 0.8) with the aid of a DAGE-MTI IR-1000 CCD camera.

Conventional whole-cell patch-clamp recordings were made in voltage- and current-clamp modes using a MultiClamp 700B amplifier (Molecular Devices). Analog signals were filtered at 10 kHz with the Digidata 1400A board (Molecular Devices) under control of pCLAMP10.3 (Molecular Devices). Patch-clamp recording pipettes with a resistance of 5–8 MΩ were filled with solution containing 128 mm K-gluconate, 4 mm NaCl, 0.0001 mm CaCl2, 10 mm HEPES, 1 mm glucose, 5 mm Mg-ATP, and 0.3 mm GTP-Li, pH 7.2 and the fluorescent light was delivered through the 40x objective.

Immunohistochemistry and confocal image capture

Following recording, 300 µM spinal slices from P2-3 Sim1Cre/+; tdTom; Ai32 mice were fixed in 4% paraformaldehyde (Electron Microscopy Science) for 10 min. Sections were then rinsed three times in 0.1% Triton X-100 (PBS-T) for 1 h total (20 min each rinse) at room temperature. Sections were then incubated in primary antibody solution for 2 days at 4°C. Primary antibody solutions consisted of 90% PBS, 10% Horse Serum (Invitrogen), and primary antibodies. Primary antibodies used were Rabbit anti DsRed (1:2000, Cat#600-401-379, Rockland) and Chicken anti GFP (1:1000, Cat#GFP-1010, Aves Labs). Following primary antibody incubation, sections were rinsed three times in PBS for 1 h total (20 min each rinse) at room temperature. Sections were then incubated in secondary antibody solution overnight at 4°C. Secondary antibody solutions consisted of 90% PBS, 10% Horse Serum (Invitrogen), Alexa Fluor 647-conjugated streptavidin (Jackson ImmunoResearch Laboratories, Inc.), and secondary antibodies. Secondary antibodies used were Fluorescein-Labelled Goat anti-Chicken IgY (1:500, Cat#F-1005, Aves Labs) and Alexa Fluor® 594-conjugated Donkey Anti-Rabbit IgG (1:500, Cat# 711-585-152, Jackson ImmunoResearch Laboratories, Inc.). Lastly, sections were rinsed in PBS for 1 h total (20 min each rinse) at room temperature. Sections were then mounted on glass slides (Fisherbrand) with Dako fluorescent mounting medium and 1.5 cover slips (VWR). All images were collected on a Zeiss LSM 710 upright confocal microscope.

Data Analysis

All recorded traces were transferred to Spike2 (Version 7.09a, Cambridge Electronic Design). The raw recordings were initially rectified and smoothed ($\tau = 0.05$ s) using Spike2.

To measure the durations of flexor and extensor bursts and the step cycle we used the smoothed signals to identify burst onset and offset times. To identify these times in noisy recordings we set a threshold that was equal to 15% of the bust amplitude (difference between maximal and minimal values) and identified intersections of the smoothed signals with the threshold. The duration of each burst was measured as a time interval between burst's onset and offset. The step cycle duration was measured as a time interval between onset times of two consecutive bursts. The average of step cycle durations and burst durations of five consecutive cycles before the light-on and all the cycles during the light were used as a pair of data before and during light, respectively. The steps interrupted at the beginning or the end of light were excluded from the calculation.

Statistical analysis was performed in Prism7 (GraphPad Software, Inc.). Wilcoxon signed-rank test was used to compare the difference between the activity before and after the light. Linear contrasts were used to determine the relationship of the burst duration difference of activities in four nerves and step cycle difference in ipsilateral and contralateral side among three intensities. One-way ANOVA was used to determine the statistical significance among the burst duration of activity in four nerves. An α-error of $P < 0.5$ was regarded as significant. Data in the Results represent the mean ± SD.

5.2 Computational Modeling

Neuron model

All neurons were simulated in the Hodgkin–Huxley style as single-compartment models. The membrane potential, V, in neurons of the left and right flexor and extensor centers was described by the following differential equation

$$C \times \frac{dV}{dt} = -I_{\mathrm{Na}} - I_{\mathrm{NaP}} - I_{\mathrm{K}} - I_{\mathrm{L}} - I_{\mathrm{SynE}} - I_{\mathrm{SynI}}, \quad (1)$$

where *C* is the membrane capacitance and *t* is time.

In all other populations, the neuronal membrane potential was described as follows:

$$\boldsymbol{C \times \frac{dV}{dt} = -I_{\mathrm{Na}} - I_{\mathrm{K}} - I_{\mathrm{L}} - I_{\mathrm{SynE}} - I_{\mathrm{SynI}} - I_{\mathrm{ChR}}.}$$

where *C* is the membrane capacitance and *t* is time.

In all other populations, the neuronal membrane potential was described as follows:

$$\boldsymbol{C} \times \frac{\boldsymbol{dV}}{\boldsymbol{dt}} = -\boldsymbol{I}_{\mathrm{Na}} - \boldsymbol{I}_{\mathbf{K}} - \boldsymbol{I}_{\mathbf{L}} - \boldsymbol{I}_{\mathrm{SynE}} - \boldsymbol{I}_{\mathrm{SynI}} - \boldsymbol{I}_{\mathrm{ChR}}. \quad (2)$$

The ionic currents in Eqs. (1) and (2) were described as follows:

$$\begin{aligned} I_{\mathrm{Na}} &= \bar{g}_{\mathrm{Na}} \times m_{\mathrm{Na}}^3 \times h_{\mathrm{Na}} \times (V - E_{\mathrm{Na}}); \\ I_{\mathrm{NaP}} &= \bar{g}_{\mathrm{NaP}} \times m_{\mathrm{NaP}} \times h_{\mathrm{NaP}} \times (V - E_{\mathrm{Na}}); \\ I_{\mathrm{K}} &= \bar{g}_{\mathrm{K}} \times m_{\mathrm{K}}^4 \times (V - E_{\mathrm{K}}); \\ I_{\mathrm{L}} &= g_{\mathrm{L}} \times (V - E_{\mathrm{L}}); \\ I_{\mathrm{ChR}} &= g_{\mathrm{ChR}} \times (V - E_{\mathrm{ChR}}), \end{aligned} \quad (3)$$

where I_{Na} is the fast Na^+ current with maximal conductance $\bar{g}_{\mathrm{Na}}$; I_{NaP} is the persistent (slowly inactivating) Na^+ current with maximal conductance $\bar{g}_{\mathrm{NaP}}$ (present only in RG neurons); I_{K} is the delayed-rectifier K^+ current with maximal conductance $\bar{g}_K$; I_{L} is the leakage current with constant conductance g_{L}; I_{ChR} is the channelrhodopsin current with the conductance g_{ChR} (present only in V3 neurons). E_{Na}, E_{K}, E_{L}, and E_{ChR} are the reversal potentials for Na^+, K^+, leakage, and channelrhodopsin currents, respectively; variables m and h with indexes indicating ionic currents are the activation and inactivation variables of the corresponding ionic channels.

Activation m and inactivation h of voltage-dependent ionic channels (e.g., Na, NaP, and K) in Eq. (3) were described by the following differential equations:

$$\begin{aligned} \tau_{mi}(V) \times \frac{d}{dt} m_i &= m_{\infty i}(V) - m_i; \\ \tau_{hi}(V) \times \frac{d}{dt} h_i &= h_{\infty i}(V) - h_i, \end{aligned} \quad (4)$$

where $m_{\infty i}(V)$ and $h_{\infty i}(V)$ define the voltage-dependent steady-state activation and inactivation of the channel i, respectively, and $\tau_{mi}(V)$ and $\tau_{hi}(V)$ define the corresponding time constants. Activation of the sodium channels is considered to be instantaneous. The expressions for channel kinetics in Eq. (4) are described as follows:

$$\begin{aligned} &m_{\infty \mathrm{Na}}(V) = (1 + \exp(-(V + 34)/7.8))^{-1};\ \tau_{m\mathrm{Na}} = 0; \\ &h_{\infty \mathrm{Na}} = (1 + \exp((V + 55)/7))^{-1}; \tau_{h\mathrm{Na}} = 20/(\exp((V + 50)/15) + \exp(-(\mathrm{V} + 50)/16); \\ &m_{\infty \mathrm{NaP}} = (1 + \exp(-(V + 47.1)/3.1))^{-1};\ \tau_{m\mathrm{NaP}} = 0; \\ &h_{\infty \mathrm{NaP}} = (1 + \exp((V + 60)/6.8))^{-1};\ \tau_{h\mathrm{NaP}} = 8000/\cosh((V + 60)/13.6); \\ &m_{\infty \mathrm{K}} = (1 + \exp(-(V + 28)/4))^{-1};\ \tau_{m\mathrm{K}} = 3.5/\cosh((V + 40)/40); \\ &h_{\mathrm{K}} = 1. \end{aligned} \quad (5)$$

The maximal conductances for ionic currents and the leak reversal potentials, E_{L}, for different populations are given in Table 4.1.

The synaptic excitatory (I_{SynE} with conductance g_{SynE} and reversal potential E_{SynE}) and inhibitory (I_{SynI} with conductance g_{SynI} and reversal potential E_{SynI}) currents were described as follows:

$$I_{\mathrm{SynE}} = g_{\mathrm{SynE}} \times (V - E_{\mathrm{SynE}});$$
$$I_{\mathrm{SynI}} = g_{\mathrm{SynI}} \times (V - E_{\mathrm{SynI}}). \quad (6)$$

where g_{SynE} and g_{SynI} are equal to zero at rest and are activated by the excitatory or inhibitory inputs, respectively:

$$g_{\mathrm{SynE}i}(t) = \bar{g}_{\mathrm{E}} \times \sum_j S\{w_{ji}\} \times \sum_{t_{kj}<t} \exp(-(t - t_{kj})/\tau_{\mathrm{SynE}}); \quad (7)$$
$$g_{\mathrm{SynI}i}(t) = \bar{g}_{\mathrm{I}} \times \sum_j S\{-w_{ji}\} \times \sum_{t_{kj}<t} \exp(-(t - t_{kj})/\tau_{\mathrm{SynI}}),$$

where $S\{x\} = x$, if $x \geq 0$, and 0 if $x < 0$. Each spike arriving to neuron i in a target population from neuron j in a source population at time t_{kj} increases the excitatory synaptic conductance by $\bar{g}_{\mathrm{E}} \times w_{ji}$ if the synaptic weight $w_{ji} > 0$, or increases the inhibitory synaptic conductance by $-\bar{g}_{\mathrm{E}} \times w_{ji}$ if the synaptic weight $w_{ji} < 0$. $\bar{g}_{\mathrm{E}}$ and $\bar{g}_{\mathrm{I}}$ define an increase in the excitatory or inhibitory synaptic conductance, respectively, produced by one arriving spike at $|w_{ji}| = 1$. τ_{SynE} and τ_{SynI} are the decay time constants for g_{SynE} and g_{SynI}, respectively.

The following general neuronal parameters were assigned: C =1 μF·cm^{-2}; E_{Na} = 55 mV; E_{K} = − 80 mV; E_{ChR} = -10 mV; E_{SynE} = −10 mV; E_{SynI} = −70 mV; $\bar{g}_{\mathrm{E}} = \bar{g}_{\mathrm{I}} =$ 0.05 mS/cm^2; $\tau_{\mathrm{SynE}} = \tau_{\mathrm{SynI}}$ = 5 ms.

Neuron populations

Each neuron population in the model contained 50–200 neurons. The numbers of neurons in each population are shown in Table 1.

Random synaptic connections between the neurons of interacting populations were assigned prior to each simulation based on probability of connection, p, so that, if a population A was assigned to receive an excitatory (or inhibitory) input from a population B, then each neuron in population A would get the corresponding synaptic input from each neuron in population B with the probability $p\{A, B\}$. If $p\{A, B\}<1$, a random number generator was used to define the existence of each synaptic connection; otherwise (if $p\{A, B\}= 1$) each neuron in population A received synaptic input from each neuron of population B. Values of synaptic weights (w_{ji}) were set using random generator and were based on average values of these weights $\overline{w}$ and variances, which were define as 5% of $\overline{w}$ for excitatory connections ($\overline{w}> 0$) and 10% of $\overline{w}$ for inhibitory connections ($\overline{w}< 0$). The average weights and probabilities of connections are specified in Table 4.2.

Heterogeneity of neurons within each population was provided by random distributions of the base values of the mean leakage reversal potentials $\bar{E}_{\mathrm{Li0}}$ (see mean values ± SD for each *i*-th population in Table 4.1) and initial conditions for the values of membrane potential and channel kinetics variables. The base values of $\bar{E}_{\mathrm{Li0}}$ and all initial conditions were assigned prior to simulations from their defined average values and variances using a random number generator, and a settling period of 10-200 s was allowed in each simulation.

Simulations of changes in the locomotor frequency by neuroactive drugs and application of photostimulation

In the model, the frequency of rhythmic oscillations depended on the parameter α, that defined the level of average neuronal excitation in each population *i* (Shevtsova et al., 2015): $\bar{E}_{\mathrm{Li}} = \bar{E}_{\mathrm{Li0}} \times (1 - \alpha)$ where $\bar{E}_{\mathrm{Li0}}$ represents the base value of mean leakage reversal potential in the population at α=0 (see Table 4.1).

To simulate the effect of photostimulation, we selectively activated the V3 neurons either bi- or unilaterally by increasing the channelrhodopsin current conductance (g_{ChR}), which was set to 0 in control conditions.

To estimate changes in model behavior after increase of the channelrhodopsin current conductance ($\boldsymbol{g}_{\mathrm{ChR}}$), we used two methods. In the first method, simulations were run at the fixed value of $\boldsymbol{g}_{\mathrm{ChR}}$. (Figures 4.8, 4.10, and 4.11B2). The values of $\boldsymbol{g}_{\mathrm{ChR}}$ for these particular simulations are indicated in the corresponding figure legends. This method was also used to estimate the robustness of the model and simulate variability of experimental condition and individual spinal cords (Figures 4.9B1, B1and 12). To do this, we performed a series of simulations for both experimental conditions (bilateral and unilateral activation of V3 neurons) when parameters α, defining the level of average neuronal excitation in each population, and $\boldsymbol{g}_{\mathrm{ChR}}$, characterizing intensity of photostimulation were randomly chosen in the range [0.01, 0.06] for α and [0.18, 0.4] for $\boldsymbol{g}_{\mathrm{ChR}}$. For each pair $\{\alpha, \boldsymbol{g}_{\mathrm{ChR}}\}$ a simulation was run and average values for flexor and extensor burst durations

and oscillation period were calculated and compared with control condition when the model behavior was estimated with the same α and $\boldsymbol{g_{Ch} = 0}$.

In the second method, the integrated population activities were computed continuously during slow-ramp increase of $\boldsymbol{g}_{\mathrm{ChR}}$. This method was used to study the effect of stimulation intensity on model behavior in more detail (see Figures 4.10A and 4.11A1-B1). The value of $\boldsymbol{g}_{\mathrm{ChR}}$ was slowly increased from 0 to 0.4 (0.01 during 100 s of simulated time). For each locomotor cycle durations of flexion and extension phases or number of ipsilateral flexor bursts were calculated and plotted against the parameter $\boldsymbol{g}_{\mathrm{ChR}}$.

Computer simulations

All simulations were performed using the custom neural simulation package NSM 2.5.11 developed at Drexel University by S. N. Markin, I. A. Rybak, and N. A. Shevtsova. This simulation package was previously used for the development of several spinal cord models (Rybak et al., 2006a, b, 2013; McCrea and Rybak, 2007, 2008; Zhong et al., 2012; Shevtsova et al., 2015; Shevtsova and Rybak, 2016). Differential equations were solved using the exponential Euler integration method with a step size of 0.1 ms. Simulation results were saved as ASCI files containing time moments of spikes for RG populations. Model configuration files to create the simulations presented in the paper are available at https://github.com/RybakLab/nsm/tree/master/models/Danner-2019-V3.

Data analysis in computer simulations

The results of simulations were processed by custom Matlab scripts (The Mathworks, Inc., Matlab 2019a). To assess the model behavior, the averaged integrated activities of flexor and extensor centers (average number of spikes per neuron) were used to calculate the flexor and extensor burst durations and oscillation period. The timing of onsets and offsets of flexor and extensor bursts was determined at a threshold level equal to 10–25% of the average difference between maximal and minimal burst amplitude for particular population in the current simulation. The locomotor period was defined as the duration between two consecutive onsets of the extensor centers. Duration of individual simulations depended on the value of parameter α, and to robustly estimate average value of burst

duration and oscillation period in the first method, the first 10–20 transitional cycles were omitted to allow stabilization of model variables, and the values of model parameters were averaged for 10–20 consecutive cycles. In the second method, to validate our results we selectively run additional simulation with a slower ramp increase (0.01 during 500 s of simulated time) or with a fixed value of parameter in proximity of bifurcation points.

6 Figures

Figure 4.1 Investigation of sim1 cell in Sim1Cre/+; Ai32 mouse.

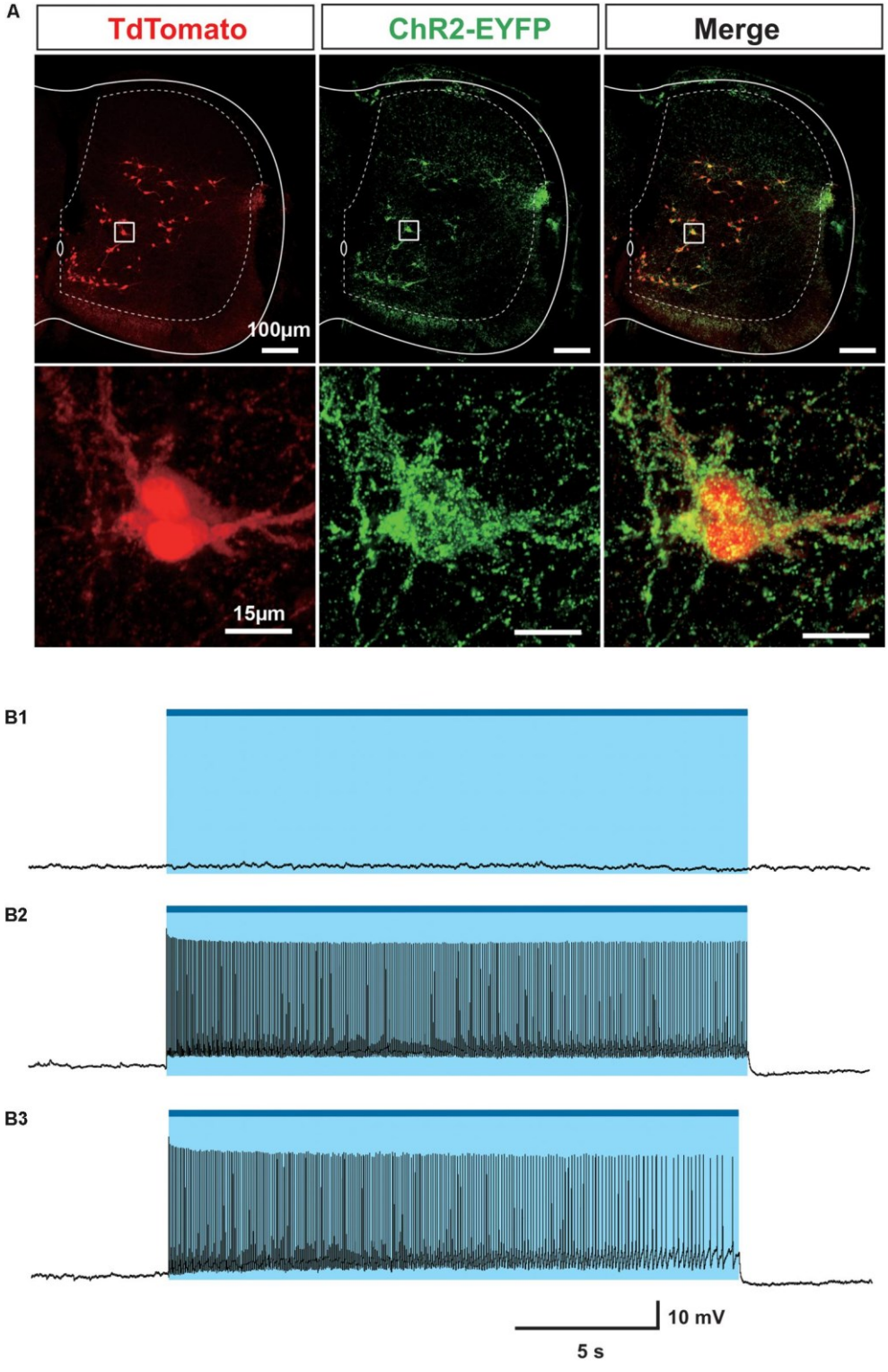

Figure 4. 1 Investigation of Sim1 cell in Sim1Cre/+; Ai32 mouse.

(A) ChR2-EYFP (Green) and tdTom (red) co-express in Sim1 + V3 INs in the spinal cord of Sim1Cre/+; tdTom; Ai32 mice. Upper: representative image of a cross section of a spinal cord from Sim1Cre/+; tdTom; Ai32 mouse. Lower: enlarged image of the insets.

(B1) Light did not activate EYFP negative cell. (B2) Patch clamp recordings of Sim1Cre/+; Ai32 cell with optical activation. (B3) Patch clamp recording of Sim1Cre/+; Ai32 cell with optical activation with fast synaptic transmission blocker. Blue bar and shaded blue area represent the optical activation (light-on) period.

Figure 4.2 Symmetric optical activation of both sides of V3 INs in L2 ventral region during drug-evoked fictive locomotion and changes in ENG characteristics.

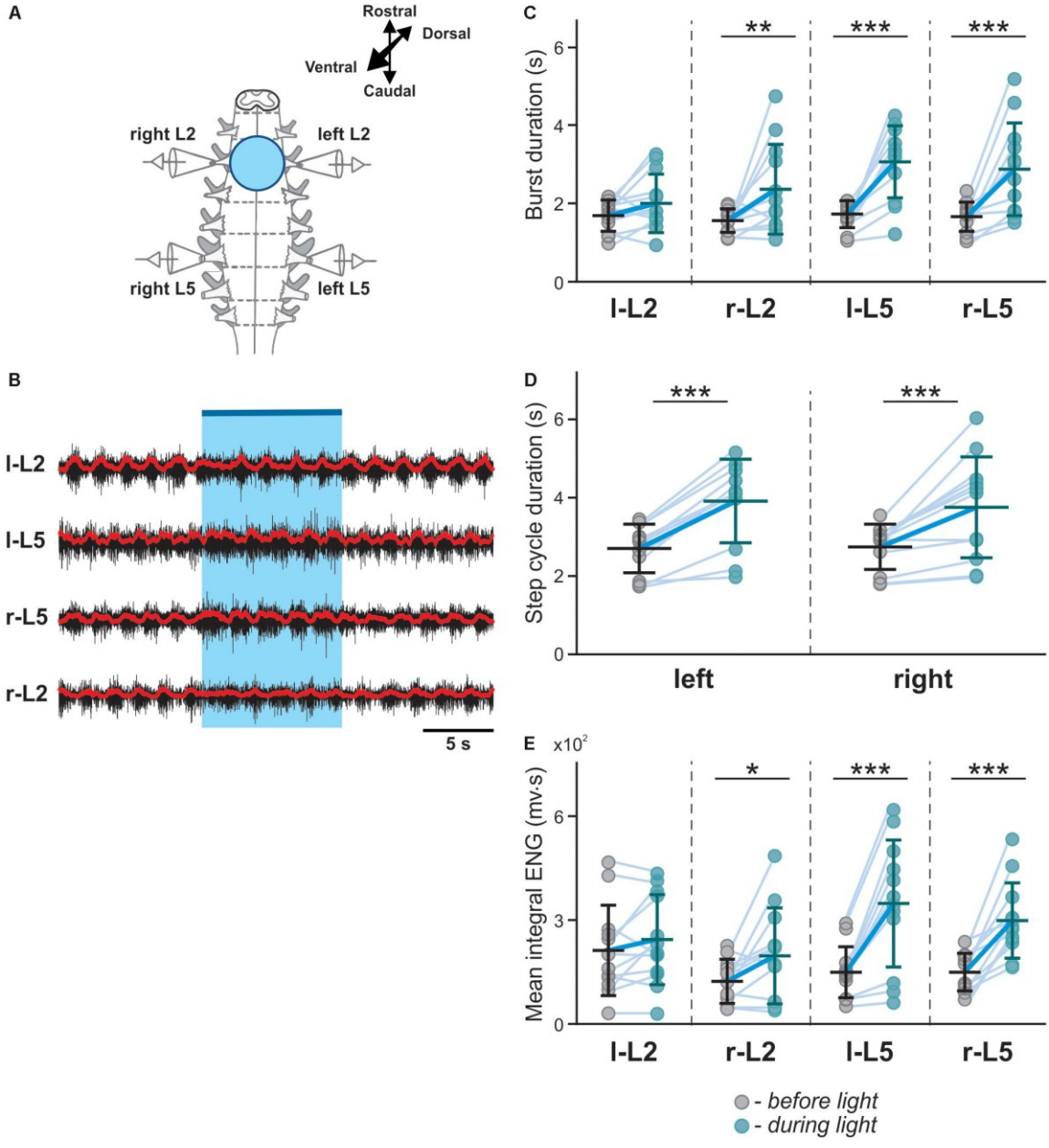

Figure 4.2 Symmetric optical activation of both sides of V3 INs in L2 ventral region during drug-evoked fictive locomotion and changes in ENG characteristics.

(A) Experimental setup.

(B) Optical activation of lumbar V3 INs increases the intensity of extensor motor output and slows oscillation frequency of drug-evoked fictive locomotion. Fictive locomotion was induced by drug cocktail (5-HT 8 μM, NMDA 8 μM) in Sim1cre-Ai32 cord. The blue bar on the top and shaded blue area represent the optical stimulation period. Red lines are rectified and smoothed traces of the original ENG recordings (black).

(C–E) Burst duration, step cycle duration, and mean integral ENG during drug-induced locomotor-like activity (n = 12) before (gray circles) and during (blue circles) optical activation. Each circle represents the average value of estimated parameter for one trace. Light blue lines connecting two circles represent parameter increase in one cord. Thick, dark blue line represent the average of increase. * indicates $P < 0.05$, ** indicates $0.01 < P < 0.05$, *** indicates $0.0001 < P < 0.001$.

Figure 4.3 Biased optical activation of V3 INs in spinal segment L2 and corresponding changes in ENG characteristics in spinal segment L2 and L5 during drug-induced locomotor-like activity.

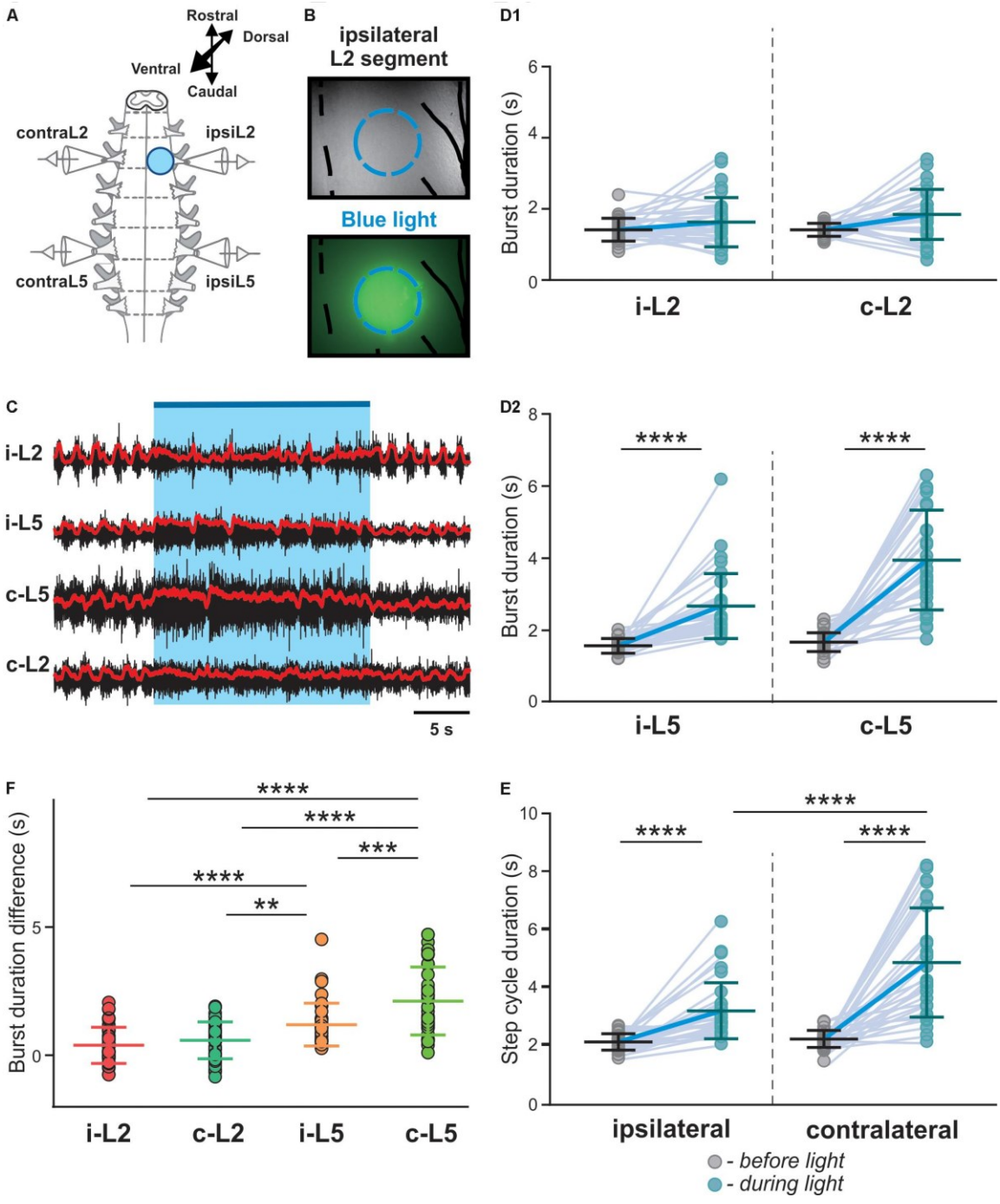

Figure 4.3 Biased optical activation of V3 INs in spinal segment L2 and corresponding changes in ENG characteristics in spinal segment L2 and L5 during drug-induced locomotor-like activity.

(A) Illustration of experimental setup for recording motor activity evoked by optical stimulation on the left spinal segment L2 from ventral side during drug-evoked fictive locomotion.

(B) Image of the optical stimulation area. Black dashed line represents the midline of spinal cord. Blue dashed circle illustrates the light illuminated region. Black line on the right shows the frame of Nerve L2 and lateral edge of the spinal cord.

(C) Recording trace during optical stimulation. Biased optical activation of V3 INs in spinal segment L2 leads to asymmetrical left-right extensor motor activity. Blue bar and area indicate the stimulation period. Red lines are rectified and smoothed traces of the original ENG recordings (black).

(D1, D2) Average of burst duration of L2 (D1) and L5 (D2) during drug-induced locomotor-like activity (n = 33) before (gray circles) and during (blue circles) optical stimulation in ipsilateral and contralateral cord.

(E) The average of step cycle duration of ipsilateral and contralateral L5 activities during drug-induced locomotor-like activity (n = 33) before (gray circles) and during (blue circles) optical stimulation. Light blue lines connecting two circles represent change in one cord. Thick, dark blue line represent the average of change. **** indicates $P < 0.0001$.

(F) Average of locomotor burst duration difference between before and during biased optical stimulation. ** indicates $0.001 < P < 0.01$, *** indicates $0.0001 < P < 0.001$, **** indicates $P < 0.0001$; n = 33.

Figure 4.4 V3 activated contralateral extensor motor activity is correlated with optical stimulation intensity.

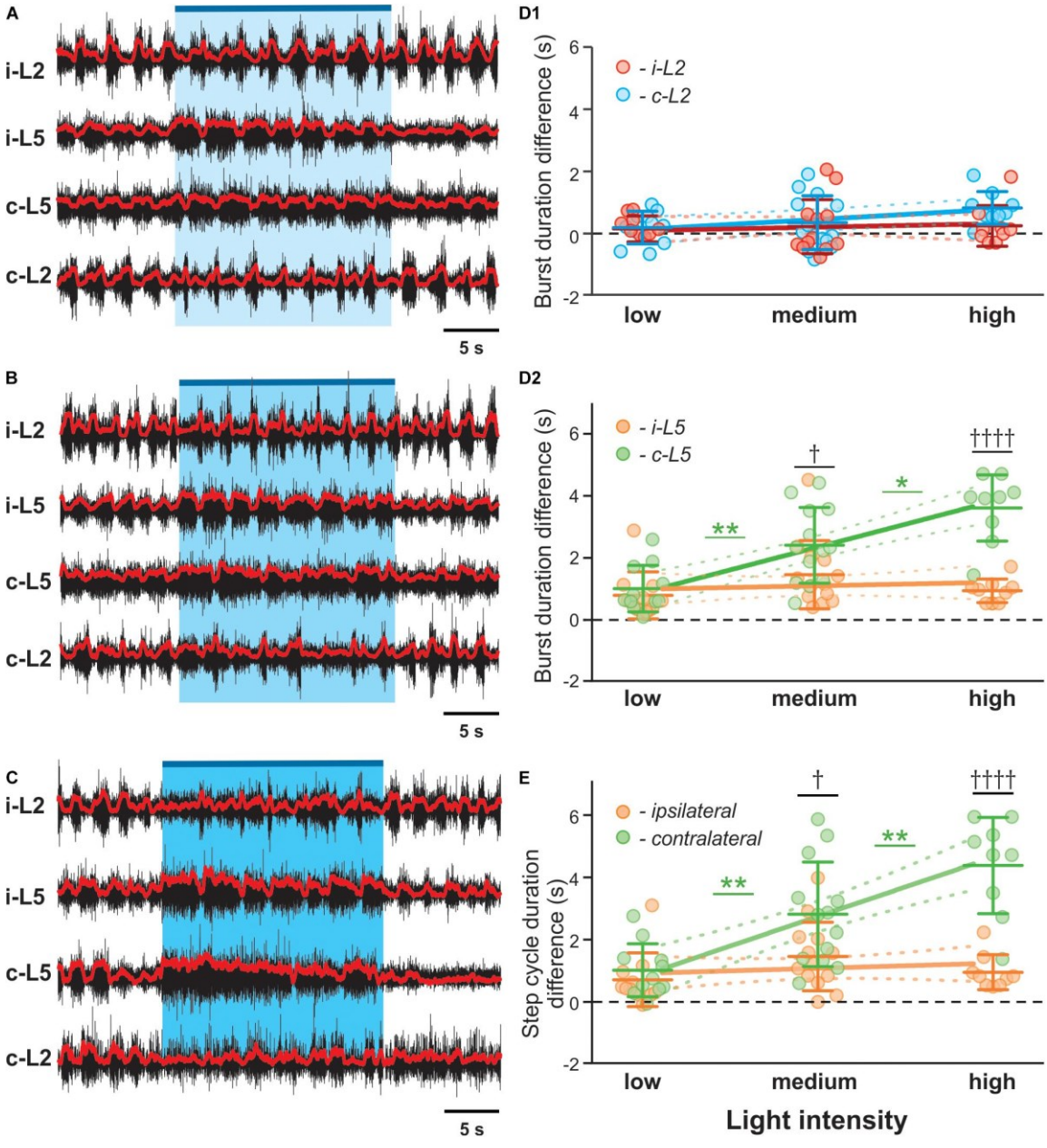

Figure 4.4 V3 activated contralateral extensor motor activity is correlated with optical stimulation intensity.

Representative traces of locomotor activity induced by drug (5-HT 8 μM, NMDA 8 μM) in Sim1Cre/+; Ai32 cord at low (A), medium (B), and high (C) light intensity. Blue bar on the top of each trace and shaded blue area represent the optical stimulation period. The brightness of blue shaded area indicates light intensity.

(D1, D2, E) Dependence of ENG characteristics on light intensity during biased optical stimulation. Average of burst duration difference of L2 (D1) and L5 (D2) between before and during optical stimulation under low, medium, and high stimulation intensity during drug-induced locomotor-like activity (low n = 11, medium n = 13, high n = 9). ∗ Indicates $0.01 < P < 0.05$, ∗∗ indicates $0.001 < P < 0.01$. † indicates $0.01 < P < 0.05$, †††† indicates $P < 0.0001$. Linear regression slope is orange for ipsilateral L5 and light green for contralateral L5 and red for ipsilateral L2 and blue for contralateral L2.

(E) Step cycle period difference between ipsilateral and contralateral L5 under low, medium and high stimulation intensity during drug-induced locomotor-like activity (low n = 11, medium n = 13, high n = 9). †††† indicates $P < 0.0001$, ∗∗ indicates $0.001 < P < 0.01$. Slope of contralateral L5 burst duration and step cycle difference are significantly non-zero.

Figure 4.5 Model schematics of the bilateral spinal circuits consisting of two interconnected rhythm generators.

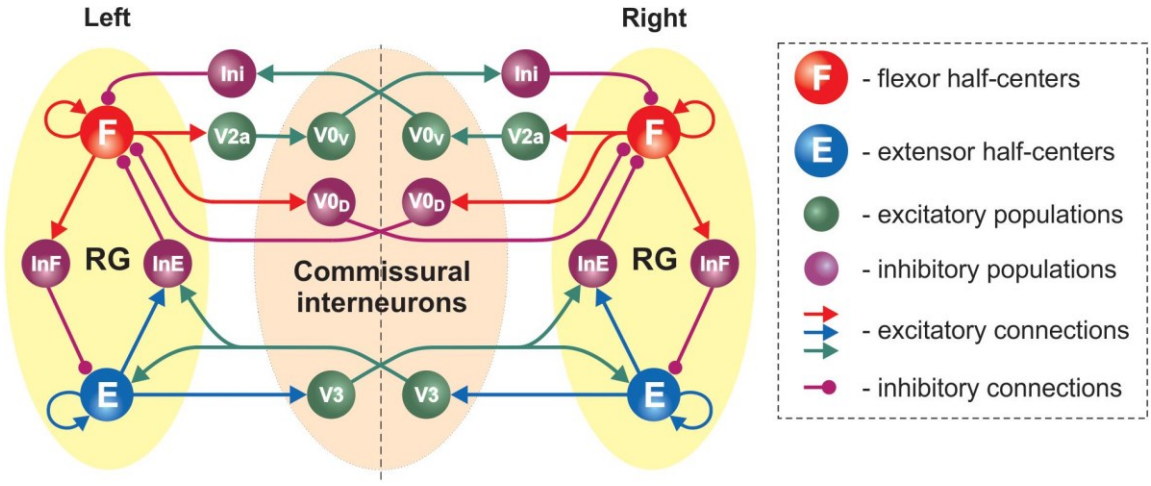

Figure 4.5 Model schematics of the bilateral spinal circuits consisting of two interconnected rhythm generators.

Spheres represent neural populations and lines the synaptic connections between them. The rhythm generator (RG) in each side includes flexor and extensor centers (F and E, respectively) interacting via the inhibitory InF and InE populations. The left and right RGs interact via CINs (V0D, V0V, and V3).

Figure 4.6 Model performance under normal conditions.

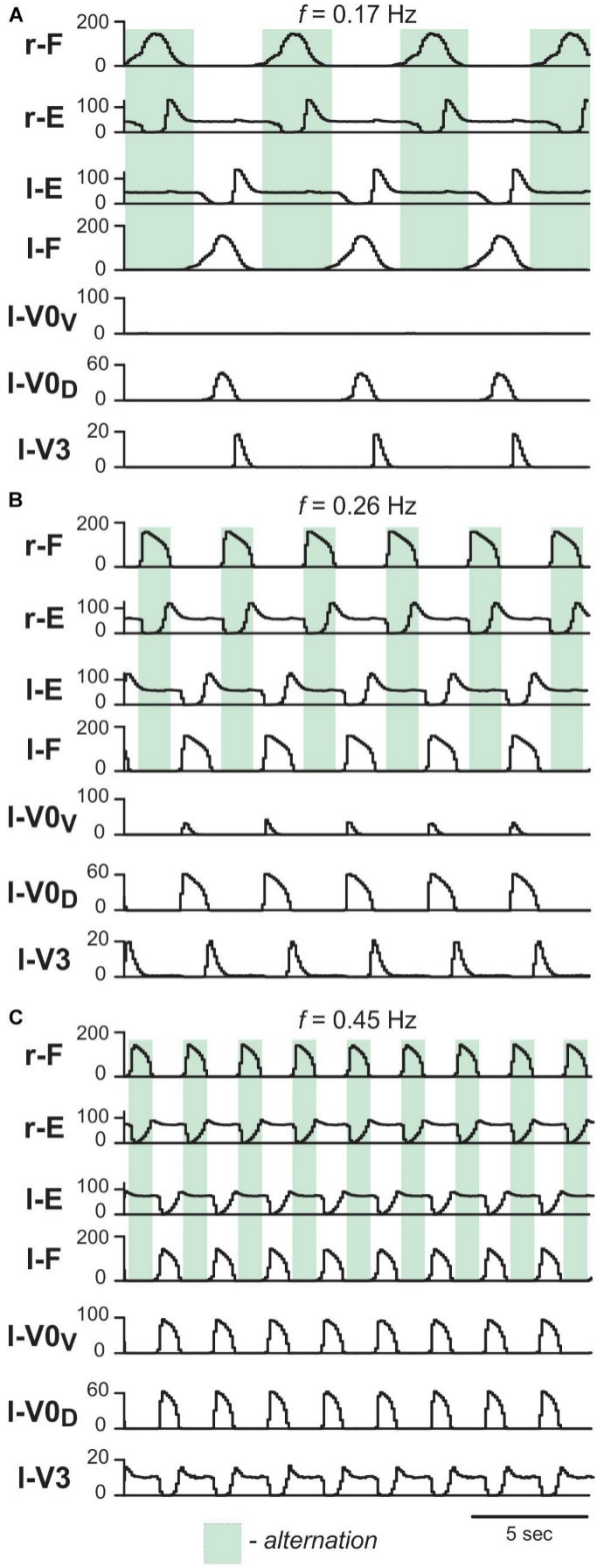

Figure 4.6. Model performance under normal conditions. Integrated population activities of flexor (F) and extensor (E) rhythm generator centers and left CINs are shown at low (A; $\alpha = 0.01$), medium (B; $\alpha = 0.03$), and high excitation levels (C; $\alpha = 0.09$). Activities of populations in this and following figures are shown as average histograms of neuron activity [spikes/ (N × s), where N is a number of neurons in population; bin = 100 ms]. Shaded green areas show intervals of right flexor activities. r-: right; l-: left.

Figure 4.7 Model performance after removal of V0V, V0D and all V0 CINs.

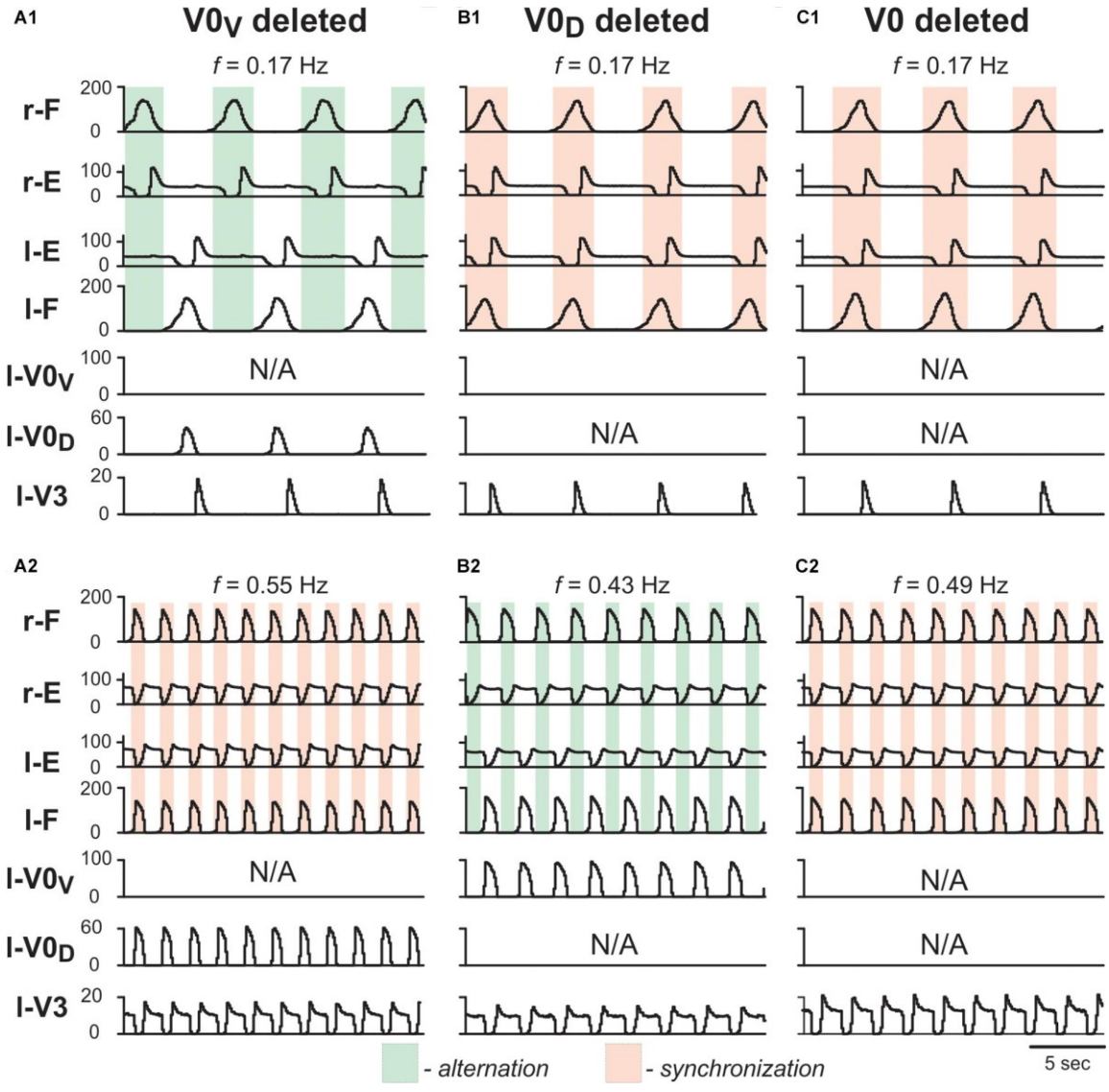

Figure 4.7 Model performance after removal of V0V, V0D and all V0 CINs.

Integrated population activities of flexor and extensor rhythm generator centers (F and E, respectively) and left CINs are shown after removal of V0V (A1,A2), V0D (B1,B2), and all V0 (C1,C2), at a low (A1,B1,C1; $\alpha = 0.01$) and a high (A2,B2,C2; $\alpha = 0.08$) excitation level and oscillation frequency. Shaded areas show intervals of right flexor activities. Green indicates left–right alternation and pink left–right synchronization. r-: right; l-: left.

Figure 4.8 Effect of bilateral stimulation of V3 CINs during fictive locomotion in the model.

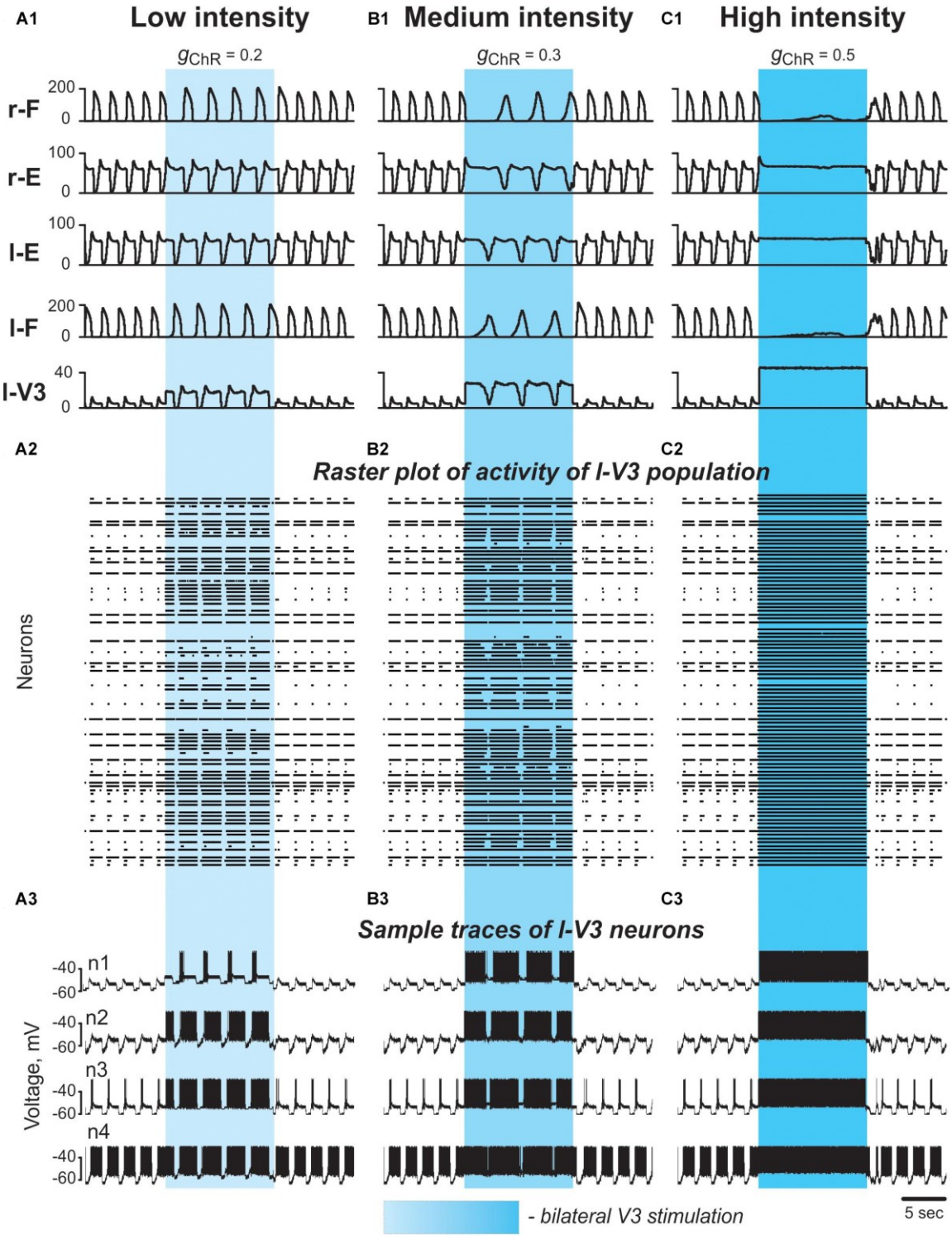

Figure 4.8 Effect of bilateral stimulation of V3 CINs during fictive locomotion in the model.

(A1–A3) Low V3-stimulation intensity (gChR = 0.2). (B1–B3) Medium V3-stimulation intensity (gChR = 0.3). (C1–C3) High V3-stimulation intensity (gChR = 0.5). Stimulation was applied to all V3 neurons (on both sides of the cord). For all stimulations fictive locomotion was evoked at $\alpha = 0.06$. (A1, B1, C1) Integrated population activities of the flexor and extensor rhythm generator centers and the left V3 population. (A2, B2, C2) Raster plots of spikes elicited by neurons in the left V3 population. (A3, B3, C3) Traces of the membrane potential of sample neurons in the left V3 population with different excitability. Shaded blue areas show the interval when V3 stimulation was applied. r-: right; l-: left.

Figure 4.9 Effect of bilateral stimulation of V3 INs on flexor and extensor burst duration s and oscillation period in the model.

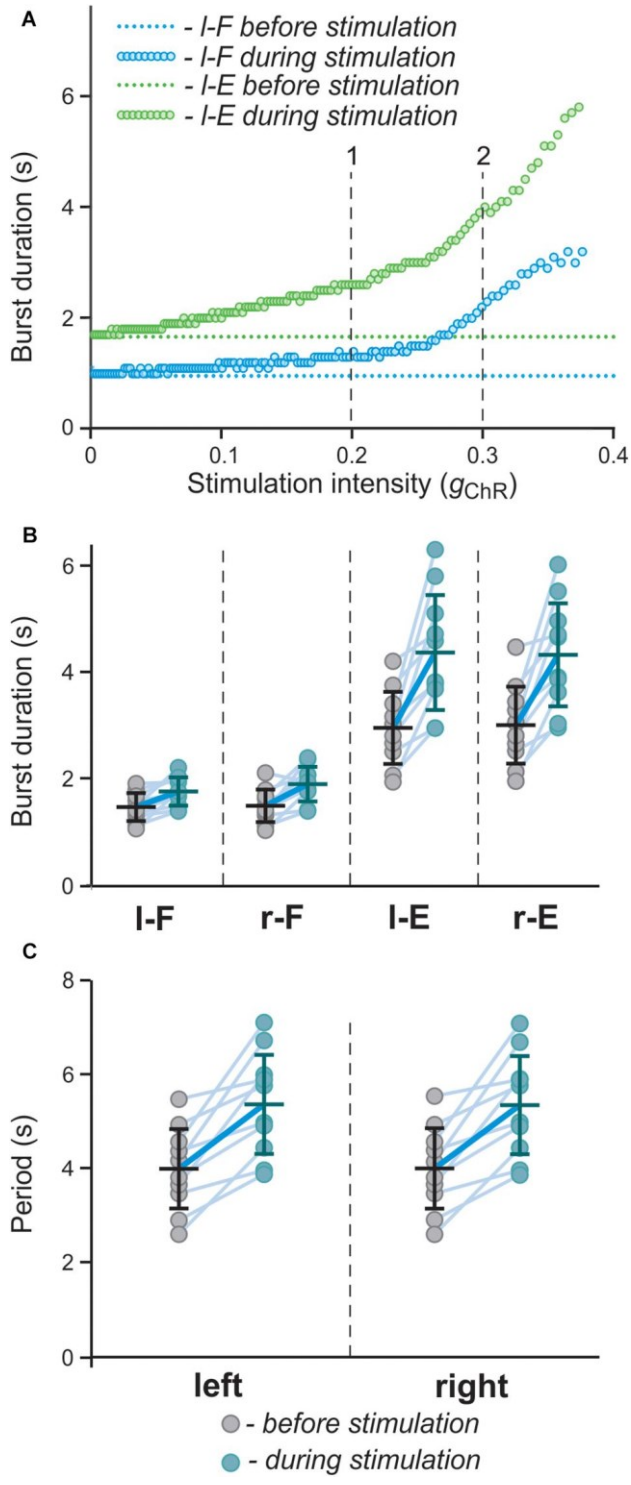

Figure 4.9 Effect of bilateral stimulation of V3 INs on flexor and extensor burst duration s and oscillation period in the model.

(A) Dependence of flexor and extensor burst duration on stimulation intensity (gChR; shown for the left side only). Intensity of stimulation was gradually changed from 0 to 0.4. The vertical lines (1 and 2) correspond to simulations shown in Figures 4.8A1, A2, respectively.

(B, C) Flexor and extensor burst duration and period of oscillations in a series of model experiments (n = 12) with randomly chosen parameters α and gChR before (gray circles) and during (blue circles) bilateral stimulation of V3 populations. Each circle represents the average value of estimated parameter for one simulation. Light blue lines connecting two circles represent parameter increase in one simulation Thick, dark blue line represent the average of increase.

Figure 4.10 Effect of unilateral stimulation of V3 CINs during fictive locomotion in the model.

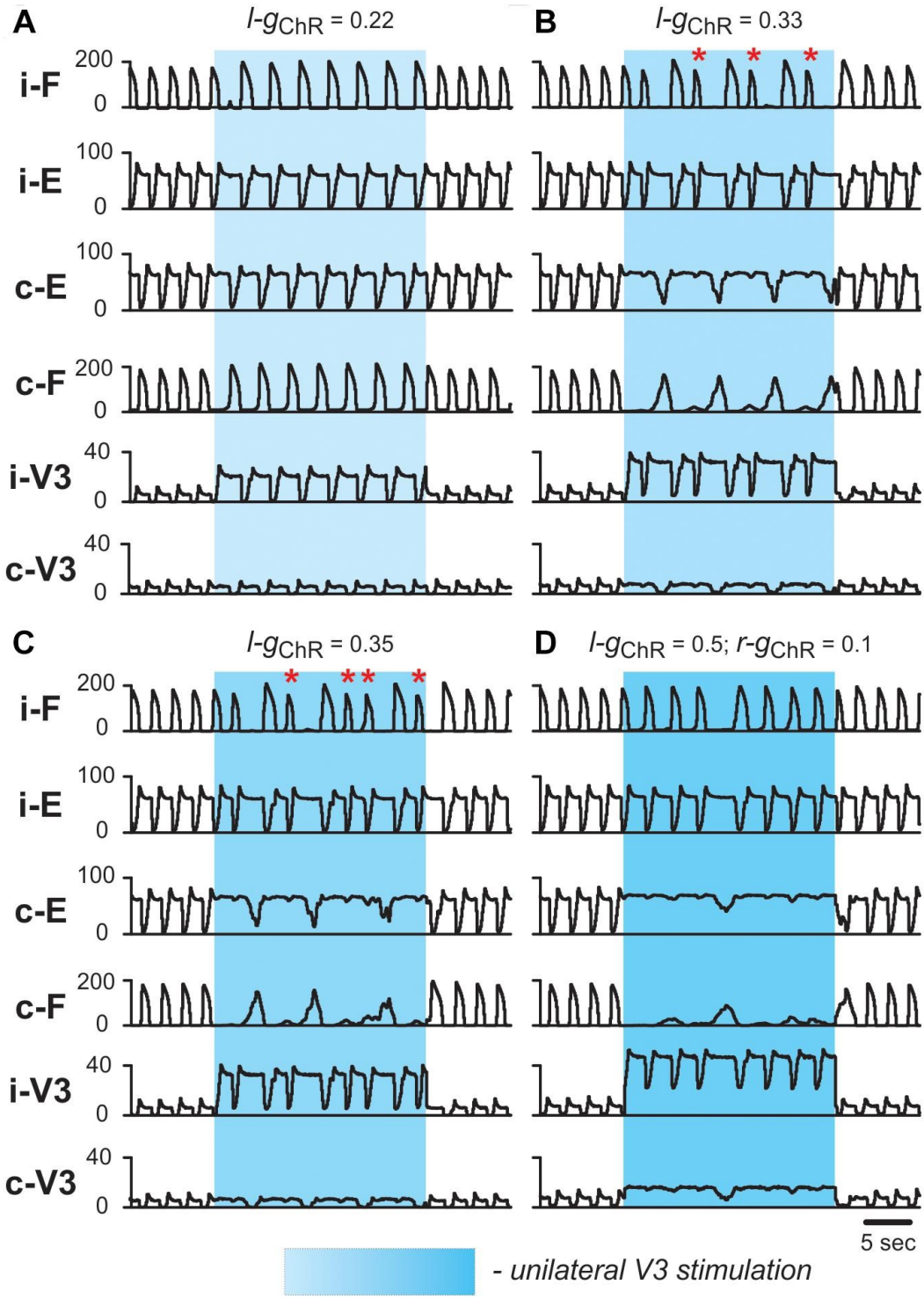

Figure 4.10 Effect of unilateral stimulation of V3 CINs during fictive locomotion in the model.

Fictive locomotion was evoked at $\alpha = 0.065$. All panels show integrated population activities of the flexor (F) and extensor (E) rhythm generator centers and the V3 populations ipsi- and contralateral to the stimulation. Shaded blue areas show the interval when V3-stimulation was applied. Four different stimulation intensities are shown: (A) gChR = 0.22; (B) gChR = 0.33; (C) gChR = 0.35; (D) gChR = 0.5 in ipsilateral and gChR = 0.1 in contralateral V3 population. Red asterisks mark additional flexor bursts on ipsilateral side. i-: ipsilateral; c-: contralateral.

Figure 4.11 Effect of unilateral stimulation intensity of V3 INs on flexor and extensor burst durations and oscillation period in the model.

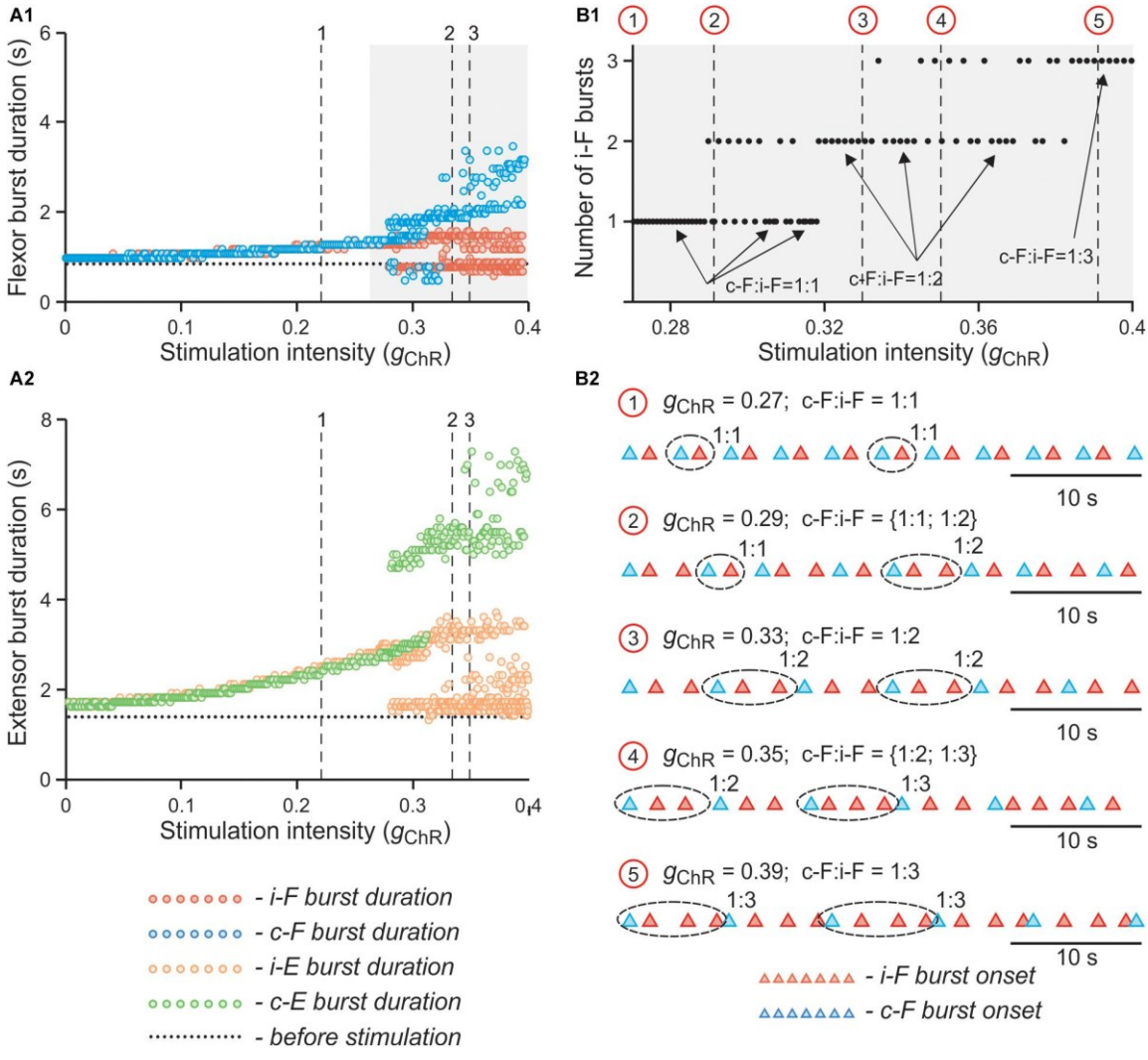

Figure 4.11 Effect of unilateral stimulation intensity of V3 INs on flexor and extensor burst durations and oscillation period in the model.

(A1, A2) Dependence of flexor (A1) and extensor (A2) burst durations on intensity of stimulation (gChR) when stimulation was applied to the left V3 population. Intensity of stimulation was gradually changed from 0 to 0.4. The vertical lines (1, 2 and 3) correspond to simulations shown in Figures 4.10A–C, respectively.

(B1, B2) Dependence of number of additional ipsilateral flexor bursts during single contralateral period on parameter gChR at higher values of stimulation intensity In (B1), gChR was gradually changed from 0.27 to 0.4. Arrows indicate 1:1, 1:2, and 1:3 ratios between the number of ipsi- and contralateral flexor bursts. Red circles and vertical lines indicate selected values of gChR for which additional simulations were run when gChR was fixed. In (B2), the timing of flexor burst onsets for these simulations are shown. The corresponding values of gChR for each simulation are indicated above each trace. Traces are shown for 40 s of simulated time. i-: ipsilateral; c-: contralateral; F - flexor rhythm generator center.

Figure 4.12 Effect of unilateral stimulation of V3 INs on flexor and extensor burst durations and oscillation period in the model.

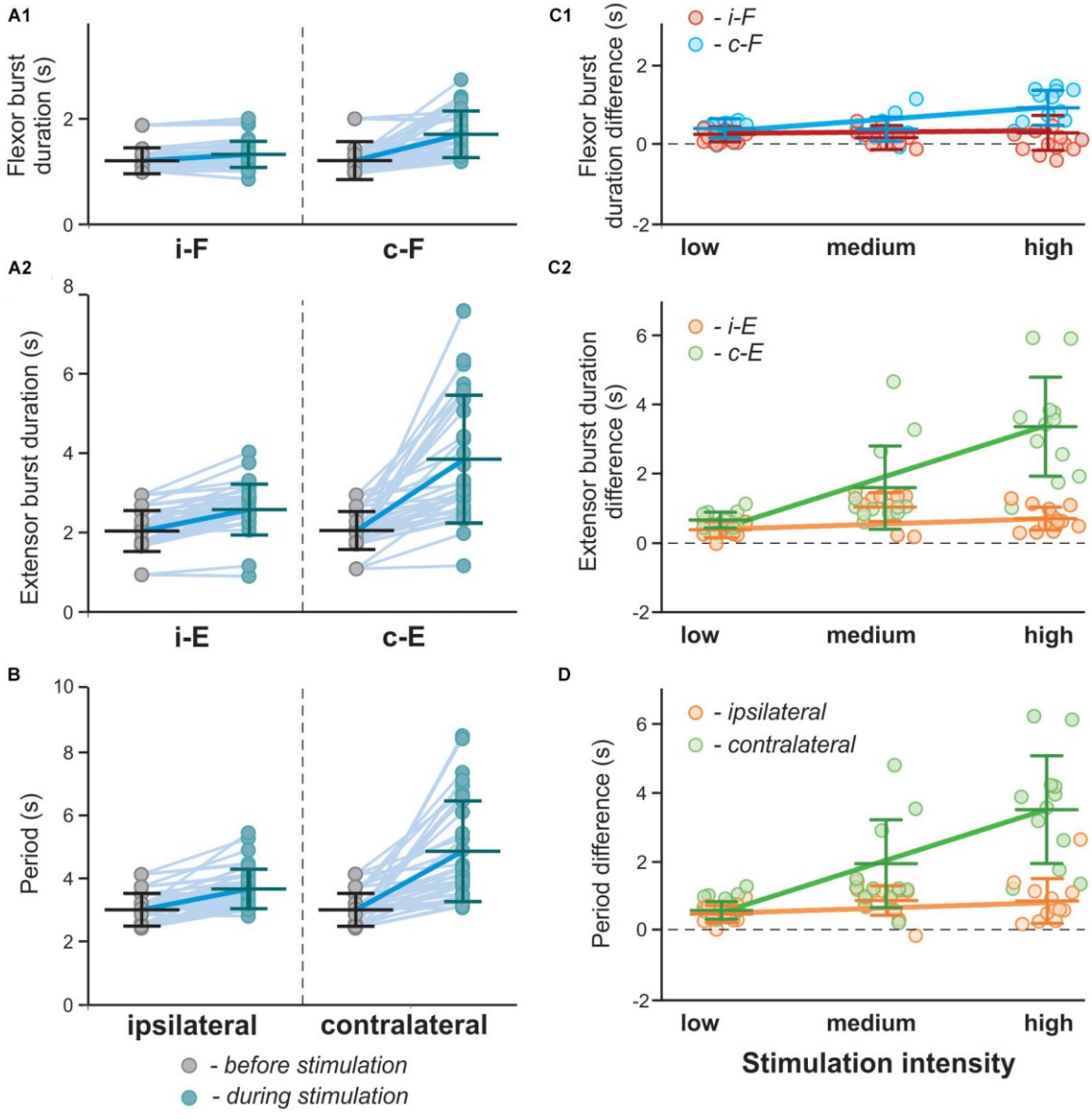

Figure 4.12 Effect of unilateral stimulation of V3 INs on flexor and extensor burst durations and oscillation period in the model.

(A1, A2, B) Flexor (A1) and extensor (A2) burst duration and period of oscillations (B) in a series of model experiments with randomly chosen parameters α and gChR before (gray circles) and during (blue circles) stimulation of the left V3 populations. Each circle represents the average value of estimated parameter for one simulation. Light blue lines connecting two circles represent parameter change in one simulation Thick, dark blue line represent the average of change.

(C1, C2, D) Differences in flexor (C1) and extensor (C2) burst duration and period of oscillations (D) for the above modeling experiments estimated according to stimulation intensity. Low stimulation intensity corresponds to gChR $\in$ [0.18,0.25], medium, gChR $\in$ [0.26,0.33], in stimulations with high intensity gChR $\in$ [0.33,0.4]. Linear regression slopes are orange for ipsilateral and green for contralateral extensor centers and red for ipsilateral and blue for contralateral flexor extensor centers. i-: ipsilateral; c-: contralateral.

7 Tables

Table 4. 1 Number of neurons and neuron parameters in different populations.

Neuron type	N, number of neurons	$\bar{g}_{Na}$, mS/cm^2	$\bar{g}_{NaP}$, mS/cm^2	$\bar{g}_K$, mS/cm^2	g_L, mS/cm^2	$\bar{E}_{LO}$, mV
F	200	25	0.75(±0.00375)	2	0.07	−67(±0.67)
E	100	25	0.75(±0.00375)	2	0.07	−60(±0.6)
InF	100	10		5	0.1	−67(±1.34)
InE	100	10		5	0.1	−72(±1.44)
V0D	50	10		5	0.1	−68(±2.04)
V2a	50	40		5	0.8	−60.5(±1.21)
V0V	50	10		5	0.1	−62(±1.24)
Ini	50	10		5	0.1	−64(±1.28)
V3	100	10		5	0.1	−68(±2.04)

Table 4. 2 Average weights $\bar{w}_{ji}$ and probabilities (p) of synaptic connections.

Source population	Target populations ($\bar{w}_{ji}$, probability of connection p)
i-F	i-F(0.009, $p = 0.1$);
	i-InF(0.01, $p = 0.1$);
	i-V2a(0.01, $p = 0.1$);
	i-$V0_D$(0.06, $p = 0.1$)
i-E	i-E(0.018, $p = 0.1$);
	i-InE(0.12, $p = 0.1$);
	i-V3(0.2, $p = 0.05$)
i-InF	i-E(−0.15, $p = 0.1$)
i-InE	i-F(−0.3, $p = 0.1$)
i-Ini	i-F(−0.5, $p = 0.1$)
i-V2a	i-$V0_V$(1.5, $p = 0.1$)
i-$V0_V$	c-Ini(1.5, $p = 0.1$)
i-$V0_D$	c-F (−0.18, $p = 0.1$)
i-V3	c-E(0.05, $p = 0.05$);
	c-inE(1, $p = 0.05$)

Prefixes i- and c- indicate ipsi- and contralateral populations.

CHAPTER 5. CONCLUSION AND FUTURE DIRECTION

V3 INs are a major group of glutamatergic commissural neurons in the spinal cord. They directly innervate MNs as well as other ventral INs. Previous studies of our lab have shown that V3 INs are heterogeneous population and differentially recruited during walking and swimming. Chopek et al. (2019) demonstrated the microcircuit comprised by two V3 sub-populations and local MNs. Acutely silencing of V3 INs caused unstable gaits in walking mice and generated imbalanced and less robust rhythmic fictive locomotion in isolated neonatal spinal cords. Nonetheless, the functions of V3 INs are way more than that and the functions of each V3 sub-population still remain unclear. This thesis work has revealed several functions of V3 INs in different locomotion and identified one sub-population of V3 INs.

In chapter2, I illustrated the function of lumbo-cervical projecting V3 INs that provide a direct excitatory drive to cervical locomotor networks during medium locomotor speeds and likely be essential for robust alternation between left-right and synchronization of diagonal fore-rear limbs to perform trotting gait. However, there is no direct evidence to show that the lack of fore-hindlimb coordination shown in V3OFF mice related to this sub-population of V3 INs. Therefore, to further confirm the correlation of lumbo-cervical projecting V3 INs and fore-hindlimb coordination phenotype shown in V3OFF mice, specific deletion of this sub-population is required. Chemogenetic technologies might shine the light on this problem. Designer Receptor Exclusively Activated by Designer Drugs (DREADDs)-based chemogenetic tools are now commonly used to manipulate the activity of defined neuron population in different behaviours (Roth, 2016). DREADDs are a mutated form of the muscarinic acetylcholine receptor, in which the binding site for acetylcholine has been removed and a new binding site for a normally-inert compound, Clozapine-N-Oxide (CNO), has been created. This technology allows selective manipulation of G protein-coupled receptor (GPRC) signaling transduction in defined neuron population by application of drug, clozapine-N-oxide (CNO) in freely moving animals (Alexander et al., 2009; Armbruster et al., 2007; Bourane et al., 2015). In addition,

adeno-associated viral (AAV) vectors encoding the inhibitory DREADD receptor, hM4D, can be genetically modified to be dependent on the flippase (Flp) -mediated recombinase system to have functional expression (Seibler & Bode, 1997; Bonaventura et al., 2019). Therefore, in the future, I plan to generate the transgenic mouse strain that have Flp recombinase specifically expressed in Sim1 cells. By injecting Flp-dependent retrograde AAV encoding hM4D DREADD receptor into cervical region, the receptor could be specifically expressed in lumbar V3 INs that have long projection to cervical region. Then, the locomotion of these mutant mice will be tested to see whether they still lack the coordination between fore-hindlimb.

In chapter3, I systematically examined the kinematics and muscle activities of hind limbs of V3OFF mice in three behaviours and demonstrated two functions of spinal V3 INs. The first function of V3 INs is to regulate ankle extensor muscle activity during E3 phase and hip-distal joint coordination during swing-stance transition phase in weight-bearing behaviours. Since the swing-stance transition phase is always superimposed with contralateral propelling phase, we speculate that V3 INs might synchronize the activity of extensor muscles of left and right hindlimbs. In chapter4, we combined experimental data with modelling study to illustrate the connectivity of V3 INs in CPG circuit and suggest that V3 INs may mediate left–right synchronization in certain conditions. Therefore, the next step is to test whether the effect we observed *in vitro* is associated with the speculation we made from *in vivo* experiments and which subpopulation of V3 INs is responsible for this.

In addition, we found that V3OFF mice lacked the excitability of hip locomotor network during all behaviours and did not recover the hip movement after spinal cord injury. It has been shown that proprioceptive afferent from hip muscles is essential for the initiation of locomotion and sensory afferents, proprioceptive and cutaneous, are critical for the motor function regained after spinal cord injury (Bui & Stifani et al., 2016; Pearson & Rossignol, 1991; Shah et al., 2016; Takeoka et al., 2014, 2019; Wenger et al., 2016). Furthermore, as described above, V3 INs may also be involved in sensorimotor pathway for regulating ankle extensor muscle activity. Immunohistochemistry study of our lab shows that V3 INs receive proprioceptive input in higher lumbar region. Therefore, in the future, we like to

explore the V3 INs function in the recovery of locomotion after spinal cord injury and check if optical stimulation of V3 INs in lumbar region could promote the locomotion recovery after spinal cord injury.

REFERENCE

Abourachid, A., Herbin, M., Hackert, R., Maes, L., & Martin, V. (2007). Experimental study of coordination patterns during unsteady locomotion in mammals. Journal of Experimental Biology, 210(2), 366–372.

Adrian, E. D. (1931). Potential changes in the isolated nervous system of Dytiscus marginalis. The Journal of Physiology, 72(1), 132–151.

Akay, T., Acharya, H. J., Fouad, K., & Pearson, K. G. (2006). Behavioral and Electromyographic Characterization of Mice Lacking EphA4 Receptors. Journal of Neurophysiology, 96(2), 642–651.

Akay, T., Tourtellotte, W. G., Arber, S., & Jessell, T. M. (2014). Degradation of mouse locomotor pattern in the absence of proprioceptive sensory feedback. Proceedings of the National Academy of Sciences, 111(47), 16877–16882.

Alaynick, W. A., Jessell, T. M., & Pfaff, S. L. (2011). SnapShot: Spinal Cord Development. Cell, 146(1), 178–178.e1.

Al-Mosawie, A., Wilson, J. M., & Brownstone, R. M. (2007). Heterogeneity of V2-derived interneurons in the adult mouse spinal cord. European Journal of Neuroscience, 26(11), 3003–3015.

Alvarez, F.J., Jonas, P.C., Sapir, T., Hartley, R.P., Berrocal, M.C., Geiman, E.J., Todd, A.J., & Goulding, M. (2005). Postnatal phenotype and localization of spinal cord V1 derived interneurons. The Journal of comparative neurology, 493 2, 177-92.

Andersson O, Grillner S, Lindquist M, Zomlefer M. (1978) Peripheral control of the spinal pattern generators for locomotion in cat. Brain Res. 1978 Jul 21;150(3):625-30.

Andersson O, Grillner S. (1981) Peripheral control of the cat's step cycle. I. Phase dependent effects of ramp-movements of the hip during "fictive locomotion". Acta Physiol Scand. 1981 Sep;113(1):89-101.

Andersson, L. S., Larhammar, M., Memic, F., Wootz, H., Schwochow, D., Rubin, C.-J., … Kullander, K. (2012). Mutations in DMRT3 affect locomotion in horses and spinal circuit function in mice. Nature, 488(7413), 642–646.

Angeli, C. A., Edgerton, V. R., Gerasimenko, Y. P., & Harkema, S. J. (2014). Altering spinal cord excitability enables voluntary movements after chronic complete paralysis in humans. Brain, 137(5), 1394–1409.

Arber, S. (2012). Motor Circuits in Action: Specification, Connectivity, and Function. Neuron, 74(6), 975–989.

Ballion, B., Morin, D., & Viala, D. (2001). Forelimb locomotor generators and quadrupedal locomotion in the neonatal rat. European Journal of Neuroscience, 14(10), 1727–1738.

Barthe, J.-Y., & Clarac, F. (1997). Modulation of the spinal network for locomotion by substance P in the neonatal rat. ExpFerimental Brain Research, 115(3), 485–492.

Batka, R. J., Brown, T. J., Mcmillan, K. P., Meadows, R. M., Jones, K. J., & Haulcomb, M. M. (2014). The Need for Speed in Rodent Locomotion Analyses. The Anatomical Record, 297(10), 1839–1864.

Bellardita, C., & Kiehn, O. (2015). Phenotypic Characterization of Speed-Associated Gait Changes in Mice Reveals Modular Organization of Locomotor Networks. Current Biology, 25(11), 1426–1436.

Benito-Gonzalez, A., & Alvarez, F. J. (2012). Renshaw Cells and Ia Inhibitory Interneurons Are Generated at Different Times from p1 Progenitors and Differentiate Shortly after Exiting the Cell Cycle. Journal of Neuroscience, 32(4), 1156–1170.

Betley, J., Wright, C.V., Kawaguchi, Y., Erdélyi, F., Szabó, G.J., Jessell, T.M., & Kaltschmidt, J.A. (2009). Stringent Specificity in the Construction of a GABAergic Presynaptic Inhibitory Circuit. Cell, 139, 161-174.

Bikoff, J.B., Gabitto, M.I., Rivard, A.F., Drobac, E., Machado, T.A., Miri, A., Brenner-Morton, S., Famojure, E., Diaz, C., Alvarez, F.J., Mentis, G.Z., & Jessell, T.M. (2016). Spinal Inhibitory Interneuron Diversity Delineates Variant Motor Microcircuits. Cell, 165, 207-219.

Bonnot, A., & Morin, D. (1998b). Hemisegmental localisation of rhythmic networks in the lumbosacral spinal cord of neonate mouse. Brain Research, 793(1-2), 136–148.

Bonnot, A., Morin, D., & Viala, D. (1998a). Genesis of spontaneous rhythmic motor patterns in the lumbosacral spinal cord of neonate mouse. Developmental Brain Research, 108(1-2), 89–99.

Bourane, S., Grossmann, K.S., Britz, O., Dalet, A., Barrio, M.G., Stam, F.J., García-Campmany, L., Koch, S.L., & Goulding, M. (2015). Identification of a Spinal Circuit for Light Touch and Fine Motor Control. Cell, 160, 503-515.

Bouyer LJ, Rossignol S. (1998) The contribution of cutaneous inputs to locomotion in the intact and the spinal cat. Ann N Y Acad Sci. 1998 Nov 16;860:508-12.

Bouyer LJ, Rossignol S. (2003a) Contribution of cutaneous inputs from the hindpaw to the control of locomotion. I. Intact cats. J Neurophysiol. 2003 Dec;90(6):3625-39. Epub 2003 Aug 27.

Bouyer LJ, Rossignol S. (2003b) Contribution of cutaneous inputs from the hindpaw to the control of locomotion. II. Spinal cats. J Neurophysiol. 2003 Dec;90(6):3640-53. Epub 2003 Aug 27.

Bracci, E., Ballerini, L., & Nistri, A. (1996). Localization of Rhythmogenic Networks Responsible for Spontaneous Bursts Induced by Strychnine and Bicuculline in the Rat Isolated Spinal Cord. The Journal of Neuroscience, 16(21), 7063–7076.

Branchereau, P., Morin, D., Bonnot, A., Ballion, B., Chapron, J., & Viala, D. (2000). Development of lumbar rhythmic networks: from embryonic to neonate locomotor-like patterns in the mouse. Brain Research Bulletin, 53(5), 711–718.

Briscoe, J., Pierani, A., Jessell, T. M., & Ericson, J. (2000). A Homeodomain Protein Code Specifies Progenitor Cell Identity and Neuronal Fate in the Ventral Neural Tube. Cell, 101(4), 435–445.

Brown, T. G. (1912). The Factors in Rhythmic Activity of the Nervous System. Proceedings of the Royal Society B: Biological Sciences, 85(579), 278–289.

Brownstone, R.M., & Wilson, J.M. (2008). Strategies for delineating spinal locomotor rhythm-generating networks and the possible role of Hb9 interneurones in rhythmogenesis. Brain Research Reviews, 57, 64-76.

Buford JA, Smith JL. (1990) Adaptive control for backward quadrupedal walking. III. Stumbling corrective reactions and cutaneous reflex sensitivity. J Neurophysiol. 1993 Sep;70(3):1102-14.

Burke, R. E., Degtyarenko, A. M., & Simon, E. S. (2001). Patterns of Locomotor Drive to Motoneurons and Last-Order Interneurons: Clues to the Structure of the CPG. Journal of Neurophysiology, 86(1), 447–462.

Burrill, J.D., Morán, L.O., Goulding, M.D., & Saueressig, H. (1997). PAX2 is expressed in multiple spinal cord interneurons, including a population of EN1+ interneurons that require PAX6 for their development. Development, 124 22, 4493-503 .

Butt, S. J. B., & Kiehn, O. (2003). Functional Identification of Interneurons Responsible for Left-Right Coordination of Hindlimbs in Mammals. Neuron, 38(6), 953–963.

Butt, S.J., Harris-Warrick, R.M., & Kiehn, O. (2002). Firing properties of identified interneuron populations in the mammalian hindlimb central pattern generator. The Journal of neuroscience : the official journal of the Society for Neuroscience, 22 22, 9961-71 .

Capogrosso, M., Wenger, N., Raspopovic, S., Musienko, P., Beauparlant, J., Bassi Luciani, L., … Micera, S. (2013). A Computational Model for Epidural Electrical Stimulation of Spinal Sensorimotor Circuits. Journal of Neuroscience, 33(49), 19326–19340.

Capogrosso, M., Wenger, N., Raspopovic, S., Musienko, P., Beauparlant, J., Bassi Luciani, L., … Micera, S. (2013). A Computational Model for Epidural Electrical Stimulation of Spinal Sensorimotor Circuits. Journal of Neuroscience, 33(49), 19326–19340.

Carlson-Kuhta, P., Trank, T. V., & Smith, J. L. (1998). Forms of Forward Quadrupedal Locomotion. II. A Comparison of Posture, Hindlimb Kinematics, and Motor Patterns for Upslope and Level Walking. Journal of Neurophysiology, 79(4), 1687–1701.

Cazalets, J., Borde, M., & Clarac, F. (1995). Localization and organization of the central pattern generator for hindlimb locomotion in newborn rat. The Journal of Neuroscience, 15(7), 4943–4951.

Cazalets, J., Borde, M., & Clarac, F. (1996). The synaptic drive from the spinal locomotor network to motoneurons in the newborn rat. The Journal of Neuroscience, 16(1), 298–306.

Clarac, F. (2008). Some historical reflections on the neural control of locomotion. Brain Research Reviews, 57(1), 13–21.

Clarke, K.A., & Still, J.W. (1999). Gait Analysis in the Mouse. Physiology & Behavior, 66, 723-729.

Clarke, K.A., & Still, J.W. (2001). Development and consistency of gait in the mouse. Physiology & Behavior, 73, 159-164.

Conway BA, Hultborn H, & Kiehn O. (1987) Proprioceptive input resets central locomotor rhythm in the spinal cat. Exp Brain Res. 1987;68(3):643-56.

Cowley, K. C., & Schmidt, B. J. (1994a). A comparison of motor patterns induced by , acetylcholine and serotonin in the in vitro neonatal rat spinal cord. Neuroscience Letters, 171(1-2), 147–150.

Cowley, K. C., & Schmidt, B. J. (1994b). Some limitations of ventral root recordings for monitoring locomotion in the in vitro neonatal rat spinal cord preparation. Neuroscience Letters, 171(1-2), 142–146.

Cowley, K. C., & Schmidt, B. J. (1995). Effects of inhibitory amino acid antagonists on reciprocal inhibitory interactions during rhythmic motor activity in the in vitro neonatal rat spinal cord. Journal of Neurophysiology, 74(3), 1109–1117.

Cowley, K. C., & Schmidt, B. J. (1997). Regional Distribution of the Locomotor Pattern-Generating Network in the Neonatal Rat Spinal Cord. Journal of Neurophysiology, 77(1), 247–259.

Crone, S.A., Quinlan, K.A., Zagoraiou, L., Droho, S., Restrepo, C.E., Lundfald, L., Endo, T., Setlak, J., Jessell, T.M., Kiehn, O., & Sharma, K. (2008). Genetic Ablation of V2a Ipsilateral Interneurons Disrupts Left-Right Locomotor Coordination in Mammalian Spinal Cord. Neuron, 60, 70-83.

Crone, S.A., Zhong, G., Harris-Warrick, R.M., & Sharma, K. (2009). In mice lacking V2a interneurons, gait depends on speed of locomotion. The Journal of neuroscience: the official journal of the Society for Neuroscience, 29 21, 7098-109.

Dagg, A. I., & Windsor, D. E. (1972). Swimming in northern terrestrial mammals. Canadian Journal of Zoology, 50(1), 117–130.

D'Angelo, E., & Casali, S. (2012). Seeking a unified framework for cerebellar function and dysfunction: from circuit operations to cognition. Front. Neural Circuits.

Danner, S.M., Zhang, H., Shevtsova, N.A., Borowska-Fielding, J., Deska-Gauthier, D., Rybak, I.A., & Zhang, Y. (2019). Spinal V3 INs and Left–Right Coordination in Mammalian Locomotion. Frontiers in Cellular Neuroscience, 13.

De Leon, R., Hodgson, J. A., Roy, R. R., & Edgerton, V. R. (1994). Extensor- and flexor-like modulation within motor pools of the rat hindlimb during treadmill locomotion and swimming. Brain Research, 654(2), 241–250.

Degtyarenko, A. M., Simon, E. S., & Burke, R. E. (1998). Locomotor Modulation of Disynaptic EPSPs From the Mesencephalic Locomotor Region in Cat Motoneurons. Journal of Neurophysiology, 80(6), 3284–3296.

Deska-Gauthier, D., & Zhang, Y. (2019). The functional diversity of spinal interneurons and locomotor control. Current Opinion in Physiology.

Donelan, J. M., & Pearson, K. G. (2004). Contribution of sensory feedback to ongoing ankle extensor activity during the stance phase of walking. Canadian Journal of Physiology and Pharmacology, 82(8-9), 589–598.

Dougherty, K. J., & Kiehn, O. (2010). Firing and Cellular Properties of V2a Interneurons in the Rodent Spinal Cord. Journal of Neuroscience, 30(1), 24–37.

Drew, T., & Marigold, D. S. (2015). Taking the next step: cortical contributions to the control of locomotion. Current Opinion in Neurobiology, 33, 25–33.

Duysens J, Pearson KG. (1976) The role of cutaneous afferents from the distal hindlimb in the regulation of the step cycle of thalamic cats. Exp Brain Res. 1976 Jan 26;24:245-55.

Duysens J, Stein RB. (1978) Reflexes induced by nerve stimulation in walking cats with implanted cuff electrodes. Exp Brain Res. 1978 Jun 19;32(2):213-24.

Duysens, J. (1977). Reflex control of locomotion as revealed by stimulation of cutaneous afferents in spontaneously walking premammillary cats. Journal of Neurophysiology, 40(4), 737–751.

Duysens, J., & Forner-Cordero, A. (2019). A controller perspective on biological gait control: Reflexes and central pattern generators. Annu. Rev. Control., 48, 392-400.

Dyck, J., Lanuza, G. M., & Gosgnach, S. (2012). Functional characterization of dI6 interneurons in the neonatal mouse spinal cord. Journal of Neurophysiology, 107(12), 3256–3266.

Engberg, I., & Lundberg, A. (1962). An electromyographic analysis of stepping in the cat. Experientia, 18(4), 174–176.

Engberg, I., & Lundberg, A. (1969). An Electromyographic Analysis of Muscular Activity in the Hindlimb of the Cat during Unrestrained Locomotion. Acta Physiologica Scandinavica, 75(4), 614–630.

English, A. W. M., & Weeks, O. I. (1987). An anatomical and functional analysis of cat biceps femoris and semitendinosus muscles. Journal of Morphology, 191(2), 161–175.

Ericson, J., Rashbass, P., Schedl, A., Brenner-Morton, S., Kawakami, A., van Heyningen, V., … Briscoe, J. (1997). Pax6 Controls Progenitor Cell Identity and Neuronal Fate in Response to Graded Shh Signaling. Cell, 90(1), 169–180.

Ericson, J., Thor, S., Edlund, T., Jessell, T., & Yamada, T. (1992). Early stages of motor neuron differentiation revealed by expression of homeobox gene Islet-1. Science, 256(5063), 1555–1560.

Ferreira-Pinto, M. J., Ruder, L., Capelli, P., & Arber, S. (2018). Connecting Circuits for Supraspinal Control of Locomotion. Neuron, 100(2), 361–374.

Fink, A.J., Croce, K.R., Huang, Z.J., Abbott, L.F., Jessell, T.M., & Azim, E. (2014). Presynaptic inhibition of spinal sensory feedback ensures smooth movement. Nature, 509, 43 - 48.

Fleshman, J. W., Lev-Tov, A., & Burke, R. E. (1984). Peripheral and central control of flexor digitorum longus and flexor hallucis longus motoneurons: The synaptic basis of functional diversity. Experimental Brain Research, 54(1).

Forssberg H, Grillner S, Halbertsma J. (1980) The locomotion of the low spinal cat. I. Coordination within a hindlimb. Acta Physiol Scand. 1980 Mar;108(3):269-81.

Forssberg H, Grillner S, Rossignol S. (1975) Phase dependent reflex reversal during walking in chronic spinal cats. Brain Res. 1975 Feb 21;85(1):103-7.

Forssberg H, Grillner S, Rossignol S. (1977) Phasic gain control of reflexes from the dorsum of the paw during spinal locomotion. Brain Res. 1977 Aug 19;132(1):121-39.

Forssberg H. (1979) Stumbling corrective reaction: a phase-dependent compensatory reaction during locomotion. J Neurophysiol. 1979 Jul;42(4):936-53.

Forssberg, H., Grillner, S., & Rossignol, S. (1975). Phase dependent reflex reversal during walking in chronic spinal cats. Brain Research, 85(1), 103–107.

Fouad, K., & Pearson, K.G. (1997). Effects of extensor muscle afferents on the timing of locomotor activity during walking in adult rats. Brain Research, 749, 320-328.

Fowler, E.G., Gregor, R.J., Hodgson, J.A., & Roy, R.R. (1993). Relationship between ankle muscle and joint kinetics during the stance phase of locomotion in the cat. Journal of biomechanics, 26 4-5, 465-83.

Frigon, A., & Rossignol, S. (2006). Experiments and models of sensorimotor interactions during locomotion. Biological Cybernetics, 95(6), 607–627.

Fukuoka, Y., & Kimura, H. (2009). Dynamic locomotion of a biomorphic quadruped 'Tekken' robot using various gaits: walk, trot, free-gait and bound. Applied Bionics and Biomechanics, 6, 63-71.

Fukuoka, Y., Habu, Y., & Fukui, T. (2015). A simple rule for quadrupedal gait generation determined by leg loading feedback: a modeling study. Scientific Reports, 5.

Gabitto, M.I., Pakman, A., Bikoff, J.B., Abbott, L.F., Jessell, T.M., & Paninski, L. (2016). Bayesian Sparse Regression Analysis Documents the Diversity of Spinal Inhibitory Interneurons. Cell, 165, 220-233.

Garcia-Rill, E. (1986). The basal ganglia and the locomotor regions. Brain Research Reviews, 11(1), 47–63.

Gerasimenko Y, Roy RR, Edgerton VR. (2008) Epidural stimulation: comparison of the spinal circuits that generate and control locomotion in rats, cats, and humans. Exp Neurol. 2008 Feb;209(2):417-25. Epub 2007 Aug 1.

Gerasimenko, Y. P., Avelev, V. D., Nikitin, O. A., & Lavrov, I. A. (2003). Neuroscience and Behavioral Physiology, 33(3), 247–254.

Gerasimenko, Y. P., Lavrov, I. A., Courtine, G., Ichiyama, R. M., Dy, C. J., Zhong, H., … Edgerton, V. R. (2006). Spinal cord reflexes induced by epidural spinal cord stimulation in normal awake rats. Journal of Neuroscience Methods, 157(2), 253–263.

Gerasimenko, Y. P., Makarovskii, A. N., & Nikitin, O. A. (2002). Neuroscience and Behavioral Physiology, 32(4), 417–423.

Gerasimenko, Y. P., Preston, C., Zhong, H., Roy, R. R., Edgerton, V. R., & SHAH, P. (2019). Rostral lumbar segments are the key controllers of hindlimb locomotor rhythmicity in the adult spinal rat. Journal of Neurophysiology.

Giuliani CA, Smith JL. (1987) Stepping behaviors in chronic spinal cats with one hindlimb deafferented. J Neurosci. 1987 Aug;7(8):2537-46.

Glasgow, S.M., Henke, R.M., MacDonald, R.J., Wright, C.V., & Johnson, J.E. (2005). Ptf1a determines GABAergic over glutamatergic neuronal cell fate in the spinal cord dorsal horn. Development.

Goldberger ME (1988) Partial and complete deafferentation of cat hindlimb: the contribution of behavioral substitution to recovery of motor function. Exp Brain Res. 1988;73(2):343-53.

Gorassini, M. A., Prochazka, A., Hiebert, G. W., & Gauthier, M. J. (1994). Corrective responses to loss of ground support during walking. I. Intact cats. Journal of Neurophysiology, 71(2), 603–610.

Gosgnach, S., Bikoff, J. B., Dougherty, K. J., El Manira, A., Lanuza, G. M., & Zhang, Y. (2017). Delineating the Diversity of Spinal Interneurons in Locomotor Circuits. The Journal of Neuroscience, 37(45), 10835–10841.

Gosgnach, S., Lanuza, G.M., Butt, S.J., Saueressig, H., Zhang, Y., Velasquez, T., Riethmacher, D., Callaway, E.M., Kiehn, O., & Goulding, M. (2006). V1 spinal neurons regulate the speed of vertebrate locomotor outputs. Nature, 440, 215-219.

Goslow, G. E., Reinking, R. M., & Stuart, D. G. (1973). The cat step cycle: Hind limb joint angles and muscle lengths during unrestrained locomotion. Journal of Morphology, 141(1), 1–41.

Goulding, M. (2009). Circuits controlling vertebrate locomotion: moving in a new direction. Nature Reviews Neuroscience, 10, 507-518.

Goulding, M., & Lamar, E. (2000). Neuronal patterning: Making stripes in the spinal cord. Current Biology, 10(15), R565–R568.

Graham Brown, T. (1911). The Intrinsic Factors in the Act of Progression in the Mammal. Proceedings of the Royal Society B: Biological Sciences, 84(572), 308–319.

Graham Brown, T. (1912). The Factors in Rhythmic Activity of the Nervous System. Proceedings of the Royal Society of London. Series B, Containing Papers of a Biological Character, 85(579), 278-289,

Graham Brown, T. (1914). On the nature of the fundamental activity of the nervous centres; together with an analysis of the conditioning of rhythmic activity in progression, and a theory of the evolution of function in the nervous system. The Journal of physiology, 48(1), 18–46.

Grasso, R., Bianchi, L., & Lacquaniti, F. (1998). Motor Patterns for Human Gait: Backward Versus Forward Locomotion. Journal of Neurophysiology, 80(4), 1868–1885.

Grillner S, Rossignol S. (1978) On the initiation of the swing phase of locomotion in chronic spinal cats. Brain Res. 1978 May 12;146(2):269-77.

Grillner S, Wallén P. (1984). How does the lamprey central nervous system make thelamprey swim?J Exp Biol112: 337–357.

Grillner S, Zangger P. (1984) The effect of dorsal root transection on the efferent motor pattern in the cat's hindlimb during locomotion. Acta Physiol Scand. 1984 Mar;120(3):393-405.

Grillner, S. (1975). Locomotion in vertebrates: central mechanisms and reflex interaction. Physiological Reviews, 55(2), 247–304.

Grillner, S. (1981). Control of Locomotion in Bipeds, Tetrapods, and Fish. In: Handbook of Physiology, The Nervous System, Motor Control, edited by V. B. Brooks. Bethesda, MD: Am. Physiol. Soc., 1981, p. 1179-1236.

Grillner, S. (2006). Biological pattern generation: the cellular and computational logic of networks in motion. Neuron 52, 751–66. doi:10.1016/ j.neuron. 2006.11.008.

Grillner, S., & El Manira, A. (2019). Current Principles of Motor Control, with Special Reference to Vertebrate Locomotion. Physiological Reviews.

Grillner, S., & Robertson, B. (2015). The basal ganglia downstream control of brainstem motor centres—an evolutionarily conserved strategy. Current Opinion in Neurobiology, 33, 47–52.

Grillner, S., & Zangger, P. (1979). On the central generation of locomotion in the low spinal cat. Experimental Brain Research, 34(2).

Grillner, S., Mcclellan, A., Sigvardt, K.A., Wallén, P., & Wilen, M.M. (1981). Activation of NMDA-receptors elicits "fictive locomotion" in lamprey spinal cord in vitro. Acta physiologica Scandinavica, 113 4, 549-51.

Grillner, S., Zangger, P., 1975. How detailed is the central pattern generation for locomotion? Brain Res. 88 (2), 367–371.

Gross, M. K., Dottori, M., & Goulding, M. (2002). Lbx1 Specifies Somatosensory Association Interneurons in the Dorsal Spinal Cord. Neuron, 34(4), 535–549.

Gruner, J. A., Altman, J., & Spivack, N. (1980). Effects of arrested cerebellar development on locomotion in the rat. Experimental Brain Research, 40(4).

Gruner, J.A., & Altman, J. (1980). Swimming in the rat: analysis of locomotor performance in comparison to stepping. Exp. Brain Res. 40, 374–382.

Guertin, P., Angel, M. J., Perreault, M. C., & McCrea, D. A. (1995). Ankle extensor group I afferents excite extensors throughout the hindlimb during fictive locomotion in the cat. The Journal of Physiology, 487(1), 197–209.

Hägglund, M., Borgius, L., Dougherty, K.J., & Kiehn, O. (2010). Activation of groups of excitatory neurons in the mammalian spinal cord or hindbrain evokes locomotion. Nature Neuroscience, 13, 246-252.

Hägglund, M., Dougherty, K.J., Borgius, L., Itohara, S., Iwasato, T., & Kiehn, O. (2013). Optogenetic dissection reveals multiple rhythmogenic modules underlying locomotion. Proceedings of the National Academy of Sciences of the United States of America, 110 28, 11589-94.

Halbertsma, J.M. (1983). The stride cycle of the cat: the modelling of locomotion by computerized analysis of automatic recordings. Acta physiologica Scandinavica. Supplementum, 521, 1-75.

Haque, F., Rancic, V., Zhang, W.Y., Clugston, R.D., Ballanyi, K., & Gosgnach, S. (2018). WT1-Expressing Interneurons Regulate Left-Right Alternation during Mammalian Locomotor Activity. The Journal of neuroscience: the official journal of the Society for Neuroscience, 38 25, 5666-5676.

Harris-Warrick, R.M. (2014). Locomotor Pattern Generation in the Rodent Spinal Cord. Encyclopedia of Computational Neuroscience.

Heglund, N.C., & Taylor, C.R. (1988). Speed, stride frequency and energy cost per stride: how do they change with body size and gait? The Journal of experimental biology, 138, 301-18.

Herbin, M., Hackert, R., Gasc, J.-P., & Renous, S. (2007). Gait parameters of treadmill versus overground locomotion in mouse. Behavioural Brain Research, 181(2), 173–179.

Herman R., Cook T., Cozzens B., Freedman W. (1973) Control of Postural Reactions in Man: The Initiation of Gait. In: Stein R.B., Pearson K.G., Smith R.S., Redford J.B. (eds) Control of Posture and Locomotion. Advances in Behavioral Biology, vol 7. Springer, Boston, MA

Herzog, W., Leonard, T.R., & Guimarães, A.C. (1993). Forces in gastrocnemius, soleus, and plantaris tendons of the freely moving cat. Journal of biomechanics, 26 8, 945-53 .

Higashijima, S., Masino, M.A., Mandel, G., & Fetcho, J.R. (2004). Engrailed-1 expression marks a primitive class of inhibitory spinal interneuron. The Journal of neuroscience : the official journal of the Society for Neuroscience, 24 25, 5827-39 .

Hildebrand, M. (1976). "Analysis of tetrapod gaits: general considerations and symmetrical gaits," in Neural Control of Movement, eds R. Herman, S. Grillner, P. S. Stein, and D. G. Stuart (New York, NY: Plenum Press), 203–236.

Hildebrand, M. (1977). Analysis of Asymmetrical Gaits. Journal of Mammalogy, 58(2), 131–156.

Hildebrand, M. (1989). The Quadrupedal Gaits of Vertebrates. BioScience, 39(11), 766–775.

Hofstoetter, U. S., Danner, S. M., Freundl, B., Binder, H., Mayr, W., Rattay, F., & Minassian, K. (2015). Periodic modulation of repetitively elicited monosynaptic reflexes of the human lumbosacral spinal cord. Journal of Neurophysiology, 114(1), 400–410.

Hughes, G.M., & Wiersma, C.A. (1960). The Co-ordination of Swimmeret Movements in the Crayfish, Procambarus Clarkii (Girard).

Hultborn, H., & Nielsen, J. B. (2007). Spinal control of locomotion ? from cat to man. Acta Physiologica, 189(2), 111–121.

Hutchison, D. L., Roy, R. R., Bodine-Fowler, S., Hodgson, J. A., & Reggie Edgerton, V. (1989). Electromyographic (EMG) amplitude patterns in the proximal and distal compartments of the cat semitendinosus during various motor tasks. Brain Research, 479(1), 56–64.

Ichiyama, R. M., Gerasimenko, Y. P., Zhong, H., Roy, R. R., & Edgerton, V. R. (2005). Hindlimb stepping movements in complete spinal rats induced by epidural spinal cord stimulation. Neuroscience Letters, 383(3), 339–344.

Jankowska, E., Jukes, M.G., Lund, S., Lundberg, A. (1967a). The effect of DOPA on the spinal cord. 5, Reciprocal organization of pathways transmitting excitatory action to alpha motoneurones of flexors and extensors. Acta Physiol. Scand. 70, 369–388.

Jankowska, E., Jukes, M. G., Lund, S., and Lundberg, A. (1967b).The effect of DOPA on the spinal cord. 6. Half-centre organization of interneurons transmitting effects from the flexor reflex afferents. Acta Physiol. Scand.

70, 389–402.

Jessell, T.M. (2000). Neuronal specification in the spinal cord: inductive signals and transcriptional codes. Nature Reviews Genetics, 1, 20-29.

Jiang, Z., Carlin, K. P., & Brownstone, R. M. (1999). An in vitro functionally mature mouse spinal cord preparation for the study of spinal motor networks. Brain Research, 816(2), 493–499.

Jordan, L. M., Liu, J., Hedlund, P. B., Akay, T., & Pearson, K. G. (2008). Descending command systems for the initiation of locomotion in mammals. Brain Research Reviews, 57(1), 183–191.

Karunaratne, A., Hargrave, M., Poh, A., & Yamada, T. (2002). GATA Proteins Identify a Novel Ventral Interneuron Subclass in the Developing Chick Spinal Cord. Developmental Biology, 249(1), 30–43.

Kiehn, O. (2006). Locomotor circuits in the mammalian spinal cord. Annu. Rev. Neurosci. 29, 279–306. doi:10.1146/ annurev.neuro. 29.051605.112910.

Kiehn, O. (2011). Development and functional organization of spinal locomotor circuits. Curr. Opin. Neurobiol. 21, 100–9. doi:10.1016/ j. conb.2010.09.004.

Kiehn, O. (2016). Decoding the organization of spinal circuits that control locomotion. Nature Reviews Neuroscience, 17(4), 224–238.

Kiehn, O., & Kjaerulff, O. (1996). Spatiotemporal characteristics of 5-HT and dopamine-induced rhythmic hindlimb activity in the in vitro neonatal rat. Journal of neurophysiology, 75 4, 1472-82.

Kiehn, O., Sillar, K. T., Kjaerulff, O., & McDearmid, J. R. (1999). Effects of Noradrenaline on Locomotor Rhythm–Generating Networks in the Isolated Neonatal Rat Spinal Cord. Journal of Neurophysiology, 82(2), 741–746.

Kjaerulff, O., & Kiehn, O. (1996). Distribution of Networks Generating and Coordinating Locomotor Activity in the Neonatal Rat Spinal CordIn Vitro: A Lesion Study. The Journal of Neuroscience, 16(18), 5777–5794.

Kjaerulff, O., & Kiehn, O. (1997). Crossed rhythmic synaptic input to motoneurons during selective activation of the contralateral spinal locomotor network. The Journal of neuroscience: the official journal of the Society for Neuroscience, 17 24, 9433-47 .

Kriellaars DJ, Brownstone RM, Noga BR, Jordan LM. (1994) Mechanical entrainment of fictive locomotion in the decerebrate cat. J Neurophysiol. 1994 Jun;71(6):2074-86.

Kudo, N., & Yamada, T. (1987). N-Methyl-d,l-aspartate-induced locomotor activity in a spinal cord-indlimb muscles preparation of the newborn rat studied in vitro. Neuroscience Letters, 75, 43-48.

Kuhtz-Buschbeck, J. P., Boczek-Funcke, A., Illert, M., & Weinhardt, C. (1994). X-Ray Study of the Cat Hindlimb During Treadmill Locomotion. European Journal of Neuroscience, 6(7), 1187–1198.

Ladenbauer, J., Minassian, K., Hofstoetter, U. S., Dimitrijevic, M. R., & Rattay, F. (2010). Stimulation of the Human Lumbar Spinal Cord With Implanted and Surface Electrodes: A Computer Simulation Study. IEEE Transactions on Neural Systems and Rehabilitation Engineering, 18(6), 637–645.

Lafreniere-Roula, M., & McCrea, D. A. (2005). Deletions of Rhythmic Motoneuron Activity During Fictive Locomotion and Scratch Provide Clues to the Organization of the Mammalian Central Pattern Generator. Journal of Neurophysiology, 94(2), 1120–1132.

Lai, H.C., Seal, R.P., & Johnson, J.E. (2016). Making sense out of spinal cord somatosensory development. Development, 143, 3434 - 3448.

Lanuza, G. M., Gosgnach, S., Pierani, A., Jessell, T. M., & Goulding, M. (2004). Genetic Identification of Spinal Interneurons that Coordinate Left-Right Locomotor Activity Necessary for Walking Movements. Neuron, 42(3), 375–386.

Leblond, H., L'Espérance, M., Orsal, D., & Rossignol, S. (2003). Treadmill Locomotion in the Intact and Spinal Mouse. The Journal of Neuroscience, 23(36), 11411–11419.

Lee, K., & Jessell, T.M. (1999). The specification of dorsal cell fates in the vertebrate central nervous system. Annual review of neuroscience, 22, 261-94.

Lemieux, M., Josset, N., Roussel, M., Couraud, S., & Bretzner, F. (2016). Speed-Dependent Modulation of the Locomotor Behavior in Adult Mice Reveals Attractor and Transitional Gaits. Frontiers in Neuroscience, 10.

Loeb, G. E. (1993). The distal hindlimb musculature of the cat: interanimal variability of locomotor activity and cutaneous reflexes. Experimental Brain Research, 96(1), 125–140.

Lundfald, L., Restrepo, C.E., Butt, S.J., Peng, C., Droho, S., Endo, T., Zeilhofer, H.U., Sharma, K., & Kiehn, O. (2007). Phenotype of V2-derived interneurons and their

relationship to the axon guidance molecule EphA4 in the developing mouse spinal cord. The European journal of neuroscience, 26 11, 2989-3002.

Markin, S. N., Lemay, M. A., Prilutsky, B. I., & Rybak, I. A. (2012). Motoneuronal and muscle synergies involved in cat hindlimb control during fictive and real locomotion: a comparison study. Journal of Neurophysiology, 107(8), 2057–2071.

Mayer, W.P., & Akay, T. (2018). Stumbling corrective reaction elicited by mechanical and electrical stimulation of the saphenous nerve in walking mice. The Journal of experimental biology, 221 Pt 13.

Mayer, W.P., Murray, A.J., Brenner-Morton, S., Jessell, T.M., Tourtellotte, W.G., & Akay, T. (2018). Role of muscle spindle feedback in regulating muscle activity strength during walking at different speed in mice. Journal of neurophysiology, 120 5, 2484-2497.

McClellan, A. D. (1984). Descending control and sensory gating of “fictive” swimming and turning responses elicited in an in vitro preparation of the lamprey brainstem/spinal cord. Brain Research, 302(1), 151–162.

McCrea D, Quevedo J, Fedirchuk B, Gosgnach S. (2005) The stumbling correction reaction during fictive locomotion in the cat. Ann N Y Acad Sci. 1998 Nov 16; 860: 502-4.

McCrea, D.A., & Rybak, I.A. (2008). Organization of mammalian locomotor rhythm and pattern generation. Brain Research Reviews, 57, 134-146.

McVea, D. A., & Pearson, K. G. (2007). Long-Lasting, Context-Dependent Modification of Stepping in the Cat After Repeated Stumbling-Corrective Responses. Journal of Neurophysiology, 97(1), 659–669.

Mena-Segovia, J., & Bolam, J. P. (2017). Rethinking the Pedunculopontine Nucleus: From Cellular Organization to Function. Neuron, 94(1), 7–18.

Mendes, C. S., Bartos, I., Márka, Z., Akay, T., Márka, S., & Mann, R. S. (2015). Quantification of gait parameters in freely walking rodents. BMC Biology, 13(1).

Miller, S., Van Der Burg, J., & Van Der Meché, F. G. A. (1975). Locomotion in the cat: Basic programmes of movement. Brain Research, 91(2), 239–253.

Minassian, K., Persy, I., Rattay, F., Pinter, M. M., Kern, H., & Dimitrijevic, M. R. (2007). Human lumbar cord circuitries can be activated by extrinsic tonic input to generate locomotor-like activity. Human Movement Science, 26(2), 275–295.

Moran-Rivard, L., Kagawa, T., Saueressig, H., Gross, M. K., Burrill, J., & Goulding, M. (2001). Evx1 Is a Postmitotic Determinant of V0 Interneuron Identity in the Spinal Cord. Neuron, 29(2), 385–399.

Moschovakis, A. K., Sholomenko, G. N., & Burke, R. E. (1991). Differential control of short latency cutaneous excitation in cat FDL motoneurons during fictive locomotion. Experimental Brain Research, 83(3).

Müller, T., Brohmann, H., Pierani, A., Heppenstall, P. A., Lewin, G. R., Jessell, T. M., & Birchmeier, C. (2002). The Homeodomain Factor Lbx1 Distinguishes Two Major Programs of Neuronal Differentiation in the Dorsal Spinal Cord. Neuron, 34(4), 551–562.

Muroyama, Y., Fujiwara, Y., Orkin, S. H., & Rowitch, D. H. (2005). Specification of astrocytes by bHLH protein SCL in a restricted region of the neural tube. Nature, 438(7066), 360–363.

Nilsson, J., Thorstensson, A., & Halbertsma, J. (1985). Changes in leg movements and muscle activity with speed of locomotion and mode of progression in humans. Acta Physiologica Scandinavica, 123(4), 457–475.

Nishimaru, H., Takizawa, H., & Kudo, N. (2000). 5-Hydroxytryptamine-induced locomotor rhythm in the neonatal mouse spinal cord in vitro. Neuroscience Letters, 280(3), 187–190.

O'Donovan, M. J., Pinter, M. J., Dum, R. P., & Burke, R. E. (1982). Actions of FDL and FHL muscles in intact cats: functional dissociation between anatomical synergists. Journal of Neurophysiology, 47(6), 1126–1143.

Orlovskiĭ GN, Fel'dman AG. (1972) The role of afferentation in the generation of walking movements. Neirofiziologiia. 1972 Jul-Aug;4(4):401-9.

Orlovskiĭ, G.N., & Fel'dman, A.G. (1972). Classification of lumbosacral neurons by their discharge pattern during evoked locomotion. Neurophysiology, 4, 311-317.

Orlovskiĭ, G.N., & Fel'dman, A.G. (1972). Classification of the neurons of the lumbo-sacral region of the spinal cord in accordance with their discharge patterns during provoked locomotion. Translated from Neirofiziologiia, Vol. 4, No. 4, pp. 4t0-417.

Pearson KG, Ramirez JM, Jiang W. (1992) Entrainment of the locomotor rhythm by group Ib afferents from ankle extensor muscles in spinal cats. Exp Brain Res. 1992;90(3):557-66.

Pearson KG, Rossignol S. (1991) Fictive motor patterns in chronic spinal cats. J Neurophysiol. 1991 Dec;66(6):1874-87.

Pearson, K. G. (2008). Role of sensory feedback in the control of stance duration in walking cats. Brain Research Reviews, 57(1), 222–227.

Pearson, K. G., & Collins, D. F. (1993). Reversal of the influence of group Ib afferents from plantaris on activity in medial gastrocnemius muscle during locomotor activity. Journal of Neurophysiology, 70(3), 1009–1017.

Pearson, K. G., Acharya, H., & Fouad, K. (2005). A new electrode configuration for recording electromyographic activity in behaving mice. Journal of Neuroscience Methods, 148(1), 36–42.

Pearson, K.G. (2004). Generating the walking gait: role of sensory feedback. Progress in brain research, 143, 123-9.

Peng, C.-Y., Yajima, H., Burns, C. E., Zon, L. I., Sisodia, S. S., Pfaff, S. L., & Sharma, K. (2007). Notch and MAML Signaling Drives Scl-Dependent Interneuron Diversity in the Spinal Cord. Neuron, 53(6), 813–827.

Perreault MC, Angel MJ, Guertin P, McCrea DA. (1995) Effects of stimulation of hindlimb flexor group II afferents during fictive locomotion in the cat. J Physiol. 1995 Aug 15;487(1):211-20.

Perret C., Cabelguen JM., Orsal D. (1988) Analysis of the Pattern of Activity in "Knee Flexor" Motoneurons During Locomotion in the Cat. In: Gurfinkel V.S., Ioffe M.E., Massion J., Roll J.P. (eds) Stance and Motion. Springer, Boston, MA

Perret, C., & Cabelguen, J.-M. (1976). Central and reflex participation in the timing of locomotor activations of a bifunctional muscle, the semi-tendinosus, in the cat. Brain Research, 106(2), 390–395.

Perret, C., & Cabelguen, J.-M. (1980). Main characteristics of the hindlimb locomotor cycle in the decorticate cat with special reference to bifunctional muscles. Brain Research, 187(2), 333–352.

Phllipson, M. 1905. L' autonomie et la centralisation dans le système nerveux des animaux. Trav Lab Physiol Inst Solvay Bruxelles 7: 1-208.

Pierani, A., Moran-Rivard, L., Sunshine, M., Littman, D., Goulding, M., & Jessell, T. (2001). Control of Interneuron Fate in the Developing Spinal Cord by the Progenitor Homeodomain Protein Dbx1. Neuron, 29(2), 367–384.

Pocratsky, A. M., Burke, D. A., Morehouse, J. R., Beare, J. E., Riegler, A. S., Tsoulfas, P., … Magnuson, D. S. K. (2017). Reversible silencing of lumbar spinal interneurons unmasks a task-specific network for securing hindlimb alternation. Nature Communications, 8(1).

Proske, U., & Gandevia, S.C. (2012). The proprioceptive senses: their roles in signaling body shape, body position and movement, and muscle force. Physiological reviews, 92 4, 1651-97.

Quevedo, J., Stecina, K., Gosgnach, S., & McCrea, D. A. (2005). Stumbling Corrective Reaction During Fictive Locomotion in the Cat. Journal of Neurophysiology, 94(3), 2045–2052.

Quinlan, K. A., & Kiehn, O. (2007). Segmental, Synaptic Actions of Commissural Interneurons in the Mouse Spinal Cord. Journal of Neuroscience, 27(24), 6521–6530.

Quinlan, K.A., Kajtaz, E., Ciolino, J.D., Imhoff-Manuel, R.D., Tresch, M.C., Heckman, C.J., & Tysseling, V.M. (2017). Chronic electromyograms in treadmill running SOD1 mice reveal early changes in muscle activation. The Journal of Physiology, 595, 5387–5400.

Rabe, N., Gezelius, H., Vallstedt, A., Memic, F., & Kullander, K. (2009). Netrin-1-Dependent Spinal Interneuron Subtypes Are Required for the Formation of Left-Right Alternating Locomotor Circuitry. Journal of Neuroscience, 29(50), 15642–15649.

Rasmussen, S., Chan, A. K., & Goslow, G. E. (1978). The cat step cycle: Electromyographic patterns for hindlimb muscles during posture and unrestrained locomotion. Journal of Morphology, 155(3), 253–269.

Rattay, F., Minassian, K., & Dimitrijevic, M. (2000). Epidural electrical stimulation of posterior structures of the human lumbosacral cord: 2. quantitative analysis by computer modeling. Spinal Cord, 38(8), 473–489.

Roelink, H., Porter, J., Chiang, C., Tanabe, Y., Chang, D., Beachy, P., & Jessell, T. (1995). Floor plate and motor neuron induction by different concentrations of the amino-terminal cleavage product of sonic hedgehog autoproteolysis. Cell, 81(3), 445–455.

Rossignol S, Dubuc R, Gossard JP. (2006) Dynamic sensorimotor interactions in locomotion. Physiol Rev. 2006 Jan;86(1):89-154.

Rossignol, S. (1996). Neural control of stereotypic limb movements," in Handbook of Physiology, eds L. B. Rowell and J. Shepherd (Bethesda, MD: American Physiological Society), 173–216.

Rovainen, C. M. (1983). Generation of respiratory activity by the lamprey brain exposed to picrotoxin and strychnine, and weak synaptic inhibition in motoneurons. Neuroscience, 10(3), 875–882.

Ruder L, Takeoka A, Arber S. (2016). Long-distance descending spinal neurons ensure quadrupedal locomotor stability. Neuron 92: 1063–1078.

Rybak, I.A., Shevtsova, N.A., Lafrenière-Roula, M., & McCrea, D.A. (2006). Modelling spinal circuitry involved in locomotor pattern generation: insights from deletions during fictive locomotion. The Journal of physiology, 577 Pt 2, 617- 39.

Ryczko, D. & Dubuc, R. (2013). The multifunctional mesencephalic locomotor region. Current Pharmaceutical Design, 19, 4448–4470.

Ryczko, D., & Dubuc, R. (2017). Dopamine and the Brainstem Locomotor Networks: From Lamprey to Human. Frontiers in Neuroscience, 11.

Santuz, A., Akay, T., Mayer, W.P., Wells, T.L., Schroll, A., & Arampatzis, A. (2019). Modular organization of murine locomotor pattern in the presence and absence of sensory feedback from muscle spindles. The Journal of physiology, 597 12, 3147- 3165.

Sapir, T. (2004). Pax6 and Engrailed 1 Regulate Two Distinct Aspects of Renshaw Cell Development. Journal of Neuroscience, 24(5), 1255–1264.

Saueressig, H., Burrill, J.D., & Goulding, M.D. (1999). Engrailed-1 and netrin-1 regulate axon pathfinding by association interneurons that project to motor neurons. Development, 126 19, 4201-12.

Sayenko, D. G., Angeli, C., Harkema, S. J., Edgerton, V. R., & Gerasimenko, Y. P. (2014). Neuromodulation of evoked muscle potentials induced by epidural spinal-cord stimulation in paralyzed individuals. Journal of Neurophysiology, 111(5), 1088–1099.

Serradj, N., & Jamon, M. (2009). The adaptation of limb kinematics to increasing walking speeds in freely moving mice 129/Sv and C57BL/6. Behavioural Brain Research, 201(1), 59–65.

Shah, P. K., Sureddi, S., Alam, M., Zhong, H., Roy, R. R., Edgerton, V. R., & Gerasimenko, Y. (2016). Unique Spatiotemporal Neuromodulation of the Lumbosacral Circuitry Shapes Locomotor Success after Spinal Cord Injury. Journal of Neurotrauma, 33(18), 1709–1723.

Sherrington CS. (1910) Flexion-reflex of the limb, crossed extension-reflex, and reflex stepping and standing. J Physiol. 1910 Apr 26;40(1-2):28-121.

Shevtsova, N. A., Talpalar, A. E., Markin, S. N., Harris-Warrick, R. M., Kiehn, O., & Rybak, I. A. (2015). Organization of left-right coordination of neuronal activity in the mammalian spinal cord: Insights from computational modelling. The Journal of Physiology, 593(11), 2403–2426.

Shik, M.L., & Orlovsky, G.N. (1976). Neurophysiology of locomotor automatism. Physiological reviews, 56 3, 465-501.

Shik, M.L., Severin, F.V., Orlovsky, G.N. (1966). Control of walking and running by means of electrical stimulation of the mid-brain. Biophysics 11, 756–765.

Shik, M.L., Severin, F.V., Orlovsky, G.N. (1969). Control of walking and running by means of electrical stimulation of the mesencephalon. Electroencephalogr. Clin. Neurophysiol. 26, 549.

Smith, E., Hargrave, M., Yamada, T., Begley, C. G., & Little, M. H. (2002). Coexpression of SCL and GATA3 in the V2 interneurons of the developing mouse spinal cord. Developmental Dynamics, 224(2), 231–237.

Smith, J. C., & Feldman, J. L. (1987). In vitro brainstem-spinal cord preparations for study of motor systems for mammalian respiration and locomotion. Journal of Neuroscience Methods, 21(2-4), 321–333.

Smith, J. C., Feldman, J. L., & Schmidt, B. J. (1988). Neural mechanisms generating locomotion studied in mammalian brain stem-spinal cord in vitro. The FASEB Journal, 2(7), 2283–2288.

Smith, J., Chung, S., & Zernicke, R. (1993). Gait-related motor patterns and hindlimb kinetics for the cat trot and gallop. Experimental Brain Research, 94(2).

Smith, J.C. & Feldman, J.L. (1985) Motor patterns for respiration and locomotion generated by an in vitro brainstem-spinal cord from neonatal rat, Soc. Neurosci. Abstr., 11: 24.

Smith, J.C. & Feldman, J.L. (1986) Role of chloride-dependent synaptic inhibition in respiratory pattern generation. Studies in an in vitro mammalian brainstem-spinal cord preparation, Fed. Proc., 45: 518.

Smith, J.L., Edgerton, V.R., Betts, B.J., & Collatos, T.C. (1977). EMG of slow and fast ankle extensors of cat during posture, locomotion, and jumping. Journal of neurophysiology, 40 3, 503-13.

Sqalli-Houssaini, Y., & Cazalets, J.-R. (2000). Noradrenergic control of locomotor networks in the in vitro spinal cord of the neonatal rat. Brain Research, 852(1), 100–109.

Stam, F.J., Hendricks, T.J., Zhang, J., Geiman, E.J., Francius, C., Labosky, P.A., Clotman, F., & Goulding, M. (2012). Renshaw cell interneuron specialization is controlled by a temporally restricted transcription factor program. Development, 139 1, 179-90.

Stein, P. S. G. (2004). Neuronal control of turtle hindlimb motor rhythms. Journal of Comparative Physiology A, 191(3), 213–229.

Taccola, G., Gad, P., Culaclii, S., Wang, P.-M., Liu, W., & Edgerton, V. R. (2020). Acute neuromodulation restores spinally-induced motor responses after severe spinal cord injury. Experimental Neurology, 113246.

Takakusaki, K. (2013). Neurophysiology of gait: From the spinal cord to the frontal lobe. Movement Disorders, 28(11), 1483–1491.

Takeoka, A., Vollenweider, I., Courtine, G., & Arber, S. (2014). Muscle Spindle Feedback Directs Locomotor Recovery and Circuit Reorganization after Spinal Cord Injury. Cell, 159(7), 1626–1639.

Talpalar, A. E., Bouvier, J., Borgius, L., Fortin, G., Pierani, A., & Kiehn, O. (2013). Dual-mode operation of neuronal networks involved in left–right alternation. Nature, 500(7460), 85–88.

Thaler, J. P., Lee, S.-K., Jurata, L. W., Gill, G. N., & Pfaff, S. L. (2002). LIM Factor Lhx3 Contributes to the Specification of Motor Neuron and Interneuron Identity through Cell-Type-Specific Protein-Protein Interactions. Cell, 110(2), 237–249.

Tourtellotte, W.G., & Milbrandt, J. (1998). Sensory ataxia and muscle spindle agenesis in mice lacking the transcription factor Egr3. Nature Genetics, 20, 87-91.

Tysseling, V.M., Janes, L., Imhoff, R., Quinlan, K.A., Lookabaugh, B., Ramalingam, S., Heckman, C.J., & Tresch, M.C. (2013). Design and evaluation of a chronic EMG multichannel detection system for long-term recordings of hindlimb muscles in behaving mice. Journal of electromyography and kinesiology: official journal of the International Society of Electrophysiological Kinesiology, 23 3, 531-9.

Viala, D., & Buser, P. (1971). Modalités d'obtention de rythmes locomoteurs chez le lapin spinal par traitements pharmacologiques (DOPA, 5-HTP, d-amphétamine). Brain Research, 35(1), 151–165.

Walmsley, B., Hodgson, J. A., & Burke, R. E. (1978). Forces produced by medial gastrocnemius and soleus muscles during locomotion in freely moving cats. Journal of Neurophysiology, 41(5), 1203–1216.

Wenger N, Moraud EM, Gandar J, Musienko P, Capogrosso M, Baud L, Le Goff CG, Barraud Q, Pavlova N, Dominici N, Minev IR, Asboth L, Hirsch A, Duis S, Kreider J, Mortera A, Haverbeck O, Kraus S, Schmitz F, DiGiovanna J, van den Brand R, Bloch J, Detemple P, Lacour SP, Bézard E, Micera S, Courtine G. (2016) Spatiotemporal neuromodulation therapies engaging muscle synergies improve motor control after spinal cord injury. Nat Med. 2016 Feb;22(2):138-45.

Whelan, P., Bonnot, A., & O'Donovan, M. J. (2000). Properties of Rhythmic Activity Generated by the Isolated Spinal Cord of the Neonatal Mouse. Journal of Neurophysiology, 84(6), 2821–2833.

Wildner, H., Das Gupta, R., Brohl, D., Heppenstall, P. A., Zeilhofer, H. U., & Birchmeier, C. (2013). Genome-Wide Expression Analysis of Ptf1a- and Ascl1-Deficient Mice Reveals New Markers for Distinct Dorsal Horn Interneuron Populations Contributing to Nociceptive Reflex Plasticity. Journal of Neuroscience, 33(17), 7299–7307.

Wilson, D.M. (1961). The Central Nervous Control of Flight in a Locust. J. Exp. Biol. 38, 471–490.

Wilson, R. J. ., Chersa, T., & Whelan, P. . (2003). Tissue PO2 and the effects of hypoxia on the generation of locomotor-like activity in the in vitro spinal cord of the neonatal mouse. Neuroscience, 117(1), 183–196.

Windhorst, U. (2007). Muscle proprioceptive feedback and spinal networks. Brain Research Bulletin, 73(4-6), 155–202.

Wisleder, D., Zernicke, R. F., & Smith, J. L. (1990). Speed-related changes in hindlimb intersegmental dynamics during the swing phase of cat locomotion. Experimental Brain Research, 79(3).

Yamaguchi, T. (2004). The central pattern generator for forelimb locomotion in the cat. Progress in brain research, 143, 115-22.

Zagoraiou, L., Akay, T., Martin, J. F., Brownstone, R. M., Jessell, T. M., & Miles, G. B. (2009). A Cluster of Cholinergic Premotor Interneurons Modulates Mouse Locomotor Activity. Neuron, 64(5), 645–662.

Zaporozhets, E., Cowley, K.C., & Schmidt, B.J. (2006). Propriospinal neurons contribute to bulbospinal transmission of the locomotor command signal in the neonatal rat spinal cord. The Journal of physiology, 572 Pt 2, 443-58.

Zhong H, Roy RR, Nakada KK, Zdunowski S, Khalili N, de Leon RD, Edgerton VR. (2012) Accommodation of the spinal cat to a tripping perturbation. Front Physiol. 2012 May 1; 3:112. doi: 10.3389/fphys.2012.00112. eCollection 2012.

Zhong, G., Díaz-Ríos, M., & Harris-Warrick, R. M. (2006a). Serotonin Modulates the Properties of Ascending Commissural Interneurons in the Neonatal Mouse Spinal Cord. Journal of Neurophysiology, 95(3), 1545–1555.

Zhong, G., Diaz-Rios, M., & Harris-Warrick, R. M. (2006b). Intrinsic and Functional Differences among Commissural Interneurons during Fictive Locomotion and Serotonergic Modulation in the Neonatal Mouse. Journal of Neuroscience, 26(24), 6509–6517.

Zhong, G., Droho, S., Crone, S.A., Dietz, S.B., Kwan, A.C., Webb, W.W., Sharma, K., & Harris-Warrick, R.M. (2010). Electrophysiological characterization of V2a interneurons and their locomotor-related activity in the neonatal mouse spinal cord. The Journal of neuroscience: the official journal of the Society for Neuroscience, 30 1, 170-82.

Zhong, G., Shevtsova, N.A., Rybak, I.A., & Harris-Warrick, R.M. (2012). Neuronal activity in the isolated mouse spinal cord during spontaneous deletions in fictive locomotion: insights into locomotor central pattern generator organization. The Journal of physiology, 590 19, 4735-59.

Zhong, H., Roy, R. R., Nakada, K. K., Zdunowski, S., Khalili, N., de Leon, R. D., & Edgerton, V. R. (2012). Accommodation of the Spinal Cat to a Tripping Perturbation. Front Physiol. 2012 May 1; 3:112.

Zhou, Y., Yamamoto, M., & Engel, J.D. (2000). GATA2 is required for the generation of V2 interneurons. Development, 127 17, 3829-38.

APPENDIX

Copyright permission letters

ELSEVIER LICENSE
TERMS AND CONDITIONS

May 25, 2020

This Agreement between 421 Larry Uteck Boulevard ("You") and Elsevier ("Elsevier") consists of your license details and the terms and conditions provided by Elsevier and Copyright Clearance Center.

License Number	4787180270996
License date	Mar 13, 2020
Licensed Content Publisher	Elsevier
Licensed Content Publication	Brain Research Reviews
Licensed Content Title	Some historical reflections on the neural control of locomotion
Licensed Content Author	François Clarac
Licensed Content Date	Jan 1, 2008
Licensed Content Volume	57
Licensed Content Issue	1
Licensed Content Pages	9
Start Page	13
End Page	21
Type of Use	reuse in a thesis/dissertation

Portion	figures/tables/illustrations
Number of figures/tables/illustrations	1
Format	both print and electronic
Are you the author of this Elsevier article?	No
Will you be translating?	No
Title	PhD
Institution name	dalhousie university
Expected presentation date	Apr 2020
Portions	Figure 1.1
Requestor Location	421 Larry Uteck Boulevard 421 Larry Uteck Boulevard 206 halifax, NS b3m0g7 Canada Attn: 421 Larry Uteck Boulevard
Publisher Tax ID	GB 494 6272 12
Total	0.00 CAD
Terms and Conditions	

INTRODUCTION

1. The publisher for this copyrighted material is Elsevier. By clicking "accept" in connection with completing this licensing transaction, you agree that the following terms and conditions apply to this transaction (along with the Billing and Payment terms and conditions

ELSEVIER LICENSE
TERMS AND CONDITIONS

May 25, 2020

This Agreement between 421 Larry Uteck Boulevard ("You") and Elsevier ("Elsevier") consists of your license details and the terms and conditions provided by Elsevier and Copyright Clearance Center.

License Number	4787211434676
License date	Mar 13, 2020
Licensed Content Publisher	Elsevier
Licensed Content Publication	Cell
Licensed Content Title	SnapShot: Spinal Cord Development
Licensed Content Author	William A. Alaynick,Thomas M. Jessell,Samuel L. Pfaff
Licensed Content Date	Jul 8, 2011
Licensed Content Volume	146
Licensed Content Issue	1
Licensed Content Pages	2
Start Page	178
End Page	178.e1
Type of Use	reuse in a thesis/dissertation

Portion	figures/tables/illustrations
Number of figures/tables/illustrations	1
Format	both print and electronic
Are you the author of this Elsevier article?	No
Will you be translating?	No
Title	PhD
Institution name	dalhousie university
Expected presentation date	Apr 2020
Order reference number	Figure 1.6
Portions	Figure 1
Requestor Location	421 Larry Uteck Boulevard 421 Larry Uteck Boulevard 206 halifax, NS b3m0g7 Canada Attn: 421 Larry Uteck Boulevard
Publisher Tax ID	GB 494 6272 12
Total	0.00 CAD
Terms and Conditions	

INTRODUCTION

1. The publisher for this copyrighted material is Elsevier. By clicking "accept" in connection with completing this licensing transaction, you agree that the following terms and conditions

apply to this transaction (along with the Billing and Payment terms and conditions established by Copyright Clearance Center, Inc. ("CCC"), at the time that you opened your Rightslink account and that are available at any time at http://myaccount.copyright.com).

GENERAL TERMS

2. Elsevier hereby grants you permission to reproduce the aforementioned material subject to the terms and conditions indicated.

3. Acknowledgement: If any part of the material to be used (for example, figures) has appeared in our publication with credit or acknowledgement to another source, permission must also be sought from that source. If such permission is not obtained then that material may not be included in your publication/copies. Suitable acknowledgement to the source must be made, either as a footnote or in a reference list at the end of your publication, as follows:

"Reprinted from Publication title, Vol /edition number, Author(s), Title of article / title of chapter, Pages No., Copyright (Year), with permission from Elsevier [OR APPLICABLE SOCIETY COPYRIGHT OWNER]." Also Lancet special credit - "Reprinted from The Lancet, Vol. number, Author(s), Title of article, Pages No., Copyright (Year), with permission from Elsevier."

4. Reproduction of this material is confined to the purpose and/or media for which permission is hereby given.

5. Altering/Modifying Material: Not Permitted. However figures and illustrations may be altered/adapted minimally to serve your work. Any other abbreviations, additions, deletions and/or any other alterations shall be made only with prior written authorization of Elsevier Ltd. (Please contact Elsevier at permissions@elsevier.com). No modifications can be made to any Lancet figures/tables and they must be reproduced in full.

6. If the permission fee for the requested use of our material is waived in this instance, please be advised that your future requests for Elsevier materials may attract a fee.

7. Reservation of Rights: Publisher reserves all rights not specifically granted in the combination of (i) the license details provided by you and accepted in the course of this licensing transaction, (ii) these terms and conditions and (iii) CCC's Billing and Payment terms and conditions.

8. License Contingent Upon Payment: While you may exercise the rights licensed immediately upon issuance of the license at the end of the licensing process for the transaction, provided that you have disclosed complete and accurate details of your proposed use, no license is finally effective unless and until full payment is received from you (either by publisher or by CCC) as provided in CCC's Billing and Payment terms and conditions. If full payment is not received on a timely basis, then any license preliminarily granted shall be deemed automatically revoked and shall be void as if never granted. Further, in the event that you breach any of these terms and conditions or any of CCC's Billing and Payment terms and conditions, the license is automatically revoked and shall be void as if never granted. Use of materials as described in a revoked license, as well as any use of the materials beyond the scope of an unrevoked license, may constitute copyright infringement and publisher reserves the right to take any and all action to protect its copyright in the materials.

9. Warranties: Publisher makes no representations or warranties with respect to the licensed material.

10. Indemnity: You hereby indemnify and agree to hold harmless publisher and CCC, and their respective officers, directors, employees and agents, from and against any and all claims arising out of your use of the licensed material other than as specifically authorized pursuant to this license.

11. No Transfer of License: This license is personal to you and may not be sublicensed, assigned, or transferred by you to any other person without publisher's written permission.

12. No Amendment Except in Writing: This license may not be amended except in a writing signed by both parties (or, in the case of publisher, by CCC on publisher's behalf).

13. Objection to Contrary Terms: Publisher hereby objects to any terms contained in any purchase order, acknowledgment, check endorsement or other writing prepared by you, which terms are inconsistent with these terms and conditions or CCC's Billing and Payment terms and conditions. These terms and conditions, together with CCC's Billing and Payment terms and conditions (which are incorporated herein), comprise the entire agreement between you and publisher (and CCC) concerning this licensing transaction. In the event of any conflict between your obligations established by these terms and conditions and those established by CCC's Billing and Payment terms and conditions, these terms and conditions shall control.

14. Revocation: Elsevier or Copyright Clearance Center may deny the permissions described in this License at their sole discretion, for any reason or no reason, with a full refund payable to you. Notice of such denial will be made using the contact information provided by you. Failure to receive such notice will not alter or invalidate the denial. In no event will Elsevier or Copyright Clearance Center be responsible or liable for any costs, expenses or damage incurred by you as a result of a denial of your permission request, other than a refund of the amount(s) paid by you to Elsevier and/or Copyright Clearance Center for denied permissions.

LIMITED LICENSE

The following terms and conditions apply only to specific license types:

15. **Translation**: This permission is granted for non-exclusive world **English** rights only unless your license was granted for translation rights. If you licensed translation rights you may only translate this content into the languages you requested. A professional translator must perform all translations and reproduce the content word for word preserving the integrity of the article.

16. **Posting licensed content on any Website**: The following terms and conditions apply as follows: Licensing material from an Elsevier journal: All content posted to the web site must maintain the copyright information line on the bottom of each image; A hyper-text must be included to the Homepage of the journal from which you are licensing at http://www.sciencedirect.com/science/journal/xxxxx or the Elsevier homepage for books at http://www.elsevier.com; Central Storage: This license does not include permission for a scanned version of the material to be stored in a central repository such as that provided by Heron/XanEdu.

Licensing material from an Elsevier book: A hyper-text link must be included to the Elsevier homepage at http://www.elsevier.com . All content posted to the web site must maintain the copyright information line on the bottom of each image.

Posting licensed content on Electronic reserve: In addition to the above the following

clauses are applicable: The web site must be password-protected and made available only to bona fide students registered on a relevant course. This permission is granted for 1 year only. You may obtain a new license for future website posting.

17. **For journal authors:** the following clauses are applicable in addition to the above:

Preprints:

A preprint is an author's own write-up of research results and analysis, it has not been peer-reviewed, nor has it had any other value added to it by a publisher (such as formatting, copyright, technical enhancement etc.).

Authors can share their preprints anywhere at any time. Preprints should not be added to or enhanced in any way in order to appear more like, or to substitute for, the final versions of articles however authors can update their preprints on arXiv or RePEc with their Accepted Author Manuscript (see below).

If accepted for publication, we encourage authors to link from the preprint to their formal publication via its DOI. Millions of researchers have access to the formal publications on ScienceDirect, and so links will help users to find, access, cite and use the best available version. Please note that Cell Press, The Lancet and some society-owned have different preprint policies. Information on these policies is available on the journal homepage.

Accepted Author Manuscripts: An accepted author manuscript is the manuscript of an article that has been accepted for publication and which typically includes author-incorporated changes suggested during submission, peer review and editor-author communications.

Authors can share their accepted author manuscript:

- immediately
  - via their non-commercial person homepage or blog
  - by updating a preprint in arXiv or RePEc with the accepted manuscript
  - via their research institute or institutional repository for internal institutional uses or as part of an invitation-only research collaboration work-group
  - directly by providing copies to their students or to research collaborators for their personal use
  - for private scholarly sharing as part of an invitation-only work group on commercial sites with which Elsevier has an agreement
- After the embargo period
  - via non-commercial hosting platforms such as their institutional repository
  - via commercial sites with which Elsevier has an agreement

In all cases accepted manuscripts should:

- link to the formal publication via its DOI
- bear a CC-BY-NC-ND license - this is easy to do
- if aggregated with other manuscripts, for example in a repository or other site, be shared in alignment with our hosting policy not be added to or enhanced in any way to appear more like, or to substitute for, the published journal article.

Published journal article (JPA): A published journal article (PJA) is the definitive final record of published research that appears or will appear in the journal and embodies all value-adding publishing activities including peer review co-ordination, copy-editing, formatting, (if relevant) pagination and online enrichment.

If any part of the material to be used (for example, figures) has appeared in our publication with credit or acknowledgement to another source it is the responsibility of the user to ensure their reuse complies with the terms and conditions determined by the rights holder.

Additional Terms & Conditions applicable to each Creative Commons user license:

CC BY: The CC-BY license allows users to copy, to create extracts, abstracts and new works from the Article, to alter and revise the Article and to make commercial use of the Article (including reuse and/or resale of the Article by commercial entities), provided the user gives appropriate credit (with a link to the formal publication through the relevant DOI), provides a link to the license, indicates if changes were made and the licensor is not represented as endorsing the use made of the work. The full details of the license are available at http://creativecommons.org/licenses/by/4.0.

CC BY NC SA: The CC BY-NC-SA license allows users to copy, to create extracts, abstracts and new works from the Article, to alter and revise the Article, provided this is not done for commercial purposes, and that the user gives appropriate credit (with a link to the formal publication through the relevant DOI), provides a link to the license, indicates if changes were made and the licensor is not represented as endorsing the use made of the work. Further, any new works must be made available on the same conditions. The full details of the license are available at http://creativecommons.org/licenses/by-nc-sa/4.0.

CC BY NC ND: The CC BY-NC-ND license allows users to copy and distribute the Article, provided this is not done for commercial purposes and further does not permit distribution of the Article if it is changed or edited in any way, and provided the user gives appropriate credit (with a link to the formal publication through the relevant DOI), provides a link to the license, and that the licensor is not represented as endorsing the use made of the work. The full details of the license are available at http://creativecommons.org/licenses/by-nc-nd/4.0. Any commercial reuse of Open Access articles published with a CC BY NC SA or CC BY NC ND license requires permission from Elsevier and will be subject to a fee.

Commercial reuse includes:

- Associating advertising with the full text of the Article
- Charging fees for document delivery or access
- Article aggregation
- Systematic distribution via e-mail lists or share buttons

Posting or linking by commercial companies for use by customers of those companies.

20. **Other Conditions**:

v1.9

Questions? customercare@copyright.com or +1-855-239-3415 (toll free in the US) or +1-978-646-2777.

JOHN WILEY AND SONS LICENSE
TERMS AND CONDITIONS

May 25, 2020

This Agreement between 421 Larry Uteck Boulevard ("You") and John Wiley and Sons ("John Wiley and Sons") consists of your license details and the terms and conditions provided by John Wiley and Sons and Copyright Clearance Center.

License Number	4787210909481
License date	Mar 13, 2020
Licensed Content Publisher	John Wiley and Sons
Licensed Content Publication	Journal of Physiology
Licensed Content Title	Modelling spinal circuitry involved in locomotor pattern generation: insights from deletions during fictive locomotion
Licensed Content Author	Ilya A. Rybak, Natalia A. Shevtsova, Myriam Lafreniere-Roula, et al
Licensed Content Date	Nov 24, 2006
Licensed Content Volume	577
Licensed Content Issue	2
Licensed Content Pages	23

Type of use	Dissertation/Thesis
Requestor type	University/Academic
Format	Print and electronic
Portion	Figure/table
Number of figures/tables	1
Will you be translating?	No
Title	PhD
Expected presentation date	Apr 2020
Order reference number	Figure 1.4
Portions	Figure 2A
Requestor Location	421 Larry Uteck Boulevard 421 Larry Uteck Boulevard 206 halifax, NS b3m0g7 Canada Attn: 421 Larry Uteck Boulevard
Publisher Tax ID	EU826007151
Total	0.00 CAD

Terms and Conditions

TERMS AND CONDITIONS

license or interest to any trademark, trade name, service mark or other branding ("Marks") of WILEY or its licensors is granted hereunder, and you agree that you shall not assert any such right, license or interest with respect thereto

- NEITHER WILEY NOR ITS LICENSORS MAKES ANY WARRANTY OR REPRESENTATION OF ANY KIND TO YOU OR ANY THIRD PARTY, EXPRESS, IMPLIED OR STATUTORY, WITH RESPECT TO THE MATERIALS OR THE ACCURACY OF ANY INFORMATION CONTAINED IN THE MATERIALS, INCLUDING, WITHOUT LIMITATION, ANY IMPLIED WARRANTY OF MERCHANTABILITY, ACCURACY, SATISFACTORY QUALITY, FITNESS FOR A PARTICULAR PURPOSE, USABILITY, INTEGRATION OR NON-INFRINGEMENT AND ALL SUCH WARRANTIES ARE HEREBY EXCLUDED BY WILEY AND ITS LICENSORS AND WAIVED BY YOU.

- WILEY shall have the right to terminate this Agreement immediately upon breach of this Agreement by you.

- You shall indemnify, defend and hold harmless WILEY, its Licensors and their respective directors, officers, agents and employees, from and against any actual or threatened claims, demands, causes of action or proceedings arising from any breach of this Agreement by you.

- IN NO EVENT SHALL WILEY OR ITS LICENSORS BE LIABLE TO YOU OR ANY OTHER PARTY OR ANY OTHER PERSON OR ENTITY FOR ANY SPECIAL, CONSEQUENTIAL, INCIDENTAL, INDIRECT, EXEMPLARY OR PUNITIVE DAMAGES, HOWEVER CAUSED, ARISING OUT OF OR IN CONNECTION WITH THE DOWNLOADING, PROVISIONING, VIEWING OR USE OF THE MATERIALS REGARDLESS OF THE FORM OF ACTION, WHETHER FOR BREACH OF CONTRACT, BREACH OF WARRANTY, TORT, NEGLIGENCE, INFRINGEMENT OR OTHERWISE (INCLUDING, WITHOUT LIMITATION, DAMAGES BASED ON LOSS OF PROFITS, DATA, FILES, USE, BUSINESS OPPORTUNITY OR CLAIMS OF THIRD PARTIES), AND WHETHER OR NOT THE PARTY HAS BEEN ADVISED OF THE POSSIBILITY OF SUCH DAMAGES. THIS LIMITATION SHALL APPLY NOTWITHSTANDING ANY FAILURE OF ESSENTIAL PURPOSE OF ANY LIMITED REMEDY PROVIDED HEREIN.

- Should any provision of this Agreement be held by a court of competent jurisdiction to be illegal, invalid, or unenforceable, that provision shall be deemed amended to achieve as nearly as possible the same economic effect as the original provision, and the legality, validity and enforceability of the remaining provisions of this Agreement shall not be affected or impaired thereby.

- The failure of either party to enforce any term or condition of this Agreement shall not constitute a waiver of either party's right to enforce each and every term and condition of this Agreement. No breach under this agreement shall be deemed waived or excused by either party unless such waiver or consent is in writing signed by the party granting such waiver or consent. The waiver by or consent of a party to a breach of any provision of this Agreement shall not operate or be construed as a waiver of or consent to any other or subsequent breach by such other party.

- This Agreement may not be assigned (including by operation of law or otherwise) by you without WILEY's prior written consent.

- Any fee required for this permission shall be non-refundable after thirty (30) days from receipt by the CCC.
- These terms and conditions together with CCC's Billing and Payment terms and conditions (which are incorporated herein) form the entire agreement between you and WILEY concerning this licensing transaction and (in the absence of fraud) supersedes all prior agreements and representations of the parties, oral or written. This Agreement may not be amended except in writing signed by both parties. This Agreement shall be binding upon and inure to the benefit of the parties' successors, legal representatives, and authorized assigns.
- In the event of any conflict between your obligations established by these terms and conditions and those established by CCC's Billing and Payment terms and conditions, these terms and conditions shall prevail.
- WILEY expressly reserves all rights not specifically granted in the combination of (i) the license details provided by you and accepted in the course of this licensing transaction, (ii) these terms and conditions and (iii) CCC's Billing and Payment terms and conditions.
- This Agreement will be void if the Type of Use, Format, Circulation, or Requestor Type was misrepresented during the licensing process.
- This Agreement shall be governed by and construed in accordance with the laws of the State of New York, USA, without regards to such state's conflict of law rules. Any legal action, suit or proceeding arising out of or relating to these Terms and Conditions or the breach thereof shall be instituted in a court of competent jurisdiction in New York County in the State of New York in the United States of America and each party hereby consents and submits to the personal jurisdiction of such court, waives any objection to venue in such court and consents to service of process by registered or certified mail, return receipt requested, at the last known address of such party.

WILEY OPEN ACCESS TERMS AND CONDITIONS

Wiley Publishes Open Access Articles in fully Open Access Journals and in Subscription journals offering Online Open. Although most of the fully Open Access journals publish open access articles under the terms of the Creative Commons Attribution (CC BY) License only, the subscription journals and a few of the Open Access Journals offer a choice of Creative Commons Licenses. The license type is clearly identified on the article.

The Creative Commons Attribution License

The Creative Commons Attribution License (CC-BY) allows users to copy, distribute and transmit an article, adapt the article and make commercial use of the article. The CC-BY license permits commercial and non-

Creative Commons Attribution Non-Commercial License

The Creative Commons Attribution Non-Commercial (CC-BY-NC)License permits use, distribution and reproduction in any medium, provided the original work is properly cited and is not used for commercial purposes.(see below)

Creative Commons Attribution-Non-Commercial-NoDerivs License

The Creative Commons Attribution Non-Commercial-NoDerivs License (CC-BY-NC-ND) permits use, distribution and reproduction in any medium, provided the original work is properly cited, is not used for commercial purposes and no modifications or adaptations are made. (see below)

Use by commercial "for-profit" organizations

Use of Wiley Open Access articles for commercial, promotional, or marketing purposes requires further explicit permission from Wiley and will be subject to a fee.

Further details can be found on Wiley Online Library
http://olabout.wiley.com/WileyCDA/Section/id-410895.html

Other Terms and Conditions:

v1.10 Last updated September 2015

Questions? customercare@copyright.com or +1-855-239-3415 (toll free in the US) or +1-978-646-2777.

JOHN WILEY AND SONS LICENSE
TERMS AND CONDITIONS

May 25, 2020

This Agreement between 421 Larry Uteck Boulevard ("You") and John Wiley and Sons ("John Wiley and Sons") consists of your license details and the terms and conditions provided by John Wiley and Sons and Copyright Clearance Center.

License Number	4787211008504
License date	Mar 13, 2020
Licensed Content Publisher	John Wiley and Sons
Licensed Content Publication	Journal of Physiology
Licensed Content Title	Neuronal activity in the isolated mouse spinal cord during spontaneous deletions in fictive locomotion: insights into locomotor central pattern generator organization
Licensed Content Author	Ronald M. Harris-Warrick, Ilya A. Rybak, Natalia A. Shevtsova, et al
Licensed Content Date	Sep 7, 2012
Licensed Content Volume	590
Licensed Content Issue	19

Licensed Content Pages	25
Type of use	Dissertation/Thesis
Requestor type	University/Academic
Format	Print and electronic
Portion	Figure/table
Number of figures/tables	1
Will you be translating?	No
Title	PhD
Expected presentation date	Apr 2020
Order reference number	Figure 1.5
Portions	Figure 9B
Requestor Location	421 Larry Uteck Boulevard 421 Larry Uteck Boulevard 206 halifax, NS b3m0g7 Canada Attn: 421 Larry Uteck Boulevard
Publisher Tax ID	EU826007151

Total 0.00 CAD

Terms and Conditions

TERMS AND CONDITIONS

This copyrighted material is owned by or exclusively licensed to John Wiley & Sons, Inc. or one of its group companies (each a"Wiley Company") or handled on behalf of a society with which a Wiley Company has exclusive publishing rights in relation to a particular work (collectively "WILEY"). By clicking "accept" in connection with completing this licensing transaction, you agree that the following terms and conditions apply to this transaction (along with the billing and payment terms and conditions established by the Copyright Clearance Center Inc., ("CCC's Billing and Payment terms and conditions"), at the time that you opened your RightsLink account (these are available at any time at http://myaccount.copyright.com).

Terms and Conditions

- The materials you have requested permission to reproduce or reuse (the "Wiley Materials") are protected by copyright.
- You are hereby granted a personal, non-exclusive, non-sub licensable (on a stand-alone basis), non-transferable, worldwide, limited license to reproduce the Wiley Materials for the purpose specified in the licensing process. This license, **and any CONTENT (PDF or image file) purchased as part of your order,** is for a one-time use only and limited to any maximum distribution number specified in the license. The first instance of republication or reuse granted by this license must be completed within two years of the date of the grant of this license (although copies prepared before the end date may be distributed thereafter). The Wiley Materials shall not be used in any other manner or for any other purpose, beyond what is granted in the license. Permission is granted subject to an appropriate acknowledgement given to the author, title of the material/book/journal and the publisher. You shall also duplicate the copyright notice that appears in the Wiley publication in your use of the Wiley Material. Permission is also granted on the understanding that nowhere in the text is a previously published source acknowledged for all or part of this Wiley Material. Any third party content is expressly excluded from this permission.
- With respect to the Wiley Materials, all rights are reserved. Except as expressly granted by the terms of the license, no part of the Wiley Materials may be copied, modified, adapted (except for minor reformatting required by the new Publication), translated, reproduced, transferred or distributed, in any form or by any means, and no derivative works may be made based on the Wiley Materials without the prior permission of the respective copyright owner.**For STM Signatory Publishers clearing permission under the terms of the STM Permissions Guidelines only, the terms of the license are extended to include subsequent editions and for editions in other languages, provided such editions are for the work as a whole in situ and does not involve the separate exploitation of the permitted figures or extracts,** You may not alter, remove or suppress in any manner any copyright, trademark or other notices displayed by the Wiley Materials. You may not license, rent, sell, loan, lease, pledge, offer as security, transfer or assign the Wiley Materials on a stand-alone

basis, or any of the rights granted to you hereunder to any other person.

- The Wiley Materials and all of the intellectual property rights therein shall at all times remain the exclusive property of John Wiley & Sons Inc, the Wiley Companies, or their respective licensors, and your interest therein is only that of having possession of and the right to reproduce the Wiley Materials pursuant to Section 2 herein during the continuance of this Agreement. You agree that you own no right, title or interest in or to the Wiley Materials or any of the intellectual property rights therein. You shall have no rights hereunder other than the license as provided for above in Section 2. No right, license or interest to any trademark, trade name, service mark or other branding ("Marks") of WILEY or its licensors is granted hereunder, and you agree that you shall not assert any such right, license or interest with respect thereto

- NEITHER WILEY NOR ITS LICENSORS MAKES ANY WARRANTY OR REPRESENTATION OF ANY KIND TO YOU OR ANY THIRD PARTY, EXPRESS, IMPLIED OR STATUTORY, WITH RESPECT TO THE MATERIALS OR THE ACCURACY OF ANY INFORMATION CONTAINED IN THE MATERIALS, INCLUDING, WITHOUT LIMITATION, ANY IMPLIED WARRANTY OF MERCHANTABILITY, ACCURACY, SATISFACTORY QUALITY, FITNESS FOR A PARTICULAR PURPOSE, USABILITY, INTEGRATION OR NON-INFRINGEMENT AND ALL SUCH WARRANTIES ARE HEREBY EXCLUDED BY WILEY AND ITS LICENSORS AND WAIVED BY YOU.

- WILEY shall have the right to terminate this Agreement immediately upon breach of this Agreement by you.

- You shall indemnify, defend and hold harmless WILEY, its Licensors and their respective directors, officers, agents and employees, from and against any actual or threatened claims, demands, causes of action or proceedings arising from any breach of this Agreement by you.

- IN NO EVENT SHALL WILEY OR ITS LICENSORS BE LIABLE TO YOU OR ANY OTHER PARTY OR ANY OTHER PERSON OR ENTITY FOR ANY SPECIAL, CONSEQUENTIAL, INCIDENTAL, INDIRECT, EXEMPLARY OR PUNITIVE DAMAGES, HOWEVER CAUSED, ARISING OUT OF OR IN CONNECTION WITH THE DOWNLOADING, PROVISIONING, VIEWING OR USE OF THE MATERIALS REGARDLESS OF THE FORM OF ACTION, WHETHER FOR BREACH OF CONTRACT, BREACH OF WARRANTY, TORT, NEGLIGENCE, INFRINGEMENT OR OTHERWISE (INCLUDING, WITHOUT LIMITATION, DAMAGES BASED ON LOSS OF PROFITS, DATA, FILES, USE, BUSINESS OPPORTUNITY OR CLAIMS OF THIRD PARTIES), AND WHETHER OR NOT THE PARTY HAS BEEN ADVISED OF THE POSSIBILITY OF SUCH DAMAGES. THIS LIMITATION SHALL APPLY NOTWITHSTANDING ANY FAILURE OF ESSENTIAL PURPOSE OF ANY LIMITED REMEDY PROVIDED HEREIN.

- Should any provision of this Agreement be held by a court of competent jurisdiction to be illegal, invalid, or unenforceable, that provision shall be deemed amended to achieve as nearly as possible the same economic effect as the original provision, and the legality, validity and enforceability of the remaining provisions of this Agreement shall not be affected or impaired thereby.

- The failure of either party to enforce any term or condition of this Agreement shall not constitute a waiver of either party's right to enforce each and every term and condition of this Agreement. No breach under this agreement shall be deemed waived or excused by either party unless such waiver or consent is in writing signed by the party granting such waiver or consent. The waiver by or consent of a party to a breach of any provision of this Agreement shall not operate or be construed as a waiver of or consent to any other or subsequent breach by such other party.

- This Agreement may not be assigned (including by operation of law or otherwise) by you without WILEY's prior written consent.

- Any fee required for this permission shall be non-refundable after thirty (30) days from receipt by the CCC.

- These terms and conditions together with CCC's Billing and Payment terms and conditions (which are incorporated herein) form the entire agreement between you and WILEY concerning this licensing transaction and (in the absence of fraud) supersedes all prior agreements and representations of the parties, oral or written. This Agreement may not be amended except in writing signed by both parties. This Agreement shall be binding upon and inure to the benefit of the parties' successors, legal representatives, and authorized assigns.

- In the event of any conflict between your obligations established by these terms and conditions and those established by CCC's Billing and Payment terms and conditions, these terms and conditions shall prevail.

- WILEY expressly reserves all rights not specifically granted in the combination of (i) the license details provided by you and accepted in the course of this licensing transaction, (ii) these terms and conditions and (iii) CCC's Billing and Payment terms and conditions.

- This Agreement will be void if the Type of Use, Format, Circulation, or Requestor Type was misrepresented during the licensing process.

- This Agreement shall be governed by and construed in accordance with the laws of the State of New York, USA, without regards to such state's conflict of law rules. Any legal action, suit or proceeding arising out of or relating to these Terms and Conditions or the breach thereof shall be instituted in a court of competent jurisdiction in New York County in the State of New York in the United States of America and each party hereby consents and submits to the personal jurisdiction of such court, waives any objection to venue in such court and consents to service of process by registered or certified mail, return receipt requested, at the last known address of such party.

WILEY OPEN ACCESS TERMS AND CONDITIONS

Wiley Publishes Open Access Articles in fully Open Access Journals and in Subscription journals offering Online Open. Although most of the fully Open Access journals publish open access articles under the terms of the Creative Commons Attribution (CC BY) License only, the subscription journals and a few of the Open Access Journals offer a choice of Creative Commons Licenses. The license type is clearly identified on the article.

The Creative Commons Attribution License

The Creative Commons Attribution License (CC-BY) allows users to copy, distribute and transmit an article, adapt the article and make commercial use of the article. The CC-BY license permits commercial and non-

Creative Commons Attribution Non-Commercial License

The Creative Commons Attribution Non-Commercial (CC-BY-NC)License permits use, distribution and reproduction in any medium, provided the original work is properly cited and is not used for commercial purposes.(see below)

Creative Commons Attribution-Non-Commercial-NoDerivs License

The Creative Commons Attribution Non-Commercial-NoDerivs License (CC-BY-NC-ND) permits use, distribution and reproduction in any medium, provided the original work is properly cited, is not used for commercial purposes and no modifications or adaptations are made. (see below)

Use by commercial "for-profit" organizations

Use of Wiley Open Access articles for commercial, promotional, or marketing purposes requires further explicit permission from Wiley and will be subject to a fee.

Further details can be found on Wiley Online Library
http://olabout.wiley.com/WileyCDA/Section/id-410895.html

Other Terms and Conditions:

v1.10 Last updated September 2015

Questions? customercare@copyright.com or +1-855-239-3415 (toll free in the US) or +1-978-646-2777.

THE AMERICAN PHYSIOLOGICAL SOCIETY LICENSE
TERMS AND CONDITIONS

May 25, 2020

This Agreement between 421 Larry Uteck Boulevard ("You") and The American Physiological Society ("The American Physiological Society") consists of your license details and the terms and conditions provided by The American Physiological Society and Copyright Clearance Center.

License Number	4791390679824
License date	Mar 17, 2020
Licensed Content Publisher	The American Physiological Society
Licensed Content Publication	Journal of Neurophysiology
Licensed Content Title	Motoneuronal and muscle synergies involved in cat hindlimb control during fictive and real locomotion: a comparison study
Licensed Content Author	Sergey N. Markin, Michel A. Lemay, Boris I. Prilutsky, et al
Licensed Content Date	Apr 15, 2012
Licensed Content Volume	107
Licensed Content Issue	8
Type of Use	Thesis/Dissertation
Requestor type	non-profit academic/educational

Readers being charged a fee for this work	No
Format	print and electronic
Portion	figures/tables/images
Number of figures/tables/images	2
Will you be translating?	no
World Rights	no
Order reference number	
Title	PhD
Institution name	dalhousie university
Expected presentation date	Apr 2020
Portions	Figure 1.2
Requestor Location	421 Larry Uteck Boulevard 421 Larry Uteck Boulevard 206 halifax, NS b3m0g7 Canada Attn: 421 Larry Uteck Boulevard
Billing Type	Invoice
Billing Address	421 Larry Uteck Boulevard 421 Larry Uteck Boulevard 206

halifax, NS b3m0g7
Canada
Attn: 421 Larry Uteck Boulevard

Total 0.00 CAD

Terms and Conditions

Terms and Conditions:

Figures/Tables/Images are available to the requestor from the APS journals website at http://www.the-aps.org/publications/journals/. The obtaining of content is a separate transaction and does not involve Rightslink or CCC, and is the responsibility of the permission seeker. Higher resolution images are available at additional charge from APS; please contact cvillemez@the-aps.org

Original Authors of Published Works: To see a full list of original authors rights concerning their own published work http://www.the-aps.org/publications/authorinfo/copyright.htm

Content reuse rights awarded by the APS may be exercised immediately upon issuance of this license, provided full disclosure and complete and accurate details of the proposed reuse have been made; no license is finally granted unless and until full payment is received either by the publisher or by CCC as provided in CCC's Billing and Payment Terms and Conditions. If full payment is not received on a timely basis, then any license preliminarily granted shall be deemed automatically revoked and shall be void as if never granted. Further, in the event that you breach any of these Terms and Conditions or any of CCC's Billing and Payment Terms and Conditions, the license is automatically revoked and shall be void as if never granted. Use of materials as described in a revoked license, as well as any use of the materials beyond the scope of the license, may constitute copyright infringement and the Publisher reserves the right to take action to protect its copyright of its materials.

The APS makes no representations or warranties with respect to the licensed material. You hereby indemnify and agree to hold harmless the publisher and CCC, and their respective officers, directors, employees and agents, from and against any and all claims arising out of your use of the licensed material other than as specifically authorized pursuant to this license.

This license is personal to you /your organization and may not be sublicensed, assigned, or transferred by you /your organization to another person /organization without the publisher's permission.This license may not be amended except in writing signed by both parties, or in the case of the publisher, by CCC on the publisher's behalf.

The APS reserves all rights not specifically granted in the combination of (i) the license details provided by you and accepted in the course of this licensing transaction, (ii) these Terms and Conditions and (iii) CCC's Billing and Payment Terms and Conditions.

v1.0

Questions? customercare@copyright.com or +1-855-239-3415 (toll free in the US) or +1-978-646-2777.